PULMONARY DELIVERY OF PNEUMOCCOCAL VACCINE USING NANOCOMPOSITE MICROPARTICLE CARRIERS VIA DRY POWDER INHALATION

IMAN MOHAMMED ALFAGIH

A thesis submitted in partial fulfilment of the
requirements of Liverpool John Moores University
for the degree of Doctor of Philosophy

February 2015

Acknowledgement

Table of Contents

List of Figures

List of Tables

List of abbreviation

¹H-NMR	Proton nuclear magnetic resonance
¹H-NMR	Proton nuclear magnetic resonance
APCs	Antigen presenting cells
BAL	Bronchoalveolar lavage
BALT	bronchus-associated lymphoid tissue
BCA	Bicinchoninic acid
BCG	Bacillus calmette-guerin
BSA	Bovine serum albumin
CbpA	Choline binding protein A
CD	Circular dichroism
CHL	Chitosan hydrochloride
CLSM	Confocal laser scanning microscopy
DCM	Dichloromethane
DCs	Dendritic cells
DIC	Disseminated intravascular coagulation
DL	Drug loading
DMSO	Dimethyl sulfoxide
DNA	Deoxyribonucleic acid
DOE	Design of experiments
DPIs	Dry powder inhalers
DSC	Differential scanning calorimeter
EAP	External aqueous phase
EE	Encapsulation efficiency
ELISA	Enzyme-linked immunosorbent assay
FCS	Fetal calf serum

FDA	Food and drug administration
FPD	Fine particle dose
FPF	Fine particle fraction
GPC	Gel permeation chromatography
HBsAg	Hepatitis B Antigen
HDL	High drug loading
IAP	Internal aqueous phase
IgA	Immunoglobulin A
IL	interleukin
INF	Interferon
LDL	Low drug loading
LPS	Lipopolysaccharides
M cells	Macro fold cells
MALT	mucosal-associated lymphoid tissue
mDCs	Myeloid dendritic cells
MHC	Major histocompatibility complex
MMAD	Mass median aerodynamic diameter
MTT	3-4, 5-dimethylthiazol-2-yl-2,5-diphenyl tetrazolium bromide
MW	Molecular weight
NCMPs	Nanocomposite microparticles
NGI	Next generation impactor
NPs	Nanoparticles
OP	Organic phase
PBS	Phosphate buffer saline
PCL	poly-(ε-caprolactone)
PCV	Pneumococcal conjugate vaccine

pDCs	Plasmacytoid dendritic cells
PDI	Poly dispersity index
PEG	Polyethylene glycol
PEI	polyethyleneimine
PGA-co-PDL	Poly (glycerol adipate-co-ω-pentadecalactone)
PLA	Poly (L-lactic acid)
PLGA	Poly (lactic-co-glycolic –acid)
pMDIs	Pressurised Metered dose inhalers
PPV	Pneumococcal polysaccharide vaccine
PspA	Pneumococcal surface protein A
PVA	Poly vinyl alcohol
RNA	Ribonucleic acid
S/N	Single-o-noise ratio
SCF	Supercritical fluid
SD	Standard deviation
SDS-PAGE	Sodium dodecyl sulfate poly (acrylamide) gel electrophoresis
SEM	Scaning electron microscope
SPS	Smaller particle size
TGA	Thermos gravimetric analysis
TNF-α	Tumor necrosis factor-alpha
w/o/w	Water-in-oil-in-water

Abstract

S. pneumoniae is one of the most significant human pathogens, causing high morbidity and mortality rates globally. Although there are vaccine available such as PPV 23, PCV7, PCV10, and PCV13, they are ineffective in some situations due to the differing epidemiology of various serotypes depending on the site of infection and the geographical location. Furthermore, they are expensive to produce and distribute. Universal research is presently concentrated on establishing other pneumococcal-vaccine approaches such as using pneumococcal surface protein A (PspA) which relate to pathogenesis and are common to all serotypes. In this study polymeric nanoparticles (NPs) encapsulating PspA4Pro were incorporated into microcarriers using L-leucine and spray dried to produce nanocomposite microparticles (NCMPs) dry powder for inhalation.

Parameters for the preparation of protein-loaded polyester poly (Glycerol Adipate-co-ω-Pentadecalactone), (PGA-co-PDL) NCMPs were optimised using Taguchi design and BSA as a model protein, by the double emulsion solvent evaporation method followed by spray drying. Particle size was mainly affected by the polymer mass and small particle size $\leq$ 500nm was achieved. The most important factor for obtaining a high BSA loading was BSA concentration. The spray drying process was optimised to produce NCMPs with a porous corrugated surface, 50% yield, MMAD of 1.71±0.10 μm and FPF% of 78.57±0.1%.

Adsorption of chitosan hydrochloride (CHL) onto PGA-co-PDL NPs can be used as successful strategies to produce cationic NPs. Cationic NPs were prepared with similar particle size to anionic NPs $\leq$ 500nm. The *In vitro* aerosolisation performance of cationic NPs/NCMPs showed FPF% of 46.79±11.21% and MMAD of 1.49±0.29 μm. Further cell viability studies on A549 cell line showed a good profile with a cell viability of 79±4.7% for anionic NPs/NCMPs and 78.85±9.96% for cationic

NPs/NCMPs at 2.5 mg/ml concentration after 24 h exposure. The previous results introduced a successful method for preparing anionic and cationic NPs/NCMPs for delivering PspA4Pro as dry powder via inhalation. The particle size of PspAPro4 loaded anionic NPs and cationic NPs were 310±25.3 nm and 409.7±49.5 nm, respectively, to be effectively taken up by dendritic cells (DCs). The PspA4Pro loading in anionic NPs was 65.73±5.6 µg/mg and in cationic NPs was 9.84±1.4 µg/mg. The PspA4Pro released from anionic and cationic NPs/NCMPs preserved its primary and secondary structure as evaluated by SDS-PAGE and circular dichroism. *In vitro* release studies showed that the anionic NPs/NCMPs formulations achieved a cumulative release of 21.01±1.5% while the cationic NPs/NCMPs formulation released 83.13 ±0.84% after 48 h. DCs uptake studies provide evidence of particles uptake by DCs upon incubation for 1 h as visualized by confocal microscopy. These results indicate the use of optimised methods for developing polymeric based NCMPs for vaccine delivery via inhalation against pneumococcal diseases.

1. General Introduction

1. Introduction

1.1 *Streptococcus pneumoniae*

In the late 1880s George M. Sternberg (1838–1915), a US Army physician, and Louis J. Pasteur (1822–1895) independently isolated *Streptococcus pneumoniae* from rabbits. The rabbits injected with human saliva extracted from patients with pneumococcal disease developed fatal septicaemia (1). Both researchers described the same organism; named *Microbe septicemique du salive* by Pasteur and *Micrococcus pasteuri* by Sternberg. In 1886 this organism was referred to as *Pneumococcus* by Fraenkel because of its liability to cause pulmonary disease (2). It was renamed *Diplococcus pneumoniae* in 1920 a nomination clearly describing pairs of cocci inducing pneumonia. In 1974, the pneumococcus was given its current name, *Streptococcus pneumoniae*, mainly due to its distinguishing growth as chains of cocci in liquid media (2).

S. pneumoniae is one of the most significant human pathogens, causing high morbidity and mortality rates globally (3). Asymptomatic human nasopharyngeal carriage is the main reservoir of *S. pneumoniae* and it colonizes the nasopharynx up to 60% in healthy children and 30% in healthy adults (3). This harmless organism becomes a major human pathogen when the immunity of the host is weakened as in young children, adult, elderly or immunocompromised patients. However, the relationship between the carriage and the development of natural immunity is not clear (3).

1.2 *S. pneumoniae* virulence components

S. pneumoniae is a gram-positive encapsulated bacterium (4). It has a wide range of virulence components that are presented as cell surface proteins, toxins or secreted proteins (Figure 1-1). The most important of these virulence components is the polysaccharide capsule. According to the structure of the capsules (serotypes), *S.*

pneumoniae are divided into 94 serotypes. Just 20-30 of the common serotypes account

for 62% of invasive infections globally (5).
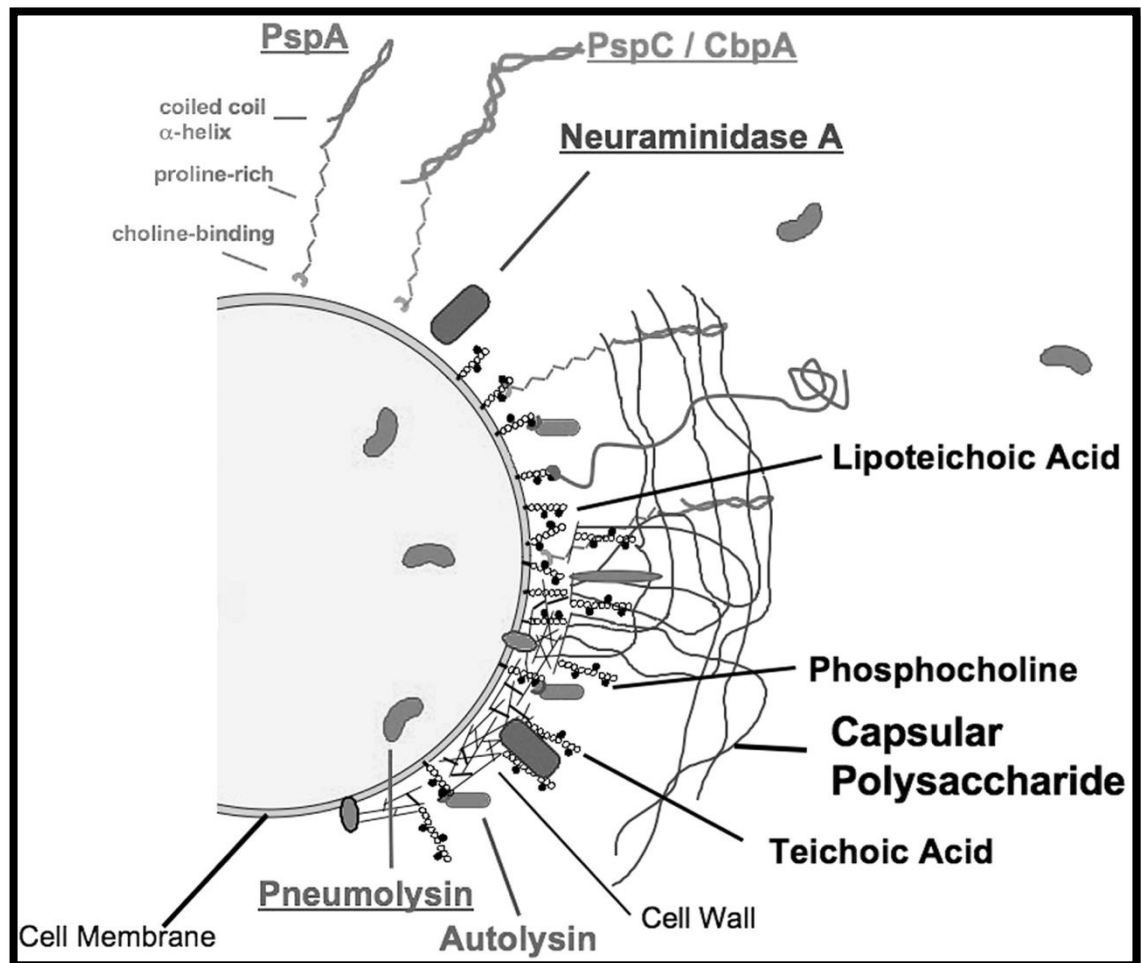
Figure 1-1: Virulence components of *S. pneumoniae*. PspA: pneumococcal surface protein A; PspC: pneumococcal surface protein C; CbpA: choline-binding protein A (with permission from (6)).

The epidemiology of various serotypes differs depends on site of infection, vaccine use

and the geographical location (6). The function of each virulence factor in the

pathophysiology of the disease is ongoing. These virulence components have been

discussed in detail (6) and Figure 1-2 shows the important virulence components of *S.

pneumoniae* and their function in disease development (6).
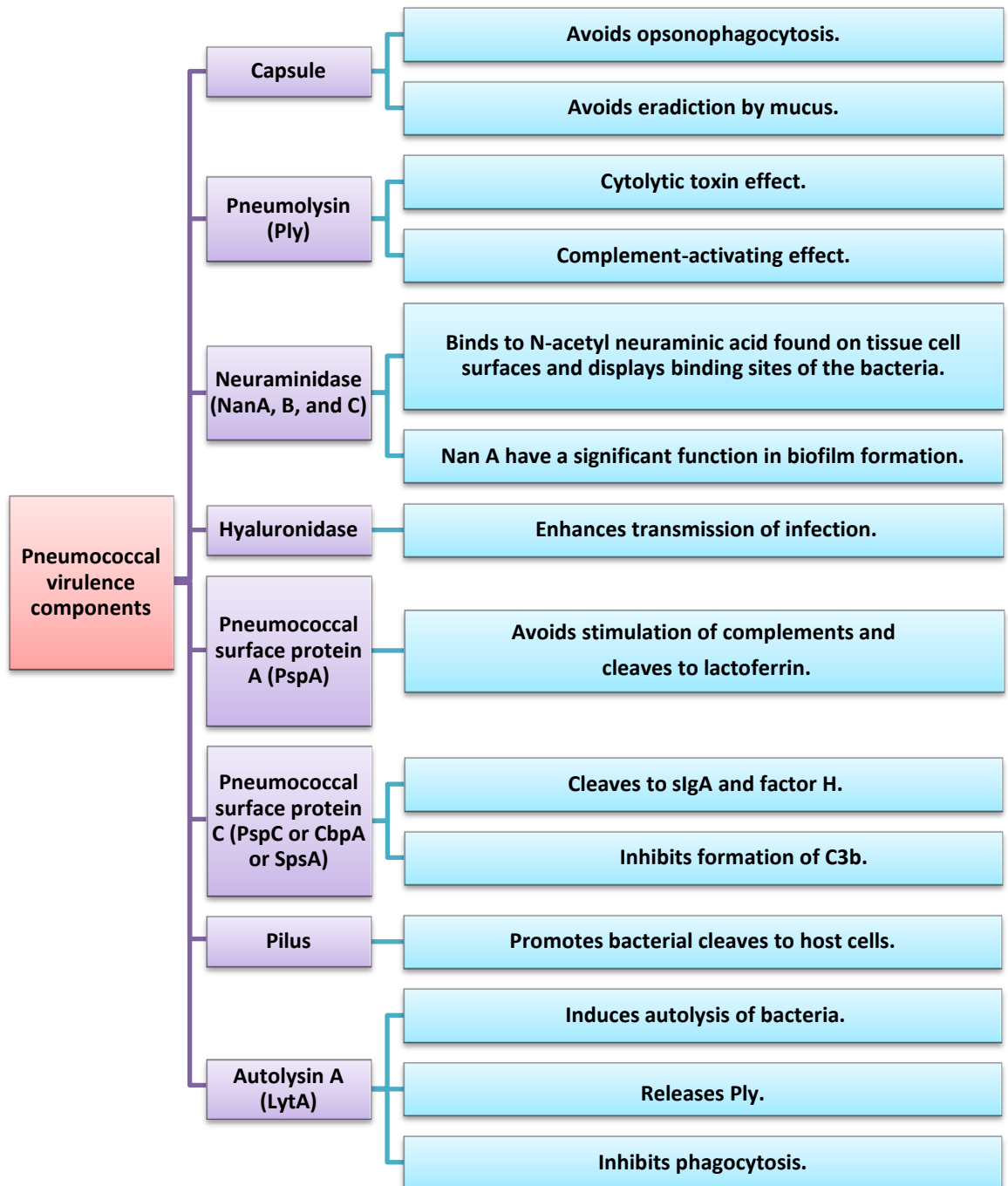
Figure 1-2: Most significant virulence factors of *S. pneumoniae* and their function in disease development.

1.3   Pneumococcal disease

S. pneumoniae are generally transmitted by air droplets or direct contact with contaminated respiratory secretions and they are implicated in both non-invasive and invasive diseases (7).

Non-invasive pneumococcal diseases (e.g. otitis media, sinusitis, and bronchitis) are generally not life threating conditions, but lead to discomfort and loss of school or work days (4). The Health Protection Agency estimates that non-invasive pneumococcal diseases lead to approximately 60,000 general practitioner visits per year (4). Additionally, there is a possibility to develop invasive pneumococcal diseases (4).

The most important manifestations of invasive pneumococcal diseases are pneumonia, bacterial meningitis, and septicaemia which are life threatening conditions (8; 9).

Pneumonia can develop when bacteria invade the lower respiratory tract (Figure 1-3). The alveoli and intracellular spaces fill with macrophages, due to the inflammatory response of the immune system. This leads to the production of a fibrin-rich exudate which fills the infected and adjacent alveolar spaces, making them stick together and so airless. Furthermore, neutrophils proliferate causing pulmonary oedema which deteriorates lung expansion (8). The patient presents with a persistent dry or productive cough, fever, dyspnoea, rigors, and pleuritic pain (10). The first-line choice of the antibiotic amoxicillin or doxycycline is suggested for all cases (4). Due to an extensive increase in antimicrobial resistance it is difficult to implement effective antimicrobial therapy (3). When *S. pneumoniae* reach the blood stream they will cause bacteraemia (Figure 1-3) and induce an immune response that can be devastating. Macrophages stimulate the release of tumour necrosis factor-alpha (TNF-α), leading to vasodilation which causes an increase in vascular permeability and drop in blood pressure. The aim of this reaction is to permit an influx of neutrophils and other lymphocytes to the site of infection to defend host cells (9).
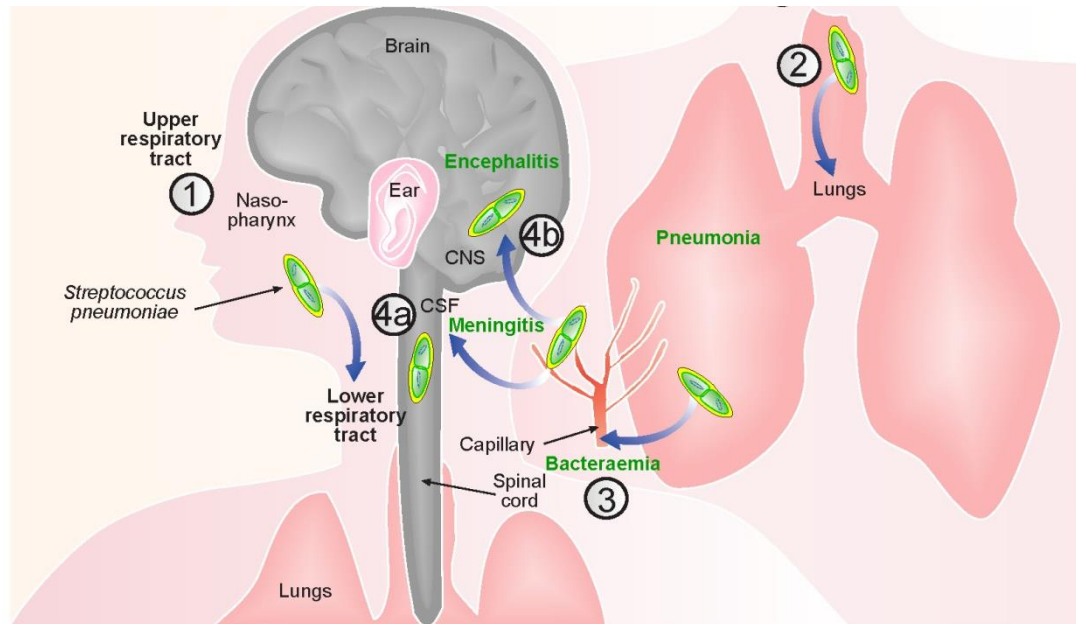
Figure 1-3: General path of *S. pneumoniae* spread from the nasopharynx (1) is invading the lower respiratory tract and leading to pneumonia (2). The lung inflammation can then allow leak out of *S. pneumonia* into the blood stream leading to bacteraemia (3), but can also cause spread to the cerebrospinal fluid (CSF) via the capillary networks leading to meningitis (4a), also *S. pneumonia* can spread into the central nervous system (CNS) leading to encephalitis (4b); but this occurs rarely (with permission from http://www.immunopaedia.org.za/index.php?id=750 (11)).

The consequences can be a massive loss of plasma volume due to leakage into the tissues (oedema). Moreover, the TNF-α stimulates disseminated intravascular coagulation (DIC), leading to clots in the capillaries, which withhold blood flow to vital organs and consume the clotting proteins in the general circulation, causing multiple organ failure (9).

When *S. pneumoniae* cross the blood-brain barrier in large numbers (Figure 1-3), it is thought that the immune system tries to remove the pathogens and this can lead to tissue damage. Neutrophils are engaged at the site of infection to engulf the bacteria and release products e.g. nitric oxide, superoxide anion, and hydrogen peroxide that are toxic to the bacteria and host tissue. This is considered to have importance in the damage to neurons that can cause the sequalae commonly observed after pneumococcal

meningitis. Up to 30 % of surviving patients suffer from sensomotor deficit, hearing loss, and cognitive impairment (8; 11).

The common clinical symptoms of meningitis are headache, fever, neck stiffness and altered mental status. In children less than 5 years old presenting symptoms may be nonspecific such as fever, vomiting, irritability, and drowsiness (12). The first line treatment is antibiotics such as cephalosporin e.g. cefoxamine which can cross the blood brain barrier and corticosteroids such as dexamethasone to prevent complications from excessive inflammation (12).

In the UK, community-acquired pneumonia is an important cause of morbidity and mortality with rate of 5–11 per 1000 adults (4) with hospital admission indicated for 22-42 % of the overall community-acquired pneumonia (13). Furthermore, the case fatality rate of 47.2 % for more than 85 years and 5.6 % for less than 65 years of age has been reported displaying the burden of community acquired pneumonia in aging population (14). In Europe, estimates show that the cost due to pneumonia is approximately € 10.1 billion annually with indirect costs due to lost work days amounting to € 3.6 billion (14). It is a worldwide problem; but, in low middle income countries, morbidity and mortality are highest in children under age of 5 years (15). In 2010, the Health Protection Agency assessed that there were 40,000 admissions to hospital per year due to pneumococcal pneumonia, where 10 % needed intensive care and 10–12 % of cases will lead to death (16). Many studies show an incidence for community acquired pneumonia 1.6-9 cases per 1000 adult population with the financial burden globally estimated to be US $ 4.8 billion for adult aged more than 65 years and US $ 3.6 billion for adults aged less than 65 years (17; 18; 19; 20).

A review of disease burden in children under the age of five reported that in 2007, of an estimated 9 million child deaths, around 1.8 million were due to pneumococcal diseases (15). The situation is worse in low middle income countries, where 90% of these deaths

occur. In addition, pneumonia is implicated in the death of the elderly and immunocompromised individuals (21).

The death rate from pneumococcal meningitis is around 16 – 37 %, and up to 50 % adults who recover will have neurological abnormalities (12). It has been accepted that many of these invasive pneumococcal disease and accompanied deaths can be avoided by vaccination (21).

1.4 Pneumococcal vaccine

Vaccines are antigenic formulations utilized to initiate immunity to establish protection against infectious diseases (22). There are two different types of pneumococcal vaccine currently available: pneumococcal polysaccharide vaccine (PPV) and pneumococcal conjugate vaccine (PCV).

1.4.1 Pneumococcal polysaccharide vaccine (PPV)

Pneumococcal polysaccharide vaccine (PPV) consists of a plain polysaccharide capsule covering the outer surface of the pneumococcus. In 1977, a 14-serotype pneumococcal capsular polysaccharide vaccine was approved for use but was replaced in 1983 after the current 23-serotypes vaccine (Pneumovax, Merck & Co) was licensed (3). Pneumovax (PPV23) contains 23 capsular polysaccharides from the most common *S. pneumoniae* serotypes associated with pneumococcal infections and it is administered by intramuscular or subcutaneous injection (3).

Polysaccharides mainly provoke a B-cell dependent immune response (23). This vaccine was highly effective in children above 2 years of age and young adults with re-vaccination after 5–6 years (4; 24). Its main limitation was the inability to stimulate a significant immune response in children under 2 years of age probably due to their immature immune systems (4; 24). In the elderly (above 65 years old) research suggests that immunization was short-term as antibody titres decreased rapidly from the highest concentrations measured one month after immunization. The administration of

8

additional doses of PPV to maintain immunity in the elderly is restrained, as antibody titres after following doses of PPV are similar or lower than after primary immunization. This phenomenon, known as ''hyporesponsiveness'' has also been noticed after meningococcal polysaccharide immunization. Researchers have suggested that hyporesponsiveness is a result of the consumption of the peripheral B-cell pool by plain polysaccharide antigens that urge B cells into terminal differentiation, without replacing the B-cell pool (23). Additionally, PPV is not suitable for immunocompromised patients (4). Moreover, PPV does not induce mucosal immunity so has no influence on the nasopharyngeal carriage of the *S. pneumoniae* (4). In the UK, this vaccine was only indicated for children and young adults who were in high-risk groups, i.e. with underlying medical conditions such as non-functioning spleen, chronic heart diseases, and renal or liver dysfunction (4; 25).

To enhance the immune response to the capsular polysaccharide in children less than 2 years of age, elderly and immunocompromised patients, a new form vaccine where capsular polysaccharides are conjugated to one of various proteins were developed (4).

1.4.2   Pneumococcal conjugate vaccine (PCV)

Pneumococcal conjugate vaccines (PCV) have been prepared by coupling capsular polysaccharides to several carrier proteins including; tetanus toxoid, diphtheria toxoid, CRM197 (a nontoxic mutant of diphtheria toxin), pneumolysin, and meningococcal outer membrane proteins (7). The protein stimulates a T-cell dependent immune response leading to immune memory and, as a result, induces a booster response (4).

This type of vaccine overcomes the issue with immune response seen with PPV in children under the age of 2 years. The first PCV 7 (Prevenar 7, Wyeth) included purified capsular polysaccharides of seven serotypes conjugated to CRM197 and administered by intramuscular injection (26).

In 2002, PCV was initially recommended for children in the higher risk clinical groups (such as heart, renal, and liver disease) in the UK (4) and in 2006, PCV was added in the national programme for all children under the age of 2 years (4; 25). In 2010, a PCV including 13 serotypes replaced the 7-valent vaccine in the national programme (4). Prevenar 13 (Pfizer Inc) was available in 2011 for active immunisation for the prevention of invasive pneumococcal disease in adults aged above 50 years. Researchers suggest that there is a decrease in cases of community-acquired pneumonia and invasive pneumococcal disease from the serotypes included in the PCV (4).

Regardless of Prevnars protection against vaccine serotypes, it has been demonstrated to evoke serotype redistribution; the substitution of vaccine serotypes by strains not included by the vaccine (3). Thus, the appearance of less common serotypes is anticipated to be more frequent. Serotype substitution is a serious concern, especially in regions with an increased disease burden, due to its ability to change the landscape of disease rapidly (3). However, the vaccine is mainly produced for U.S. and European epidemiological settings, so for low middle income countries it has only a limited coverage of the serotypes provoking invasive pneumococcal diseases (3). In Asia and Africa there are considerable variations in serotype distribution (3). This vaccine is also more expensive than all the other vaccines in the national immunization programmes in many low middle income countries. The unit price of a vial of PPV23 (Pneumovax II, Sanofi Pasteur MSD) is £8.32 and for a vial of PCV13 (Prevenar 13, Pfizer) is £49.10 (retrieved from the British National Formulary 63, 2012). The cost of administration is expected to be 10 min' time of a band 7 advanced nurse, as seen in the Health Protection Agency (now Public Health England) research on seasonal influenza vaccination program. The average cost of administration was evaluated at £6.92 per vaccine (27). However, according to the Royal College of General Practitioners data 54.5% of pneumococcal vaccinations will be co-administered with influenza

vaccination so there is no additional administration cost. In addition, the PCV requires a three-dose vaccination regimen (27). To broaden the protection, the development of a protein-based pneumococcal vaccine could be a feasible and preferable alternative (3).

1.4.3   Pneumococcal protein-based vaccine

Pneumococcal proteins relate to pathogenesis and are common to all serotypes. Over the last twenty years, many pneumococcal protein antigens have been examined for their virulence and vaccine ability. These involve pneumolysin (Ply) toxoid (PdB); choline binding proteins PspA and PspC (also called CbpA or SpsA); metal binding lipoprotein (PsaA); iron uptake ABC transporters PiuA and PiaA; heat shock protein (ClpP); neuraminidases A and B; LytA and hyaluronidase; and pneumococcal histidine triad (Pht) proteins PhtB and PhtE. All the proteins listed above have demonstrated a significant level of protection against systemic challenge with different *S. pneumoniae* serotypes in animal models but not all have been fully evaluated or directly compared, and the outcomes are highly reliant on the mouse strain and challenge strain examined (28).

PspA has gained a special focus, and is a surface protein located on the cell wall in all strains of pneumococci (Figure 1-1). It has N-terminal α-helical domain displayed on the bacterial surface and a repeated region of C-terminal choline-binding that attaches the molecule to the bacterial cell wall (29). There are different PspA sequences, mainly in the N-terminal domain, and according to the similarity of the sequence, PspA is categorised into three families where there is a high serological cross-reactivity between the various families. Around 95% of *S. pneumoniae* strains have PspA categorized in family 1 or family 2 (29). PspA is a critical pneumococcal virulence factor, mainly interfering with host complement function (29). PspA avoids the accumulation of complement on the surface of the bacterium which leads to inhibition of clearance and phagocytosis of *S. pneumoniae* (30). PspA also prevents bactericidal activity by

lactoferrin (30). Lactoferrin is a human protein located on mucosal surfaces and its main function is to bind to elemental iron preventing its use by bacteria on mucosal surfaces. It has been demonstrated that the α-helical domain of PspA binds lactoferrin and may be a means by which pneumococci can either utilize environmental iron or inhibit one mechanism of host defence (31). Some studies showed that PspA vaccine protects mice against a lethal challenge with *S. pneumoniae* through the generation of anti-PspA serum antibodies that are highly cross reactive to other strains (30).

Consequently, it is essential to formulate novel adjuvants - substances that augment an immune response in order to evoke sufficient responses (30) and/or delivery system for the preparation of efficient vaccines that can defend against different strains of *S. pneumoniae* and improve patient compliance by using a tolerable dose regimen. PspA has been the object of many studies examining different vaccine delivery systems such as the delivery of PspA with live attenuated bacteria such as salmonella (32) and via co-administration with a whole-cell pertussis vaccine (33). Furthermore, nano-preparations such as gold nanoparticles (34), nanogel-based vaccine formulations (35), and biodegradable polyanhydride nanoparticles containing PspA have been previously examined (30).

1.5   Pulmonary drug delivery

1.5.1   Lung anatomy and physiology

The respiratory tract comprises the conducting and respiratory airways (Figure 1-4). The lung, weighing about one kilogram, is divided by pleural membranes into lobes; three on the right and two on the left (36). Inhaled air travels through the nose and mouth, passes from the larynx and trachea to 16 generations of conductive bronchi and bronchioles. Alveoli begin to appear from the 17th generation of bronchioles (respiratory airways) and by the 20th generation of airways, the alveoli result in alveolar ducts (36). Blind sacs lined with alveoli known as alveolar sacs become evident at the

23rd generation. Nearly 300 million alveoli are present in the lung and provide a surface area of exchange of 80–90 sq. m (36). On the bronchial surface the submucosal glands and the 'goblet cells' secrete mucus. The mucus lining the conducting airways is transported towards the mouth in accordance with the movement of cilia found on the ciliated columnar cells followed by swallowing of the mucus transported to the mouth.
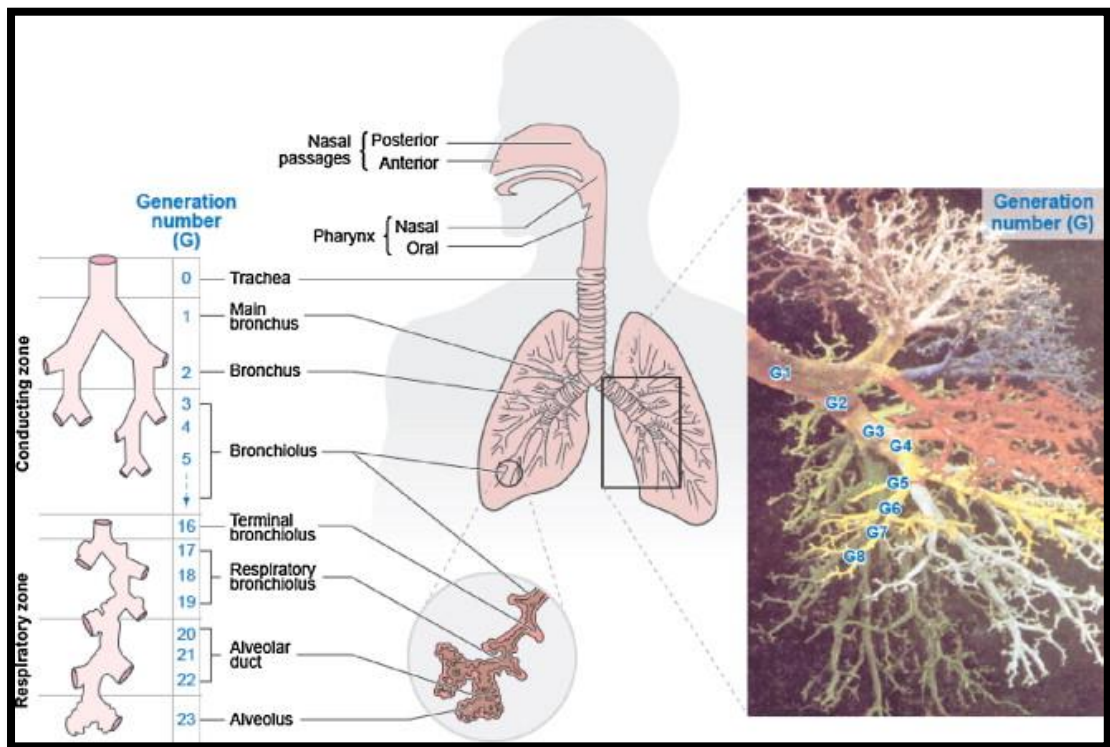
Figure 1-4: Diagram of the human respiratory tract (with permission from (37)).

This movement is primarily responsible for removing any foreign materials that enter the bronchial area (36). The alveoli and the pulmonary capillaries are separated by a barrier consisting of endothelial cells, interstitial space and pneumocytes (pulmonary epithelial cells). The pneumocytes are divided into two types; type I and type II cells. Type I cells are very flat and cover the alveolar surface enhancing the gaseous exchange between the alveoli and blood whereas type II cells are irregularly shaped which produce and secrete surfactants (36; 37).

1.5.2   The lung as a delivery site for drugs

The pulmonary region as a site of drug administration provides many advantages that can be divided into two different categories; one related to the lung and the other related to the drug delivery system. The advantages of the lung include the large surface area of approximately 80 m² available for drug absorption, thin epithelium in the alveolar lung tissue (around 0.1 - 0.5 μm thick), lower enzymatic activity than the gastrointestinal system, and large vascularisation that can enable the efficient systemic delivery of drugs. The advantages of the pulmonary delivery system include: the non-invasive method of delivery and the reduced risk of cross contamination due to the reuse of needles and syringes (38). The reuse of needles is a major obstacle in low middle income countries and global rates of 10.4 – 20.9 million infections per year caused by vulnerable injections were reported, with vaccines representing 5 to 15% of all injections administered (39). Nearly 80 % of infections transmitted by injections are hepatitis B, followed by hepatitis C, while less than 1 % of infections are HIV (39). In addition, such an approach diminishes a serious waste disposal problem and eliminates needle stick injuries, in both patients and healthcare workers. Following a needle stick injury the transmission risk from an infected patient to medical person is estimated as 0.3% for HIV, and 3-10% for hepatitis B. Around 2 million of 35 million medical personal are infected by needle stick injuries (39). Additional benefit applies for patients who need a substitute for needle-based therapy due to fear of injections enhancing patient compliance and leading to improved treatment outcomes (38).

Pulmonary delivery would be useful for mass immunization campaigns when there is an outbreak of a disease that is usually contained by vaccination. In these circumstances, important factors are; speed (the number of vaccinations per unit of time), easy and pain free delivery, no requirement for trained medical personnel and the elimination of cold-chain requirements. Most available vaccine preparations are dependent on the effective

availability of continuous refrigerator storage conditions to maintain vaccine stability. This cold chain requirement presents significant difficulties in the effective performance of immunization campaigns in low middle income countries where a regular and stable supply of electricity and cold-chain storage is often unavailable (39).

In a clinical research study where volunteers could choose between an intranasal virosomal influenza vaccine and an injection formulation, around 97 % choose the nasal vaccine. When they were asked for the reason, 14% answered that they were afraid of injections. This is in agreement with other investigations, where around 10% of the people reported injection phobia (39).

Despite the many advantages, both the lung anatomy and properties of the delivery system present limitations for pulmonary drug administration. An important obstacle for the absorption of inhaled drugs is the thick lung epithelium (around 50 – 60 µm) in the trachea although this decreases in the alveoli to around 0.1 - 0.5 µm (36). Additionally, mucociliary clearance, lung mucus and enzymes such as proteases which degrade macromolecules, act as barriers for the absorption of drugs through the pulmonary region (36).

Moreover, there are some important factors that influence the delivery of drugs through the lung: the patient, the inhalation pattern, and the properties of the aerosol system e.g. the morphology, particle size etc. Deep lung delivery requires the production of particles with an aerodynamic diameter between $1 – 5$ µm. The aerodynamic diameter (d_{ae}) is defined as the diameter of a sphere with a density of 1 g/cm^3 in air characterized by the same velocity in air as that of the particle being examined and represented by the following equation:

$$d_{ae} = d_g \sqrt{\frac{\rho}{\rho_a}} \qquad\qquad \textbf{Equation 1-1}$$

where ρ is the mass density of the particle, ρ_a is the unit density (1 g/cm^3) and d_g is the geometric diameter (36).

1.5.3 Pulmonary delivery of vaccines

The mucosal surface of the respiratory system is the main entrance for airborne pathogens. Many researchers have shown that the induction of systemic immunity by parenteral immunization can clear systemic infections efficiently but is unable to protect the mucosal surface (40). The antibodies produced due to systemic immunity; do not provide mucosal immunity to the mucosal surface, which is the main entry site for airborne pathogens. Thus mucosal immunisation affords the first line defence, through stimulation of the production of the secretory IgA (sIgA) which does not allow the bacterial or viral binding to the mucosal surface so avoids colonisation (41; 42; 43). Several studies examined the development of mucosal vaccine without use of the adjuvant; however the results showed poor immunogenic response. Thus different methods have been used to enhance the mucosal vaccine immunogenic properties, by using adjuvants e.g. polymeric nano/microparticles such as PLGA (44; 45), and chitosan nano/microparticles (46; 47), liposomes (48; 49), and cholera toxin (50; 51).

Also, due to the extensive mucosal surface area available to inhaled particles upon deposition, an efficient system for delivering vaccines in aerosol particle form might enable the delivery of vaccines at lower doses than via the parenteral route (43).

The mucosal immune system in the respiratory tract produces a wide range of protection, as the respiratory tract involves a large network of bronchus-associated lymphoid tissue (BALT); the respiratory part of mucosal-associated lymphoid tissue (MALT), extensive dendritic cells (DCs) network that line the respiratory epithelium in the submucosa and on the alveoli and the macrophages network in the interstitium and on the alveolar surface (52). BALT readily shares antigenic information and are known to induce systemic immunity (42).

MALT epithelial surfaces are occupied with nonciliated macro-fold cells (M cells) which function as antigen-sampling. M cells are responsible for transporting antigens

from mucosal surfaces to the underlying lymphoid tissues (Figure 1-5). Following the antigen getting into the lymphoid tissues, the antigens are up taken and processed by antigen presenting cells (APCs): DCs and macrophages, and presented to B cells and T cells found in the lymphoid tissues. This leads to activation of T-cells which provoke IgG and IgA-committed B-cell maturation in the germinal centre of the MALT. At the end, antigen-specific CD4+ T-cells and activated B-cells will travel through the draining lymph nodes and the thoracic duct to the systemic circulation and other mucosal effector sites, where IgA+ B cell in the presence of interleukin-5 (IL-5) and interleukin-6 (IL-6), secreted by CD-4+ T helper 2 (TH2) cells, differentiate in to IgA producing plasma cells, which develop IgA antibodies. Whereas IgG-committed B-cells, after stimulation by TH2 cells differentiate in to IgG producing plasma cells, which develop IgG antibodies (40).

1.5.4 Dendritic cells

Antigen uptake by DCs induces antigen-specific adaptive immunity (53). The innate immunity (Table 1-1) is an immediate protective response with broad action upon entry of a pathogen. The innate immunity depends on natural defence mechanisms that are applied to rapidly attack the invading pathogen. The innate system consist of epithelial barriers; mucosal membranes; phagocytes (monocytes, macrophages, and neutrophils); complements, natural killer cells; cytokines produced by the phagocytes; and DCs. These constituents promote phagocytosis and lysis of pathogen. The bone-marrow derived DCs with multiple long membranous projections share common characteristic with macrophages, and thus shares an overlapping function of phagocytosis. DCs function as APCs to activate naïve T cells (53; 54).
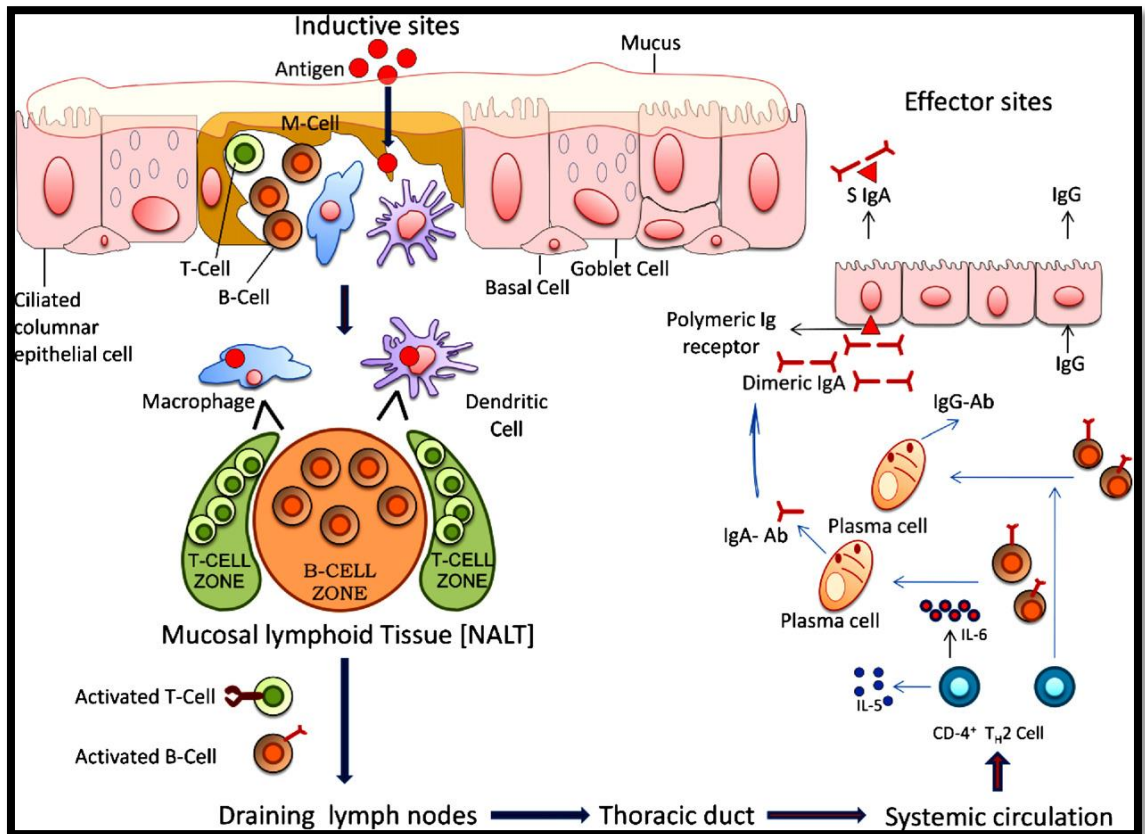
Figure 1-5: Simple scheme illustrates the stimulation of humoral immunity in the bronchus-associated lymphoid tissue (BALT). On the mucosal surface, M-cells transport antigen through sub-mucosa. Followed by antigen processing by DCs and macrophages and presenting to naïve T-cells in the mucosal lymph nodes and induce naïve T-cells. Then, the activated cells stimulate B-cell maturation in the original centre of the BALT. At the end, CD4+ T-cells (specific to the antigen) and stimulated B-cells will travel through the draining lymph nodes and the thoracic duct to the systemic circulation. Then CD-4+ T helper 2 (TH2) cells secrete interleukin-5 (IL-5) and interleukin-6 (IL-6) leading to IgA+ B and IgG+ B cells differentiation in to IgA generating plasma cells which develop IgA antibody and IgG generating plasma cells which develop IgG antibody, respectively (with permission from (54))**.**

Table 1-1: Main components of immune system.

Immunity						
Innate Immunity	•	Complement				
	•	Natural killer				
	•	Autophagy				
	•	Dendritic cells				
	•	Phagocytosis	•	Macrophages		
			•	Neutrophils		
			•	Monocytes		
Adaptive Immunity	•	Humoral	•	B cells	•	Antibodies
					•	Memory cells
	•	Cellular	•	T cells	•	CD4+
					•	CD8+

Antigens entering the body are taken up by immature DCs which develop into mature cells. The DCs uptake, process and present antigen through major histocompatibility complex (MHC) class I and II pathways for identification by the T-cell receptors found on T-cells to start an immune response. This process is known as antigen presentation and typically occurs in the lymph node region (55). It is considered that soon after antigen presentation, the DCs go through apoptosis in the lymph nodes (36).

Once activated, the naïve T cells initiate the adaptive immune response (acquired immunity) (56). Adaptive immunity (Table 1-1) is delayed but highly specific to a pathogen. The adaptive response includes the humoral immunity mediated by B cells, antibodies and complements and cellular immunity mediated by T cells activation. This immune specific response develops an immune memory for that pathogen (57).

Recently it was found that there are approximately five different subsets of DCs in the murine conducting airways; resident DCs, plasmacytoid DCs, alveolar DCs, inflammatory DCs and interferon-producing killer DCs (58). The information available on these subsets of DCs in the human lung is limited due to the problem of obtaining lung tissue, as they cannot be recovered from the bronchoalveolar lavage (BAL) fluid. On the other hand, human alveolar macrophages are extensively studied because they are available in BAL. Immature DCs have a higher antigen presenting cells function but

poor phagocytic function, while the alveolar macrophages are primarily phagocytes and have a lower antigen presenting cell function (36).

The lung region is composed of two main areas: the conducting airways and the lung parenchyma (Figure 1-6). The conducting airways mucosal surface includes ciliated epithelial cells, interspersed goblet cells, macrophages and DCs.

The DCs in this area are mainly made up of myeloid DCs (mDCs), with a small percentage of plasmacytoid DCs (pDCs) (Figure 1-7). These mDCs have a greater ability for antigen uptake but lower potential to provoke the T cells. Furthermore; human DCs are generated from haematopoietic stem cells, mDCs from bone marrow–derived monocyte precursors and pDCs from lymphoid progenitors. The mDCs and pDCs are stimulated by various groups of antigenic stimuli so their activity will be reflected by the expression of various cell surface receptors such as Toll-like receptors (TLRs).

The lung parenchyma includes the lung interstitium, respiratory and terminal bronchioles, and alveoli and is primarily composed of 80% macrophages and 20% DCs and T cells. The 'immature' resident DCs have a high ability to detect, capture and process the encountered antigen (36). Human DCs are recognized by the over expression of human leukocyte antigen (HLA) DR (main histocompatibility complex class II). Furthermore, the specific markers to identify the mDCs involve CD11c+, CD1a+, BDCA-1+, BDCA-3+, HLA-DR+ while for the pDCs they are CD11c−, HLADR+, BDCA-2+ and CD123+ (59; 60).
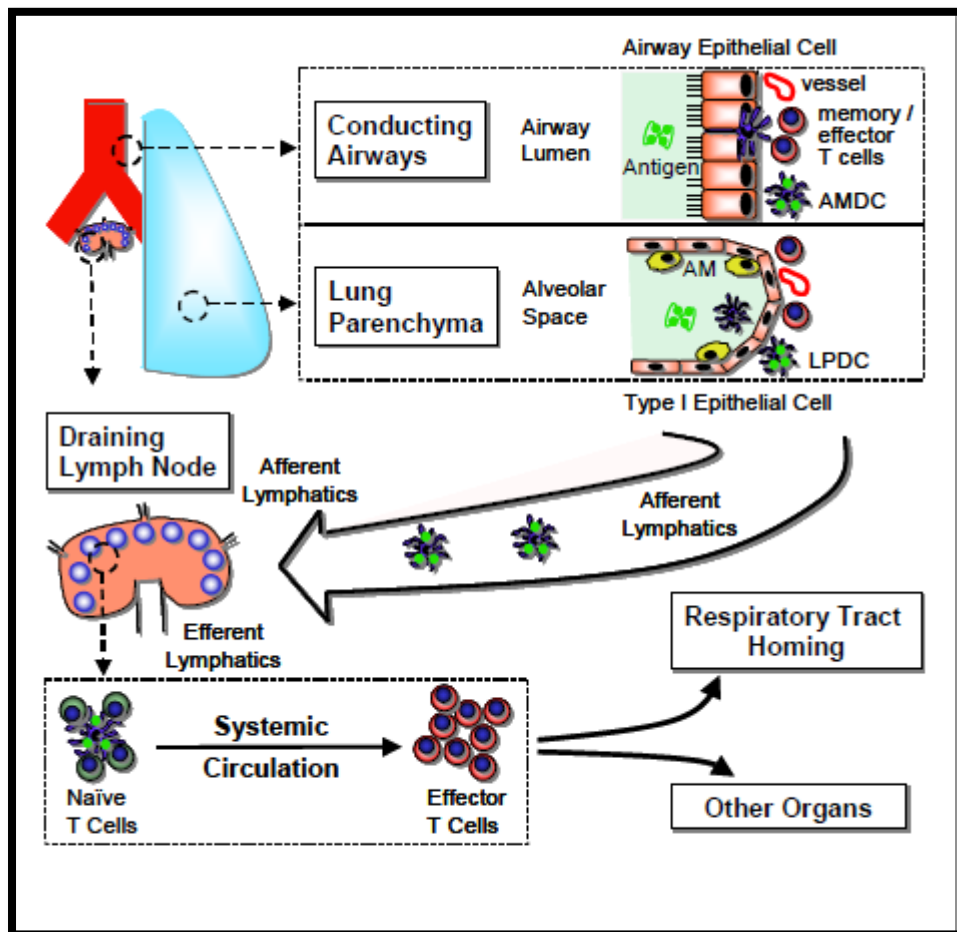
Figure 1-6: Respiratory immune system. AMDC: airway mucosal DCs, LPDC: lung parenchymal DCs (with permission from (59)).
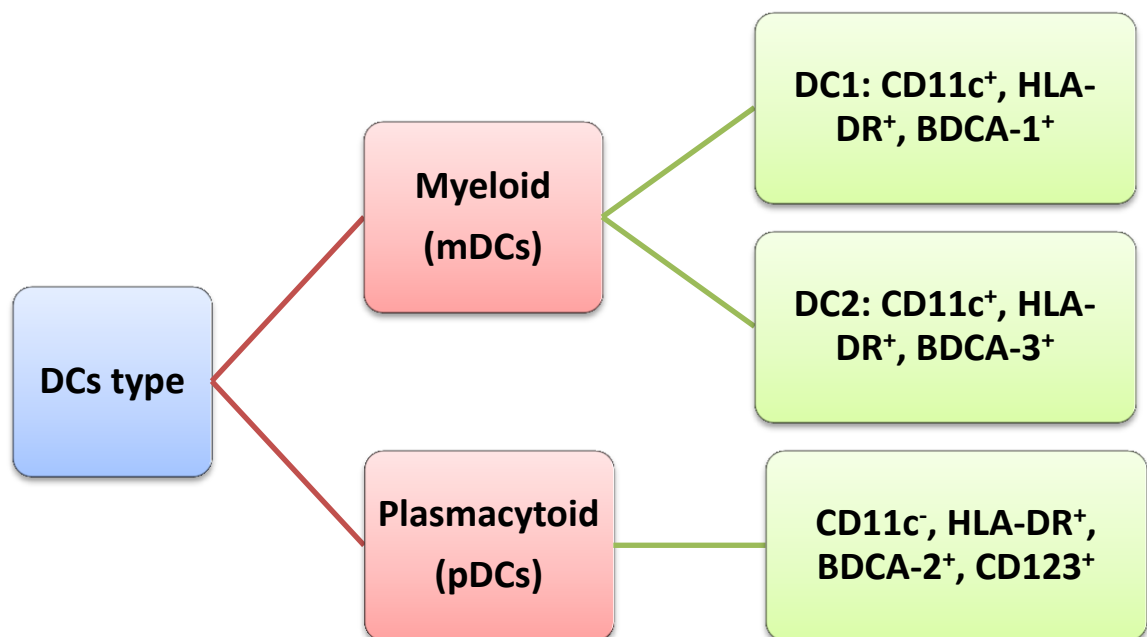
Figure 1-7: Respiratory tract DCs described in the human. BDCA, blood dendritic cell antigen; HLA, human leukocyte antigen.

1.6 Polymers for the pulmonary administration of vaccines

A vaccine delivery system can be defined as a formulation or device that helps with the administration of a vaccine to the patient, enhancing its potency and safety and initiating an immune response as mentioned above (61). A wide range of polymers, both natural and synthetic, have previously been explored for the preparation of biodegradable nano/micro-particles for pulmonary vaccine delivery. Natural polymers e.g. albumin, cyclodextrin, collagen, gelatin, chitosan, and alginate; and synthetic polymers e.g. polyacrylates, polyanhydrides, and polyesters such as poly (lactic acid-co-glycolic acid) (PLGA) and poly (L-lactic acid) (PLA) have been utilized for the formulation of biodegradable delivery systems (Table 1-2).

Table 1-2: Some examples of polymer for pulmonary vaccine delivery.

Type of polymer	Examples	Advantages	Disadvantages
Natural	Albumin, cyclodextrin, collagen, gelatin, chitosan, and alginate	Biocompatible, low cost, high aqueous solubility and comparatively short duration of drug release.	Presence of extraneous contaminants, batch variability, low hydrophobicity (40).
Synthetic	polyacrylates, polyanhydrides, and polyesters such as PLGA and PLA	Reproducible, controlled molecular weight, copolymer composition, and degradation rate.	Limited solubility (40).

Natural polymers generally have a relatively rapid release of therapeutic agent while the main characteristic of synthetic polymers is the ability to render sustained release of the active ingredient for a long period e.g. days to several weeks and can also modify the degradation rate based on molecular weight and polymer composition. Much research has been carried out to assess the potential of antigen-encapsulated microparticles for the preparation of a single dose vaccine through sustained release of the antigen avoiding the requirement for a booster dose. This would be advantageous in low and

middle income countries, where access to healthcare facilities and infrastructure can be difficult (61).

The polyester, PLGA is one of the most extensively explored polymers for drug delivery due to the FDA approval of different products that are commercially available in different grades and ratios of lactic and glycolic acid. However, PLGA hydrolysis results in the accumulation of acidic monomers, lactic and glycolic acids, thereby leading to a significant decrease in the pH of the environment and denaturation of the encapsulated proteins and local inflammation (22).

In recent years, advances in polymer chemistry have led to the development of various novel biodegradable polymers as alternatives to PLGA (62). Here at Liverpool John Moores University poly (glycerol adipate-co-ω-pentadecalactone, PGA-co-PDL) has been developed as a novel delivery system (62).

PGA-co-PDL (Figure 1-8) can be synthesized via the lipase, *Candida antarctica,* catalyzed combined condensation and ring opening copolymerization of activated diacid, glycerol and lactone monomers (63).
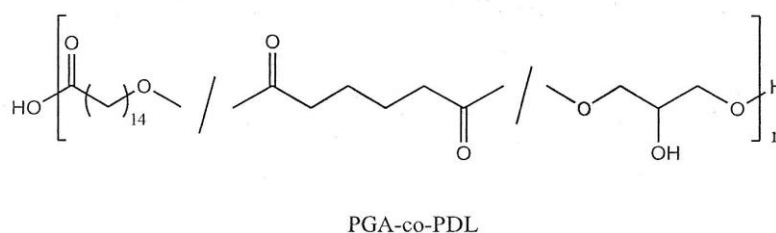
PGA-co-PDL

Figure 1-8: Chemical structure of PGA-co-PDL.

This enzyme catalysed polymerization reaction exploits the regioselectivity of this lipase for primary hydroxyl groups offering protection of the secondary glycerol hydroxyl group that would otherwise react during the polymerization reaction. Although it is possible to synthesise this polymer chemically useing protecting groups this would involve more synthetic steps and probably lead to hydrolysis of the polymer backbone

(62). Also, the enzymatic method does not require the toxic chemical or metal catalysts used in conventional chemical synthesis.

PGA-co-PDL is expected to degrade through hydrolysis of ester bonds which will release adipic acid which is less acidic than glycolic acid and lactic acid produced by hydrolysis of PGLA. PGA-co-PDL has a similar but more disordered structure than poly-ε-caprolactone (PCL, semi-crystalline polymer) due to the randomly nature of polymerisation. Thompson *et al.* revealed that PGA-co-PDL was made from a random mixture of diacid, glycerol and lactone monomers by using ^{13}C NMR hence PGA-co-PDL should degrade quicker than PCL (62). Moreover, the presence of the pendant hydroxyl group enables the covalent attachment of moieties to the polymer backbone to modify the polymer physical and chemical characteristics (64).

This polymer has been investigated by our group for the delivery of small molecules e.g. dexamethasone phosphate (63), model drugs e.g. ibuprofen (65) and sodium fluorescein (66), and macromolecules e.g. α-chymotrypsin (64), and DNase I (67).

Another study proposed that PGA-co-PDL microparticles could be considered as carriers for pulmonary delivery. The results showed a good aerosol performance of PGA-co-PDL microparticles with fine particle fraction (%FPF) of 43.38±5.61% and mass median aerodynamic diameter (MMAD) 3.43±0.58 μm. Also, the toxicity studies at 5 mg/ml using human bronchial epithelial 16HBE14o- cell lines demonstrating the safety of PGA-co-PDL microparticles (85.57±5.44 % cell viability) compared to PLGA microparticles (60.66±6.75 % cell viability) after 72 h treatment (66). These results indicated that PGA-co-PDL could be a promising pulmonary drug delivery system affording a protective matrix and faster release of drug in a short period of time in comparison with PLGA (66). More recently we have developed PGA-co-PDL nanoparticles (NPs) for delivery of a model protein, bovine serum albumin (BSA) (68). The aerosolisation studies showed a good aerosolisation performance and deep lung

deposition with FPF% of 76.95±5.61% and MMAD of 1.21±0.67 μm. The structure stability and integrity studies using SDS-PAGE and CD confirmed the primary and secondary structure of the released BSA. These results indicate that PGA-co-PDL NPs may be a promising carrier for pulmonary protein delivery (68).

1.6.1 Nanoparticles for pulmonary administration of vaccine

Nanoparticles are particles with diameters size in range of 1 to 1000 nm (62; 69). Polymeric NPs can improve the immune response by an adjuvant-like effect (40). When the antigen is encapsulated in NPs it is modified to a particulate pattern and this form can be more antigenic than the soluble antigen form due to the fact that these particulate forms have similar dimensions to pathogen to which the immune system structured to fight (40; 61). This particulate delivery of antigen will enhance DCs uptake and consequently antigen transfer to lymph node and so induce immune response (61). Most likely, the particulate antigen delivered to the lower respiratory tract area prevents the rapid clearance by alveolar macrophages and thereby enhances uptake by the epithelial M cells on mucosal surface. These cells, as a component of BALT, sample the environment for antigens and share antigenic information with DCs found in lymphoid tissue and induces secretory local IgA production. The NPs may then be transported to secondary lymph-nodes where they enhance induction of the systemic immune response (43).

Another approach to enhance immune response (adjuvant-like effect) is to use chitosan or chitosan derivatives to prepare or to modify the surface of the NPs encapsulating antigen. Vila *et. al.* studied the use of low molecular weight chitosan (23 and 38 kDa) in preparation of NPs as nasal delivery system for vaccine using tetanus toxoid as a model antigen. The NPs sizes were in the 350 nm with a positive charge (+40 mV). These NPs were administered via intranasal route and produced higher and long-term IgG titres (humoral immune response) in comparison with the antigen solution. Moreover, the IgA

titres (mucosal immune response) after 6 months following administration of NPs was significantly more than that resulted after the antigen solution administration (70).

Sayın *et. al*. prepared tetanus toxoid loaded NPs using *N*-trimethyl chitosan and mono-*N*-carboxymethyl chitosan for mucosal vaccination. The particle size range was 40–400 nm, and a negative surface charge for mono-*N*-carboxymethyl chitosan and positive surface charge for *N*-trimethyl chitosan and high loading efficacy >90 %. Immunity studies showed an increased in immune responses in Balb/c mice after intranasal administration of NPs. *N*-trimethyl chitosan NPs with positive surface charge produced high level of serum IgG titres in comparison with mono-*N*-carboxymethyl chitosan NPs with negative surface charge (71). Pawar *et. al.* developed hepatitis B surface antigen loaded PLGA microparticles coated by chitosan or trimethyl chitosan. Following intranasal administration of coated PLGA microparticles to mice showed a higher anti-HBsAg titer when compared to uncoated PLGA microparticles (72).

Table 1-3 shows some recent research on polymeric based particles for pulmonary vaccine delivery.

Table 1-3: Recent research (non-exhaustive list) on polymeric nanoparticles based pulmonary vaccine delivery.

Polymer	Antigen	Reference
Poly(D,L-lactide) (PLA)	Hepatitis B surface antigen	(73)
Poly(D,L-lactide-co-glycolide) (PLGA)	Hepatitis B surface antigen	(73)
N-Trimethyl chitosan (TMC)	Diphtheria toxoid	(52)
poly(lactic-co-glycolic acid) (PLGA)/polyethylene glycol (PEG)	Recombinant hepatitis B surface antigen	(74)
Chitosan	DNA (tuberculosis)	(75)
Poly-L-lactide (PLA)	*Yersinia pestis* F1 and V subunit	(76)

1.6.2 Preparation of nanoparticles

Protein and peptide encapsulation in NPs has been achieved by various methods such as emulsion solvent evaporation, salting out, and solvent displacement/solvent diffusion. Each method of protein encapsulation has its own advantages and disadvantages and each protein or peptide requires its own specific conditions depending on stability, solubilisation, controlled release, and elimination. The method of encapsulation is therefore entirely based on the physicochemical activity of the protein and its intended application (77).

1.6.2.1 Emulsification/Solvent Evaporation/extraction

Water-oil-water (w/o/w) double emulsion techniques (Figure 1-9.A) have been commonly applied as parameters such as particle size and drug loading can be controlled by varying the type, viscosity and amount of organic and aqueous phases, stir rate and temperature which can easily be adjusted (78). This method is best suited to encapsulate water soluble drugs such as peptides, proteins, and vaccines, unlike the o/w method which is better for water-insoluble drugs like steroids (79). In the double emulsion method an aqueous solution of the active ingredient is dispersed in an organic phase containing polymer (e.g. PLGA in dichloromethane) to form the first w/o emulsion. This emulsion is then dispersed in a large volume of water containing an emulsifier/stabiliser such as poly (vinyl alcohol), PVA, to form the w/o/w emulsion. The dispersion is performed using a homogenizer, high pressure homogenizer or ultrasound (22). The emulsion is then subjected to solvent removal by extraction or evaporation processes (80). With the solvent extraction method, the double emulsion is added to a large amount of water or an aqueous cosolvent, (e.g. acetone in an aqueous solution).
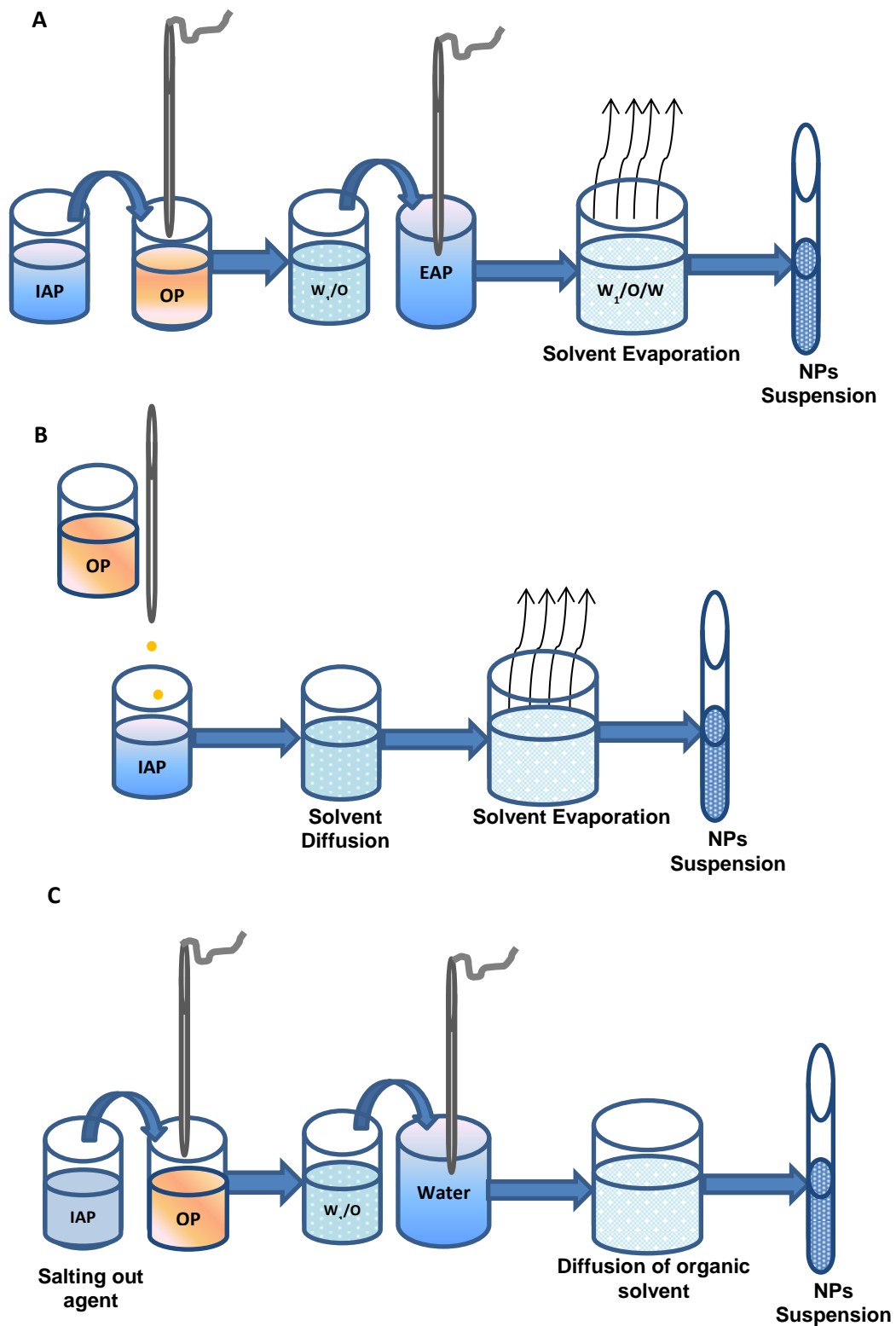
Figure 1-9: Methods of preparation of nano/microparticles: **(A)** emulsification/solvent evaporation method, **(B)** emulsification and solvent diffusion method and **(C)** salting out method.

One disadvantage of the double emulsion method is the removal of the solvent from the emulsion during which the water/oil (w/o) emulsion droplets are exposed to a large amount of water and this may lead to lower antigen loading and encapsulation efficiency, and an initial burst release. During solvent removal from the emulsion, antigen molecules can diffuse out from the emulsion into the aqueous solution and can also accumulate on the surface of particles, as they become hardened, leading to a high initial burst release (78). Additionally, the antigen is exposed to a harsh environment at the interface between the aqueous and organic phases and the high shear force during nanoparticle formulation (61). To improve protein stability and integrity stabilizers such as carrier proteins (e.g., albumin), surfactants or molecules such as trehalose and mannitol can also be added to the aqueous phase (22).

Singh *et al.* produced poly-(ε-caprolactone) (PCL) NPs loaded with diphtheria toxoid using a double emulsion solvent evaporation method to study their use as a mucosal vaccine delivery system. The internal aqueous phase containing diphtheria toxoid and 0.25 ml 10%w/v polyvinyl alcohol (PVA) was emulsified with the organic phase (100 mg of PCL in 5 mL of dichloromethane), by homogenization at 12,000 rpm for 2 min. This w/o emulsion was added to a 25ml of 1.25% w/v PVA solution, and then homogenised for 5min at 12,000 rpm. The preparations were then stirred magnetically at room temperature for 18 h to allow solvent evaporation and NPs formation. The NPs produced were approximately 267±3 nm in size and preserved diphtheria toxoid integrity as confirmed by sodium dodecyl sulfate poly (acrylamide) gel electrophoresis (SDS-PAGE) study (81).

1.6.2.2 Emulsification/Solvent Diffusion

In the solvent diffusion (solvent displacement) technique (Figure 1-9.B), the polymer and protein are dissolved in a partially water soluble solvent and then saturated with water with strong stirring. Then the polymer–water saturated solvent phase is emulsified

in an aqueous solution containing a stabilizer, leading to solvent diffusion to the external phase and elimination by evaporation leading to the production of NPs (77). This technique is simple, provides high encapsulation efficiency without homogenization, has high batch to batch reproducibility, is easy to scale up, and produces a narrow size distribution of protein NPs (77).

The problem of protein hydration and the presence of hydrophobic interfaces resulted in protein irreversible aggregation inside the NPs. These problems can be solved by the addition of stabilizers such as PEO (77). BSA and immune-γ-globulin (IgG) encapsulated in polyethylene oxide- PLGA (PEO–PLGA) using this technique showed high encapsulation efficiency (58.9%) and a slow rate of *in vitro* release (77).

1.6.2.3 Salting out

In the salting out technique (Figure 1-9.C) the polymer is solubilised in a water miscible organic solvent (e.g. tetrahydrofuran) then this solution is added to an aqueous solution containing salting out agents (e.g. magnesium chloride and stabilizer) under continuous stirring leading to the formation of primary emulsion. Dilution of the primary emulsion through addition of a large quantity of water under mild stirring leads to a reduction in salt concentration and promotes the diffusion of the organic solvent into the aqueous phase leading to the formation of NPs. Finally the NPs formed are isolated from the salting out agents either by centrifugation or cross-flow filtration. The major benefit of the salting out method is that it reduces protein unfolding and inactivation (77). The main disadvantages of the salting out method are the removal of the salting out agent and possible interactions between the salting out agents and drugs (36). Konnan *et al.* fabricated NPs by a salting out technique. The organic phase containing PLGA and PLA in THF was emulsified with an aqueous solution of PVA and a salting out agent (magnesium chloride hexahydrate) by mechanical stirring. A large volume of water was added to the o/w emulsion leading to diffusion of the water-miscible organic solvent

into the aqueous solution forming NPs with particle size ranging from 102 to 200 nm (82).

1.6.3 Factors affecting uptake of nanoparticles by dendritic cells

To achieve an optimum immune response upon administration of particulate antigens through the pulmonary mucosal route, it is essential to optimize the particles for size, surface charge and hydrophobicity. These parameters can also influence differential uptake by DCs, which play an important role in developing the immune response (73).

1.6.3.1 Hydrophobicity

The hydrophobicity of NPs can make a difference in the cellular uptake because more hydrophobic NPs have a tendency to adsorb more to the cell surface compared to their hydrophilic counterparts, perhaps because of enhanced nonspecific interaction with the hydrophobic cell surface (83).

Thomas *et al* prepared porous poly (L-lactic acid) (PLA) and PLGA NPs for pulmonary delivery of hepatitis B vaccine. They investigated the effects of particle size and hydrophobicity on mucosal and cell-mediated immune response. Hydrophobic NPs larger than 500 nm evoked a stronger increase in secretory IgA, interleukin-2 and interferon-γ levels in comparison with hydrophilic NPs less than 500 nm (73).

Researchers have demonstrated that particles formulated using hydrophobic polymers are more prone to phagocytosis than hydrophilic polymers (84; 85). For example, particles prepared from poly-(ε-caprolactone), which is more hydrophobic than PLGA, are removed by phagocytosis more efficiently and generate a stronger immune response to diptheria toxoid (81). However, there are many reports that shows the PLGA with a hydrophilic surface are promptly taken up by the dendritic cells (55; 86).

1.6.3.2 Surface charge

The surface charge of the particles plays an important role in generating an immune response. Cationic particles are effectively taken up by DCs. The ionic interaction

between the positive charge on the particles surface and the negative charge on the cell surface generates a successful bond and promotes particle uptake (87). Thomas *et al* have shown that cationic PLGA microspheres containing HBsAg significantly enhanced the mucosal and cell mediated immune response in comparison with PLGA microspheres (88). Modifying PLGA microspheres with chitosan resulted in an increase in mucosal residence time and enhanced immunogenicity (41).

Chitosan nanoparticles with encapsulated DNA plasmid encoding eight T-cell epitopes from *M. tuberculosis* were administered intratracheally to the lungs of mice and induced the maturation of DCs, increased levels of IFN-γ secretion in comparison with DNA plasmid solution alone (75). The exact mechanism of action of chitosan is unclear and may be attributed to mucoadhesive characteristics, increased cell penetration, enhanced cell interaction and immune-modulating responses (39).

1.6.3.3 Particle size

There are contradictory studies on the effect of particle size on the initiation of immune responses. Some reports demonstrate that particles of about 5 μm can efficiently initiate an immune response after mucosal administration; on the other hand other reports revealed that particles of about 1 μm are taken up by antigen presenting cells more efficiently than 500 and 200 nm size particles resulting in a stronger immune response (73). In conflict to these studies, others showed that particles of about 500 nm or less were optimal for DCs uptake compared to particles of 1- 5 μm in size (89).

DCs and macrophages are able to take up any particles of a similar size to the pathogens (up to 10 μm) so it is expected that both micro and nano particles can be easily taken up by both cells. However, to target vaccine antigens to DCs, NPs are preferred over microparticles. This restricted level of particle uptake by DCs in comparison with macrophages has been attributed to the different functions that these two cell types have for immune response. The macrophages remove foreign particles efficiently leading to

clearance while DCs are responsible for antigen take-up to an extent that is necessary to induce an immune response (89). Some research has demonstrated that DCs more efficiently take up small particles of a size similar to the viral size (around 20-200 nm), while macrophages phagocytose larger bacterial sized particles. There is an inverted relationship between particle size and the ability of uptake by DCs that could be attributed to the large surface area of the nanoparticles which promote rapid degradation and faster release of the encapsulated antigens within the cells. Moreover, the large surface area promotes higher protein loading through adsorption (87).

Recently Foged *et al.* demonstrated that particle size, surface charge, shape, and composition of the substance to be delivered all have a major function in controlling particle uptake by human DCs. Moreover, it was resolved that for the highest uptake by DCs the desired particle size was 0.5 μm (diameter). Large particles (> 1 μm) uptake was highly promoted when they showed a positive surface charge (89). Furthermore, Manolova *et al.* showed that upon intracutaneous injection of polystyrene beads of different sizes, the large particles (500–2000 nm) connected with DCs from the site of administration and relied extensively on them for cellular transport, while small particles (20–200 nm) and virus-like particles (30 nm) were transported freely to the lymph nodes and were present in lymph nodes resident DCs (90).

1.6.4 Technical concerns of nanoparticle pulmonary delivery

NPs do not deposit efficiently in the lungs leading to the exhalation of the majority of the inhaled dose (91). Particulate systems incorporating NPs into micron-scale structures have been developed to solve the problem of delivering NPs to the lungs; such as embedding NPs within an inert 'microcarrier', porous nanoparticle-aggregate particles (PNAPs), agglomerated NPs (91) and nanocomposite microparticles (NCMPs) (92) as a dry powder. These systems are designed to dissolute in the lung lining fluid,

releasing the NPs from the inert carrier (93). The methods of preparation and administration of dry powder formulations are described below in more details.

1.7 Methods of preparation of dry powder for inhalation

1.7.1 Freeze drying

Freeze drying (or lyophilisation) involves first freezing the sample then removing the water via sublimation under vacuum. The drawbacks of this method are; slow processing, expense and the production of stresses on the antigen through the freezing and drying phases (36). The presence of a stabilizer is essential to protect the active ingredient, avoid agglomeration and to confirm suitable reconstitution ability. Carbohydrates such as sucrose, mannitol, dextran or lactose alone, or in presence of surfactants e.g. poloxamer 188 or polyvinyl alcohol are often added as stabilizers to protect the active ingredient and avoid coalescence. The ratio of nanoparticles to sugar acts as a determining factor in the stability and long term storage of the final form. Research on long term stability of these particles demonstrated that the use of cryoprotective agents during freeze drying decreased the particle growth in comparison with non cryoprotective preparations. For example, formulations freeze-dried in the presence of sucrose and trehalose at 2% and 3% w/v had more controlled particle size and performed better than when mannitol was used at the same concentrations (36). However, freeze drying is technically time consuming and expensive for macromolecules (94).

1.7.2 Spray drying

Spray drying is a one-step technique which transforms liquid formulations to a dried form. The liquid formulation can be a suspension or an emulsion that is atomized to a spray form and passed through hot air leading to the rapid evaporation of the solvent to produce dried particles. The dried particles are then separated from the gas by means of a cyclone (95). The characteristics of the particles produced rely on the type of feed

(e.g. suspension or emulsion) as well as the spray drying parameters such as solid concentration, solvent type and composition, solution feed rate, inlet temperature, gas type and flow rate, etc. (78).

For pulmonary drug delivery the main advantages of using spray drying is the possibility to manage and alter the different parameters mentioned above. This results in optimization of dry powder properties such as size, morphology and density, as well as macroscopic powder characteristics such as bulk density, flowability and dispersibility. Furthermore, spray dryers can be easily scaled up for industrial production (95). However, high inlet temperature, separation of final powder and particles loss in lab-scale spray -dryers are disadvantageous. The spray drying technique was previously applied to prepare microparticles loaded with insulin, tetanus toxoid (TT), recombinant human erythropoietin (rhEPO), and BSA (78).

1.7.3 Spray freeze drying

The spray-freezedrying method includes spraying an aqueous solution of drug into a spray chamber containing a cryogenic liquid (such as liquid nitrogen) leading to formation of frozen droplets which are then lyophilized to form porous dry powder particles suitable for inhalation. The main advantage of the spray-freeze-drying method is the ability to produce particles with controllable sizes and, as it is carried out at sub-ambient temperature, heat sensitive polymers and highly potent macromolecules can be formulated into dry powder preparations. The main disadvantage of this method is the stresses due to freezing and drying, which may lead to irreversible damage to proteins. This is indicated as structural denaturation, aggregation and loss of biological activity upon reconstitution. Furthermore, loss of stability due to unfolding and aggregation still present a main challenge and also it is time consuming, and expensive (95).

Amorij *et al.* demonstrated that an influenza subunit vaccine powder prepared by spray-freeze-drying using oligosaccharide inulin as a stabilizer and administered through the

lung to BALB/c mice stimulated systemic humoral (IgG), cell-mediated (Il-4, IFN-γ) and mucosal immune responses (IgA, IgG). While vaccination with a solution subunit vaccine through the pulmonary or intramuscular route only lead to systemic humoral (IgG) immune responses concluding that powder vaccine preparations could be advantageous for immunization (96).

1.7.4 Supercritical fluid

Supercritical fluids (SCF) are compressed gases or liquids above their critical temperatures (Tc) and pressures (Pc), and have many advantages of both gases and liquids. The solvating power and density can be managed by changing the pressure and temperature. Commonly used SCF include carbon dioxide (CO_2), acetone, propane, nitrous oxide (N_2O), chlorodifluoromethane, propane, water, diethyl ether, or mixture. In addition to its low cost and non-toxicity supercritical CO_2 is the most widely used SCF because of its accessible critical point at 31°C and 74 bar makes it suitable for processing thermolabile solutes as an alternative to conventional organic solvents. There are two main fundamental processes for particle drying with SCF. The first uses SCF as a solvent and the other as an antisolvent. In the first process, the drug is dissolved in the SCF, suddenly decompressed and then the solution is moved through an opening and rapidly expanded at low pressure. Rapid Expansion of a Supercritical Solution (RESS) applies with this concept. In the second type of process, the solute is insoluble in SCF so it utilizes SCF as an antisolvent. A solute is solubilised in an organic solvent followed by absorption of the SCF by the organic solvent. The liquid phase then expands and the solvation power decreased leading to particle formation. The following are processes that employ this second principle. Gas Anti-Solvent (GAS), Aerosol Solvent Extraction System (ASES), Supercritical Fluid Antisolvent (SAS), Precipitation with Compressed Antisolvent (PCA), Solution Enhanced Dispersion by Supercritical Fluids (SEDS), and supercritical fluid extraction of emulsion (SFEE). By applying these

methods the particles can be formulated with the desired shape and size and any drawbacks on the macromolecules can be decreased. A comprehensive discussion of these methods has recently been published (94).

The dry particulate prepared by SCF techniques are often less charged than those prepared mechanically making them flow more easily and thus more freely dispensed from a DPI. Moreover, SCF techniques allow the preparation of inhalable powder that are more uniform in terms of particle-size, distribution, crystallinity and morphology than those prepared by jet milling. Regardless of its ability, SCF is still considered as a rising technology that is still to be fully explored for DPI preparations; with increased concerns about the possibility of the denaturing effects of the solvents/antisolvents used in this technique (36; 94).

Amidi *et al.* prepared diphtheria toxoid containing microparticles by a SCF spraying process, resulting in dry powder microparticles with a median volume diameter between 2 and 3 μm. Immunization of guinea pigs with diphtheria toxoid -N-Trimethyl chitosan microparticles via the pulmonary route lead to a strong immune response as showed by the induction of IgM, IgG, IgG1 and IgG2 antibodies comparable to or significantly higher than those obtained with subcutaneous administration of alum-adsorbed diphtheria toxoid showing an effective pulmonary delivery system of diphtheria toxoid antigen (52).

1.8   Aerosol as a delivery system for pulmonary vaccine

Inhalation devices can be divided into three different categories: the nebulizer, the pressurized metered dose inhaler (MDIs), and the dry powder inhaler (DPIs).

1.8.1   Nebulizer

There are two major types of nebulizers: jet nebulizers and ultrasonic nebulizers. The jet nebulizer uses the movement of compressed air or oxygen through a narrow opening, leading to a low pressure area next to a liquid feed tube which results in pulling up the

drug solution from the fluid reservoir and splitting it into droplets in the gas stream. The ultrasonic nebulizer uses a piezoelectric crystal vibrating at a high frequency to generate a fountain of liquid in the nebulizer chamber (97). Nebulization provides a constant output with minimum patient skills, large dose can be delivered, and disposable nebulizers are cheap (98).

Pulmonary vaccination research has been carried out using nebulization of live, attenuated organisms such as tularemia, measles, attenuated *Mycobacterium bovis* in Bacille Calmette-Guérin (BCG), and rubella. However there is a potency loss obstacle as demonstrated when complex molecules broke down due to the shear force of the jet nebulizer. For example, a measles vaccine experienced about a 71 % loss of potency after nebulization (98). Nebulization has many drawbacks; it is bulky, requires large volumes of clean water and an electricity supply, has a long-time of administration, is expensive, has poor efficiency, has low reproducibility, high risk of bacterial contamination, needs continuous cleaning, and sometimes requires the use of compressor or gas cylinder which are impractical in low and middle income countries and in vaccine campaigns (95).

1.8.2 Pressurized-meter dose inhaler

In pMDIs, the drug formulation is either suspended or dissolved under pressure in a liquefied propellant in a canister provided with a valve to measure accurate doses and a positioner (95). Few vaccines have been administered using pMDIs. The main reason being the use of a hydrophobic propellant is too harsh for most antigens. Brown *et al*. administered *Streptococcus suis* bacteria into the lung of swine using liquefied dimethylether as propellant and only approximately 30-50 % of antigenicity in the respirable bacteria was preserved (98).

1.8.3 Dry powder inhaler

Dry powder inhalers (DPIs) are cheap, simple, efficient, compact and disposable devices for single dose delivery and hence are ideal devices for antigen delivery. Most antigens are macromolecules (e.g. proteins, peptides, and polysaccharides) and are highly susceptible to chemical and physical degradation in liquid preparations. Administration of macromolecules as dry powder aerosols through the pulmonary route has been widely studied as a promising non-parenteral route for drug delivery that affords enhanced stability in comparison with traditional liquid dosage form. Proteins stability can also be enhanced by preparing them in a dry, solid state with excipients such as lactose, inulin and L-leucine (99; 100). The excipient that is approved by FDA for dry powder inhalation is lactose (98; 101). Recently, D-mannitol is available in the form of pulmonary diagnostic DPIs as Aridol[TM] which approved by US food and drug administration office and in the form of DPIs for the treatment of cystic fibrosis and chronic bronchitis as Bronchitol[TM] which aapproved by approved European regulatory committee (102). Many studies demonstrated the stability of measles vaccine without refrigeration when prepared as dry powder formulations (103; 104). Furthermore, DPIs can reach larger deposition efficiency, do not require an external driving force, and can be utilized by patients more simply than liquid formulations. Also DPIs vaccines can overcome the need of the cold chain which is a necessity for liquid vaccine preparations making the shipping and handling of the vaccine cheap and easier (38). However, this type would not be suitable for infant and children less than 4 years old due to the difficulty in reliable control of breathing pattern in this group (105).

The possibility of using dry powder aerosol vaccines has previously been investigated. Influenza subunit vaccines formulated as dry powder using spray-freeze-drying were revealed to induce superior systemic and mucosal humoral and cell-mediated immune responses in mice when administered via the pulmonary route in comparison with liquid

vaccines delivered by the pulmonary or the intramuscular route (96). The efficiency of spray-dried NPs administered by inhalation of Bacille Calmette-Gue´rin (BCG) in inducing immunity against Mycobacterium tuberculosis has been studied in guinea pigs, and specific immune responses have been shown in macaques after aerosol delivery of a measles vaccine (106).

Lu *et. al.* prepared recombinant antigen 85B protein-PLGA microparticles as dry powder in respirable size to be administered to the guinea pig via inhalation in single or multiple doses of homologous and heterologous antigens to protect against tuberculosis. A single dose of Bacille Calmette–Guérin (BCG) administered subcutaneously was applied as the positive control and as part of immunisation plans. Immunized guinea pigs were challenged with a low-dose aerosol of *Mycobacterium tuberculosis* H37Rv to evaluate the amount of protection assessed as decrease in bacterial burden (CFU) in the lungs and spleens of animals. Histopathological evaluation and morphometric assessment of these tissues were also carried out. The heterologous strategy of BCG prime–Ag85B PLGA microparticles aerosol boosts showed enhanced protection against bacterial infection, as identified by a decrease in bacterial burden CFU in both the lungs and spleens of treated animals compared with untreated. However, there was no statistical difference in the bacterial burdens data between the BCG and BCG-BCG groups. The histopathological and morphometric evaluation of lung and spleen tissue showed the positive effect of BCG prime–Ag85B PLGA vaccination by evaluating a smaller area of tissue affected and number and size of granulomas noticed in the tissues of guinea pigs vaccinated via the lung. Hence, it was concluded that direct vaccination via the lung by these microparticles improved the protection provided by primary immunization with BCG against tuberculosis in guinea pigs. Due to the fact that a substantial percentage of the people around the world have been vaccinated with BCG

in early childhood, a boosting dose with aerosol may be a potential method to augment and extend the immunity due to BCG-immunisation (107).

Recently, Agarkhedkar *et al.* carried out Phase I clinical study to examine the safety and immune responses of measles vaccine dry powder for inhalation. The study included three groups: the first group treated with measles vaccine dry powder using Puffhaler®, the second group treated with measles vaccine dry powder using Solovent^{TM}, and the third group treated using the licensed subcutaneous measles vaccine. The results showed a good safety and immunogenicity profile of measles vaccine dry powder using Puffhaler® and Solovent^{TM} in comparison with subcutaneous measles vaccine (108).

Moreover, it has been indicated that dry particulate antigens, in comparison with solubilized antigens, are taken up more efficiently by APCs, leading to a strong immune response (99).

Saluja *et al* also demonstrated immunization through the pulmonary route using dry powder inhalation leading to a strong immune response in comparison with conventional liquid preparation administered intramuscularly or via the pulmonary route (38).

The formulation of vaccines as dry powder for inhalation seems to be a promising new method to vaccination.

1.9   Thesis hypothesis

Dry powder inhaler aerosols of a pneumococcal protein PspA4Pro, encapsulated within nanocomposite microparticles, as a vaccine for deep lung delivery.

1.10   Thesis Aim and objectives

To design, formulate and characterise nanocomposite microparticles encapsulating pneumococcal protein PspA4Pro as a vaccine for the prevention of pneumococcal disease by dry powder pulmonary delivery.

To obtain the aim of the thesis a systematic study was designed considering the following objectives:

1) Optimisation of PGA-co-PDL NPs prepared by double emulsion solvent evaporation technique.

a. Optimisation of NPs in term of size and protein loading using factorial design.

b. Investigate the effect of chitosan hydrochloride adsorption on NPs regarding particle size and charge.

c. A study of NPs *in vitro* cell toxicity and DCs uptake.

d. Application of the optimum NPs preparation parameters for PspA4pro encapsulation.

2) Incorporation of optimum NPs into micron-scale structures NCMPs via spray drying with L-leucine as microcarrier.

a. Optimisation of NCMPs formulations in term of morphology and yield%.

b. A study of the *in vitro* aerosolisation behaviour, *in vitro* release and cell toxicity.

c. Evaluation of the stability and integrity of protein released from optimum formulations and an investigation of relative antigenicity of released PspA4pro.

2.Materials and Methods

2. Materials and methods

2.1. Materials

Material and Properties	Source
Glycerol	Sigma-Aldrich, UK
ω-pentadecalactone (PDL)	
Myo-Inositol ≥99%	
3-(4,5-dimethylthiazol-2-yl)-2,5-diphenyltetrazolium bromide (MTT)	
Dichloromethane (DCM)	
RPMI-1640 medium with L-glutamine and sodium hydrogen carbonate ($NaHCO_3$)	
antibiotic/antimycotic solution (100x)	
Glycine	
Sodium dodecyl sulfate (SDS)	
Tris hydrochloride	
Sodium chloride	
Albumin tagged with fluorescein isothiocyanate (FITC-BSA)	
Alkaline phosphate yellow liquid substrate, number P7998	
Divinyl adipate (DVA)	Fluorochem, UK
Lactose (Lactohale, LH 230)	Friesland food, Netherland.
Methanol	Fisher Scientific, UK
Chloroform	
Tetrahydrofuran (THF)	
96-well flat bottom black plates	
25 and 75 cm^2/tissue culture flask with vented cap (IWAKI brand)	
24-well tissue culture plates and 96-well flat bottom plates	
Paraformaldehyde	
Dimethyl sulfoxide (DMSO)	
Novozyme 435 (a lipase derived from *Candida antarctica* immobilized on a microporous acrylic resin)	Biocatalytics, USA
Polystyrene standards kit	Supelco, USA

PLGEL 5 μm MIXED-D 300 x 7.5 mm column	Varian, Polymer Laboratories, UK
Bovine serum albumin (BSA, Mw 67 kDa)	Avenchem, UK
Poly (vinyl alcohol) (PVA, Mw of 13- 23 kDa, 87-89% hydrolyzed)	Clariant GmbH, Frankfurt amMain, Germany.
QuantiPro bicinchoninic acid (BCA) protein assay kit Disposable Plastic Cuvets, Catalog Number C5416	Sigma, UK.
Protogel (30% acrylamide, 0.8% Bis-acrylamide stock solution 37.5:1) Protogel resolving buffer (1.5 M Tris-HCl, 0.4% SDS, pH 8.8) Protogel stacking buffer (0.5 M Tris-HCl, 0.4% SDS, pH 6.8) N, N, N`, N`,-tetramethyl ethylenediamine (TEMED) Vertical Gel Electrophoresis Units Protein loading buffer blue, BLUeye Prestained Protein Ladder	Geneflow limited, UK
Ammonium persulfate (APS)	AGT, Bioproduct, Global life science supply, UK.
Colloidal Coomassie Brilliant Blue	Severn Biotech Ltd, UK
Phosphate buffered saline tablets pH 7.3	Oxoid, UK
Chitosan hydrochloride: molecular weight: 200,000–400,000; degree of deacetylation: 80% and 95%	HEPPE MEDICAL CHITOSAN GmbH, Germany
L-leucine ≥ 99.5%	Bioultra, Sigma, UK.
Fluorescamine	Acros Organics; Morris Plains, NJ
Foetal calf serum (FCS) heat inactivated	Biosera, UK.
Adenocarcinomic human alveolar basal epithelial cell line, A 549 (CCL-185[TM]) Immature DCs; monocyte, mouse, JAWS II (CRL-11904[TM]).	American Type Culture Collection (ATCC).
Fetal bovine serum	Gibco by life

L-glutamine	technologies, UK.
Granulocyte macrophage colony-stimulating factor (GM-CSF)	
Minimum Essential Medium (MEM) alpha-nucleosides	
8-well chambered #1 cover glass system	Nunc Lab-Tek, Thermo Scientific, UK.
4′,6-diamidino-2-phenylindole, dihydrochloride (DAPI)	Invitrogen, Ltd.,UK.
Wheat Germ Agglutinin Texas RedR-X conjugate (WGA TR)	
High binding chemistry 96-well plate Costar microplate	Cole-Parmer, UK
10x fish gelatin blocking solution number 22010	Biotium, Hayward, CA.
20x TBS tween 20 buffer number 28360	was obtained from Thermo, UK.
Anti-PspA monoclonal antibody clone number 22003	QED Biosciences, San Diego, CA.
Aalkaline phosphatase conjugated goat anti-mouse IgG number 115-055 (heavy and light chain)	Jackson ImmunoResearch, West Grove, PA.
Recombinant PspA4Pro	A kind gift from Dr Eliane Miyaji and Dr Viviane Gonçalves from the Insituto Butantan, Brazil.

2.2.   General Methods

2.2.1.   Polymer synthesis

The poly glycerol adipate-co-ω-pentadecalactone (PGA-co-PDL) was synthesized via an enzyme catalysed condensation and ring opening co-polymerization reactions (Figure 2-1) as described by Thompson *et al.* (62). Briefly, a 250mL two-necked round bottom flask equipped with a centre stirrer guide and an open top condenser (to act as an outlet for the acetaldehyde produced), was charged with the monomers, glycerol (125 mmol), DVA (125 mmol), and PDL (125 mmol) and half the THF (15 ml). The flask was fitted with an overhead stirrer paddle and condenser, and immersed to the level of the solution, in a water bath (50 ˚C) and stirred for 20 min to allow the temperature to equilibrate. The Novozyme 435 (1.25 g) was added with the remaining THF (15 ml) and the reaction continued for 6 h. Upon completion, 300 ml of warm DCM was added to the flask and stirring continued to dissolve the viscous polymer. The enzyme was removed by Buchner filtration under vacuum. The solvent was removed by rotary evaporation (60 ˚C, Heidolph Laborota 4000). Methanol (100 ml) was added and the mixture agitated to precipitate the polymer and leave unreacted monomers and oligomers in solution. The solid polymer was obtained by filtration and air dried for 48 h before storing in desiccator at room temperature.

2.2.2.   Polymer characterization

2.2.2.1. Gel Permeation Chromatograph

Polymer molecular weight was characterized by Gel Permeation Chromatography (GPC) using a Viscotek system employing OmniSEC 3 software, TDA Model 300. The system was fitted with two PLGEL 5 μm MIXED-D 300 x 7.5 mm columns stored in the detector oven at 40 ˚C, and a flow rate of 1mL/min applied using chloroform as the mobile phase. The detector alignment and instrument sensitivity parameters had been previously calibrated using different molecular weight of polystyrene standard.
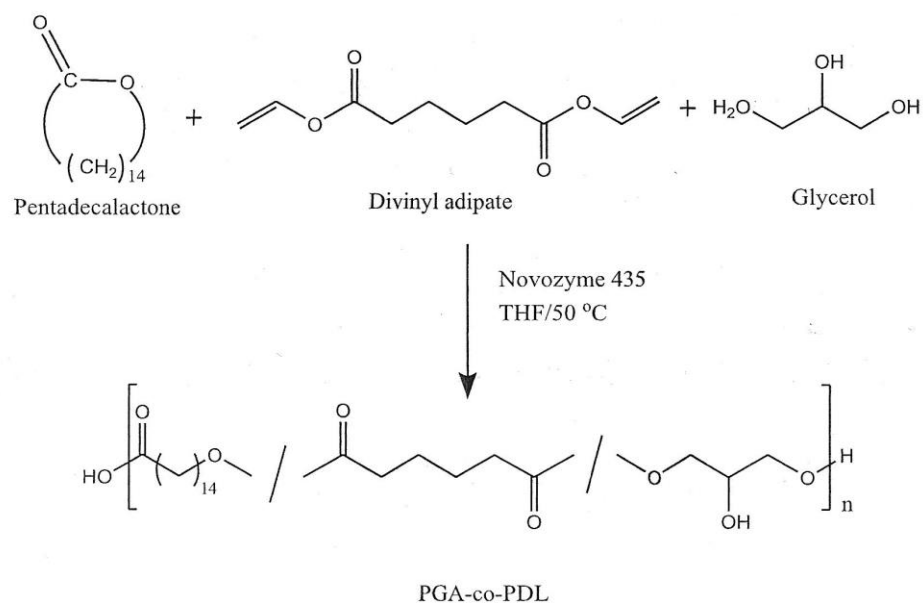
Figure 2-1: Reaction scheme for the enzymatic synthesis of poly (glycerol adipate-co-ω-pentadecalactone), PGA-co-PDL.

2.2.2.2. Proton nuclear magnetic resonance

Proton nuclear magnetic resonance (^{1}H-NMR) spectroscopy was used to confirm the chemical structure of the synthesised polymer. The ^{1}H-NMR was performed using a Bruker AVANCE 300 MHz, inverse probe with B-ACS 60 and autosampler with gradient shimming. The spectra were analysed by MestReNova software.

2.2.2.3. Differential scanning calorimeter

The melting point (T_m) and glass transition temperature (T_g) were determined using differential scanning calorimetry (DSC, Perkin Elmer 800, Pyris software). The system was calibrated with an indium reference standard. The polymer sample (3–5mg) was placed into a hermetically sealed and crimped pan. The samples were scanned at heating and cooling rate of 10 °C/min purged with nitrogen. T_m and T_g were reported from the second heating scan after previously heating to 75 ˚C followed by cooling to – 90 ˚C.

2.2.3. Nanoparticle preparation

BSA loaded PGA-co-PDL NPs were prepared by (w/o/w) double emulsion/solvent evaporation method (Figure 2-2). A Taguchi L$_{36}$ orthogonal array design of experiment was used to optimise the preparation parameters to achieve NPs of optimum particle

size and protein loading. The optimised conditions used were: internal aqueous phase (IAP) 0.5 ml of protein solution (1 %) containing PVA (1 %) was emulsified in 1 ml DCM (organic phase, OP) containing 50 mg of PGA-co-PDL, using a probe sonicator (VC X 500 Vibra-Cell[TM], Sonics & Materials, Inc., Newtown, CT, USA, 13mm probe) at 45 % amplitude for 15 sec over an ice bath. The resulting single emulsion was emulsified into 25 ml of a 1% PVA solution (external aqueous phase, EAP) using the same probe sonicator at 45 % amplitude for 30 sec to form a w/o/w double emulsion. The double emulsion was stirred magnetically for 2 h at room temperature to evaporate the DCM. The NPs were collected by centrifugation (Sigma 3-30k, SIGMA Laborzentrifugen GmbH, Germany) at 40,000 xg for 1 h at 4 ^{0}C, washing twice with distilled water. Control NPs were prepared using the same method but without protein. For particle uptake studies, fluorescein isothiocyanate (FITC-BSA) was added in the IAP.
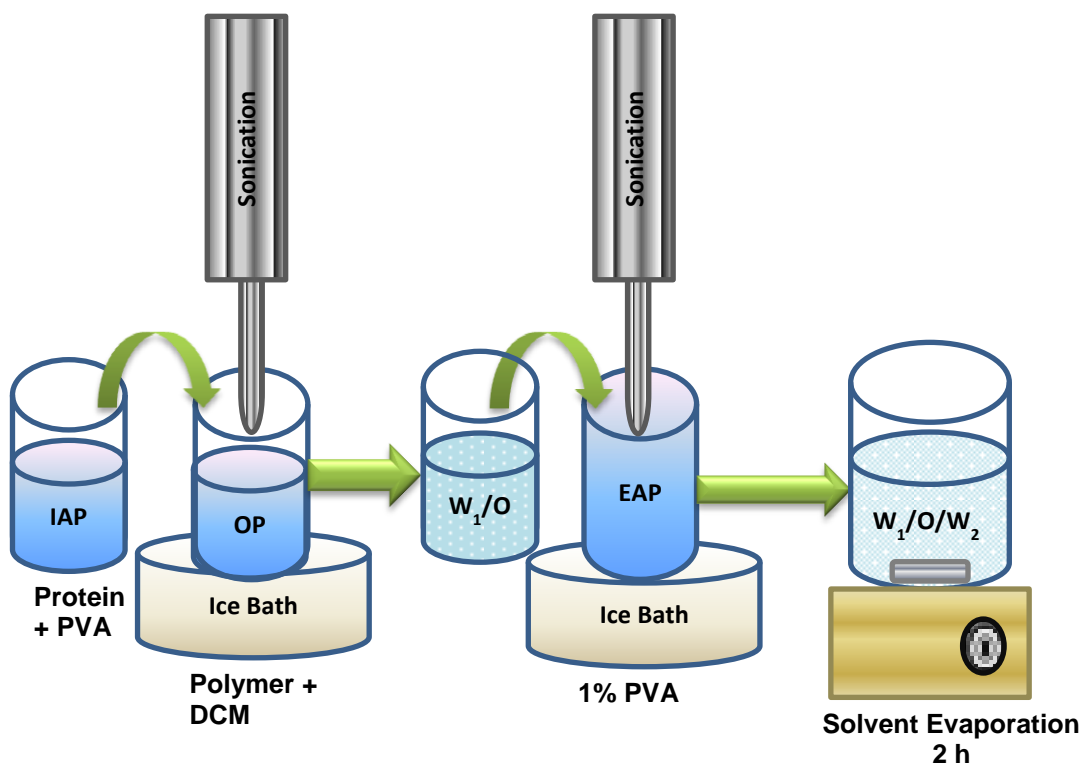
Figure 2-2: Simple scheme shows nanoparticles preparation by double emulsion solvent evaporation method.

2.2.4. Cationic nanoparticle preparation

The adsorption of CHL was achieved by two strategies as follows:

1.   The first strategy involved the adsorption of CHL onto the surface of the preformed NPs prepared as described in section 2.2.3 (109; 110):

   1.1.   To optimise the CHL concentration, NPs were suspended in an aqueous solution of CHL of varying PGA-co-PDL / CHL weight ratio from 1:0, 1:1, 1:3, 1:6, 1:8 to 1:10 with and without 1% PVA and incubated for 2 h at room temperature with magnetic stirring. The suspension was then centrifuged at 40,000 x g for 1 hour at 4 °C, and washed twice with distilled water.

   1.2.   To optimise the amount of PVA required, NPs were suspended in an aqueous solution of CHL containing PGA-co-PDL /CHL weight ratio 1:6 with 0, 0.5 or 1% PVA and incubated for 2 h at room temperature with magnetic stirring. The suspension was then centrifuged at 40,000 x g for 1 hour at 4 °C, and washed twice with distilled water.

   1.3.   To optimise the adsorption time, NPs were suspended in an aqueous solution of CHL (PGA-co-PDL / CHL weight ratio 1:6) without PVA and incubated for 2h, 4 h, 6h, 24h at room temperature with magnetic stirring. The suspension was then centrifuged at 40,000 x g for 1 hour at 4 °C, and washed twice with distilled water.

2. The second strategy involved the addition of CHL to EAP during the NPs preparation process as described in section 2.2.3 (41; 72; 111). CHL was dissolved at various concentrations (2, 4, 6, 8, 10, 16, 20 mg/ml) in the EAP. The suspension was then centrifuged at 40,000 x g for 1 hour at 4 °C, and washed with distilled water. The supernatants were further assessed for CHL adsorption to NPs.

2.2.5. Quantification of chitosan hydrochloride adsorption

The amount of CHL adsorbed on the surface of cationic NPs was determined by fluorescamine due to its high sensitivity and specificity (111). Fluorescence was produced by the reaction of fluorescamine with the primary amino groups of CHL. Fluorescamine in DMSO solution (100 µL of 0.2%) was added to the supernatant (collected from section 2 of the section 2.2.4, 20 µL) in a black 96-well fluorescent detection microplate. This was incubated for 3 h protected from light, and the fluorescence measured at an excitation wavelength of 390 nm and emission wavelength of 515 nm using a microplate reader (Clariostar BMG LABTECH, Germany). A CHL calibration curve was prepared for each experiment. The mass CHL adsorbed onto the NPs was calculated by subtracting the free CHL in the supernatant from the initial amount of CHL added, equation 2-1:

$$q = \frac{(C_i - C_e)}{W} V \qquad \textbf{Equation 2-1}$$

where q is the amount (mg) of adsorbed CHL on NPs, V is the volume of suspension (ml), W is the mass (mg) of NPs, and C_i and C_e are the initial feed concentration of CHL and the free CHL concentration (mg/ml) at equilibrium, respectively (111).

2.2.6. Adsorption isotherm models

The adsorption mechanism of CHL on NPs could be explained by using isotherm models: the Langmuir, (equation 2-2); BET (Brunauer–Emmett–Teller), (equation 2-3); Freundlich, (equation 2-4); and Halsey, (equation 2-5). The isotherm models were plotted in a linear form using the measured adsorption values. Listed below are the equations of isotherm models where, *q* is the weight of adsorbed CHL per unit weight of NPs, C_e is the equilibrium concentration of unadsorbed CHL, q_m, and *k* are constants referred to the adsorption capacity, and *b* and *n* are constant referred to the intensity of adsorption (111).

$$\frac{C_e}{q} = \frac{1}{b\,q_m} + \frac{C_e}{q_m}$$ **Equation 2-2**

$$\frac{C_e}{q-(1-C_e)} = \frac{1}{b\,q_m} + \frac{b-1}{b\,q_m}$$ **Equation 2-3**

$$\log q = \log k + \frac{1}{n}\log C_e$$ **Equation 2-4**

$$\ln q = \frac{1}{n}\ln k - \frac{1}{n}\ln(-\ln C_e)$$ **Equation 2-5**

2.2.7. Characterization of nanoparticles

2.2.7.1. *Particle Size and zeta potential*

Particle size, polydispersity index (PDI) and zeta potential were measured by laser differaction using a Zetasizer Nano ZS (Malvern Instruments Ltd, UK). An aliquot of 200 µl of the suspension was diluted with 3ml of deionized water. The diluted samples were placed into a cuvette and the measurements were conducted at ambient temperature (25 °C) (n=3).

2.2.7.2. *Encapsulation efficiency and protein loading of nanoparticles*

The amount of protein loaded in the NPs was determined by indirect and direct methods.

Direct method: the amount of protein loaded in the NPs was determined after extraction from the NPs. Ten milligrams of protein-loaded NPs was dissolved in 4 mL of DCM followed by the addition of 2 mL of distilled water. The mixture was vortexed at 1000 rpm and then placed on the shaker for extraction overnight. After centrifugation (Sigma 3-30k, SIGMA Laborzentrifugen GmbH, Germany) at 40,000 xg for 1 h at 4 ^{0}C the supernatant was removed for analysis.

Indirect method: the amount of protein loaded in the NPs was determined by measuring the amount of protein remaining in the supernatant and wash after centrifugation.

Both methods carried out using a QuantiPro bicinchoninic acid (BCA) protein assay kit (n=3). This assay is based on colorimetric detection. Protein concentration was

determined by UV spectroscopy at 562 nm (Genesys 5 spectrophotometer, Thermo Fisher Scientific Inc, Waltham, MA).

In order to eliminate any source of interfering with BCA assay in the direct method an unloaded NPs was treated as the BSA loaded NPs and used as a blank while in the indirect method the supernatant of unloaded NPs was used as a blank. A calibration curve was obtained with BSA standard solutions (2.5-30 µg/ml). The encapsulation efficiency (EE %) and drug loading (DL) were calculated according to equations 2-6 and 2-7:

$$EE \% = \frac{amount\ of\ BSA\ added - free\ amount\ of\ BSA}{amount\ of\ BSA\ added} \times 100 \qquad \textbf{Equation 2-6}$$

$$DL = \frac{actual\ amount\ of\ encapsulated\ BSA\ (\mu g)}{actual\ amount\ of\ nanoparticles\ (mg)} \qquad \textbf{Equation 2-7}$$

2.2.8. Preparation of nanocomposite microparticles by spray drying

Spray drying was used to incorporate the NP formulation into nanocomposite microparticles (NCMPs). NCMPs were prepared by spray drying NPs suspended in aqueous L-leucine solutions (at polymer-to-carrier ratio of 1:1.5 w/w) using a Büchi, B-290 mini-spray dryer (Büchi Labortechnik, Flawil, Switzerland) with a standard two-fluid nozzle (0.7 mm diameter). A Taguchi L_{27} orthogonal array design of experiment was used to optimise the parameters to achieve NCMPs of highest yield %. The optimised condition used were: feed rate 10%, aspirator capacity 100%, atomizing air flow rate 400 L/h, inlet drying temperature 100ºC (corresponding outlet temperature of approximately 42-46 ˚C), and the feed concentration 12.5 mg/ml. The dried powder was collected from the particle collecting vessel and stored in a desiccator at room temperature prior to characterization.

2.2.9. Characterization of nanocomposite microparticles

2.2.9.1.   Particle size and zeta potential

Five milligram of NCMPs were suspended in 7 ml deionized water and the measurements recorded at 25°C (n=3) to determine the geometric particle size and zeta potential by laser diffraction using a Zetasizer Nano ZS (Malvern Instruments, UK).

2.2.9.2.   Morphology of nanocomposite microparticles

Spray dried NCMPs samples were mounted on aluminum stubs (pin stubs, 13mm) layered with a sticky conductive carbon tab and coated with palladium (10-15 nm) (EmiTech K 550X Gold Sputter Coater, 25mA for 3 min), and visualized by scanning electron microscopy (SEM) (FEI – Quanta^{TM} 200 ESEM, Holland).

2.2.9.3.   Yield of spray dried nanocomposite microparticles

The yield of spray dried NCMPs (dry powder) was quantified as a percentage mass of expected total powder yield according to equation 2-8:

$$\boldsymbol{Yeild}\ \% \ = \ \frac{\boldsymbol{Weight\ of\ dry\ powder\ collected\ after\ spray\ drying}}{\boldsymbol{Weight\ of\ total\ dry\ mass\ used\ for\ the\ preparation}} \times \boldsymbol{100} \qquad \textbf{Equation 2-8}$$

2.2.9.4.   Moisture content

A thermogravimetric analyser (TGA) was used to evaluate the moisture content of dry powder after spray drying. Moisture content was measured using TGA Q50, UK equipped with TA universal analysis 2000 software. Approximately 10–15 mg of sample was weighed in a platinum pan and heated over the temperature range 25–650°C using a scanning rate of 10 °C/min purged under nitrogen at 20 ml/min. The moisture content was analysed for data collected between 25 to 120 °C.

2.2.9.5.   Powder density and primary aerodynamic diameter

The powder density of selected NCMPs powders was determined by adding approximately 0.2 g of powder to a 5 ml graduated cylinder and recording the volume. The tapped density was determined by tapped density measurements on the same

samples in a 5 ml graduated measuring cylinder until constant volume was obtained (n=3).

Theoretical primary aerodynamic diameter (d_{ae}) was calculated using data acquired from geometric particle size (d) and tapped density (ρ) according to equation 2-9.

$$\boldsymbol{d_{ae} = d\sqrt{\frac{\rho}{\rho_1}}} \qquad \textbf{Equation 2-9}$$

$\rho_1 = 1$ g/cm^3

2.2.10. *In vitro* aerosolisation studies

The aerodynamic particle size of the NCMPs was assessed using a Next Generation Impactor (NGI) (NGI is specified in the USP Chapter <601> as Apparatus 5 and Ph. Eur. Chapter 2.9.18 as Apparatus E for their use in measuring the mass distribution of pharmaceutical aerosols by aerodynamic diameter) (112). The NGI have a range of cut-off diameters at 60 L/min (Table 2-1), with particles captured on any specific stage having an aerodynamic diameter less than the preceding stage, assuming ideal collection behaviour on each stage. Optimum NCMPs samples were weighed (4- 6 capsules, each corresponding to 10-15 mg spray-dried powder) and manually loaded into hydroxypropyl methylcellulose capsules (size 3) and aerosolised via a Cyclohaler® (Teva pharma) into NGI. The capsule was punctured using the actuator of the Cyclohaler® prior to inhalation and a pump (Copley HCP5, Nottingham, UK) was used to simulate an inspiration (the flow rate was 60L/min for 4s). Prior to testing, the pre-separator was filled with 15ml of 0.15 M NaCl as washing media. The NGI stages were coated with 1% tween 80: acetone solution to eliminate particle bounce (113). Four to six capsules were emptied in each run (3 runs). Following aerosolisation, the samples were collected from each stage of the NGI, pre-separator, throat, mouth piece, inhaler, and capsule by washing with a DCM/0.15 M NaCl mixture (2:1) to dissolve the polymer and the encapsulated BSA, which was determined by QuantiPro BCA protein assay as described in section 2.2.4.2. (n=3). The emitted dose (ED) was determined as

the sum of powder deposited in mouthpiece, throat, pre-separator, NGI stages and micro-orifice collector of the NGI (MOC), the fine particle dose (FPD) was determined as the sum of powder deposited in NGI stages and MOC with aerodynamic diameters less than 4.6 μm, the fine particle fraction (FPF%) was determined as the fraction of ED deposited in the NGI and MOC with aerodynamic diameters less than 4.6 μm, and the mass median aerodynamic diameter (MMAD) was calculated from log-probability analysis.

Table 2-1: Effective cut-off diameters for NGI impactor at 60 L/min (with permission from (113))**.**

Stage	Aerodynamic cut-off diameter (μm)
1	8.1
2	4.5
3	2.9
4	1.7
5	1
6	0.6
7	0.3
MOC	< 0.3

MOC: micro-orifice collector of the NGI.

2.2.11. *In vitro* release study

Spray dried NCMPs samples (10 - 15 mg) were placed in micro tubes and dispersed in 1.2 ml of PBS (pH 7.4). The samples were incubated at 37 °C and left rotating at 20 RPM in a sample mixer (HulaMixer, Invitrogen Dynal AS, Life Technologies). At predetermined time intervals up to 48 h, the samples were centrifuged (13,000 rpm for 30 min) and 0.5 ml of the supernatant removed and replaced with fresh buffer. The supernatant was analysed by the QuantiPro BCA protein assay as described above

(n=3). The percentage cumulative protein released was calculated according to equation 2-10.

$$\% \ \textit{Cumulative protein released} = \frac{\textit{cumulative protein released}}{\textit{protein loaded}} \times 100 \qquad \textbf{Equation 2-10}$$

The % cumulative protein release data was assessed using different release models, namely zero order, first order and Higuchi's square root plot, and a correlation coefficient close to unity was used as the mechanism and order of release (114). The following plots were made: *cumulative % drug release vs. time* (zero order kinetic model); *log cumulative of % drug remaining vs. time* (first order kinetic model); cumulative *% drug release vs. square root of time* (Higuchi model).

2.2.12. Investigation of protein structure

2.2.12.1. SDS-PAGE analysis of protein integrity

The primary structure of the proteins was characterized by sodium dodecyl sulfate poly (acrylamide) gel electrophoresis (SDS-PAGE). NPs and spray dried NCMPs (10-20 mg) were suspended in 0.5-1.5 ml of phosphate buffer saline (PBS, pH 7.4). The samples were incubated at 37 °C and left rotating at 20 RPM on a sample mixer (HulaMixer, Invitrogen Dynal AS, Life Technologies) for 24 h. This was followed by centrifugation (Sigma 3-30k, SIGMA Laborzentrifugen GmbH, Germany) at 40,000 xg for 1h, and 50 µl of supernatant was withdrawn to perform SDS-PAGE. The standard was 75 µg/ml of protein in water. The SDS-PAGE was performed on a CVS10D omniPPAGE vertical gel electrophoresis system (Geneflow Limited, UK).

Sodium dodecyl sulfate poly (acrylamide) gels (10 cm W × 8 cm L × 0.5 mm thick) were freshly cast for all experiments as described in appendix- 1. Protein samples and standard were treated with protein loading buffer in a ratio (1:1) for 3 min at 95°C. The protein molecular weight marker, standard, and samples were loaded into the wells (25 µl per well). Electrophoresis was performed at a constant voltage of 100 V for 2.3 h.

Then the gel was stained with colloidal Coomassie Brilliant Blue stain (as described in appendix- 1). A Molecular Imager® Gel Doc™ XR+ System with Quantity One Software was used for the gel imaging and documentation.

2.2.12.2. Circular dichroism spectroscopy

The secondary structure of standard protein (as a control), and protein released after 48 h was determined via circular dichroism (CD) spectra using a J-815 spectropolarimeter (Jasco, UK) at 20 °C (115). Five scans were performed per sample using a 10 mm path-length cells at far-UV wavelengths from 260-180 nm at a data pitch of 0.5 nm, band width of 1 nm and a scan speed 50 nm/min. Far-UV CD spectra were collated for standard protein and protein released in PBS after 48 h. For all spectra, the baseline acquired in the absence of sample was subtracted (116). The secondary structure of the samples was estimated using the CDSSTR method (117) protein reference set 3 from the DichroWeb server (118; 119).

2.2.13. Production and purification of PspA4Pro

Recombinant PspA4Pro was produced, purified, and provided by Dr. Eliane Miyaji and Dr. Viviane Gonçalves from Centro de Biotecnologia, Instituto Butantan, São Paulo, Brazil.

The PspA4Pro was produced and purified using published methods with modifications (120; 121). PspA4Pro was produced in 5 L bioreactors by; fed-batch cultivation with defined medium including glycerol as carbon source and lactose as inducer (120) or batch cultivation with complex medium including glucose, glycerol and lactose for auto-induction (122). The purification procedure includes cell disruption in a continuous high pressure homogenizer at 500 bar for 8 min, precipitation of the homogenate with 0.1% cationic detergent cetyltrimethylammonium bromide, pellet removal by centrifugation, anion exchange chromatography in Q-Sepharose, cryoprecipitation at pH 4 and cation exchange chromatography in SP-Sepharose (121). The desired protein

purity of > 95% was reached with good yield (14-30 %). The established procedure also removed lipopolysaccharides (LPS), producing an acceptable concentration of endotoxin (0.3-0.6 EU/ml) in the final product (123). The purified protein was identified by antibodies, capable to bind lactoferrin and displayed the characteristics α-helical secondary structure.

2.2.14. *In vitro* antigenicity study of protein

The antigenicity of PspA4Pro was defined by the capability of anti-PspA antibody to bind to the released PspA4Pro. The antigenicity of PspA4Pro was measured using an enzyme-linked immunosorbent assay (ELISA) as described previously by Haughney *et al.* with modifications (30). The concentration of released PspA4Pro was adjusted to 0.5µg/ml and used to coat a high binding chemistry 96-well plate then incubated overnight at 4°C. The PspA solution was removed and PBS with 1% fish gelatin blocking buffer was added and incubated for 2 h at room temperature. Then, the fish gelatin blocking buffer was removed and the plates were washed three times with PBS containing 0.5% Tween 20 (PBS-TN). Anti-PspA monoclonal antibody (1 µg/ml) was added and the plates were incubated overnight at 4°C. Plates were washed three times with PBS-TN then alkaline phosphatase conjugated goat anti-mouse IgG (0.1 µg/mL) was added, and incubated for 2 h at room temperature before developing. For the development of the ELISA, alkaline phosphatase substrate was added (1 mg/mL). After 15 min incubation at room temperature, the colorimetric assay was carried out at an absorbance of 405 nm using a microplate reader (Epoch, BioTek Instruments Ltd, UK) and the data was described as relative antigenicity, which is presented as the ratio of absorbance between the released PspA4Pro and the native protein.

2.2.15. Cytotoxicity study

2.2.15.1.   *Normal human bronchial epithelial (A 459) cells*

2.2.15.1.1.   Cell culture

Adenocarcinomic human alveolar basal epithelial cell line (A 549) cells were cultured in RPMI-1640 medium supplemented with 10% FCS/1% Antibiotic/Antimycotic solution (complete medium) incubated at 37°C into 5%CO_2 incubator. The medium was changed every four days and cells were passed weekly using Trypsin.

2.2.15.1.2.   Cells viability study

The toxicity profiles of NPs and NCMPs were evaluated over 24 h in adenocarcinomic human alveolar basal epithelial cell line (A549) cells (passage No. 44) using 3-(4,5-dimethylthiazol-2-yl)-2,5-diphenyltetrazolium bromide (MTT) assay. Cells were cultured in 96-well plates with 100 µl ($2.5X10^5$ cells /ml) RPMI-1640 medium supplemented with 10% FCS/1% Antibiotic/Antimycotic solution for 24 h at 37°C into 5% CO_2 incubator. The wells were replaced with fresh medium (100 µl) containing NPs or NCMPs (0–2.5 mg/ml) (n=3) and 10% dimethylsulfoxide (DMSO) as a positive control and incubated for a further 24 h as above, followed by the addition of 40 µl MTT solution (5 mg/ml in PBS, pH 7.4) to each well. After incubation for a further 2 h, the medium was gently removed, and any formazan crystals generated were solubilized with 100 µl of DMSO. The absorbance of solubilised dye, which correlates with the number of living cells, was measured using a microplate reader (Epoch, BioTek Instruments Ltd, UK) at 570 nm. The cell viability (%) in each well was calculated as the absorbance ratio between NPs or NCMPs-treated and untreated control cells.

2.2.15.2.   *Dendritic cells*

2.2.15.2.1.   Cell culture

DCs were cultured in MEM alpha medium containing ribonucleosides, deoxynucleosides, 4 mM L-glutamine,1 mM sodium pyruvate, supplemented with 20 %

fetal calf serum, 5 ng/ml murine growth GM-CSF, and 1% Antibiotic/Antimycotic solution (complete growth medium) and incubated at 37°C and 5%CO_2 incubator in 25 cm^2 tissue culture flask. The medium was changed every four days and cells were passed weekly using Trypsine.

2.2.15.2.2.   Cells viability

Cells were cultured in 96-well plates with 100 μl (2.5×10^5 cells /ml) complete growth medium for 24 h at 37°C in a 5% CO_2 in an incubator. Then, complete growth medium (100 µl) containing NPs (0–5 mg/ml) (n=3) and 10% DMSO as a positive control were added to the wells and incubated for a further 4 h as above, followed by the addition of 40 μl MTT solution (5 mg/ml in PBS, pH 7.4) to each well. After a further 2 h incubation, the 96-well plate was centrifuged at 1300 g for 7 min at 4 ˚C to pellet the suspended cells then the medium was gently removed, and any formazan crystals generated were solubilized with 100 μl of DMSO. The absorbance of solubilised dye, which correlates with the number of living cells, was measured using a microplate reader (Epoch, BioTek Instruments Ltd, UK) at 570 nm. The cell viability (%) in each well was calculated as the absorbance ratio between treated and untreated control cells.

2.2.16. NPs cellular uptake by DCs

DCs uptake of FITC-BSA loaded anionic and cationic NPs was visualized using Confocal Laser Scanning Microscopy (CLSM) (Carl Zeiss lsm 710, UK). The DCs 2×10^5 cells/400 μl were plated into an 8-well chambered borosilicate cover glass system, and incubated at 37 °C and 5% CO_2 for 48 h prior to treatment with NPs. Different concentrations of FITC-BSA loaded NPs (10-40 µg/40 µl) were added to each well and incubated at 37°C and 5% CO_2 for 1 h. The suspension in each well was removed and washed using PBS. Cells were fixed for 15 min with 300 μL of 4% paraformaldehyde in PBS followed by washing with PBS. The cell membranes were counterstained with WGA TR: 100 µl WGA TR (5µg/ml) was added to each well and

incubated at 37°C and 5% CO_2 for 10 min followed by washing with PBS. The nuclei were counterstained with DAPI: 100 μl of DAPI was added to each well and incubated at 37°C and 5% CO_2 for 10 min. Followed by washing with PBS. The cells were examined using a Zeiss 510 Meta laser scanning microscope mounted on a Axiovert 200 M BP computer-controlled inverted microscope. Cells were imaged by excitation at a wavelength of 595 nm (red channel for WGA TR), and 358 nm (blue channel for DAPI), and 488 nm (green channel for FITC-BSA), using a Plan Neofluar 63×/0.30 numerical aperture (NA) objective lens. Image analysis was carried out using the Zeiss LSM software.

2.2.17. Statistical analysis

Minitab 16 Statistical Software® (Minitab Inc., PA, USA) was employed for statistical analysis and graph plotting. The data obtained were analysed statistically by one-way analysis of variance (ANOVA) with the Tukey's comparison using Minitab 16 Statistical Software® (Minitab Inc., PA, USA). Statistically significant differences were assumed when $p < 0.05$. All values are expressed as their mean ± standard deviation.

3. Pulmonary Delivery of Model Protein Using Nanocomposite Microparticle Carriers via Dry Powder Inhalation

3.1. Introduction

Pulmonary vaccination would stimulate both mucosal and systemic immune responses. The substantial networks of DCs lining the epithelium submucosa of the respiratory tract and on the alveolar surface play a significant role in inducing both systemic and local immune responses. Furthermore, s-IgA antibodies in the respiratory tract have important roles in the avoidance and control of infection at the respiratory mucosa by preventing the adherence of the pathogen and neutralizing antigen on the respiratory mucosal surfaces (52).

Immune response can be improved by using polymeric NPs containing antigen because of NPs adjuvant-like effect where the particulate pattern can be more antigenic than the soluble antigen form (40). Also, it could enhance uptake by the epithelial M cells on mucosal surface by delivering the antigen to the lower respiratory tract area and prevents the rapid clearance by alveolar macrophages. M cells share antigenic information with DCs found in lymphoid tissue and induces secretory local IgA production. Then, the NPs may be transported to secondary lymph-nodes where they enhance induction of the systemic immune response (43).

However, to gain a reliable and strong immune response upon application of particulate vaccines via the pulmonary route, it is essential to optimize the size of the delivery system (73). Studies reported that particles of ~500 nm size are more suitable for uptake than particles of 1-5 μm size (124). However, an inverse relationship had been reported between particle size and the efficiency of uptake by DCs (87).

In this study PGA-co-PDL, biodegradable polyester, was used to prepare NPs. The most common method for the encapsulation of proteins in polymer NPs is the water/oil/water (w/o/w) double-emulsion solvent evaporation method (79) and it is best suited to encapsulate water soluble drugs such as peptides, proteins, and vaccines (80).

NPs do not deposit efficiently in the lungs leading to the exhalation of the majority of the inhaled dose (91). NPs can be formulated into dry powder microparticle carriers to produce NCMPs as DPIs via spray-drying (92). This system is designed to disperse in the lung lining fluid, releasing the NPs from the inert carrier (93).

Biocompatible excipients (carbohydrates, amino acids, and lipids) are typically added to the formulation feed to afford dry powders with bulk (i.e. from microparticle carrier) and to promote the production of a desirable aerodynamic particle size and allow a rapid release of the NPs in the lung fluid lining upon inhalation. In addition, the excipients are added to the formulation to afford some level of protection to both the NPs and encapsulated drug during spray drying, especially against shear forces and increased temperatures (38).

L-leucine is one of the amino acid excipients that is commonly used in the pharmaceutical industry because of its potential to improve dispersibility and bioavailability of aerosols (125). Pure spray dried L-leucine shows hollow particles with low density, proving its ability to enhance aerosolisation (125).

To design a new dosage form in the pharmaceutical field, it is very important to identify the formulation (e.g. concentration of drug, polymer, surfactant, etc.) and preparation (e.g. homogenisation speed, time, etc.) parameters because these variables will affect the properties of the final dosage form. The use of design of experiment (DOE) is the most common method of determining the influence of different parameters on the characteristics of the dosage form being studied and to optimise the parameters to achieve the desired properties (126). Due to parameter interactions and the large number of factors implicated, optimizing these parameters by conventional DOE (e.g. factorial designs) would be considered highly exhausting and uneconomical (127). The efficient analyses of complex formulations process using statistical experimental design have been proposed by "Taguchi Orthogonal Array Design" (127). This design is a

combination of mathematical and statistical approaches included into an empirical study developed by Dr. Genichi Taguchi (128). It aims to investigate how different factors affect the mean and variance of a process performance property that defines how well the process is functioning. A number of implemented trials are proposed to find out the optimum combination of parameters that have the highest effect on the product and with the least variation from the design target (129).

The Taguchi design is a useful inexpensive method for the study of a large number of parameters and interactions within an acceptable number of trials. Also, it has the ability to optimise many extract qualitative parameters simultaneously and extraction much quantitative data with only a few experiments (129). Taguchi has conceptualised a new method to carry out the design of experiments using a special set of arrays called orthogonal arrays. The orthogonal array is a matrix of numbers arranged in columns and rows (128). These standard arrays specify a way to carry out the minimal number of experiments to give full information on all factors that affect the performance over a specific region of interest (levels). Rather than having to try all possible combination e.g. factorial design, Taguchi design test pairs of combinations (126). For example, a single replicate of 4 parameters and 3 level experiments would require 81 runs for a full factorial analysis. On the other hand, Taguchi method will require 9 runs only. Taguchi approach has previously been used in the improvement of dosage forms (126; 127).

The Taguchi method employs a signal to noise (S/N) ratio to quantify variations. These ratios are meant to be used as measures of the effect of noise (uncontrollable) factors on performance characteristics. S/N ratios take into account both amount of variability in response data and closeness of average response to the target (130). In Taguchi design, *S/N* ratio can be defined as the measure of the deviation of the response from the desired value. So, "signal" presents the mean value and "noise" presents the standard deviation. It means that lower variability in the process is ensured through maximizing

the S/N ratio (131). The variability of a characteristic is due to the noise factor such as environmental factors. Thus, optimizing process parameters by the Taguchi design leads to bringing the average quality near to the target value, and also to simultaneously decrease the variation in quality (132). The experimental condition having the maximum S/N ratio is considered the optimum condition, as the variability of characteristics is in inverse proportion to the S/N ratio (133).

There are several S/N ratios available depending upon the type of characteristics: smaller the better (equation 3-1), e.g. particle size; larger the better (equation 3-2), e.g. drug loading. In some cases, a nominal S/N ratio is the best (equation 3-3) (130).

Smaller is better:

$$\frac{S}{N} = -10 \log \sum_{k=1}^{n} \frac{y_i^2}{n} \qquad \textbf{Equation 3-1}$$

Larger is better:

$$\frac{S}{N} = -10 \log \sum_{k=1}^{n} \frac{1}{y_i^2} \frac{1}{n} \qquad \textbf{Equation 3-2}$$

Nominal S/N ratio is the best:

$$\frac{S}{N} = -10 \log \sum_{k=1}^{n} \frac{\mu}{\sigma^2} \qquad \textbf{Equation 3-3}$$

Where

$$\mu = \frac{1}{n} \sum_{k=1}^{n} y_i \qquad \textbf{Equation 3-4} \text{ and } \sigma^2 = \left(\frac{1}{n-1}\right) \sum_{k=1}^{n} (y_i - \mu)^2 \qquad \textbf{Equation 3-5}$$

And y_i donates response variables and "n" represents the number of experiments (131).

The Taguchi design method was applied in this study to examine the effects of different formulation and process parameters on the size and drug loading of NPs and yield % and morphology of NCMPs.

Bovine serum albumin (BSA) has been widely used as a model antigen mainly because of its well-recognized secondary structure (Figure 3-1) (134; 135; 136; 137). It has a molecular weight in the range of 66-69 kDa and is composed of a single long chain of about 582 amino acid residues (138). It has been used in this study as a model antigen to optimize NPs formulation for DCs uptake.
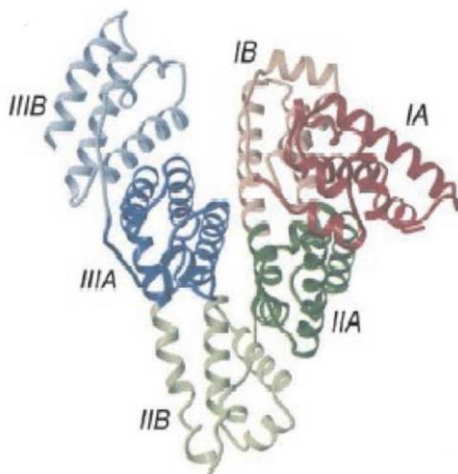
Figure 3-1: Bovine serum albumin structure includes three α-helical domains (I, II, III). Each domain contains two subdomains (A and B) (with permission from (137)**).**

3.2. Aim

The aim of this study was to formulate PGA-co-PDL NPs encapsulating bovine serum albumin (BSA), a model protein, using Taguchi design to optimize formulation parameters: particle size and drug loading. The PGA-co-PDL NPs were then incorporated into microparticle carriers (L-leucine) via spray drying to produce NCMPs carriers suitable for pulmonary delivery via DPIs.

To obtain the aim of the study a systematic study was designed considering the following aspects:

1. Formulation of NPs using double emulsion solvent evaporation technique.

2. Evaluation of the influence of formulation parameters on the particle size, encapsulation efficiency, and drug loading of BSA using Taguchi design.

3. Formulation of NCMPs via spray drying technique.

4. Evaluation of the influence of spray drying parameters on the morphology, and yield% of NCMPs using Taguchi design.

5. Examination of BSA integrity, *in vitro* aerosolisation performance, *in vitro* release, cells toxicity of optimum NCMPs.

3.3. Methods

3.3.1. Polymer synthesis and characterisation

The PGA-co-PDL was synthesised and characterised as described in section 2.2.1 and section 2.2.2 respectively.

3.3.2. Nanoparticle preparation

BSA loaded PGA-co-PDL NPs were prepared by a (w/o/w) double emulsion/solvent evaporation method. Various concentrations of aqueous BSA solutions (0.2 − 1 %) containing PVA as surfactant (1 − 10 %) were prepared. The protein solution (IAP) was emulsified in DCM (OP) containing PGA-co-PDL (50 - 200 mg), by sonication using a probe sonicator (VC X 500 Vibra-Cell^{TM}, Sonics & Materials, Inc., Newtown, CT, USA, using the 13 mm probe) for 5 - 20 seconds over an ice bath. The resulting single emulsion was emulsified into 25 ml of a 1 % PVA solution (EAP) using the same probe sonicator for 10 - 30 seconds to form a w/o/w double emulsion. The double emulsion was stirred magnetically for 2 h at room temperature to evaporate the DCM. The NPs were collected by centrifugation (Sigma 3-30k, SIGMA Laborzentrifugen GmbH, Germany) at 40,000 xg for 1 h at 4 ^{0}C, and washed twice with distilled water.

3.3.2.1. Experimental design by Taguchi method

The Taguchi design was applied in this study to evaluate the influence of IAP volume, BSA concentration, polymer amount, OP volume, PVA concentration, sonication time of IAP, sonication time of EAP, and sonication amplitude on the NPs particle size, BSA encapsulation efficiency %, and loading. The design was composed of 8 variables set at 2 levels (IAP volume, and OP volume) or 3-levels each (BSA concentration, polymer mass, PVA concentration, sonication time of IAP, sonication time of EAP, and sonication amplitude), where the mean particle size, BSA encapsulation efficiency % and loading were the dependent variables (Table 3-1). The design was constructed using L$_{36}$ orthogonal array as shown in Table 3-2. The optimum conditions were indicated by

high signal-to-noise (S/N) ratios. Where the signal factor (S) is the outcome, i.e. particle size, BSA encapsulation efficiency %, or loading and noise factors (N) include room temperature and humidity and researcher experience etc.

Optimization of the size was carried out using the Taguchi's 'smaller-is-better' criterion while optimization of the BSA encapsulation efficiency % and loading was carried out using the Taguchi's 'higher-is-better' criterion (128). The different values for the variables summarized in Table 3-1 were chosen on the basis of the tested lower and upper values for each variable following pre-formulations studies. The Taguchi design was constructed and analysed in Minitab 16 Statistical Software® (Minitab Inc., PA, USA).

Table 3-1: Double emulsion solvent evaporation processing variables, units, and levels for BSA-loaded PGA-co-PDL NPs.

Code	Variables	Unit	Levels		
			1	**2**	**3**
A	IAP volume	ml	0.25	0.5	-
B	OP volume	ml	1	2	-
C	BSA concentration	% (w/v)	0.2	0.5	1
D	Polymer mass	mg	50	100	200
E	PVA concentration	% (w/v)	1	5	10
F	Sonication time IAP	sec	5	10	15
G	Sonication time EAP	sec	10	15	30
H	Sonication Amplitude	%	30	45	65

Table 3-2: Double emulsion solvent evaporation processing variables for BSA-loaded PGA-co-PDL NPs using Taguchi design method (L$_{36}$ Orthogonal Array).

Run	A	B	C	D	E	F	G	H
1	1	1	1	1	1	1	1	1
2	1	1	2	2	2	2	2	2
3	1	1	3	3	3	3	3	3
4	1	1	1	1	1	1	2	2
5	1	1	2	2	2	2	3	3
6	1	1	3	3	3	3	1	1
7	1	1	1	1	2	3	1	2
8	1	1	2	2	3	1	2	3
9	1	1	3	3	1	2	3	1
10	1	2	1	1	3	2	1	3
11	1	2	2	2	1	3	2	1
12	1	2	3	3	2	1	3	2
13	1	2	1	2	3	1	3	2
14	1	2	2	3	1	2	1	3
15	1	2	3	1	2	3	2	1
16	1	2	1	2	3	2	1	1
17	1	2	2	3	1	3	2	2
18	1	2	3	1	2	1	3	3
19	2	1	1	2	1	3	3	3
20	2	1	2	3	2	1	1	1
21	2	1	3	1	3	2	2	2
22	2	1	1	2	2	3	3	1
23	2	1	2	3	3	1	1	2
24	2	1	3	1	1	2	2	3
25	2	1	1	3	2	1	2	3
26	2	1	2	1	3	2	3	1
27	2	1	3	2	1	3	1	2
28	2	2	1	3	2	2	2	1
29	2	2	2	1	3	3	3	2
30	2	2	3	2	1	1	1	3
31	2	2	1	3	3	3	2	3
32	2	2	2	1	1	1	3	1
33	2	2	3	2	2	2	1	2
34	2	2	1	3	1	2	3	2
35	2	2	2	1	2	3	1	3
36	2	2	3	2	3	1	2	1

Note: A: IAP volume, B: OP volume, C: BSA concentration, D: polymer mass, E: PVA concentration, F: sonication time IAP, G: sonication time EAP, H: sonication amplitude.

3.3.3. Nanoparticle characterization

The NPs were characterised for particle size, PDI, encapsulation efficiency and protein loading as described in section 2.2.7.1 and 2.2.7.2 respectively.

3.3.4. Nanocomposite microparticles preparation by spray drying

NCMPs were prepared by spray drying selected NPs formulation as described in section 2.2.8

3.3.4.1. Experimental design by Taguchi method

The Taguchi method was applied to evaluate the influence of the air flow rate, inlet drying temperature, aspirator capacity, pump rate, and feed concentration (total amount of L-leucine and NPs in the feed suspension) on the NCMPs properties. The design was composed of 5 variables each set at 3-levels (Table 3-3), where the morphology and percentage yield were the dependent variables. The design was constructed using L_{27} orthogonal array design (Table 3-4). The different values for the factors, summarized in Table 3-3 were chosen on the basis of the tested lower and upper values for each variable following pre-formulations studies. The Taguchi design was constructed in Minitab 16 Statistical Software$^{®}$ (Minitab Inc., PA, USA).

Furthermore, the optimum spray drying condition was carried out without L-leucine and with lactose or myo-inositol as alternative excipient to L-leucine.

Table 3-3: Spray drying processing variables, units, and levels for BSA-loaded PGA-co-PDL NCMPs.

Code	Variable	Unit	Level		
			1	2	3
A	Air flow	L/h	400	535	670
B	Inlet Temperature	C	50	75	100
C	Aspirator capacity	%	50	75	100
D	Feed rate	%	5	10	15
E	Feed concentration	mg/ml	12.5	6.25	4.17

Table 3-4: Spray drying processing variables for NCMPs using Taguchi design method (L$_{27}$ Orthogonal Array).

Runs	A	B	C	D	E
1	1	1	1	1	1
2	1	1	1	1	2
3	1	1	1	1	3
4	1	2	2	2	1
5	1	2	2	2	2
6	1	2	2	2	3
7	1	3	3	3	1
8	1	3	3	3	2
9	1	3	3	3	3
10	2	1	2	3	1
11	2	1	2	3	2
12	2	1	2	3	3
13	2	2	3	1	1
14	2	2	3	1	2
15	2	2	3	1	3
16	2	3	1	2	1
17	2	3	1	2	2
18	2	3	1	2	3
19	3	1	3	2	1
20	3	1	3	2	2
21	3	1	3	2	3
22	3	2	1	3	1
23	3	2	1	3	2
24	3	2	1	3	3
25	3	3	2	1	1
26	3	3	2	1	2
27	3	3	2	1	3
H	1	3	3	2	1

Note: A: air flow, B: inlet temperature, C: aspirator %, D: pump rate, E: feed concentration. Numeric values 1-27 indicate experimental run number, H indicate optimum spray drying condition that produce highest yield %.

3.3.5. Characterization of nanocomposite microparticles

NCMPs were characterised as described in section 2.2.9.

3.3.6. *In vitro* Aerosolisation studies

The *in vitro* aerosolisation studies were carried out as described in section 2.2.10.

3.3.7. *In vitro* release study

The *in vitro* release studies were carried out as described in section 2.2.11.

3.3.8. Investigation of BSA structure

The released BSA stability of primary and secondary structure were evaluated as described in section 2.2.12.

3.3.9. Cytotoxicity study

The cytotoxicity of NPs and NCMPs were determined as described in section 2.2.15.1.

3.4. Results

3.4.1. Polymer characterization

PGA-co-PDL (monomer ratio, 1:1:1) was a white powder with an average molecular weight of 16.72±0.4 KDa (n=3) as determined by GPC. The GPC chromatographs (Figure 3-2) show symmetric molecular weight distribution with small or no low molecular weight impurities and, so, low polydispersity. This was expected as the polymers were re-precipitated from methanol and any low molecular weight material would have been washed. The structure of the polymer (Figure 3-3) was confirmed from the integration pattern of peaks obtained from ^{1}H-NMR spectra (Figure 3-4) (δH CDCl3, 300 MHz): 1.34 (s, 22 H, H-g), 1.65 (m, 8 H, H-e, e′, h), 2.32 (m, 6 H, H-d, d′, i), 4.05 (q)-4.18 (m) (6 H, H-a, b, c, f), 5.2 (s, H, H-j). The T_m of the polymer was measured by DSC (Figure 3-5) and was detected to be 59.79 ˚C which is similar to previous report (66).
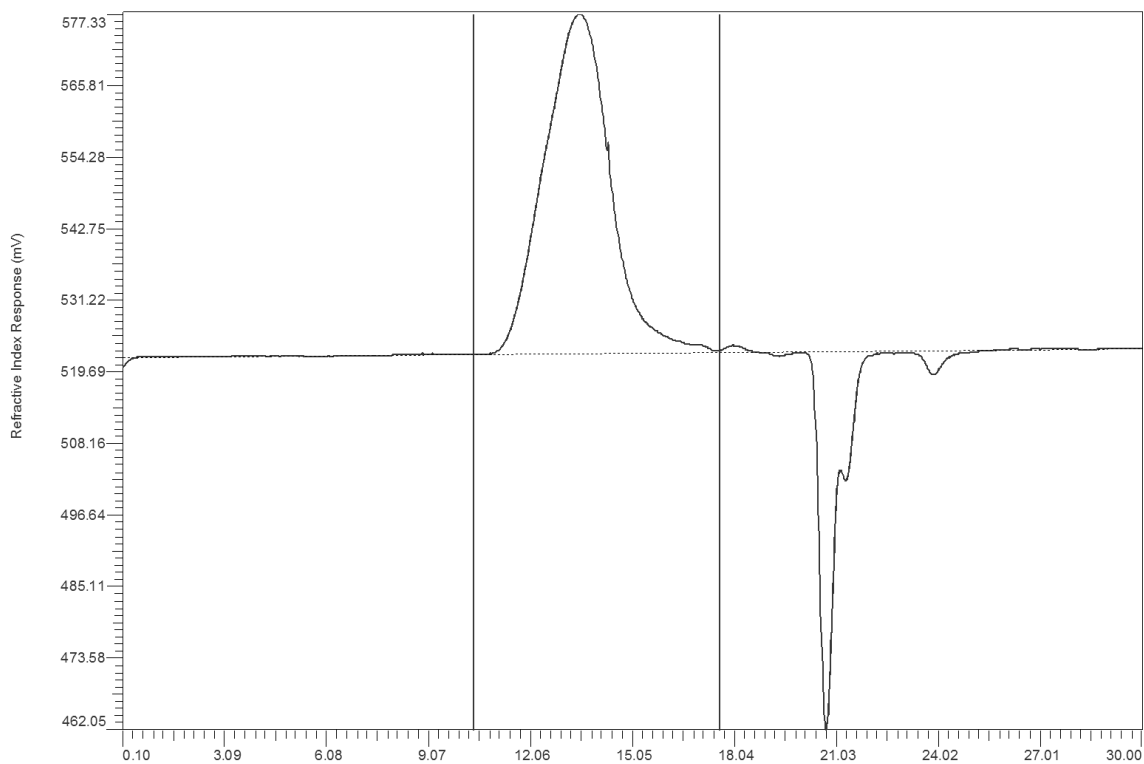
Figure 3-2: Gel Permeation Chromatography (GPC) chromatograph of PGA-co-PDL.
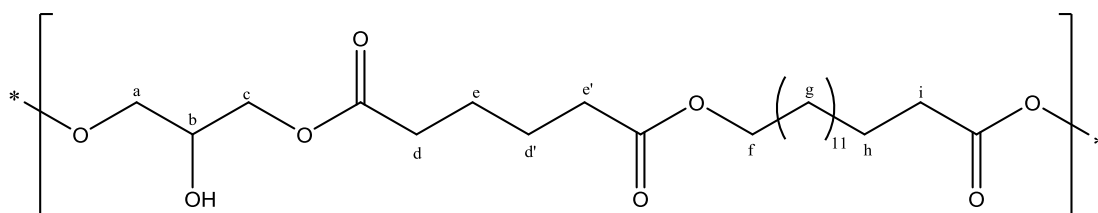
Figure 3-3: Chemical structure of PGA-co-PDL.
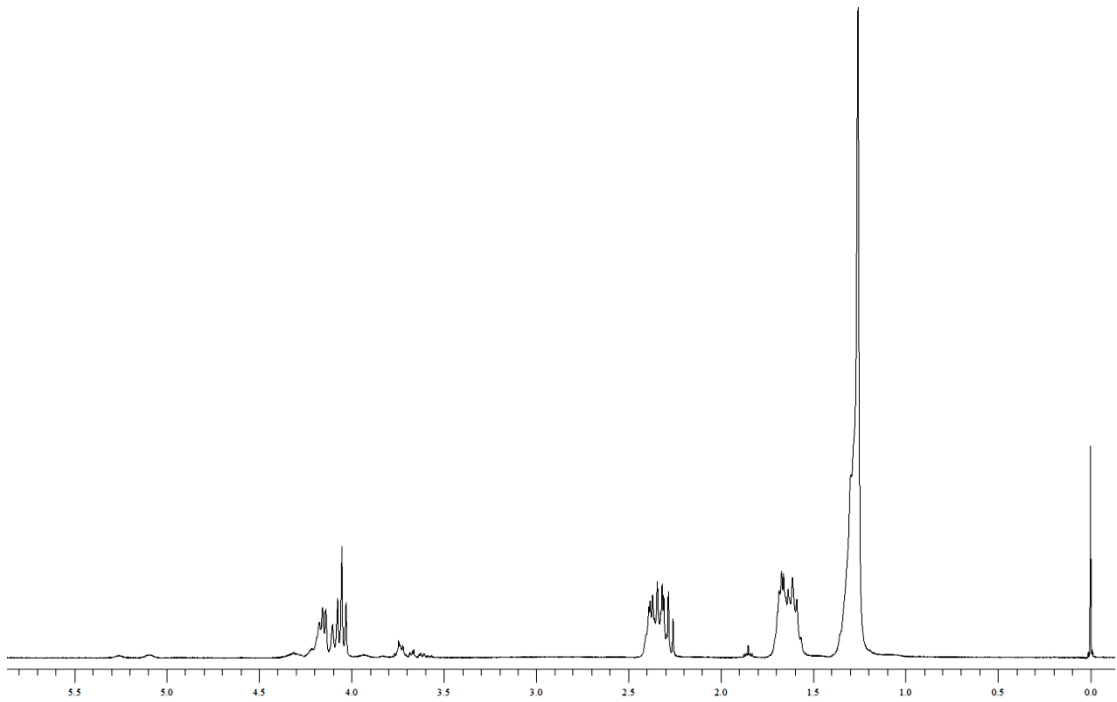
Figure 3-4: Nuclear magnetic resonance (^{1}H-NMR) spectra of PGA-co-PDL.
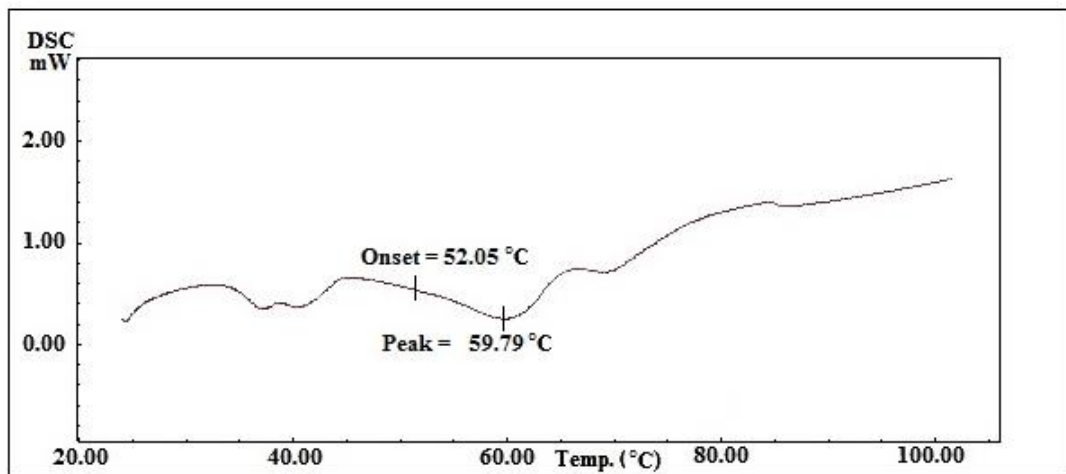
Figure 3-5: Differential scanning calorimetry (DSC) thermograms of PGA-co-PDL.

3.4.2. Optimization of the BSA-loaded NPs prepared by the double emulsion solvent evaporation method using Taguchi design

The Taguchi L_{36} orthogonal array design required 36 runs to be carried out to identify the important factors that could affect the particle size and DL of NPs and to produce the optimum conditions for each variable to achieve the smallest particle size NPs (SPS NPs), and highest drug loading NPs (HDL NPs). In Taguchi design, S/N ratio is the determination of the deviation of the response from the target value. In this study, "signal" represents the mean value while "noise" represents the standard deviation value. The highest the S/N ratio the lowest the variability in the process applied (131).

Table 3-5 represents the measured values of particle size, DL, and EE % of NPs. The measured values were converted into S/N ratio (using Minitab 16 statistical software) which was utilized for the analysis of the results. The calculated S/N ratio at different levels for each parameter were plotted in Figure 3-6 which favoured a 'smaller –is-better' S/N ratio for particle size. Also, the calculated S/N ratio at different levels for each parameter were plotted in Figure 3-7 and Figure 3-8 which favoured a 'larger-is-better' S/N ratio for DL and EE %. In order to determine which parameter had a critical impact on the particle size, DL, or EE% the range and rank were calculated. The range is the difference between the maximum and minimum S/N ratios for the parameter while the rank is the rank of each range, where rank 1 is the largest range. The factor with largest range and corresponding rank (indicating the relative importance compared to other factors) was considered as the critical factor affecting the particle size, DL, or EE % of NPs.

Analysis of results following the Taguchi design indicated particle sizes ranging from 216.17 to 2168.78 nm were obtained (Table 3-5). Based on the range, rank, and S/N response graph (Figure 3-6) for the production of SPS NPs using the Taguchi's "smaller-is-better" criterion in Minitab® 16 statistical software, the optimal conditions

Table 3-5: The experimentally measured values of particle size, polydispersity index, EE %, and DL of NPs. Data represent mean ± S.D., n=3.

Runs	Particle size (nm)	Polydispersity Index	EE (%)	DL (µg/mg)
1	574.4±120.6	0.395±0.15	36.6±1.6	3.6±0.2
2	648.5±10.5	0.209±0.1	56.3±3.3	6.9±0.4
3	1165.9±337.9	0.1805±0.2	57±0.8	7±0.1
4	498.7±4.6	0.311±0.01	23.9±3.8	2.4±0.4
5	1032.9±41.9	0.1845±0.3	45.9±4.5	5.7±0.5
6	1534.7±1484	0.1715±0.2	39.8±28	4.9±3.4
7	577.8±107.4	0.236±0.1	41.2±6.3	4.1±0.6
8	550.4±93.9	0.1455±0.2	37.5±7	4.6±0.9
9	1836.4±864	0.273±0.2	75.3±1.7	9.3±0.2
10	357.5±102	0.1585±0.03	8.4±5.9	0.8±0.6
11	349±68.9	0.124±0.1	52.1±7.2	6.4±0.9
12	325±73.3	0.162±0.03	34.5±8	4.3±0.9
13	270.8±81	0.1325±0.004	27.4±9.8	1.4±0.5
14	416.4±100.8	0.083±0.1	62.9±4.6	3.9±0.3
15	319.7±41.9	0.1415±0.002	11.4±11	5±4
16	493.1±36.1	0.243±0.06	38.9±3.8	1.9±0.2
17	443.6±47	0.1355±0.1	69.1±2.6	4.3±0.2
18	230.7±46.7	0.1005±0.01	32.9±10	15.7±4.8
19	420.8±75.9	0.081±0.1	50.7±1	5±0.1
20	1375.8±392.2	0.005±0	57.3±1.2	7.1±0.1
21	467.3±104.4	0.005±0	21.1±6.6	19.2±5.9
22	1204.7±450.6	0.342±0.1	56.1±0.36	5.6±0.04
23	2168.9±1553	0.0035±0.002	42.8±1.5	20.4±0.7
24	267±10.2	0.0615±0.07	29.5±6.3	26.8±5.8
25	554.1±88.7	0.111±0.09	56.8±2.9	2.8±0.1
26	468.2±50	0.005±0	33.2±0.7	15.8±0.3
27	493.1±104	0.046±0.05	51.4±6.6	24.5±3.1
28	535.1±3.4	0.175±0.1	53.6±0.4	2.7±0.02
29	216.2±39.9	0.1045±0.04	32.5±1.9	15.5±0.9
30	343.4±54.3	0.194±0.03	37.3±2.6	17.7±1.2
31	729.9±54.6	0.269±0.05	44.8±8.4	2.2±0.4
32	246.5±32.2	0.103±0.02	39.5±2.6	18.8±1.2
33	316.7±59.8	0.2125±0.02	38±0.3	18.1±0.1
34	430.1±207.8	0.233±0.1	62.8±3.5	3.1±0.2
35	301.5±19.6	0.095±0.12	45.2±4	21.5±1.9
36	463.5±123.4	0.246±0.03	60.9±4.5	19.2±2.1

Note: EE%: encapsulation efficiency %, DL: BSA loading.

	A1 A2	**B1 B2**	**C1 C2 C3**	**D1 D2 D3**	**E1 E2 E3**	**F1 F2 F3**	**G1 G2 G3**	**H1 H2 H3**
Range	0.73	6.31	0.57	6.88	2.3	0.78	2.02	2.66
Rank	7	2	8	1	4	6	5	3
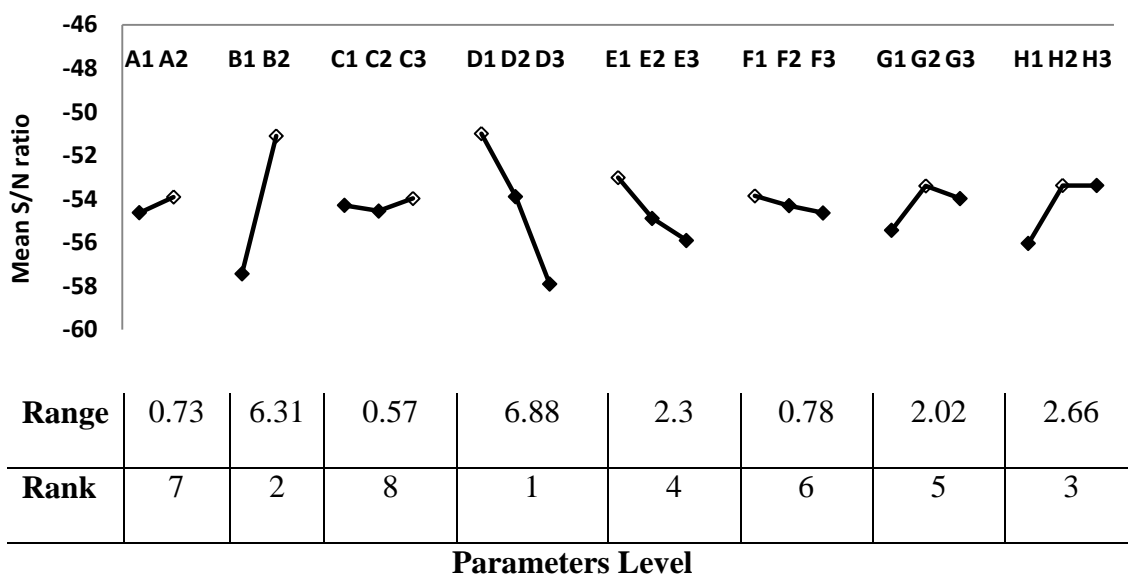
Parameters Level

Figure 3-6: Mean signal-to-noise (S/N) graph for particle size response. Letters (A-H) indicate the experimental parameters and numeric value indicates the parameter levels, ◊ indicate maximum S/N value, A: IAP volume, B: OP volume, C: BSA concentration, D: polymer mass, E: PVA concentration, F: IAP sonication time, G: EAP sonication time, H: sonication amplitude.

	A1 A2	**B1 B2**	**C1 C2 C3**	**D1 D2 D3**	**E1 E2 E3**	**F1 F2 F3**	**G1 G2 G3**	**H1 H2 H3**
Range	7.73	2.08	13.65	4.77	2.18	0.96	1.42	1.10
Rank	2	5	1	3	4	8	6	7
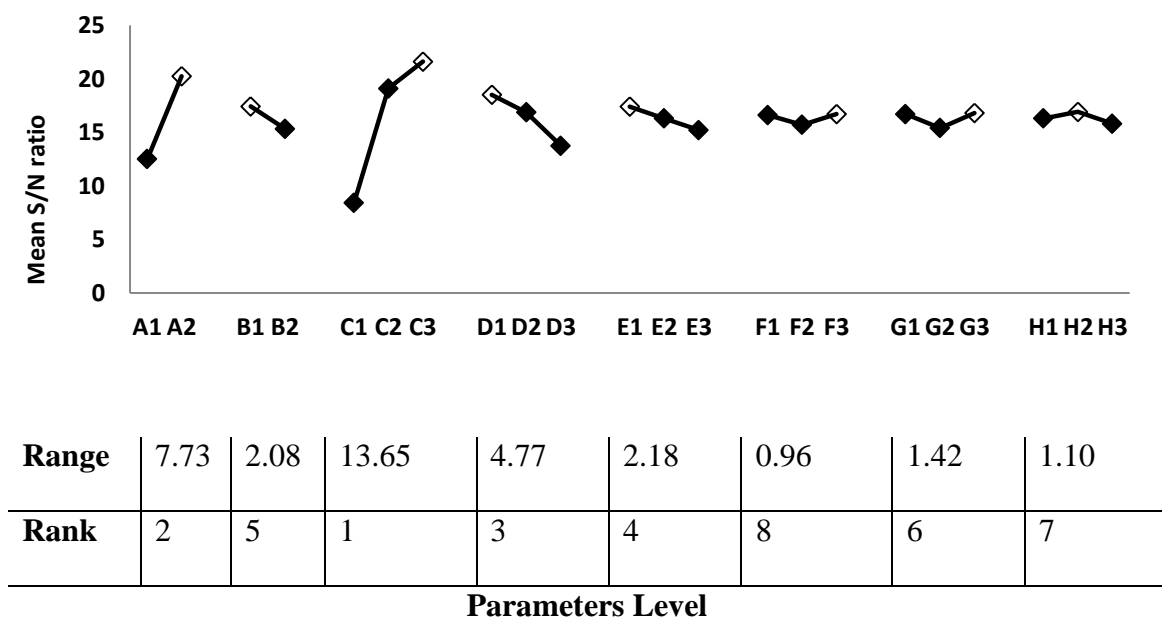
Parameters Level

Figure 3-7: Mean signal-to-noise (S/N) graph for BSA loading response. Letters (A-H) indicate the experimental parameters and numeric value indicates the parameter levels, ◊ indicate maximum S/N value, A: IAP volume, B: OP volume, C: BSA concentration, D: polymer mass, E: PVA concentration, F: IAP sonication time, G: EAP sonication time, H: sonication amplitude.

	A1 A2	B1 B2	C1 C2 C3	D1 D2 D3	E1 E2 E3	F1 F2 F3	G1 G2 G3	H1 H2 H3
Range	1.45	1.23	2.05	5.99	2.86	0.9	1.11	0.84
Rank	4	5	3	1	2	7	6	8
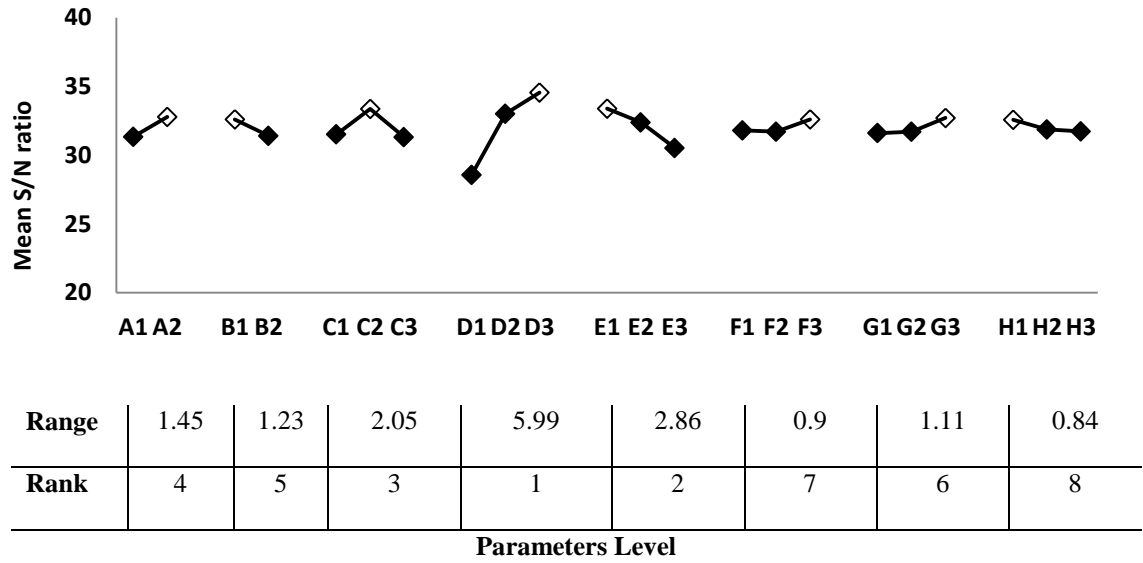
Parameters Level

Figure 3-8: Mean signal-to-noise (S/N) graph for EE% response. Letters (A-H) indicate the experimental parameters and numeric value indicates the parameter levels, ◊ indicate maximum S/N value, A: IAP volume, B: OP volume, C: BSA concentration, D: polymer mass, E: PVA concentration, F: IAP sonication time, G: EAP sonication time, H: sonication amplitude.

were A2B2C3D1E1F1G2H2. When the suggested optimized run was carried out the measured particle size obtained was 203±5.4 nm, which is lower than the minimum particle size of 216.2±39.9 nm prepared using run 29. The measured particle size obtained for unloaded SPS NPs was 224.4±10 nm. It is also worth to mention that the measured BSA loading of SPS NPs was 35.9±2.4 µg/mg using the indirect method. Also, when the direct method used to calculate DL, it was 30.02±8.1 µg/mg.

Regarding BSA loading and EE% the results (Table 3-5) of the present Taguchi design showed that DL ranged from 0.8±0.6 to 26.84± 5.8µg/mg and EE % ranged from 8.42 to 75.31%.

Based on the range, rank, and S/N response graph (Figure 3-7) for the production of HDL NPs using the Taguchi's "Larger-is-better" criterion in Minitab® 16 statistical software, the optimal conditions were A2B1C3D1E1F3G3H2. When the suggested optimized run was carried out the measured DL obtained was 43.67±2.3 µg/mg, which

is higher than the maximum DL of 26.8±5.8 µg/mg prepared using run 24. It is also worth to mention that the particle size of HDL NPs was 287±24.4 nm and for unloaded HDL NPs was 291.86±8.8 nm. Also, the drug loading measured using the direct method was 39.30±11.2 µg/mg.

The DL value calculated by the indirect method based on the assumption that there was no BSA loss during the preparation so this could explain the difference (non-significant, $p > 0.05$, ANOVA/Tukey's comparison) between the DL calculated by direct and indirect methods.

3.4.3. Optimization of the spray drying process

Spray drying was applied to incorporate the selected NPs formulation into NCMPs using L-leucine as a carrier and to enhance powder dispersion.

The Taguchi L_{27} orthogonal array design required 27 runs to be carried out to produce the optimum condition for each factor to achieve the highest yield % of dry powder.

Table 3-6 represents the structure of the Taguchi L_{27} orthogonal array design and the corresponding dry powder yield ranged from no yield to 49.78±0.17 %.

Figure 3-9 presents the mean S/N graph of the yield for each factor level. The factor with the largest range and corresponding rank (indicating the relative importance compared to other factors) was considered the critical factor affecting that yield.

Optimum conditions were suggested by high S/N ratios. Therefore, based on the range, rank, and S/N response graph for production of highest yield of dry powder using the Taguchi's "larger-is-better" criterion in Minitab 16 statistical software suggested combinations A1B3C3D2E1 (run H - Table 3-6) which produced dry powder yield of 50.96±2.26 %.

When the optimum condition carried out without the use of L-leucine there was no yield. Furthermore, when lactose used the yield was 13 % and when myo-inositol used the yield was decreased dramatically to 1 %.

Table 3-6: The experimentally measured value of yield % of NCMPs after spray drying. Data represent mean ± S.D., n=3.

Runs	Yield (%)
1	34.1±2.2
2	30.5±4.5
3	27.8±0.3
4	26.5±3.9
5	37.7±0.7
6	29.4±7.9
7	43.1±2.4
8	41.9±2.1
9	37±0.95
10	0.01±0
11	0.01±0
12	0. 01±0
13	49.8±0.2
14	41.2±0.1
15	40.8±3.5
16	38.2±1.2
17	33.3±0.8
18	26.6±1.2
19	48.6±2.5
20	35.8±2.7
21	35.7±3.1
22	0.01±0
23	0.01±0
24	0.01±0
25	38±1.1
26	21.9±0.9
27	24±1.5
H	50.9±2.3

Note: Numeric values 1-27 indicate experimental run number, H indicate optimum spray drying condition that produce highest yield %.
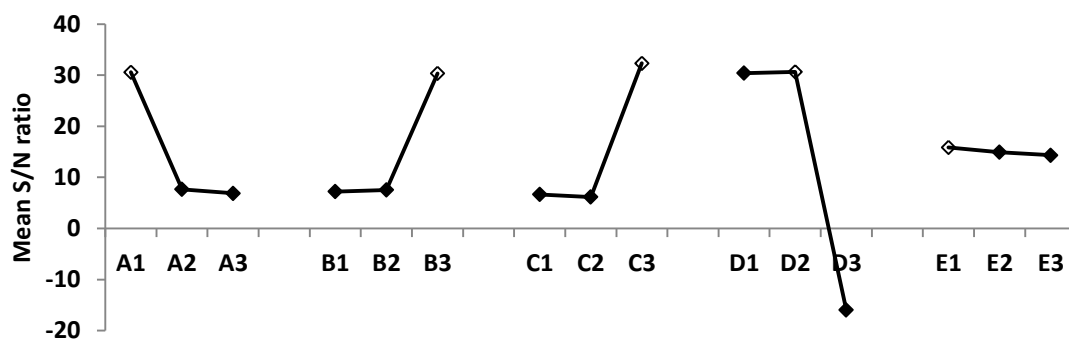
Range	23.69	23.12	26.16	46.59	1.53
Rank	3	4	2	1	5

Parameters Level

Figure 3-9: Mean signal-to-noise (S/N) graph for yield % response. Letters (A-E) indicate the experimental parameters and numeric value indicates the parameter levels, ◊ indicate maximum S/N value, A: airflow, B: inlet temperature, C: aspirator %, D: feed rate %, E: feed concentration.

The shape and surface texture of NCMPs were investigated using scanning electron microscopy (Figure 3-10). Photomicrographs of NCMPs showed irregular and porous microparticles. Figure 3-11 showed photomicrograph of run H.

From 27 spray-drying conditions run 16 and run H were selected for primary aerodynamic diameter calculation and *in vitro* aerosolisation studies. Run H had the highest yield while run 16 produced particles more porous in nature. So the selected HDL NPs and SPS NPs spray dried using run 16 and run H parameters to produce NCMPs. The formulations were given the following codes HDL 16 NCMPs, SPS 16 NCMPs, HDL H NCMPs, and SPS H NCMPs respectively.
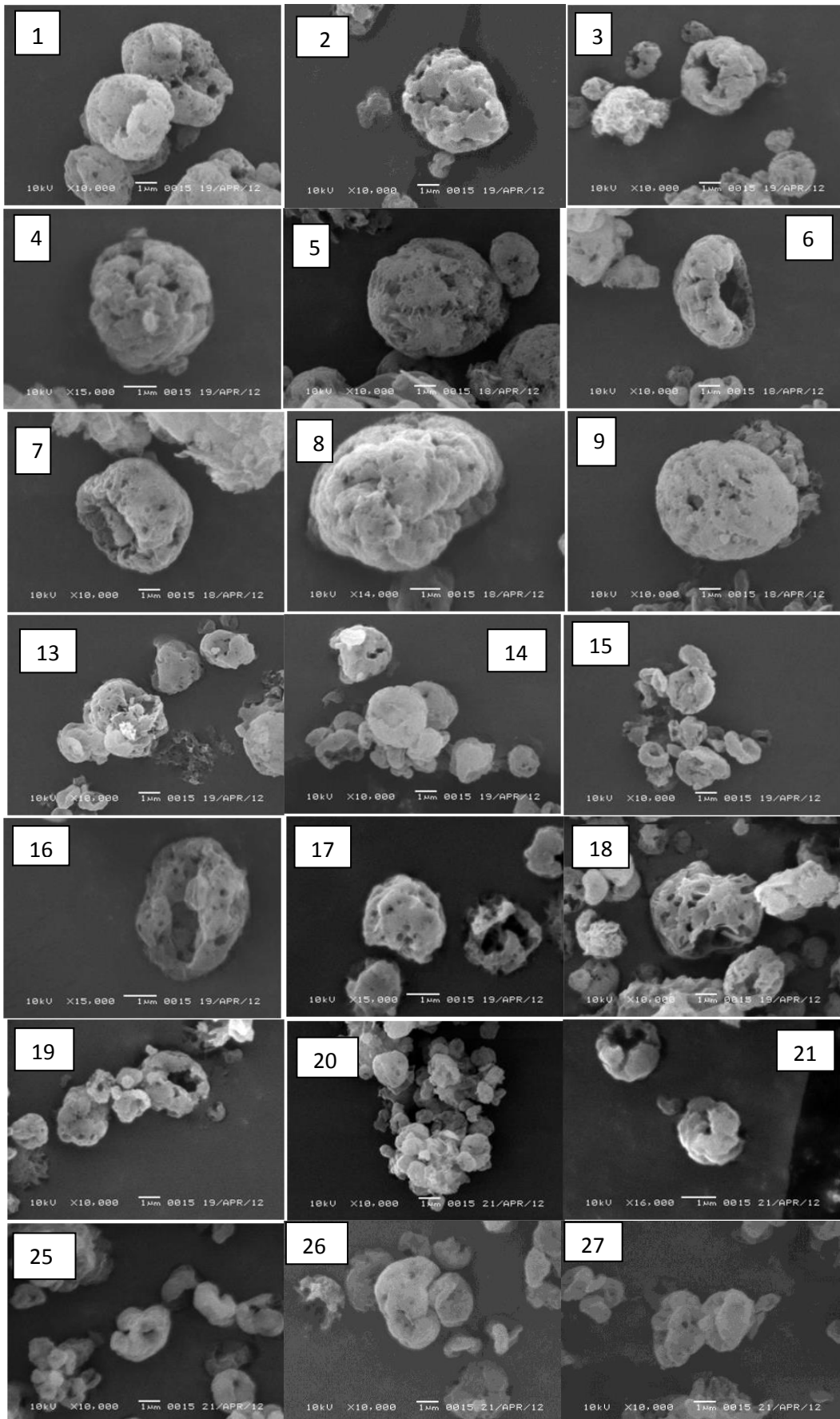
Figure 3-10: SEM images of NCMPs prepared by different spray drying conditions (numeric values 1-27 indicates run experimental number). The scale bar represents 1 μm.
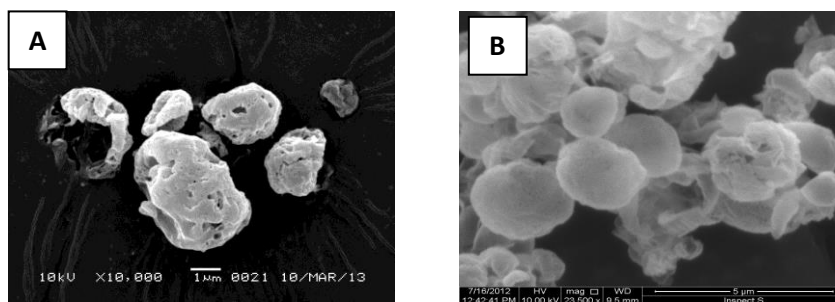
Figure 3-11: SEM images of NCMPs spray dried with run H (HDL H NCMPs) (A) and L-leucine alone spray dried with run H (B).

3.4.4. Powder density and primary aerodynamic diameter

NCMPs formulations had a geometric particle size between 1.23±0.07- 4.69±0.77 µm (Table 3-7) suitable for pulmonary delivery. The tapped densities of all formulations were similar (0.091±0.004–0.145±0.002 g cm^{-3}; Table 3-7) and were used together with the geometric particle size to calculate the theoretical aerodynamic diameter (d_{ae}). As shown in Table 3-7, the d_{ae} for all formulations was between 0.399±0.08– 1.71±0.30 µm.

Table 3-7: The geometric particle size, tapped density and theoretical aerodynamic diameter (d_{ae}) of spray-dried NCMPs. Data represent mean ± S.D., n=3.

NCMPs Formulation	Geometric particle size (µm)	Tapped density (g/cm^3)	d_{ae} (µm)
SPS 16 NCMPs	1.23±0.07	0.091±0.004	0.399±0.08
HDL 16 NCMPs	2.62±0.11	0.093±0.004	0.811±0.01
SPS H NCMPs	4.69±0.77	0.132±0.007	1.71±0.30
HDL H NCMPs	3.89±0.37	0.145±0.002	1.45±0.14

SPS 16 NCMPs, HDL 16 NCMPs: SPS NPs and HDL NPs spray dried using run 16.

SPS H NCMPs, HDL H NCMPs: SPS NPs and HDL NPs spray dried using run H.

3.4.5. *In vitro* aerosolisation studies for SPS and HDL nanocomposite microparticles

The percent mass of BSA recovered from the NGI was approximately 76 %, which is within pharmacopeia limit (75 − 125 %) of the average delivered dose (139). BSA deposition data obtained from NCMPs (Table 3-8) indicated there was no significant difference in FPD, FPF % and MMAD between SPS 16 NCMPs and SPS H NCMPs and between HDL 16 NCMPs and HDL H NCMPs (p>0.05, ANOVA/Tukey's comparison). But run H produced the highest yield% of powder (50%). So run H was applied as spray drying condition for the rest of this study. Formulations SPS H NCMPs and HDL H NCMPs were further investigated.

Table 3-8: The Fine particle dose (FPD), fine particle fraction (FPF), and mass median aerodynamic diameter (MMAD) of NCMPs. Data represent mean ± S.D, n=3.

Code	FPD (μg)	FPF (%)	MMAD (μm)	Yield %
SPS 16 NCMPs	49.12±12.5	70.97±4.7	1.5±0.40	36.0±2.7
HDL 16 NCMPs	59.26±6.00	79.60±7.0	1.6±0.20	38.2±1.2
SPS H NCMPs	38.04±2.80	64.32±1.6	1.49±0.13	46.4±7.9
HDL H NCMPs	45.00±7.40	78.57±0.1	1.71±0.10	50.9±2.3

SPS 16 NCMPs, HDL 16 NCMPs: SPS NPs and HDL NPs spray dried using run 16. SPS H NCMPs, HDL H NCMPs: SPS NPs and HDL NPs spray dried using run H.

3.4.6. In Vitro Release Studies

In vitro release studies comparing SPS H NCMPs and HDL H NCMPs formulations were performed (Figure 3-12). Both formulations showed biphasic release profiles with a first initial burst release followed by a second continuous sustained release phase over 48h. A significant difference (p<0.05, ANOVA/Tukey's) was noted in the release profile (24 − 48 h) of HDL H NCMPs and SPS H NCMPs, with HDL H NCMPs achieving 38.77±3% release after 48 h compared to SPS H NCMPs with (20.84±4.2%).

In this study, BSA was released from SPS H NCMPs and HDL H NCMPs formulations according to the Higuchi diffusion model (r^2 value of 0.981 and 0.955, respectively), and the release rate constant were $k_1 (h^{-1/2})$ 2.7021 and 5.3653, respectively (Table 3-9). Therefore, the sustained release of BSA from spray-dried NCMPs appears to be a diffusion-limited process. Accordingly HDL H NCMPs was selected for further investigation in this study.
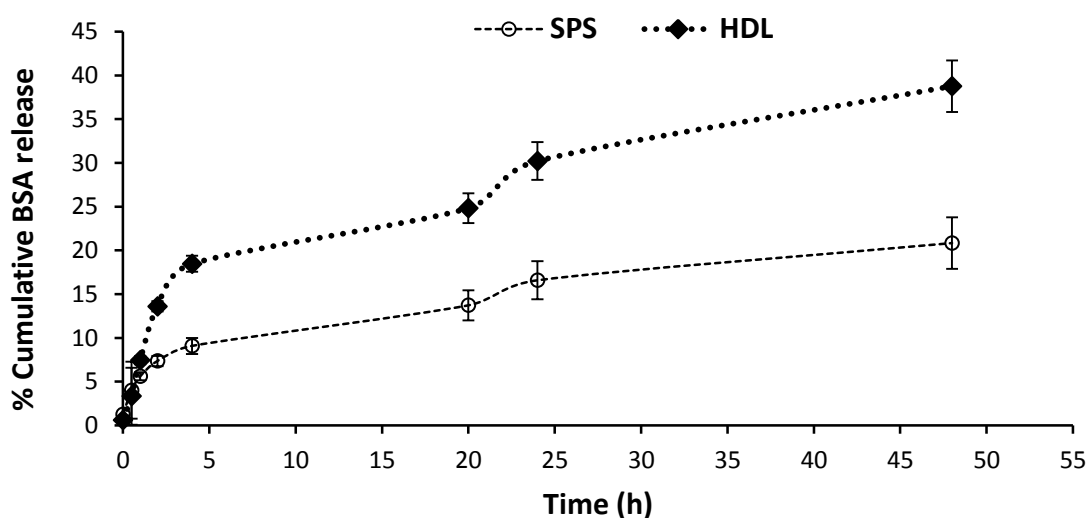
Figure 3-12: Cumulative *in-vitro* release of BSA from NCMPs in PBS buffer at 37°C. Data represent mean ± S.D., n=3.

Table 3-9: Release parameters of BSA from NCMPs.

Formulation	Zero Order		First order		Higuchi	
	r^2	$k_o (h^{-1})$	r^2	$k_1 (h^{-1})$	r^2	$k_1 (h^{-1/2})$
HDL H NCMPs	0.842	0.72	0.886	-0.004	0.955	5.3653
SPS H NCMPs	0.881	0.366	0.899	-0.0018	0.981	2.7021

SPS H NCMPs, HDL H NCMPs: SPS NPs and HDL NPs spray dried using run H.

3.4.7. Moisture content

The moisture content in HDL NCMPs was reported using TGA and the thermogram (Figure 3-13) demonstrates that the dry powder formulation had a residual moisture content of 0.2±0.03 % w/w.
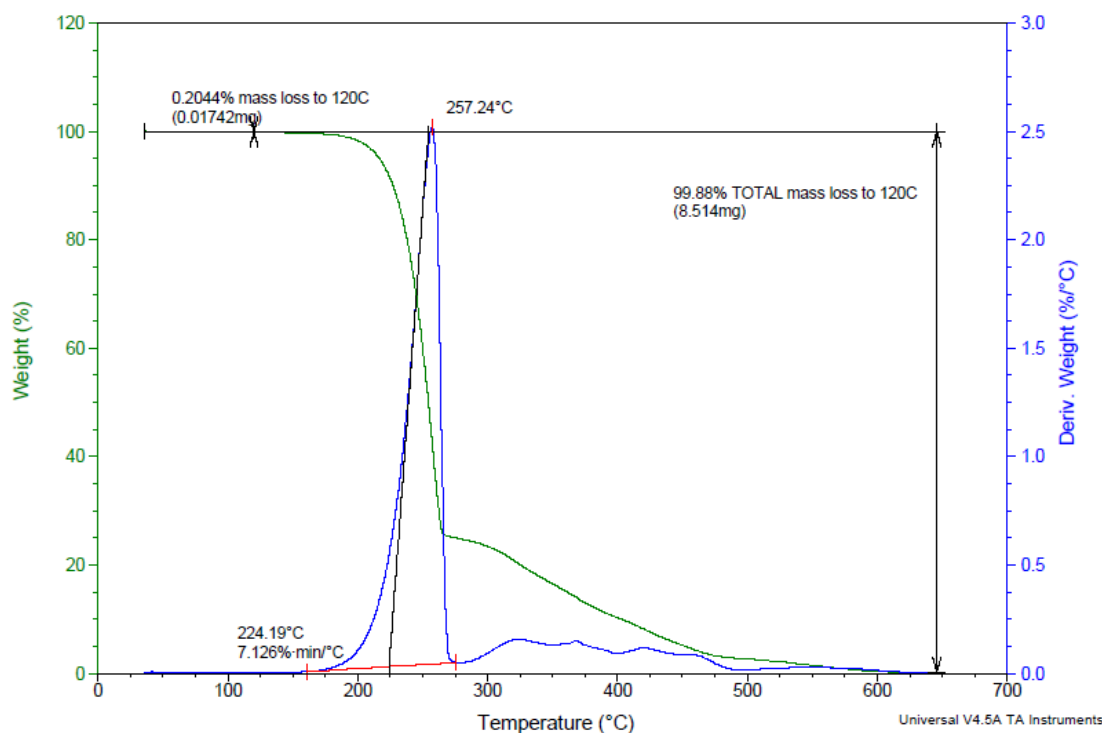
Figure 3-13: Thermogram of NCMPs reported using thermal gravimetric analysis.

3.4.8. Investigation of BSA structure

The primary structure of BSA released from NPs or NCMPs was analysed by SDS-PAGE followed by Coomassie brilliant blue staining. According to Figure 3-14, BSA standard and the molecular weight marker shown in Lanes 1 and 5, respectively, revealed a clear band at about 66 KDa. The BSA released from HDL NPs lanes 2 and from HDL H NCMPs lanes 3, and 4, respectively, also showed similar clear banding patterns to the BSA standard (Figure 3-14). The single lines in the gels provided

evidence that the BSA released did not suffer a significant covalent aggregation or fragmentation during the preparation methods used.
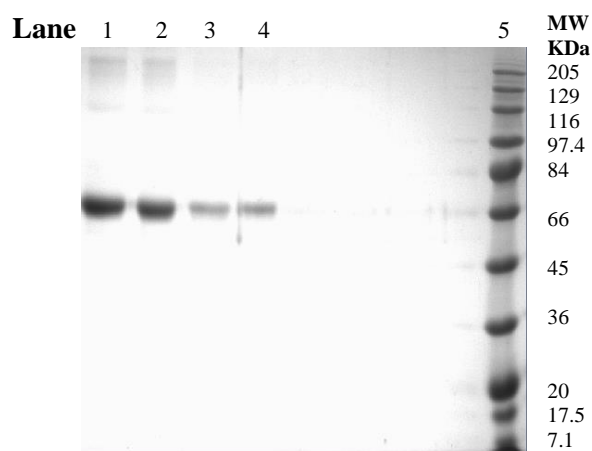
Figure 3-14: SDS-PAGE behaviour of BSA released for the assessment of BSA stability. Lanes represent, BSA standard (1), BSA released from HDL NPs (2), BSA released from HDL H NCMPs (3, 4), and molecular weight (MW) standard markers, BSA (MW 66,000), (5). Difference in band intensity was due to different loading.

The secondary structure of BSA was analysed using CD spectroscopy. Figure 3-15 shows CD spectra of the secondary structure of standard BSA and BSA released. The CD spectra present minima at 221 - 222 and 209 – 210 nm and a maximum at 195 nm for both samples, which is characteristic of an α-helical structure. In support of this data, structural analysis showed that BSA was predominantly helical displaying 51.5% helicity (Table 3-10), which is in good agreement with previous reports (140). Structural analysis of BSA released displayed double minima at 210 and 222 nm and a further spectra analysis showed a reduced level of α-helical conformation (*circa* 48.5% helical) (Table 3-10). Furthermore, a comparison of BSA released with standard BSA, showed that the α-helical content decreased by 3%, the β-sheet content increased by 3.5%, the turns content decreased by 2.5%, and the random coils' content increased by 2%, respectively.
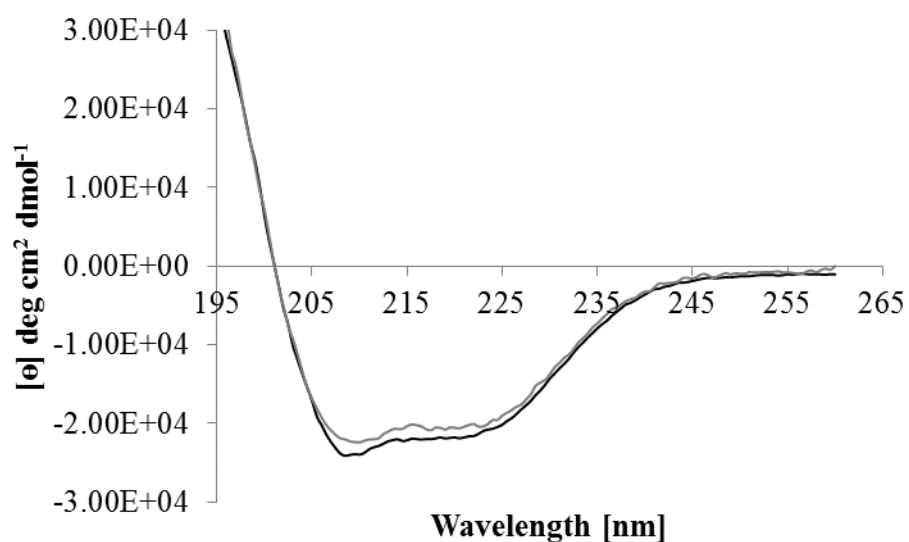
Figure 3-15: The CD spectra of BSA released from HDL NPs (grey) and BSA standard (black).

Table 3-10: The percentage of secondary structure conformation for BSA released from the selected formulation and BSA standard (means±SD, n=3).

Sample	Helix	Strands	Turns	Unordered
BSA standard	51.5 ± 0.007	21.50 ± 0.007	9.0 ± 0	17.50 ± 0.007
BSA released	48.50 ± 0.007	25.0 ± 0	6.50 ± 0.007	19.5 ± 0.007

3.4.9. Cytotoxicity study

The NPs and NCMPs appear to be well tolerated by the A549 cell line, with a cell viability of 77.7±19.6% for NPs and 79±4.7% for NCMPs (Figure 3-16) at 2.5 mg/ml concentration after 24 h exposure. There was no significant difference between cell viability of cells treated with NPs and cells treated with NCMPs ($p > 0.05$, ANOVA, Tukey's comparison). The cell viability study indicates a good toxicity profile.
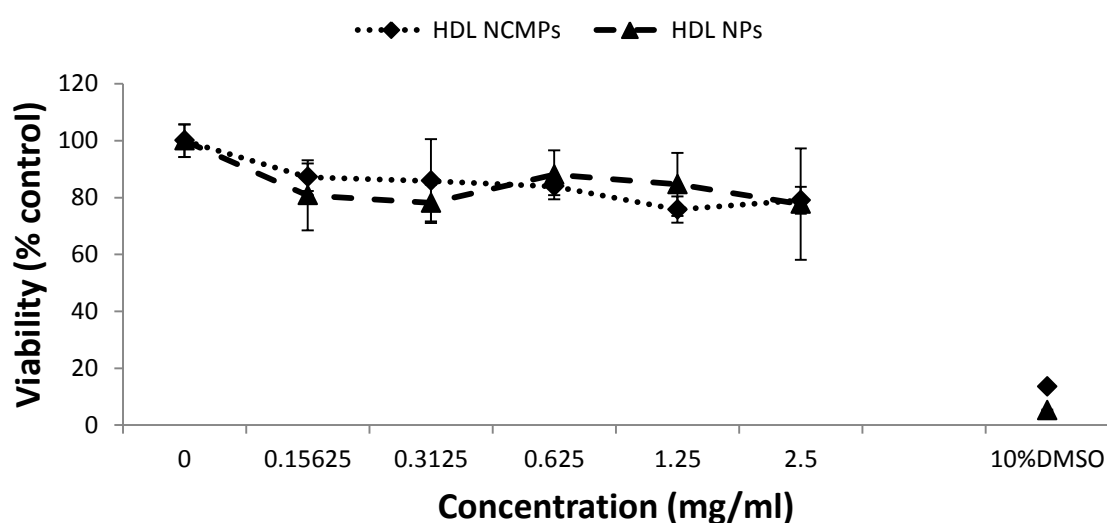
Figure 3-16: A549 cell viability measured by MTT assay after 24 h exposure to NPs and NCMPs. Data represent mean ± S.D., n=3.

3.5. Discussion

3.5.1. Preparation and characterization of NPs

The BSA loaded PGA-co-PDL NPs were prepared by a modified (w/o/w) double emulsion/solvent evaporation method (141). The aim of the Taguchi design was to determine the formulation parameters that have the greatest impact on the particles size, BSA encapsulation and loading within NPs and to optimise NPs formulation in term of particle size and BSA loading.

Also, Taguchi design uses orthogonal array saved time and decreased cost of experiments while reproducibility and consistency were maintained (142).

3.5.1.1. **Effects of the double emulsion solvent evaporation method parameters on the size of the nanoparticles**

Analysis of results following the Taguchi design indicated that the particle size of NPs was influenced by different parameters in the following order: polymer mass > OP volume > sonication amplitude>surfactant concentration> EAP sonication time and IAP sonication time > IAP volume > BSA concentration (Figure 3-6).

It can be seen that the polymer mass followed by the OP volume had the greatest influence on the particle size of NPs (i.e. rank 1 and 2, Figure 3-6). It could be noticed from Table 3-5, that four out of the thirty-six experimental runs (i.e. runs 3, 6, 9, and 23) had a particle size range of 1165.9 to 2168.9 nm These four runs shared a common parameters, which was 200mg polymer mass and 1 ml OP in the preparations. On the other hand, it could be seen from Table 3-5 that runs 10, 15, 18, 29, 32, and 35 had much smaller particle size ranging from 216.2 to 357.5 nm. These runs shared a common parameters, which was 50mg polymer mass and 2 ml OP in the preparations. In general, an increase in the mass of substances used will increase the particle size, and this was illustrated by the observation that the mass of PGA-co-PDL is the primary parameter responsible for the changes in particle size. This size increase was also observed with PLGA protein-loaded NPs or/and microparticles, when using a double emulsion solvent evaporation method (143). This effect of the polymer mass on the particle size can be attributed to the increased viscosity of the OP leading to a less efficient stirring of the medium and to increased NPs coalescence (144).

The third factor affecting particle size was sonication amplitude (i.e. rank=3, Figure 3-6) while EAP sonication time and IAP sonication time occupied the fifth and sixth rank, respectively (Figure 3-6). The rate of size reduction decreased considerably when sonication was carried out beyond the duration of 5 s for IAP or 15 s for EAP or above an amplitude of 45 %. For example, it could be noticed from Table 3-2 that runs

10 and 29 shared the important parameters: the polymer mass 50 mg, OP 2 ml and PVA concentration 10 % but differ in amplitude (65 % and 45 %, respectively) and duration of sonication for IAP (10 sec and 15 sec, respectively) and EAP (10 sec and 30 sec, respectively). These difference led to change in particle size measured (run 10: 375.5±102 nm and run 29: 216.2±39.9). Increasing amplitude lead to more fluid cavitation, this inhibited the efficiency of energy transmission and decreased the ultrasonic effect (145).

PVA concentration was directly proportional to size with 1< 5< 10% PVA (rank=4, Figure 3-6). For example, it could be noticed from Table 3-2 that runs 4 and 7 shared the important parameters (i.e. polymer mass 50 mg , OP 1 ml and sonication amplitude 45 %) but differ in PVA concentration (run 4: 1 % and run 7: 5%). This increase in PVA concentration led to increase in particle size (run 4:498.7±4.6 nm and run 7: 577.8±107.4 nm). This was associated with an increase in viscosity with an increase in PVA concentration from 1 to 5 or 10% of the IAP. This resulted in a reduced net shear stress, decreasing the diffusion speed and consequently increasing particle size. Moreover, further addition of PVA lead to an increase in NPs size because of the accumulation of excess molecules at the particle surface leading to bridging between the primary particles (146).

IAP volume and BSA concentration had minimum effect on the particle size of NPs (rank=7 and 8, respectively Figure 3-6) which have also been previously reported in literature (143). For example, it could be noticed from Table 3-2 that runs 16 and 36 shared the first 4 important parameters (i.e. polymer mass 100 mg, OP 2 ml, sonication amplitude 30 % and PA concentration 10%) but differ in BSA concentration and IAP volume (run 16: 0.2 % and 0.25 ml and run 36: 1 % and 0.5 ml, respectively). This change in BSA concentration and IAP volume led minimal change in particle size (run 16: 493.7±36.1 nm and run 36: 463.8±123.4 nm).

3.5.1.2. Effects of the double emulsion solvent evaporation method parameters on the loading of BSA

The loading capacity of NPs is a critical aspect as the higher the loading, the higher the bioavailability of drug per particle absorbed (143). A successful drug delivery system should have a high loading capacity in order to decrease the amount of drug and excipients used for manufacturing the delivery system. However, with proteins it is generally not necessary to achieve very high drug loading, because most therapeutic proteins are active at low doses (143). BSA loading expresses the ratio of the weight of BSA encapsulated to the weight of NPs.

The influence of different parameters on the DL of NPs had the following order: BSA concentration>IAP volume > polymer mass > PVA concentration > OP volume > EAP sonication time and IAP sonication time > sonication amplitude (Figure 3-7).

BSA concentration had the greatest influence on the DL (rank=1, Figure 3-7). The DL increased profoundly as the BSA concentration increased from 0.2 to 1%. This was expected from predictions based on equation 2-7 in which DL was positively proportional to the amount of BSA and also as reported in literature (143). For example, run 7 and run 18 shared three dominant factors affecting DL (i.e. rank 2, 3, and 4, Figure 3-7) which were IAP volume, polymer mass, and PVA concentration and differ in the BSA concentration (i.e. rank 1, Figure 3-7). The DL obtained when run 7 carried out was 4.1±0.6 µg/mg while run 18 produced NPs with DL 15.7±4.8 µg/mg. The difference in DL could be attributed mainly to the increased BSA concentration from 0.2 (run 7) to 1% (run 18).

IAP volume was the second factor affecting DL (i.e. rank 2, Figure 3-7), such that, the larger volume of the IAP the higher the BSA loading. This effect has been reported (141; 143; 147) and is thought to be due to a decrease in the concentration gradient between IAP and EAP. For example, run 13 and run 19 although they have an equal

BSA concentration (0.2 %) and polymer mass (100 mg) but differ in IAP volume (0.25 ml and 0.5 ml, respectively). The DL obtained with run 13 was 1.4±0.5 µg/mg and with run 19 was 5±0.1 µg/mg.

The third factor affecting DL was the polymer mass (rank=3, Figure 3-7). DL decreased substantially with increasing polymer mass from 50 to 100 to 200 mg, as predicted based on equation 2-7, in which DL is inversely proportional to the polymer mass (147). For example, run 22 and run 25 shared the predominant factors affecting DL (i.e. rank 1, and 2, Figure 3-7) which were BSA concentration and IAP volume and also have the equal PVA concentration and OP volume and differ in the polymer mass (rank= 3, Figure 3-7). The DL obtained with run 22 (polymer mass 100 mg) was 5.6±0.04 µg/mg and with run 25 (polymer mass 200 mg) was 2.8±0.1 µg/mg.

The factors that had the least effect on DL were PVA concentration, OP volume, sonication time of the EAP, sonication amplitude and sonication time of the IAP (i.e. rank= 4, 5, 6, 7, and 8, Figure 3-7).

Among the PVA concentrations used, 1% PVA was found to result in a considerably high BSA loading with no added benefit of any further increase in PVA concentration (5, and 10 %). For example, run 19 and run 22 shared the predominant factors affecting DL (i.e. rank 1, 2, and 3, Figure 3-7) which were BSA concentration, IAP volume and polymer mass and differ in the PVA concentration (1 and 5 %, respectively). The DL obtained were similar with run 19 was 5±0.1 µg/mg and with run 22 was 5.6±0.04 µg/mg. Similar observation was reported previously (148).

OP volume has an enhancing effect on DL of BSA (rank=5, Figure 3-7). The results showed that decreasing the OP volume increased DL. This could be explained by that increasing the viscosity of the OP lead to a further stabilization of the primary emulsion and lowering the diffusion of BSA through the OP (141).

Moreover, increasing the sonication time of IAP and EAP or increasing the sonication amplitude from 30 to 45 to 65% had almost no beneficial effect on the BSA loading. This has been reported previously and has been associated with BSA precipitation within the sonication probe due to high pressure and increased fluid cavitations during sonication (136; 149). For example, run 1 and run 4 shared the predominant factors affecting DL (i.e. rank 1, 2, 3, 4, and 5, Figure 3-7) which were BSA concentration, IAP volume, polymer mass, PVA concentration, and OP volume. The DL obtained with run 1 was 3.6±0.2 µg/mg and with run 4 was 2.4±0.4 µg/mg.

3.5.1.3. Effects of the double emulsion solvent evaporation method parameters on the encapsulation efficiency % of BSA

The EE % was studied because BSA is a hydrophilic compound which can easily diffuse into an EAP during the double emulsion solvent evaporation method (150).

The effect of different parameters on the EE% had the following order: polymer mass > PVA concentration > BSA concentration > IAP volume > OP volume > EAP sonication time and IAP sonication time > sonication amplitude (Figure 3-8). It is obvious from the ranking that the first four important factors affecting EE% and DL of BSA are the same but with a different order.

The polymer mass had the greatest influence on EE % of BSA. For example, run 11 and run 17 shared the predominant factors affecting EE % (i.e. rank 2, 3, 4 and 5, Figure 3-8) which were PVA concentration, BSA concentration, IAP volume, and OP volume and differ in the polymer mass (100 and 200 mg, respectively). The EE% obtained with run 11 was 52.1±7.2% and with run 17 was 69.1±2.6%. This could be correlated with the increased mass of the polymer resulting in a further stabilization of the primary emulsion and limiting the diffusion of BSA through and out of the OP due to higher viscosity of the OP (141; 151).

The second important factor affecting EE % of BSA was PVA concentration (i.e. rank=2, Figure 3-8). Among the PVA concentrations used, 1% PVA was found to result in a considerably high EE% of BSA. For example, runs 28, 31, and 34 shared the predominant factors affecting EE % (i.e. rank 1, 3, 4 and 5, Figure 3-8) which were polymer mass, BSA concentration, IAP volume, and OP volume and differ in the PVA concentration (5, 10 and 1 %, respectively). The EE% obtained were 53.6±0.4, 44.8±8.4 and 62.8±3.5 %, respectively. One possible explanation is that 1 % PVA concentration provides sufficient covering of the organic/aqueous interface so as to reduce possible leaching of the BSA. Consequently, any further increase in PVA concentration (5 and 10 %) resulted in more BSA molecules portioning into the aqueous phase during the emulsification procedure (129; 152).

BSA concentration was the third factor that affected EE % (i.e. rank= 3, Figure 3-8). The EE % of BSA increased when BSA concentration increased from 0.2 to 0.5% but interestingly it decreased as the BSA concentration increased further to 1%. For example, runs 19 and 27 shared the predominant factors affecting EE % (i.e. rank 1, 2, 4 and 5, Figure 3-8) which were polymer mass, PVA concentration, IAP volume, and OP volume and differ in the BSA concentration (0.2 and 1 %, respectively). The EE% obtained were 50.7±1 and 51.4±6.6 %, respectively. In fact, an increase in BSA concentration to high levels (1 %) is not always beneficial; this trend has been explained by the mass of polymer used being insufficient to completely encapsulate the BSA (143). Furthermore, higher concentration of BSA provide a higher BSA concentration in IAP droplets and thus increase the concentration gradient between the IAP droplets and the EAP and so increases the amount of BSA transported into the EAP (153; 154).

IAP volume was the fourth factor affecting EE % (i.e. rank=4, Figure 3-8), such that, the larger volume of the IAP the higher the BSA EE %. This effect has been reported previously (141; 143; 147) and is similar to those observed for DL. For example, run 13

and run 19 although they have an equal BSA concentration (0.2 %) and polymer mass (100 mg) but differ in IAP volume (0.25 ml and 0.5 ml, respectively). The EE% obtained with run 13 was 27.4±9.8 % and with run 19 was 50.7±1 %.

In contrast reducing OP volume has positive effect on EE % of BSA (rank=5, Figure 3-8). The results showed that reducing the OP volume increased EE %. This could be due to the higher viscosity of the OP leading to a further stabilization of the primary emulsion and minimizing the diffusion of BSA through the OP (141). For example, run 25 and run 28 shared the predominant factors affecting EE % (i.e. rank 1, 2, 3 and 4, Figure 3-8) which were polymer mass, PVA concentration, BSA concentration, and IAP volume and differ in the OP volume (1 and 2 ml, respectively). The EE% obtained were 56.8±2.9 and 53.6±0.4 %, respectively.

The sonication time of the IAP and EAP exerted similar effects on EE % (i.e. rank= 7 and 6, respectively, Figure 3-8). The results indicated that increasing the sonication time of IAP and EAP resulted in higher EE % (155). Walter *et al.* reported that when preparing PLGA microparticles the reduction in the sonication time of IAP from 20 to 10 s lead to decrease in EE% of DNA which may be due to the decrease in dispersion efficiency of the W/O emulsion (155).

Moreover, increasing the sonication amplitude from 30 to 45 to 65% had almost no beneficial effect on the BSA EE % (rank= 8, Figure 3-8). This has been reported previously and has been associated with BSA precipitation within the sonication probe due to high pressure and increased fluid cavitations during sonication (136; 149).

For example, run 14 and run 17 shared the predominant factors affecting EE % (i.e. rank 1, 2, 3, 4 and 5, Figure 3-8) which were polymer mass, PVA concentration, BSA concentration, IAP volume and OP volume with different sonication amplitude and time. The EE% obtained were 62.9±4.6 and 69.1±2.6 %, respectively.

3.5.1.4. Optimized Conditions for BSA-loaded PGA-co-PDL nanoparticles prepared by double emulsion solvent evaporation method

A precise adjustment of the various formulation and processing parameters is important to obtain NPs of a desired size and BSA loading. In this study, a particle size of ≤ 500 nm was desired to facilitate uptake of NPs by DCs (43; 98; 156) and at least 30 µg/mg proteins loading to be suitable for dosage purpose when the protein of interest, PspA, is used (30; 35; 157).

Optimum conditions were suggested by high S/N ratios. The greater the S/N ratio, the smaller is the variance of target (particle size and BSA loading) around the desired value. When the suggested optimized run was carried out the measured particle size obtained 203±5.4 nm was considered suitable for DCs uptake (158; 124; 159).

Concerning the DL, the suggested optimized run produced NPs (HDL NPs) with DL 43.67±2.3 µg/mg which is considered suitable for vaccination (7; 26; 160).

When the DL was determined using the direct method for both SPS and HDL NP there was no significant difference although the DL value decreased in comparison with indirect method.

3.5.2. Optimization of the spray drying process

Spray-drying was applied to incorporate the selected HDL NPs into NCMPs using L-leucine as a carrier and to enhance powder dispersion.

Most of the runs produced low yields (Table 3-6) due to the difficulties in dry powder collection associated with condensation inside the drying chamber and collecting vessel and the sticking tendency of dry powder to the walls of the drying chamber and collecting vessel so cannot be collected efficiently (161). Utilizing the Taguchi design revealed that the feed rate, aspirator capacity, air flow, and inlet temperature had the greatest effects on the yield of dry powder while the change in the concentration of total

solid in the spray dried suspension showed no improvement in the yield of dry powder (Figure 3-9).

The most important factor was feed rate with a negative effect on powder yield % (rank = 1, Figure 3-9). At higher feed rates of 15%, the atomizing air may not be able to break the liquid flow. Consequently, insufficient atomization and drying may cause deposition of a large amount of NCMPs on the walls of the drying chamber and the cyclone separator (161). Similar observation was reported by Motlekar *et. al.* (161). They found that the high feed rate (25 %) of the spray suspension lead to almost no yield of dry powder (161).

The second important factor was aspirator capacity (i.e. rank=2, Figure 3-9). A high aspirator flow rate created greater centrifugal force leading to an increase in the collection efficiency (162). Airflow was the third factor affecting dry powder yield (i.e. rank=3, Figure 3-9). Higher spray flow produced smaller droplet so collected less efficiently by the centrifugal force (162).

Shi and Hickey optimised spray drying condition to prepare PLGA microparticles suitable for inhalation. They found that the airflow and aspirator capacity had significant effect on the yield of dry powder. Where the airflow had negative effect, showing that powder yield decreased with the increase of the airflow while the aspirator capacity had positive effect, showing that powder yield increased with the increase of the aspirator capacity (162).

The inlet temperature of drying air ranged from 50 to 100 ℃ typically resulting in the spray dryer outlet temperature of approximately 22 to 46 ℃, respectively. The inlet temperature of drying air had considerable effects on the yield of dry powder (rank=4, Figure 3-9). It was noticed that as inlet temperature increased from 50 to 100 ℃ this resulted in an increased powder yield. It has been reported that high inlet temperature can reduce the drying time and inhibit particle aggregation (163). Furthermore, a higher

inlet temperature promotes a decrease of residual moisture by enhancing water evaporation resulting in less particles stick in the drying chamber (164).

Also, it was observed that the change in the concentration of total solid in the spray dried suspension showed no improvement in the yield of dry powder. This observation was in contrast to the results reported by Jensen *et al.* were they found that as the concentration of solid in the suspension increased the yield of dry powder increased (92).

It could be noticed from Table 3-6 that runs 10, 11, 12, 22, 23, and 24 had no yield. They shared the predominant factor (i.e. rank=1, Figure 3-9) affecting yield which is feed rate although they differ in other factors which are aspirator capacity, air flow and inlet temperature (Table 3-4). The feed rate was 15 % at this high rate the atomizing air may not be able to break the flow of the suspension also this high feed rate accompanied by lower level of aspirator capacity (50 and 75%), higher level airflow (535 and 670 L/h) and lower level of inlet temperature (50 and 75 ˚C). At these levels these factors had negative effect on yield as explained above. When these parameters adjusted to their positive level in run 7, 8, and 9 (i.e. level that produced higher yield, Table 3-4 and Table 3-6) the yield increased up to 43 %.

Optimum conditions used for the production of highest yield% (Table 3-4) of dry powder resulted in 50.96±2.26 % of NCMPs which was considered reasonable (92).

Photomicrographs of NCMPs (Figure 3-10) showed irregular and porous microparticles. This occurred due to an excessive build-up of vapour pressure during water evaporation in the spray drying process and typically occurs with hydrophobic amino acids, such as L-leucine, for improved aerosolisation performance (66; 134; 165; 166; 167; 168; 169; 170).

From 27 spray-dried formulations run 16 and run H were selected for *in vitro* aerosolisation studies. Run H had the highest yield % while run 16 produced particles

more porous in nature as presented by SEM photograph and the tapped density suggesting highly porous particles (66).

SPS H NCMPs and HDL H NCMPs formulations had a geometric particle size double of that obtained with SPS 16 NCMPs and HDL 16 NCMPs (Table 3-7). This could be due to the difference in the airflow between the run H and run 16 (400 and 535 L/h, respectively). The higher airflow produces smaller droplet size and enhancing evaporation rate and thus produces smaller particle size. This observation was reported previously with PLGA microparticles prepared by spray drying as the airflow increased the particle size decreased (162).

The theoretical aerodynamic diameters (Table 3-7) of tested formulation HDL H NCMPs, SPS H NCMPs, HDL 16 NCMPs, and SPS 16 NCMPs indicate that the spray dried NCMPs generated are suitable for pulmonary delivery.

3.5.3. *In vitro* aerosolisation and moisture content studies

BSA deposition data obtained from spray-dried formulations indicated similarity in aerosolisation performance between run 16 and run H for FPD, FPF % and MMAD (Table 3-8). SPS 16 NCMPs and HDL 16 NCMPs produced higher FPD and FPF % and this was attributed to the more porous structure of the NCMPs prepared by run 16 (134; 165). In run 16, the aspirator capacity was adjusted to 50 % which is lower than the aspirator capacity of run H (100 %). Consequently this resulted in a slower movement of the particles through the system and a longer action of the drying air upon them (171). Moreover, in run 16 the air flow was adjusted to a higher value (535 l/h) than for run H (400 l/h) which resulted in a smaller droplet size to which amphiphillic small leucine molecules can easily diffuse (163). However, the conditions associated with run H produced significantly greater yield hence run H conditions were applied for spray drying for the rest of this study.

Therefor high residual moisture content can promote particle aggregation leading a variation in particle size distribution (157). The low moisture content reported from the TGA thermogram presents a good drying efficiency therefor the dry powder formulations (HDL H NCMPs) are likely to show high storage stability.

3.5.4. *In Vitro* Release, structure stability of BSA, and cytotoxicity studies

In vitro release studies comparing SPS H NCMPs and HDL H NCMPs formulations were performed in PBS (pH=7.4). Both formulation showed biphasic release profile with a first initial burst release followed by a second continuous sustained release phase over 48h (Figure 3-12). The noticeable change in release profile at 24h after the initial burst release could be due to the distribution of BSA inside NPs or a change in degradation rate due to changed surface porosity.

In this study, BSA was released from SPS H NCMPs and HDL H NCMPs formulations according to the Higuchi diffusion model (Table 3-9). Therefore, the sustained release of BSA from spray-dried NCMPs appeared to be a diffusion-limited process.

Accordingly from *in vitro* aerosolisation and release studies HDL H NCMPs was selected for further investigation in this study.

The primary structure of BSA released from HDL NPs and HDL H NCMPs was analysed by SDS-PAGE followed by Coomassie brilliant blue staining. The BSA released showed similar clear banding patterns to the BSA standard providing evidence that the released BSA did not suffer a significant covalent aggregation or fragmentation during the preparation methods used (Figure 3-14).

The secondary structure of BSA in the formulation was analysed using CD spectroscopy, a valuable technique for analysing protein structure (115). CD of the BSA released samples (Figure 3-15) confirmed the presence of α-helix and β-sheets although these were slightly decreased in comparison with standard BSA (140; 172). But, in

protein secondary structure, this decrease (3%) considered minor and it is believed that the β-sheet structure is sometimes noticed as a special α-helix only with two amino acid residues through stretching resulting from the breakage of hydrogen bond (140; 172).

The aerosolisation data suggests a deposition mainly in the deep lung region thus cytotoxicity studies were performed on A549 cell line (adenocarcinomic human alveolar basal epithelial cells). The NPs and NCMPs appear to be well tolerated by the cells.

3.6.   Conclusion

PGA-co-PDL NPs with appropriate size (203±5.4 nm) to target DCs and therapeutic BSA loading (43.67±2.3 µg/mg) were successfully prepared using the Taguchi L_{36} orthogonal array design of experiment. The selected NPs formulations were incorporated into NCMPs using L-leucine as a carrier and to enhance powder dispersion. The highest yield % of dry powder (50%) was obtained using the Taguchi L_{27} orthogonal array design of experiment. The NCMPs had irregular and porous surface. The *in vitro* release studies showed BSA maintains its primary and secondary structure. Furthermore, aerosolisation deposition data (FPF 78.57±0.1 % and MMAD 1.71±0.1 µm) indicates deep lung deposition. Cell viability studies on A549 cells and DCs showed a low toxicity profile. This study suggests that PGA-co-PDL NCMPs should be further investigated for modification of particle surface to improve uptake by DCs and to encapsulate PspA as a therapeutic antigen to be delivered through the lung.

4. Pulmonary Delivery of Nanocomposite Microparticles Containing Model Protein Loaded Cationic nanoparticles via Inhalation

4.1. Introduction

Pulmonary vaccine delivery has recently been explored as an alternative for parenteral immunization. The extensive network DCs lining the respiratory submucosa and on the alveolar surface plays important roles in generating both mucosal and systemic immune responses (52).

The surface charge of NPs plays an important role in determining uptake of NPs by DCs and cationic particles have been shown to be more effectively taken up by DCs (75; 87; 88; 41). The ionic interaction between the positive charge on the particles surface and the negative charge on cell surface generates a successful bond and promotes particle uptake (87). Furthermore, cationic NPs have greater ability to interact with the proteoglycans on the surface of macrophages and DCs (173).

Incorporation of cationic polymers such as chitosan or chitosan derivatives have been shown to enhance the uptake of antigens by DCs and subsequently induce strong immune responses (174). Recently published researches on the use of chitosan and its derivatives as mucosal vaccine delivery systems are summarised in Table 4-1. Thomann-Harwood *et al.* have reported that chitosan nanogels carrying a model antigen, ovalbumin, have a higher association of the positively charged nanogel compared with the more neutral (mannosylated alginate coated) or negatively charged (alginate coated) nanogels (175). Also, Slütter *et al.* have demonstrated that N-trimethyl chitosan (TMC) NPs were superior over PLGA NP and PLGA/TMC NP in stimulating the maturation of DCs after nasal administration (156).

Many research groups have documented techniques of modifying NPs charge by using didodecyldimethylammoniumbromide (DMAB) as a surfactant (173; 176; 177). Jensen *et al.* have demonstrated that addition of cationic lipid dioleoyltrimethylammoniumpropane (DOTAP) into PLGA matrix during preparation of NPs resulted in cationic NPs and they further showed the use of these NPs loaded with

small interfering RNA prepared as a dry powder of RNA NPs for pulmonary delivery
(178).

Table 4-1: Recently published studies on Chitosan and chitosan derivatives as mucosal vaccine deliver systems.

Polymer	Antigen	Delivery system	Model	Route	Ref.
Chitosan	Bacillus anthracis protective antigen	Nanoparticles	*In vivo*	Nasal	(179)
Chitosan	measles antigen	Nanoparticles	*In vivo*	Oral	(180)
Chitosan	PsaA protein	Nanoparticles	*In vivo*	Intranasal	(181)
Chitosan	Human papillomavirus	Nanoparticles	*In vivo*	Intranasal	(182)
Mannose/ chitosan	Pseudomonas aeruginosa protein	Microspheres	*In vivo*	Intranasal	(183)
Chitosan/gold	Tetanus toxoid	Nanoparticles	*In vivo*	Oral	(184)
Chitosan	Influenza whole virus	Nanospheres	*In vivo*	Nasal	(185)
Chitosan	Yeast-derived PCV2 virus-like particles	Microparticles	*In vivo*	Oral	(186)
Chitosan	Recombinant enterovirus 71	Mixture	*In vivo*	Oral	(187)
Glucomannosylated chitosan	Tetanus toxoid	Nanoparticles	*In vitro*	Oral	(188)
Chitosan	DNA	Complex	*In vivo*	Intranasal	(189)
Chitosan	CPE30 peptide, C terminal 30 amino acids of clostridium perfringens enterotoxin	Nanoparticles	*In vivo*	Oral	(190)
Glycol chitosan	Hepatitis B surface antigen	Nanoparticles	*In vivo*	Intranasal	(191)
N-trimethylamino-ethylmethacrylate chitosan	Thiolated ovalbumin	Soluble conjugate	*In vivo*	Intranasal	(192)
Chitosan	Recombinant HIV-	Solution	*In vivo*	Intranasal	(193)

	1 envelope glycoprotein and tetanus toxoid			and sublingual	
Mannosylated chitosan	DNA	Nanoparticles	*In vivo*	Intranasal	(194)
Chitosan	DNA	Solution	*In vivo*	Intranasal	(195)
Glucomannosylated chitosan	Model antigen	Nanoparticles	*In vivo*	Oral	(196)
Chitosan	Diphtheria toxoid	In situ forming gel	*In vivo*	Intranasal	(197)
Chitosan	hemagglutinin (HA)-split influenza virus product	Nanoparticles	*In vivo*	Intranasal	(198)
PLGA/Chitosan	membrane protein B of Brachyspira hyodysenteriae	Microparticles	*In vivo*	Oral	(199)
Chitosan	high-mobility group box 1	Microparticles	*In vivo*	Intranasal	(200)
Chitosan/liposome	DNA	Nanoparticles	*In vivo*	Intranasal	(201)
Chitosan	P1-P30 chimeric recombinant protein	Solution	*In vivo*	Intranasal	(202)
PLGA/Chitosan	Model antigen	Nanoparticles	*In vivo*	Intranasal	(203)
PLGA/Chitosan or glycol chitosan	Hepatitis B surface Antigen	Nanoparticles	*In vivo*	Intranasal	(204)
Chitosan	Hepatitis B.	Nanoparticles	*In vivo*	Oral	(205)
Methylated N-(4-N,N-dimethylaminocinnamyl) chitosan-	Ovalbumin	Microparticles	*In vivo*	Oral	(206)
Chitosan	Ovalbumin	Microparticles	*In vivo*	Intranasal	(207)
Chitosan and trimethyl chitosan	Hepatitis B surface antigen	Nanoparticles	*In vivo*	Intranasal	(208)
N-[(2-hydroxy-3-trimethylammonium) propyl] chitosan chloride and α, β-glycerophosphate	adenovirus based Zaire Ebola virus glycoprotein antigen	hydrogel	*In vivo*	Intranasal	(209)

Here, we focused on the use of natural polymer chitosan and its derivatives. Chitosan is a biodegradable, biocompatible, cationic polysaccharide, with low toxicity and can be formulated in a number of different ways, as a solution, gel, powder, microparticles and nanoparticles. The potential application of chitosan is restricted by its low aqueous solubility but it can be chemically modified to enhance polymer processing, solubility, antimicrobial activity, and the ability to interact with other substances (71).

Recently, water-soluble chitosan hydrochloride (CHL) has been reported as a model positively charged polyelectrolyte, which may overcome the low water solubility of chitosan at neutral pH (210). However, like other cationic polymers, the strong positive charge contributes to the toxicity of the polymer. The amount of CHL can be substantially decreased by adsorbing CHL to anionic NPs. This is particularly true due to the large surface-to-volume ratio of the NPs (111). These cationic NPs could be incorporated into microparticles to produce cationic NPs/NCMPs with an aerodynamic size between 1 and 5 μm which upon inhalation can deposit deep in the lung and have access to the alveoli and the broncho associated lymphoid tissue (BALT) and are, therefore, attractive antigen carriers (52).

PGA-co-PDL has previously been used to produce NPs with negative surface charge (as described in section 2.2.3 and chapter 3) utilising PVA as a surfactant.

4.2. Aim

The aim of this study was to adsorb CHL onto PGA-co-PDL NPs with encapsulated BSA as a model protein, and optimize the preparation method and formulation parameters: particle size and zeta potential. The cationic NPs were incorporated into microcarriers (L-leucine) via spray drying to produce cationic NPs/NCMPs suitable for pulmonary delivery via DPIs.

To obtain the aim of the study a systematic study was designed considering the following aspects:

109

1.   Formulation of cationic NPs using double emulsion solvent evaporation technique.

2.   Evaluation of the influence of formulation parameters on the particle size and charge.

3.   Formulation of cationic NPs/NCMPs via spray drying technique.

4.   Examination of BSA integrity, *in vitro* aerosolisation performance, *in vitro* release, *in vitro* cells toxicity of optimum cationic NPs/NCMPs.

4.3.   Methods

4.3.1. Cationic nanoparticle preparation

The adsorption of CHL was achieved as described in section 2.2.4.

4.3.2. Cationic nanoparticle characterization

The cationic NPs were characterised for particle size, PDI, zeta potential, encapsulation efficiency and protein loading as described in sections 2.2.7.1 and 2.2.7.2 respectively.

4.3.3. Quantification of chitosan hydrochloride adsorption

The amount of CHL adsorbed on the surface of cationic NPs was evaluated as described in section 2.2.5.

4.3.4. Adsorption isotherm models

The adsorption mechanism of CHL on NPs was determined as described in section 2.2.6.

4.3.5. Chitosan   Hydrochloride   nanocomposite   microparticles preparation by spray drying

Cationic NPs/NCMPs were prepared by spray drying cationic NPs using the spray drying conditions for run H as described in section 2.2.8.

4.3.6. Characterization of Chitosan Hydrochloride nanocomposite microparticles

Cationic NPs/NCMPs morphology, yield %, moisture content and powder density and primary aerodynamic diameter were characterised as described in section 2.2.9.

4.3.7. *In vitro* aerosolisation studies

The *in vitro* aerosolisation studies were carried out as described in section 2.2.10.

4.3.8. *In vitro* release study

The *in vitro* release studies were carried out as described in section 2.2.11.

4.3.9. Investigation of BSA structure

The stability of the primary and secondary structure of released BSA was evaluated as described in section 2.2.12.

4.3.10.   Cytotoxicity study

The cytotoxicity of cationic NPs and cationic NPs/NCMPs was determined as described in section 2.2.15.1.

4.4.   Results

4.4.1. Cationic nanoparticles characterisation

4.4.1.1.   Effect of different concentrations of CHL and PVA on particle size and zeta potential

The adsorption of CHL on NPs was carried out using two strategies: the first after the formation of NPs and resuspending in CHL solution the second during the preparation of NPs with CHL added to EAP.

In the first strategy, different concentrations of CHL were used with and without 1% PVA. When 1% PVA was used the zeta potential significantly changed from negative (-17.44±1.3 mV) to around neutral (0.06±0.34 to -0.71±0.63 mV) (Figure 4-1.A)

regardless of CHL concentration (p < 0.05, ANOVA/Tukey's comparison). The particle size (445±46.87 nm) increased significantly (p < 0.05, ANOVA/Tukey's comparison) when the CHL concentration increased to 4, 8 and 30 mg/ml (Figure 4-1.B). However, at a CHL concentration of 20 and 34 mg/ml there was no significant (p > 0.05, ANOVA/Tukey's comparison) change in particle size (Figure 4-1.B).

When PVA was not included during the NPs preparation, the zeta potential was neutral at lower CHL concentrations of 4 and 8 mg/ml (p < 0.05, ANOVA/Tukey's comparison) while at higher CHL concentrations of 20 and 30 mg/ml the zeta potential was positive 11.79±2.5 and 16.73±0.98 mV respectively (p < 0.05, ANOVA/Tukey's comparison) (Figure 4-1.A). At the highest concentration of CHL 34 mg/ml the NPs surface charge once again became neutral.

The particle size increased significantly when the concentration of CHL increased to 4, and 8 mg/ml (Figure 4-1.B). However, at higher concentrations of CHL (20, 30 and 34 mg/ml) there was no significant (p>0.05, ANOVA/Tukey's comparison) difference in particle size at different concentration of CHL but it was significantly (p<0.05, ANOVA/Tukey's comparison) larger than the anionic NPs (Figure 4-1.B).

In order to use lower amount of CHL concentration of 20 mg/ml was selected to investigate the effect of PVA% on zeta potential and particle size.

Figure 4-2.A and B shows the effect of % PVA added to the CHL solution (20 mg/ml) on particle size and zeta potential of NPs. Three concentrations of PVA were compared 0, 0.5, and 1%.

Anionic NPs had a negative surface charge (-17.44±1.2 mV) but following the addition of CHL (20 mg/ml) with various amount of PVA the zeta potential changed significantly (p < 0.05, ANOVA/Tukey's comparison) from negative (-17.44±1.3 mV) to positive (11.8±2.5 mV) then neutral (-0.41±0.89 M). When the PVA concentration

was 0 and 0.5%, the particle size showed significant difference ($p < 0.05$, ANOVA/Tukey's comparison) from anionic NPs (Figure 4-2 B).
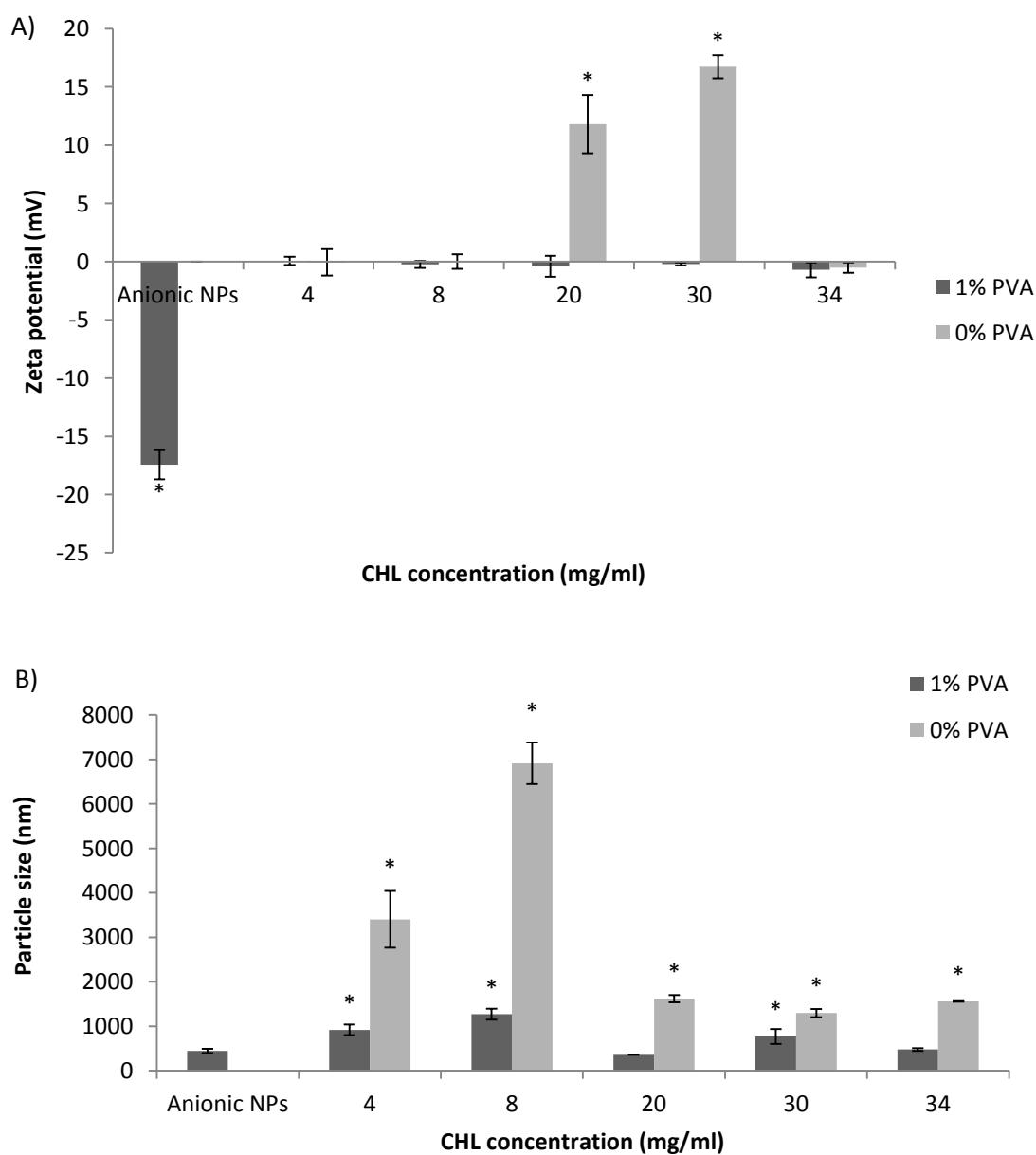
Figure 4-1: Effect of CHL (mg/ml) concentration on: A) zeta potential and B) particle size of NPs. Data represent means ±SD, n=3,* is $p < 0.05$, ANOVA/Tukey's comparison.
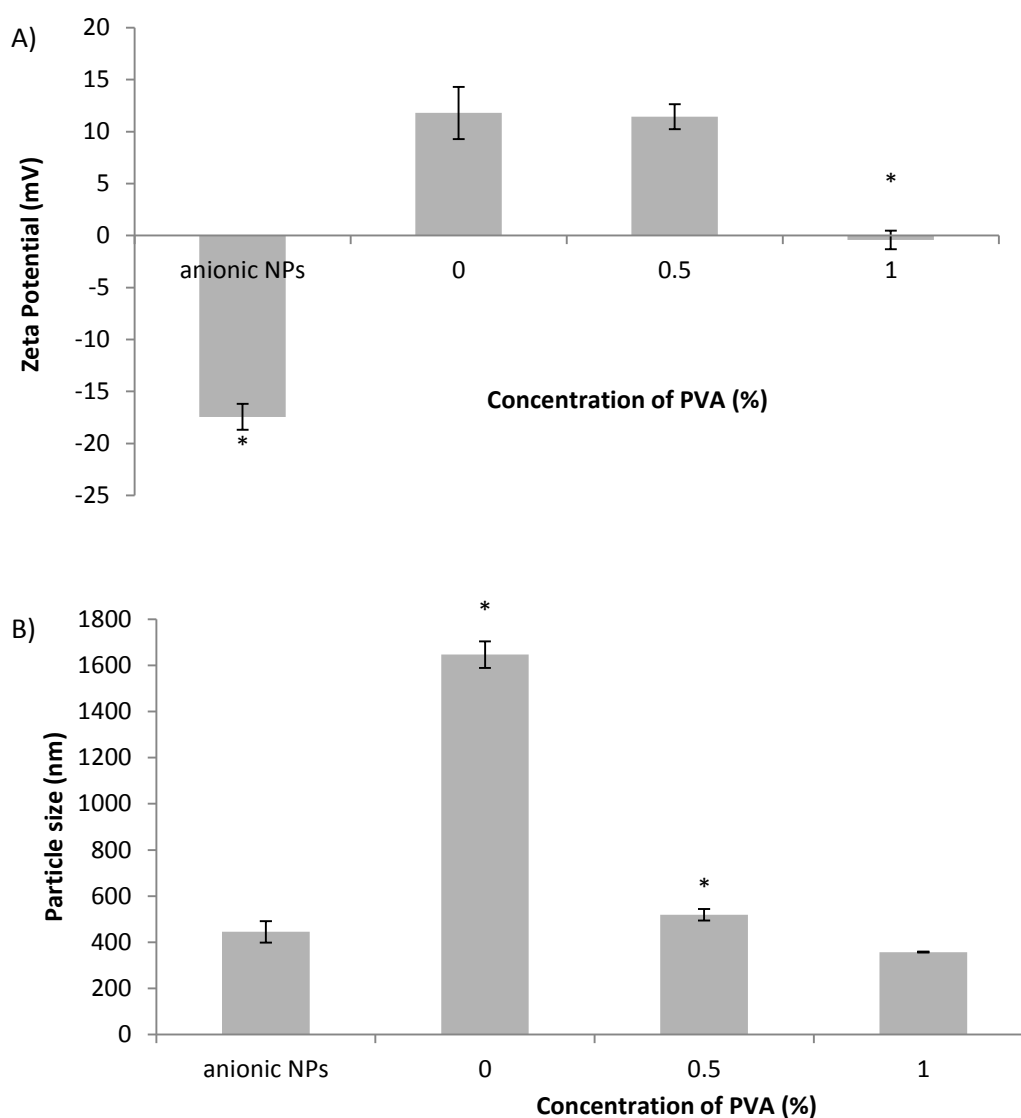
Figure 4-2: Effect of PVA % concentration on: A) zeta potential and B) particle size of NPs. Data represent means ±SD, n=3, * is p < 0.05, ANOVA/Tukey's comparison.

4.4.1.2. Effect of adsorption time

Figure 4-3.A and B shows the effect of adsorption time on zeta potential and particle size. The zeta potential changed significantly ($p<0.05$, ANOVA/Tukey,s comparison) from negative ($- 17.44\pm1.3$ mV) to positive 2 and 6 h and became neutral after 4 and 24 h. The particle size (455 ± 46.87 nm) increased significantly ($p<0.05$, ANOVA/Tukey's

comparison) after CHL adsorption in comparison with anionic NPs regardless of adsorption time.
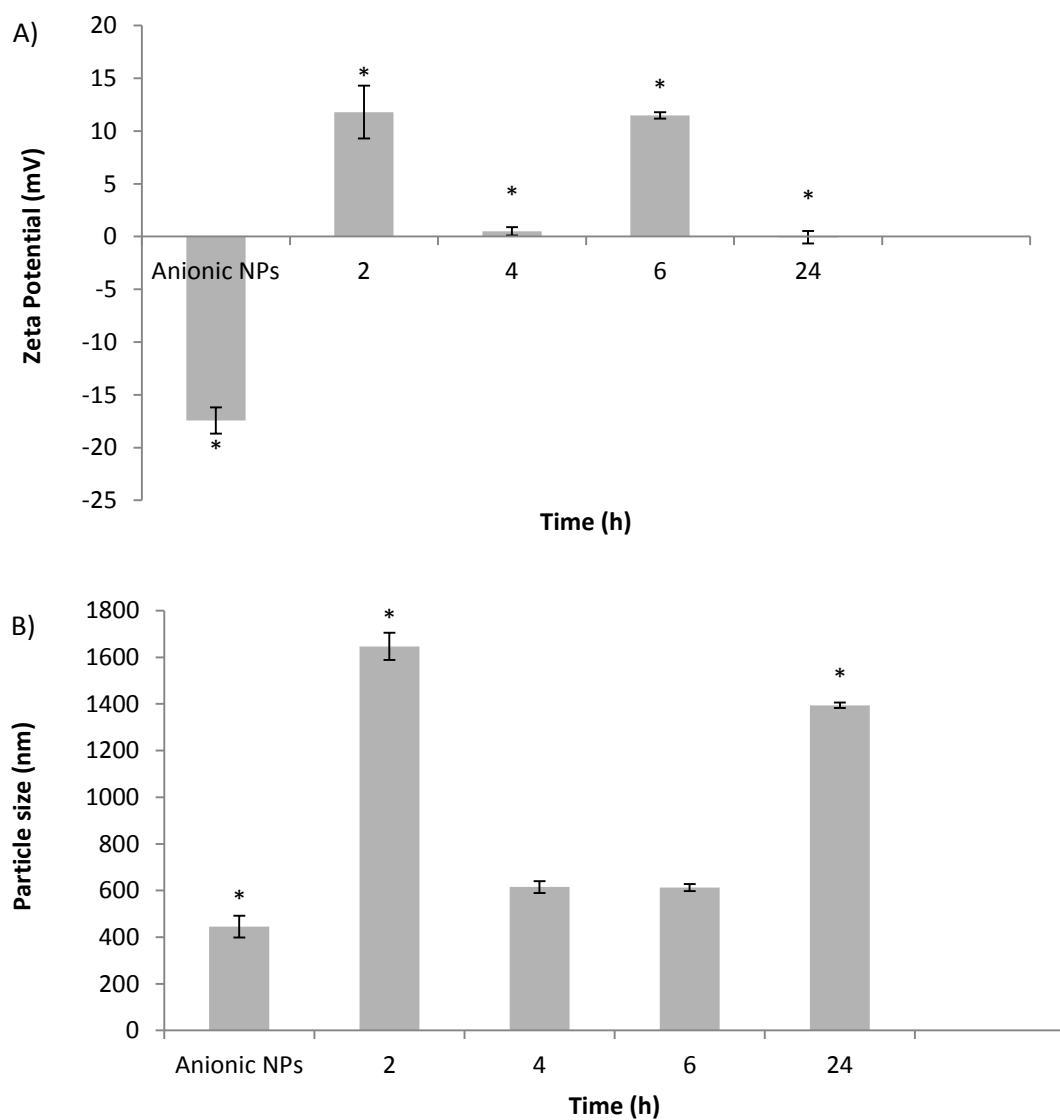
Figure 4-3: Effect of adsorption time on: A) zeta potential and B) particle size of NPs. Data represent means ±SD, n=3, * is p < 0.05, ANOVA/Tukey's comparison.

4.4.1.3.   Effect of method of addition CHL

In the second strategy CHL was added to the EAP in different concentrations (0 to 20 mg/ml) during the preparation of cationic NPs. The NPs had an electronegative (-17.44±1.2 mV) zeta potential, while all CHL - NPs were electropositive ($p < 0.05$, ANOVA/Tukey's comparison). The zeta-potential of cationic NPs increased with CHL feed concentrations up to +24 mV when produced from a CHL concentration of approximately 16–20 mg/ml (Figure 4-4.A).

The particle size (Figure 4-4.B) of anionic NPs was 445± 46.8 nm and it increased (3934±1533.7 and 2148±352.6 nm) significantly ($p < 0.05$, ANOVA/Tukey's comparison) with low concentrations of CHL ranging from 2 to 4 mg/ml (Figure 4-4.B). Whilst at higher concentrations of CHL the particle size did not significantly change ($p > 0.05$, ANOVA/Tukey's comparison).

The CHL concentration of 10 mg/ml in EAP was selected for further investigations in this study because it had similar size to anionic NPs with positive charge (Table 4-2). Furthermore, there was no significant difference ($p > 0.05$, ANOVA/Tukey's comparison) between particle size and surface charge of unloaded and BSA loaded cationic NPs at the selected concentration of CHL (10 mg/ml in EAP) Table 4-2.

4.4.2. Chitosan adsorption

The amount of CHL per mg of NPs increased significantly with the concentrations of CHL in the EAP over the entire range (0–20 mg/ml) of CHL concentrations examined (Figure 4-5). The mass of adsorbed CHL was 0.69±0.01, 1.45±0.02, 2.32±0.01, 3.44±0.38, 3.99±0.02, and 8.97±0.03 mg CHL/ mg of NPs obtained with initial CHL concentrations of 2, 4, 6, 8, 10 and 20 mg/ml, respectively. The largest mass of adsorbed CHL was obtained at 20 mg/ml CHL initial concentration with 8.97 mg CHL per mg of NPs ($p < 0.05$, ANOVA/Tukey's comparison; all values are significantly different to each other).
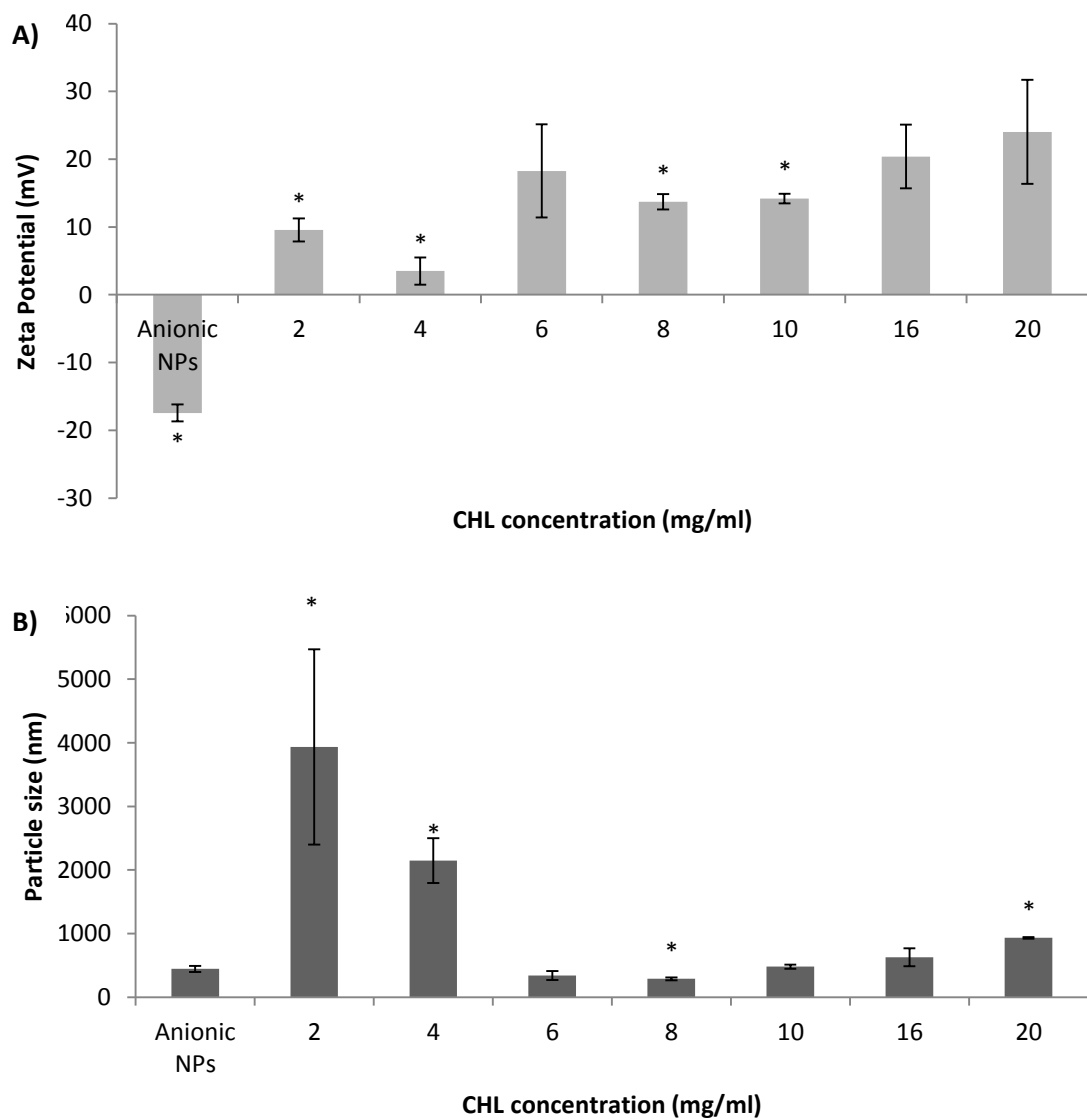
Figure 4-4: Effect of CHL concentration in EAP on: A) zeta potential and B) particle size of NPs, Data represent means ±SD, n=3, * is p < 0.05, ANOVA/Tukey's comparison.

Table 4-2: Particle size and zeta potential of selected anionic and cationic NPs with and without BSA loading. Data represent mean ± SD, n=3.

	Unloaded NPs	BSA loaded NPs
Anionic NPs*		
Particle size (nm)	403±7.80	445±46.8
Zeta Potential (mV)	-20.33±2.1	-17.44±1.20
PDI	0.244±0.03	0.209±0.05
Cationic NPs*		
Particle size (nm)	470.22±45.77	480.23±32.2
Zeta Potential (mV)	+16.88±3.10	+14.20±0.72
PDI	0.328±0.09	0.380±0.03

*NPs characterised after centrifugation.
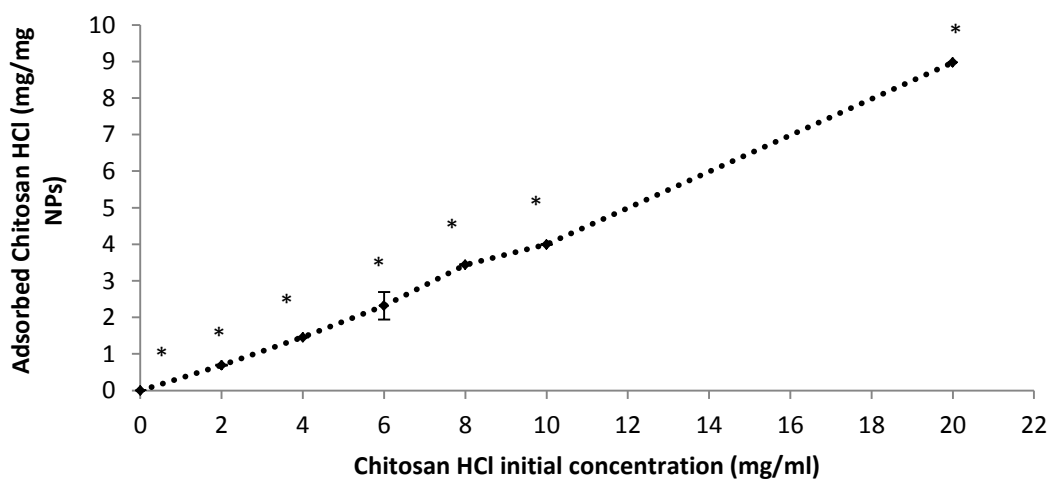
Figure 4-5: Effect of CHL concentration on the amount of CHL absorbed onto NPs. Data represent mean±SD, n=3, where * significantly different (p < 0.05, ANOVA/Tukey's comparison).

4.4.3. Adsorption isotherm model

The adsorption of CHL onto NPs did not fit with the Langmuir model over the range of CHL concentration examined (Figure 4-6.A). Even though, it had a good fit at low initial chitosan concentrations. The adsorption of CHL had a poor fit with the BET model (Figure 4-6.B). The multiplayer adsorption models including the Freundlich (Figure 4-6.C), and Halsey (Figure 4-6.D), models both had a good fit with good agreement ($r^2 > 0.9$), and the corresponding adsorption parameters were calculated (Table 4-3).

Table 4-3: Parameters derived from adsorption isotherm models by linear regression.

Isotherm equations	Adsorption capacity	Adsorption intensity	Regression coefficient
Langmuir*	q_m=1.2366	b=-0.2149	0.9167
Langmuir	q_m=2.28	b=0.146	0.8415
BET	q_m=0.4288	b=0.8561	0.0015
Freundlich	k=0.2893	n=0.5434	0.9988
Halsey	k=1.9422	n=0.5406	0.9974

*PGA-co-PDL NPs made at 0-8 mg/ml CHL initial concentration.
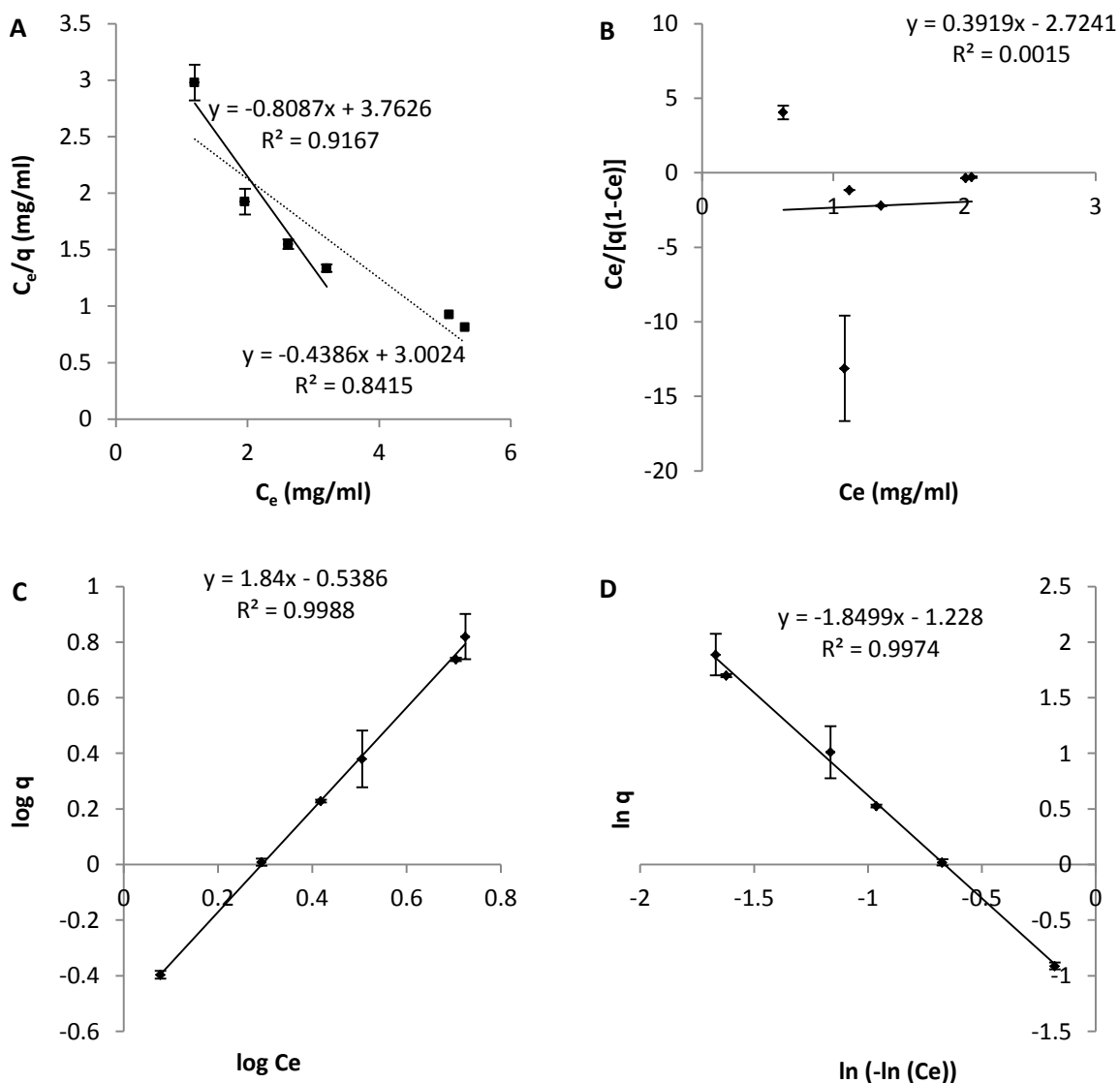
Figure 4-6: Linear representation of the four isotherm models of CHL adsorption onto NPs. C_e is the residual CHL concentrations in the suspension at equilibrium (mg/ml) and q is the amount of adsorbed CHL per unit weight of NPs. The (A) Langmuir model was fit with two regression lines plotted for low (0–8 mg/ml) (—) and the entire range of concentrations (….), respectively. The (B) BET, (C) Freundlich, and (D) Halsey models were fit using whole range of concentrations. Data represent mean±SD, n= 3.

4.4.4. BSA loading and EE%

The BSA loading of anionic NPs (43.67±2.3 µg/mg) decreased significantly ($p<0.05$, ANOVA/Tukey's comparison) in comparison with cationic NPs (7.28±1.3 µg/mg) and the BSA EE% (48±2.6 %) decreased significantly ($p<0.05$, ANOVA/Tukey's comparison) in comparison with cationic NPs (4.9±2.1 %), Table 4-4.

Table 4-4: BSA loading (µg/mg) and EE % of anionic NPs, anionic NPs/NCMPs, cationic NPs and cationic NPs/NCMPs. Data represent mean±SD, n=3.

	BSA loading (µg/mg)	EE (%)
Anionic NPs	43.67±2.3*	48.04±2.6*
Anionic NPs/NCMPs	5.37±1.7**	
Cationic NPs	7.29±1.4*	4.9±1.3*
Cationic NPs/NCMPs	1.09±0.03**	

* (Anionic vs Cationic NPs) and ** (Anionic vs Cationic NPs/NCMPs) is $p < 0.05$, ANOVA/Tukey's comparison.

4.4.5. Characterisation of nanocomposite microparticles

Spray-drying was applied to incorporate the selected cationic NPs into NCMPs using L-leucine as a carrier and to enhance powder dispersion.

The size of anionic NPs after recovery from spray-dried anionic NPs/NCMPs and cationic NPs/NCMPs in distilled water were 453.6± 19.7 nm and 490±17 nm confirming the recovery of NPs from NPs/NCMPs.

4.4.5.1. Morphology of nanocomposite microparticles

The shape and morphology of cationic NPs/NCMPs were investigated using SEM (Figure 4-7). Photomicrographs of cationic NPs/NCMPs showed irregular and porous microparticles.
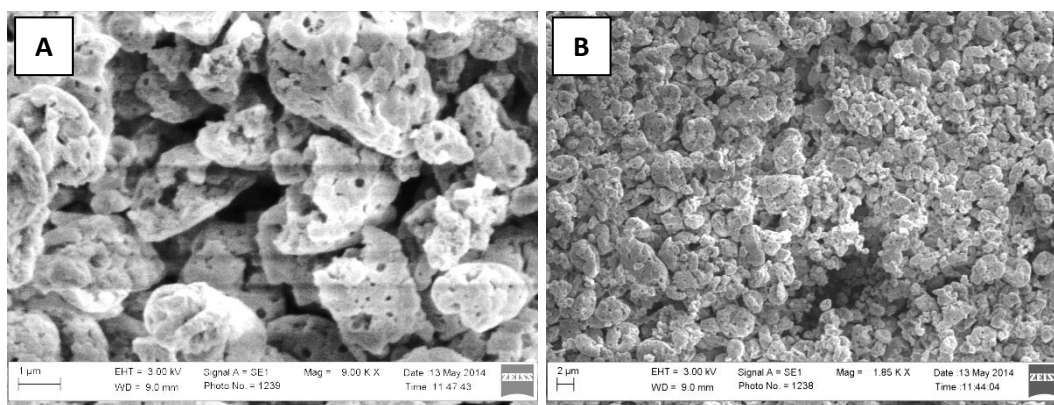
Figure 4-7: SEM images of cationic NPs/NCMPs: 1 μm scale (A) and 2 μm scale (B).

4.4.6. Powder density and primary aerodynamic diameter

Cationic NPs/NCMPs formulation had a geometric particle size of 5.52±0.64 μm (Table 4-5). The tapped density was 0.08±0.002g cm^{-3}; and this was used together with the geometric particle size to calculate the theoretical aerodynamic diameter (d_{ae}). The cationic NPs/NCMPs had the theoretical aerodynamic diameter within the respirable range.

Table 4-5: The geometric particle size, tapped density and theoretical aerodynamic diameter of cationic NPs/NCMPs. Data represent mean ± S.D., n=3.

NCMPs Formulation	Geometric particle size (μm)	Tapped density (g/cm^3)	Carr's index		d_{ae} (μm)
			%	Flowability	
Cationic NPs/NCMPs	5.52±0.64	0.08±0.002	36.71±0.83	Very poor	1.56±0.19

4.4.7. In vitro aerosolisation studies

The percent mass of BSA recovered from the NGI was approximately 89 %, which is within the pharmacopeia limits (75 − 125 %) of the average delivered dose (139). BSA deposition data obtained from anionic NPs/NCMPs and cationic NPs/NCMPs formulations (Table 4-6) indicated there was a significant difference in aerosolisation performance between these formulations for FPD, and FPF% ($p<0.05$, ANOVA/Tukey's comparison). Anionic NCMPs produced a higher FPD 45.00±4.70 µg, and FPF% 78.57±0.1% than cationic NPs/NCMPs 32.51±6.67 µg and 46.79±11.21%, respectively.

Table 4-6: The Fine particle dose (FPD), percentage fine particle fraction (FPF), and mass median aerodynamic diameter (MMAD) of cationic NPs/NCMPs. Data represent mean ± S.D., n=3.

	FPD (µg)	FPF (%)	MMAD (µm)
Cationic NPs/NCMPs	32.51±6.67	46.79±11.21	1.49±0.29

4.4.8. Investigation of BSA structure

The primary structure of BSA released from cationic NPs and cationic NPs/NCMPs was investigated using SDS-PAGE analysis. According to Figure 4-8, the BSA standard and the molecular weight marker had shown in Lanes 1 and 2, respectively, revealed a clear band at around 66 KDa. The BSA released from cationic NPs and cationic NPs/NCMPs (Lanes 3 and 4, respectively), showed similar clear banding patterns to the BSA standard. The single lines in the gels provided evidence that the entrapped BSA in the cationic NPs and cationic NPs/NCMPs samples was stable.
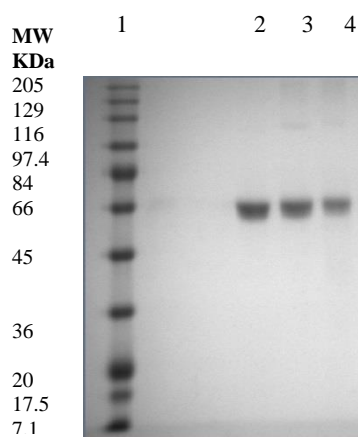
Figure 4-8: SDS-PAGE behaviour of BSA released from NPs for the assessment of BSA stability. Lanes represent, molecular weight (MW) standard markers, BSA (MW 66,000) (1), BSA standard (2), BSA released from cationic NPs (3), and BSA released from cationic NPs/NCMPs (4). Difference in band intensity was due to different loading.

The secondary structure analysis of released BSA was carried out using CD. Figure 4-9 shows the structure of standard BSA and BSA released. The CD spectra show minima at 221 - 222 and 209 − 210 nm and a maximum at 195 nm for both samples, which is characteristic of an α-helical structure. In support of these data, structural analysis showed that BSA was predominantly helical displaying 51.5% helicity (Table 4-7). In contrast to standard BSA, structural analysis of BSA released showed a reduced level of α-helical conformation (*circa* 43 % helical) (Table 4-7). Furthermore, a comparison of BSA released with standard BSA, showed that the α-helical content decreased by 8.5 %, the β-sheet content increased by 8%, the turns content decreased by 2%, and the random coils' content increased by 3%, respectively.
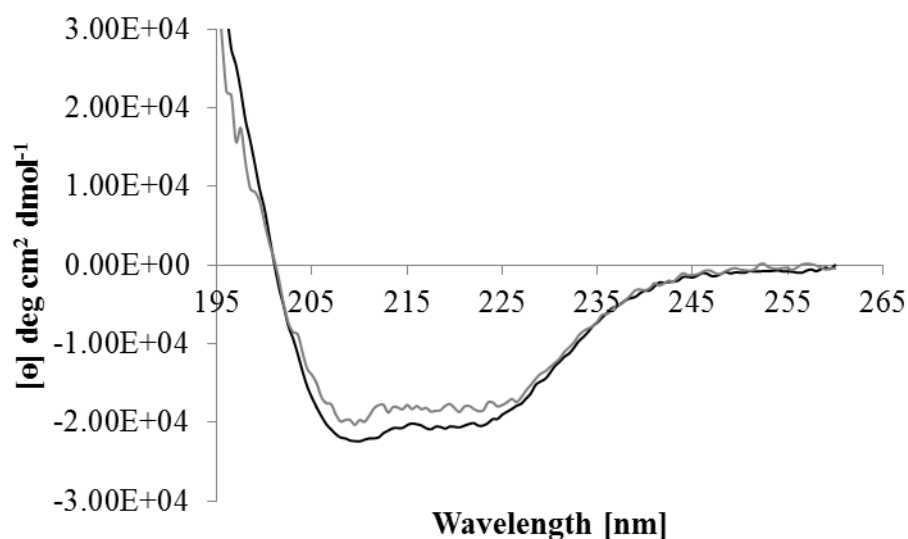
Figure 4-9: The CD spectra of BSA released from cationic NPs/NCMPs (grey) and BSA standard (black) (n=3).

Table 4-7: The percentage of secondary structure conformation for BSA standard and BSA released from cationic NPs/NCMPs (n=3).

	Helix	Strands	Turns	Unordered
BSA standard	51.5 ± 0.007	21.50 ± 0.007	9.0 ± 0	17.50 ± 0.007
BSA released	43 ± 0.007	29 ± 0.014	7 ± 0	20.5 ± 0.007

4.4.9. In Vitro Release Studies

In vitro release studies were performed on cationic NPs/NCMPs formulations and reported as cumulative percentage BSA released over time (Figure 4-10). Cationic NPs/NCMPs formulations showed a biphasic release profile. The % cumulative BSA released at time zero was considered as surface-associated BSA, the % cumulative BSA

released at the end of 4 h was considered as the initial burst phase of BSA release, and followed by a second continuous sustained release phase over 48h (Figure 4-10).

The anionic NPs/NCMPs formulations showed a lower cumulative release achieving $38.77\pm3\%$ release after 48 h (Figure 3-12). The cationic NPs/NCMPs formulations showed a higher cumulative releases, with nearly $88.93 \pm14.8\%$ of BSA released after 48 h ($p<0.05$, ANOVA/Tukey's comparison) (Figure 4-10).

In vitro release kinetics were used to determine the mechanism of BSA release. Comparison of the rates of release using zero, first order and the Higuchi rate equations are shown in Table 4-8.

BSA was released from cationic NPs/NCMPs formulations according to a dual pattern first order model with an r^2 value of 0.919. The release rate constant k_1 $(h^{-1/2})$ was -0.016, the Higuchi diffusion model r^2 value was 0.928, and the release rate constant k_1 $(h^{-1/2})$ was 9.316 (Table 4-8).
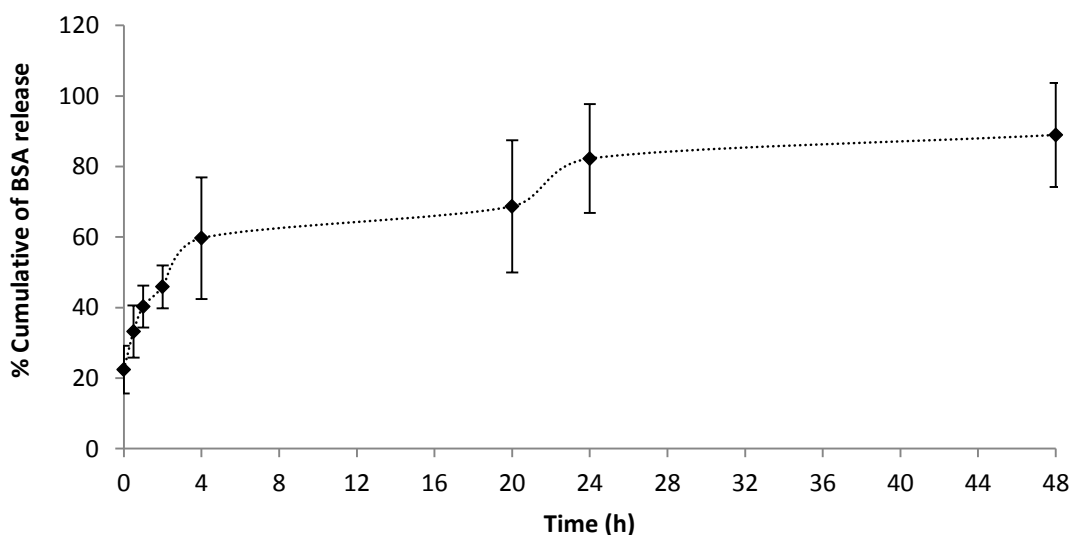
Figure 4-10: % Cumulative *in-vitro* release of BSA from cationic NPs/NCMPs in PBS buffer at 37°C. Data represent mean ± S.D., n=3.

Table 4-8: Release parameters of BSA from cationic NPs/NCMPs.

Formulation	Zero Order		First order		Higuchi	
	r^2	$k_o\ (h^{-1})$	r^2	$k_1\ (h^{-1})$	r^2	$k_1\ (h^{-1/2})$
Cationic NPs/NCMPs	0.777	1.218	0.919	-0.016	0.928	9.316

4.4.10.   Cytotoxicity study

The A549 cell line toxicity studies (Figure 4-11) of cationic NPs and cationic NPs/NCMPs showed a cell viability of 63.91±0.87% for cationic NPs and 78.85±9.96% for cationic NPs/NCMPs at a concentration of 2.5 mg/ml after 24 h exposure indicating a good toxicity profile.
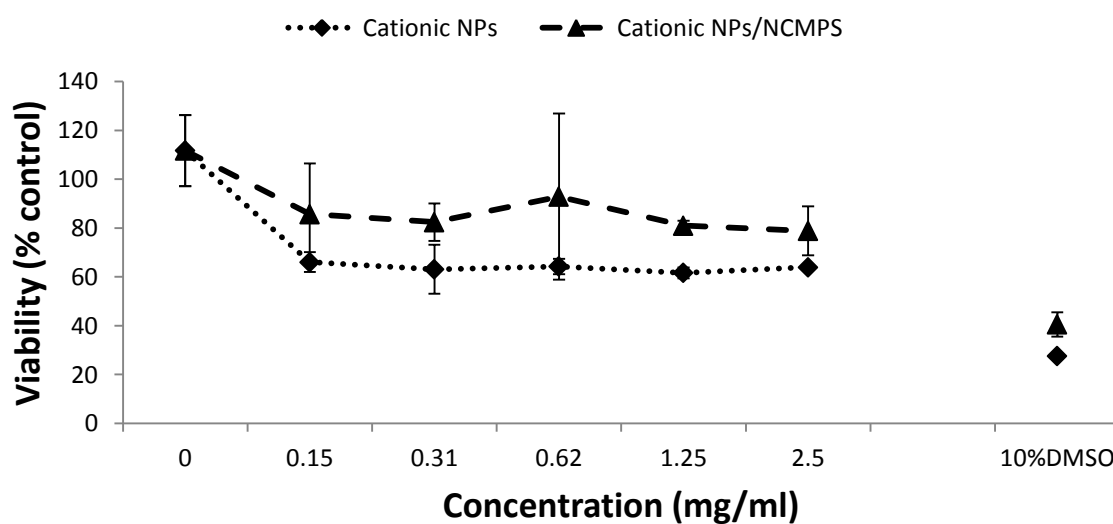
Figure 4-11: A549 cell viability measured by MTT assay after 24 h exposure to cationic NPs and cationic NPs/NCMPs. Data represent mean ± S.D., n=3.

4.5. Discussion

Adsorption of CHL was investigated in order to modify the particles surface charge, favouring potential interactions with negatively charged cell membranes and facilitating uptake by DCs (156).

4.5.1. Cationic nanoparticles characterisation

Effect of different concentrations of CHL and PVA on zeta potential and particle size

In the first strategy, different concentrations of CHL were used with and without 1% PVA. When 1% PVA was used, upon addition of CHL, the zeta potential changed from negative to neutral regardless of CHL concentration (Figure 4-1.A). This was due to the ability of the PVA layer to screen CHL charges leading to an almost neutral zeta potential value (211).

When PVA was not included the zeta potential changed from negative to neutral at lower CHL concentrations (4 and 8 mg/ml) but at higher CHL concentrations (20 and 30 mg/ml) the zeta potential changed to positive (Figure 4-1.A). Chronopoulou *et al.* reported a similar pattern with chitosan coated PLGA NPs (110). They found that in the case of lower concentrations, the relative PLGA and chitosan concentrations corresponded to a concentration close to the one of the isoelectric condition, justifying the finding that the zeta potential of the resulting coated PLGA NPs was very close to zero and then at higher concentration inverts its charge, indicating that the adsorbed chitosan reversed the NPs charge (110). At the highest concentration of CHL tested (34 mg/ml) the NPs surface charge was neutral again, probably because of the high viscosity which would decrease the efficiency of adsorption (111). This decrease in efficiency of adsorption is evident by particle size of NPs. where the increase in particle size could be attributed to particle aggregation due to absence of PVA and only small amount of CHL adsorbed.

The particle size increased significantly when the concentration of CHL increased to 8 mg/ml (Figure 4-1.B). The increase in particle size has been attributed to either the increased viscosity of the CHL solution, which lowered the shear stress on NPs during stirring, and/or the increasing amounts of CHL on the surface of the NPs (212). However, at CHL concentration of 20 and 34 mg/ml there was no significant change in particle size. This indicated a complete coating of CHL on the surface leading to CHL molecules repelling each other, preventing particle aggregation and hence an increase in particle size (111).

At the same concentration of CHL with highest PVA concentration used (1%, Figure 4-2.B) the particle size decreased significantly this is because the PVA is known to prevent particle aggregation (80).

Effect of adsorption time

Figure 4-3.A and B shows the effect of adsorption time on zeta potential and particle size. The zeta potential changed significantly from negative to positive at 2 and 6 h and became neutral after 4 and 24 h. This pattern of change in zeta potential could be attributed to interfering by BSA released from NPs which could be adsorbed by CHL on NPs surface. At 2-6 h incubation it is positive with CHT charge dominating and some aggregation of NPs. At other time points the neutral charge could be due to the release of BSA into media and aggregation of BSA which dominates the CHT adsorbed on NPs. Moreover, this was confirmed by increased particle size significantly after CHL adsorption in comparison with anionic NPs regardless of adsorption time.

Effect of method of addition CHL

In the second strategy CHL was added to EAP in different concentrations (0 to 20 mg/ml) during the NPs preparation process. Anionic NPs produced were electronegative -17.44±1.2 mV, while all cationic NPs were electropositive this confirmed the presence of CHL on NPs. The zeta-potential of cationic NPs increased with CHL feed

concentrations until a zeta-potential plateau was reached at approximately +24 mV (CHL concentration of approximately 16–20 mg/ml, Figure 4-4.A). This could be indicative of saturation in adsorption of CHL on the NPs (111; 72; 212).

The particle size of cationic NPs was heterogeneous with two populations of particles present regardless of the concentrations of CHL (Figure 4-4.B). The particle size of cationic NPs increased significantly at lower concentrations of CHL ranging from 2 to 4 mg/ml. This could be attributed to the increased viscosity of CHL, lowering the shear stress of the OP during sonication producing larger emulsion droplets and subsequently larger NPs (212). At higher concentrations of CHL (6, 10, 16 mg/ml) the particle size did not change significantly. This has been attributed to a complete coating of the NPs by CHL molecules so additional CHL would repel each other (due to similar charge) and prevent particles aggregation. Also, the pattern of change in particle size when CHL was added to the EAP was similar to that when CHL was added after NPs formation. It was observed that all cationic NPs regardless of preparation method displayed a neutral or positive charge that could be due to electrostatic interactions between the negatively charged groups (-OH) of PGA-co-PDL and the positively charged CHL inducing adsorption of CHL onto the NPs surface. Only a fraction of the amino groups would be required to neutralize the negative charges of PGA-co-PDL, whereas the remaining free amino groups could be responsible for the resulting change in the measured zeta potential (211).

The second strategy was selected to examine CHL adsorption onto NPs and to explain the mechanism of adsorption because it had positive zeta potential over the entire range of CHL concentrations examined. The cationic NPs prepared at a CHL concentration of 10 mg/ml was selected for further investigations in this study because these particles had a similar size to the anionic NPs.

The amount of adsorbed CHL per mg of NPs increased with initial CHL concentrations over the entire range (0–20 mg/ml) of CHL concentrations examined and no plateau of adsorption was reached. The continued adsorption of CHL onto NPs did not affect the apparent zeta-potential at high concentrations (greater than approximately 16–20 mg/ml). As a possible model, multiple layers of CHL only allow a small amount of CHL to influence the measured zeta-potential. Layers beyond the first few do not increase the zeta-potential because the apparent surface charge per unit area (amine groups) is constant (111).

Adsorption isotherm model

Different presumptions of the parameters of adsorption, such as the characteristics of compositions and interaction between adsorbate (CHL) and adsorbent (PGA-co-PDL) influenced the analysis of adsorption isotherms. The mechanism of adsorption can be predicted from the model that fits best with the experimental results. (111).

The first model tested was Langmuir model (Figure 4-6.A). This model described monolayer adsorption of adsorbate on the adsorbent where there is no interaction between adsorbate molecules, the adsorption is not governed by surface occupation, and equivalent adsorption sites (111).

The adsorption of CHL onto NPs did not comply with the Langmuir model at the range of CHL concentration investigated. However, the Langmuir monolayer model was valid at low concentrations (0–8 mg/ml). The monolayer adsorption capacity (q_m) was found to be 1.2366 mg/mg NPs, which corresponded to the initial concentration of CHL at 8 mg/ml. However, the Langmuir monolayer model could not explain adsorption at high concentrations of CHL.

The second model tested was BET model (Figure 4-6.B). This model did not describe the results in the concentrations range investigated. The BET model was a development of the Langmuir model (monolayer model) to include multilayer adsorption. Depending

on the BET type, the following layers are the condensed adsorbate molecules. Also, it assumed that the energies of adsorption are equal for layers after the monolayer, which is property of a uniform surface. Moreover, this model bears in mind little interactions between adsorbate and adsorbent. The adsorption model demonstrated in this study did not fit the BET type due to the ideal characteristic of this type (111).

The adsorption results for CHL were in good agreement with the Freundlich model (Figure 4-6.C). The nonlinear adsorption model was commonly described by Freundlich model. This model is applicable for multilayer adsorption with a uniform surface or a greatly non-uniform surface (111). The slope 1/n, ranging between (0.33-1.18), is a measure for the adsorption intensity or surface heterogeneity, becoming more heterogeneous as its value gets closer to zero. The calculated value of 1/n is above 1 which is an indication of a cooperative adsorption (213).

The Halsey isotherm model (Figure 4-6.D) illustrates multilayer adsorption of an adsorbate (at relatively far distances from a heterogeneous surface) which fit with the exponential relationships between the mass of adsorbate (q) and free concentration of adsorbateat equilibrium (C_e). Accordingly, the typical multilayer isotherm consisted of three sections where in the first section the adsorption is non-cooperative on a highly non-uniform surface; in the second section the adsorption is cooperative on a still non-uniform surface; and in the last section the multilayer adsorption is cooperative provoked by little van der Waals force influences at some length from the surface (111). It was found that the adsorption of CHL on NPs complied with multilayer adsorption pattern irrespective of which model was examined. The leading factor particularly in the development of the first adsorption layer was electrostatic force between CHL (with positive charge) and PGA-co-PDL surface (with negative charge). When the CHL concentration increased it is likely that the following layers of CHL adsorbed on the first layer of CHL without interaction with the NPs surface. When more CHL layers

adsorbed the CHL molecules would repel each other because of the same charge however CHL molecules interacted via hydrogen bonds, hydrophobic interactions, and van der Waal's forces. Mainly, the NPs great surface energy and surface area had a significant function in CHL multilayer adsorption (111).

BSA loading and EE %

The EE% of BSA in anionic NPs was (48±2.6 %) but this decreased significantly after CHL adsorption (4.9±2.1 %). This could be explained by electrostatic interactions between the negative charge of BSA and positive charge of CHL. The isoelectric point of BSA is 4.8 indicating it was negatively charged at pH>4.8, so could potentially adsorb cationic CHL in an aqueous solution (measured 1% in water pH =6) (214). The CHL may adsorbs some of the BSA to the surface of the NPs during the preparation and hardening process, significantly decreasing the encapsulation efficiency (109). This was confirmed by the first initial burst release phase (section 4.4.9) at time 0 h which was the result of loss of surface BSA. However, DL decreased substantially with increasing polymer amount (PGA-co-PDL and CHL), as it was expected from predictions based on the respective equation 2-2 in which DL is inversely proportional to the amount of polymer (147).

4.5.2. Cationic nanocomposite microparticles characterisation

Photomicrographs of cationic NPs/NCMPs showed irregular and porous microparticles (see section 3.5.2 for more detail and explanations). Furthermore, the size of anionic and cationic NPs after dispersing anionic and cationic NPs/NCMPs in distilled water confirmed the recovery of NPs with suitable size for uptake by DCs (89).

The cationic NPs/NCMPs formulations had a geometric particle size of 5.52±0.64 µm suitable for pulmonary delivery. The tapped density was 0.08±0.002g cm^{-3}; suggesting highly porous particles. The cationic NPs/NCMPs showed the theoretical aerodynamic diameter was in the respirable range despite having a larger geometric particle size than

anionic NPs/NCMPs. This is because the density of cationic NPs/NCMPs was lower than that of the anionic NPs/NCMPs (66).

Anionic NPs/NCMPs produced a higher FPD 45.00±4.70 μg, and FPF% 78.57±0.1% than cationic NPs/NCMPs 32.51±6.67 μg and 46.79±11.21%, respectively. This could be explained by the observation that the cationic NPs/NCMPs aggregate more and have a poorer powder flow as indicated by Carr's index. This could be attributed to incomplete powder de-aggregation as van der Waals forces between particles were not completely overcome upon inhalation despite the low density of the particles. In addition, powder aggregation of cationic NPs/NCMPs was confirmed with a Carr's index of ≥32, indicating the flow was very poor (66).

In the cationic NPs/NCMPs formulation the observed high-burst release at time zero (22.41±6.7%) could be explained by the majority of the BSA being adsorbed onto the surface (110). Also, the cationic NPs/NCMPs formulations showed a higher cumulative BSA release at the end of 48 h compared to anionic NPs/NCMPs. These differences in release patterns may be due to a combination of factors, such as BSA loading, and presence of CHL on the surface of the NPs (141). For both formulations the notable change in release profile at 20-24h after the initial burst release could be due to the distribution of BSA inside NPs or a change in degradation rate due to changed surface porosity (141). Also, it is worth noting that CHL adsorbed on NPs dissolves in water and therefore does not hinder drug diffusion from the NPs (156; 110).

A study of the *in vitro* release kinetics was carried out to determine the mechanism of BSA release. BSA was released from anionic NPs/NCMPs formulations according to the Higuchi diffusion model (for details see section 3.5.4).

However, BSA was released from cationic NPs/NCMPs formulations according to a dual pattern first order model and Higuchi diffusion model. A first order kinetics equation described the release of BSA which was not efficiently encapsulated in

cationic NPs and is available for dissolution from cationic NPs surface. This takes place immediately after introducing the formulation into the release medium (215). The Higuchi model describes the second and third part of the BSA release which appears to be a diffusion-limited process.

The primary structure of BSA released from cationic NPs and cationic NPs/NCMPs was analysed by SDS-PAGE. BSA standard and the BSA released from anionic NPs and cationic NPs/NCMPs showed similar clear banding patterns in the gels providing evidence that the BSA entrapped in cationic NPs and cationic NPs/NCMPs samples maintained its primary structure during the preparation methods used.

The secondary structure of BSA in the formulation was analysed using CD spectroscopy. Structural analysis showed that BSA was predominantly helical which is in good agreement with previous reports (172). The BSA released samples confirmed the presence of α-helix and β-sheets although these were decreased in comparison with standard BSA (140).

The aerosolisation studies indicated that the cationic NPs/NCMPs would reach the bronchial-alveolar region in the lung so cytotoxicity studies were carried out on A 549 cell line. The cationic NPs and cationic NPs/NCMPs appear to be well tolerated by the cell line at 2.5 mg/ml concentration indicating a good toxicity profile. The difference in cell viability between cationic NPs and cationic NPs/NCMPs at the same concentration could be due to dilution of cationic NPs with L-leucine for spray drying. Also, the possibility of reaching a high local concentration can be ruled out because after inhalation the dose would be spread over different part of the lungs and not be concentrated in certain area (216). Furthermore, cationic NPs have a greater ability to interact with negatively charged proteoglycans on the cell surface of macrophages and DCs (173). Kwon *et al.* have showed higher delivery of cationic NPs with ovalbumin as model antigen to bone marrow DCs in comparison with neutral NPs while the cell

viability of both cationic and neutral NPs were comparable at concentrations of 125-250 µg/mg (217). This provides an indication of the feasibility of using cationic NPs/NCMPs as safe carriers for pulmonary drug delivery (68).

4.6. Conclusion

Adsorption of CHL on PGA-co-PDL NPs can be used as a successful strategy to produce cationic NPs. Two strategies were used. The first strategy involved attachment of CHL onto the surface of the preformed NPs by physical adsorption. The second strategy involved addition of CHL to EAP during the process of NPs preparation by double emulsion solvent evaporation method. The second strategy successfully produced cationic NPs with a positive charge in the whole range of CHL concentrations examined while the first strategy failed. The adsorption of CHL on NPs complied with multilayer adsorption behaviour as indicated by Freundlich model.

The cationic NPs prepared at a CHL concentration of 10 mg/ml was selected for further investigations in this study because it has a similar size to anionic NPs with a positive zeta potential. The BSA loading for this selected formulation was 7.28±1.3 µg/mg. After spray drying, the photomicrographs of cationic NPs/NCMPs showed irregular and porous microparticles. *In vitro* aerosolisation performance of cationic NPs/NCMP FPD, and FPF% were 32.51±6.67 µg and 46.79±11.21%, respectively. The cationic NPs/NCMPs formulations showed high BSA cumulative releases, with nearly 88.93 ±14.8% of BSA released at the end of 48 h. Further cell viability studies on A549 cells showed a low toxicity profile. This study suggests that cationic NPs/NCMPs could be further investigated for encapsulation of PspA as therapeutic antigen to be delivered through the lung.

5. Pulmonary Delivery of Recombinant Pneumococcal Surface Protein A Using Different Nanocomposite Microparticle Carriers via Dry Powder Inhalation

5.1. Introduction

Over the last decades, many researchers have explored the use of pneumococcal proteins as possible replacements for current pneumococcal vaccines (PPV and PCV). A protein-based vaccine can overcome the limitations of PPV and PCV and provide protection against nasopharyngeal carriage upon mucosal delivery. One of the most promising pneumococcal proteins is pneumococcal surface protein A (PspA) which has an important role in preventing the accumulation of complement on the surface of the bacterium which leads to inhibition of clearance and phagocytosis of *S. pneumoniae* (157).

PspA is a surface protein located on the cell wall of all strains of pneumococci (Figure 5-1.A), and has an N-terminal α-helical domain exposed on the bacterial surface and a C-terminal choline-binding repeat region responsible for the attachment to the cell wall (Figure 5-1.B) (218). PspA sequences are variable, especially in the N-terminal domain, and have been classified into three families based on sequence homologies. Ninety-five percent of pneumococcal strains carry PspA of family 1 (PspA1) or family 2 (PspA2), and there is a significant serological cross-reactivity between the different families (29). Moreover, PspA has been shown to provoke protective antibodies in humans (157).

Recombinant protein based vaccines are often poorly immunogenic alone or in combination. Encapsulating PspA in polymer based particle or nanogel has been documented to improve its immunogenicity (35; 157). In previous chapters, the biodegradable PGA-co-PDL successfully encapsulated in NPs and released stable BSA. The mucosal surface of the respiratory system is the main entrance for *S. pneumoniae*. Delivery of a vaccine through the pulmonary route has been proposed for evoking an immune response at mucosal and systemic level against airborne pathogens and consequently may prevent colonization at mucosal surfaces (43; 42). Furthermore, the

stimulation of the immune system requires the successful delivery of the antigen to DCs which process the antigen and generate the immune response (217). Therefore encapsulating PspA into polymeric NPs followed by incorporation into microparticle carriers to produce NCMPs as DPIs is a promising vaccine delivery system.
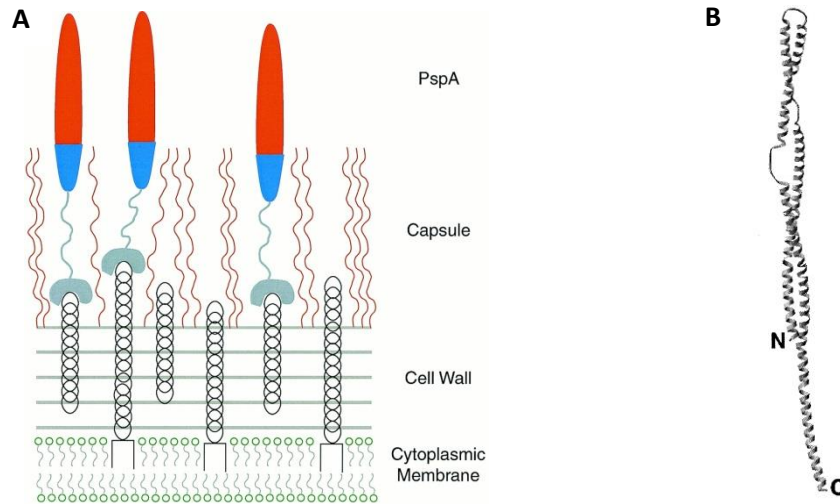
Figure 5-1: A. alignment of PspA on the cell wall of pneumococci. B. Model of PspA structure (with permission from (218))**.**

5.2. Aim

The aim of this study was to formulate anionic and cationic NPs (optimum formulations from chapters 3 and 4) encapsulating PspA followed by incorporation into microparticle carriers to produce anionic and cationic NPs/NCMPs as DPIs via spray-drying suitable for pulmonary vaccine delivery.

5.3. Methods

5.3.1. Production and purification of PspA4Pro

Recombinant PspA4Pro was produced as described in section 2.2.13.

5.3.2. Anionic and cationic NPs preparation

PspA4Pro loaded PGA-co-PDL anionic NPs were prepared by a previously optimised (w/o/w) double emulsion/solvent evaporation method as described in section 2.2.3 and section 2.2.4. Briefly, IAP containing 1% PspA4Pro and 1% PVA was emulsified in OP (DCM and 50 mg PGA-co-PDL), by sonication using a probe sonicator at 45% amplitude for 15 seconds over an ice bath. The resulting single emulsion was emulsified into 25 ml of a 1% PVA solution (EAP) using the same probe sonicator for 30 seconds to form a w/o/w double emulsion. The double emulsion was stirred magnetically for 2 h at room temperature to evaporate the DCM. The anionic NPs were collected by centrifugation (Sigma 3-30k, SIGMA Laborzentrifugen GmbH, Germany) at 40,000 xg for 1 h at 4 ^{0}C, and washed with distilled water twice. Cationic NPs were prepared using the same method except CHL 10 mg/ml was added to the EAP. Control NPs were prepared using the same method but without protein. For particle uptake studies, fluorescein isothiocyanate (FITC-BSA) was added in the IAP.

5.3.3. Anionic and cationic NPs characterization

The particle size and zeta potential, EE % and PspA4Pro loading of anionic and cationic NPs were characterised as described in section 2.2.7.

5.3.4. Preparation and characterisation of NCMPs

The anionic and cationic NPs were dispersed into L-leucine solution (1:1.5 w/w) and spray dried according to the spray drying condition described in section 2.2.8 to produce NCMPs as a dry powder for inhalation. The produced NCMPs were characterised for morphology as described in section 2.2.9.2.

5.3.5. *In vitro* release study

The in vitro release studies were performed as described in section 2.2.11.

5.3.6. Investigation of PspA4Pro structure

The released PspA4Pro was examined for primary structure stability by SDS-PAGE analysis and for secondary structure by circular dichroism spectroscopy analysis as described in section 2.2.12.

5.3.7. *In vitro* antigenicity study of PspA4Pro

The antigenicity of PspA4Pro was examined as described in section 2.2.14.

5.3.8. Cytotoxicity study

The DCs viability of anionic and cationic NPs was determined as described in section 2.2.15.2.

5.3.9. NPs cellular uptake by DCs

DCs uptake of FITC-BSA loaded anionic and cationic NPs was evaluated as described in section 2.2.16.

5.4. Results

5.4.1. Characterisation of anionic and cationic NPs

The encapsulation of PspA4Pro into anionic and cationic NPs was carried out using the processing parameters optimised in chapters 3 and 4. PspA4Pro loading into cationic particles (9.84±1.4 µg/mg) was significantly less (p<0.05, ANOVA/Tukey's comparison) than in anionic particles (65.73±5.6 µg/mg). The EE % of PspA4Pro into the anionic NPs was 75.3±6.2% which was significantly (P<0.05, ANOVA/Tukey's comparison) higher than the EE% of cationic particles (50.2±7.1%).The particle size of anionic and cationic NPs were 328.4±56.16 nm and 409.7±49.5 nm respectively, indicating a significantly increased particle size (p<0.05, ANOVA/Tukey's comparison). Table 5-1 presents the particle size, PDI, zeta potential, EE % and PspA4Pro loading of anionic and cationic NPs.

Table 5-1: Particle size, PDI, zeta potential, EE % and PspA4Pro loading of PGA-co-PDL NPs. Data represent mean ± SD, n=3.

	Anionic NPs[a]	Cationic NPs[a]
Particle size (nm)	310.4±25.3*	409.4±49.5*
PDI	0.302±0.02	0.418±0.06
Zeta potential (mV)	-29.20±0.9	21.30±1.3
EE (%)	75.3±6.2*	50.2±7.1*
PspA4Pro loading (µg/mg)	65.73±5.6*	9.84±1.4*

[a] NPs characterised after centrifugation, * significantly different (p<0.05, ANOVA/Tukey's comparison).

5.4.2. Characterisation of NCMPs

The shape and surface texture of anionic and cationic NPs/NCMPs were investigated using SEM (Figure 5-2). Photomicrographs for both formulations showed irregular and corrugated microparticles.
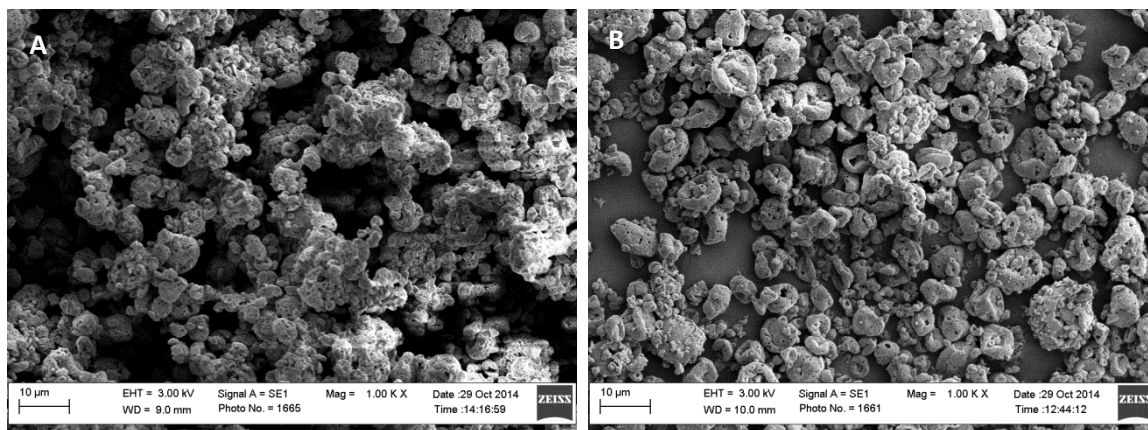
Figure 5-2: The SEM image of anionic NPs/NCMPs (A) and cationic NPs/NCMPs (B).

5.4.3. In Vitro Release Studies

In vitro release studies comparing anionic and cationic NP/NCMPs formulations were performed (Figure 5-3) and reported as the % cumulative PspA4Pro released. Anionic NPs/NCMPs formulation showed a biphasic release profile with an initial burst release (14.56±1.6%) followed by a second continuous sustained release phase over 48h. Cationic NPs/NCMPs formulation showed a biphasic release profile with the PspA4Pro released at time zero (12.76±0.11 %) considered to be surface-associated PspA4Pro, the PspA4Pro released at the end of 4 h (66.93±1.2%) was considered as the initial burst phase of PspA release, followed by a second continuous sustained release phase over 48h. The anionic NPs/NCMPs formulations showed a significantly ($p<0.05$, ANOVA/Tukey's comparison) lower cumulative release achieving only 21.01±1.5% release after 48 h compared to the cationic NPs/NCMPs formulations with nearly 83.13±0.84% of PspA4Pro released at the end of 48 h.

An *in vitro* release kinetics study was performed to determine the PspA4Pro release mechanism. Comparison of the rates of release using zero and first order and the Higuchi rate equations are shown in Table 5-2. PspA4Pro was released from anionic NPs/NCMPs formulations according to the Higuchi diffusion model (r^2 value of 0.836, and the release rate constant k_1 $(h^{-1/2})$ was 2.1 (Table 5-2). For cationic NPs/NCMPs formulations, PspA4Pro was released according to a first order model r^2 value of 0.944, and the release rate constant k_1 $(h^{-1/2})$ was 8.1 (Table 5-2).
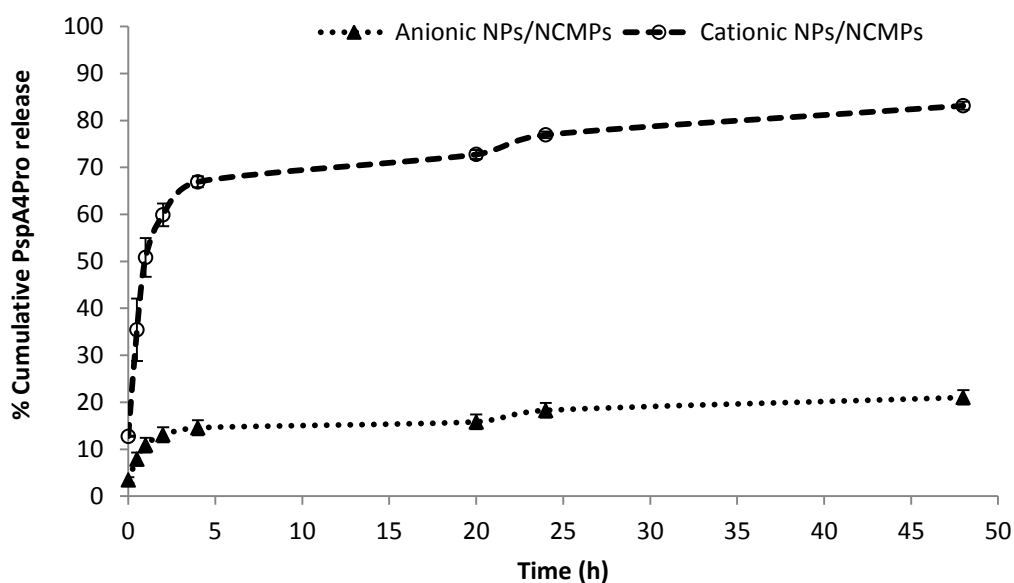
Figure 5-3: Cumulative *in-vitro* release of PspA4Pro from anionic and cationic NPs/NCMPs formulation in PBS buffer at 37°C. Data represent mean ± S.D., n=3.

Table 5-2: Release parameters of PspA4Pro from anionic and cationic NPs/NCMPs formulations.

Formulation	Zero Order		First order		Higuchi	
	r^2	k_o (h^{-1})	r^2	k_1 (h^{-1})	r^2	k_1 $(h^{-1/2})$
Anionic NPs/NCMPs	0.671	0.27	0.699	-0.0014	0.836	2.1
Cationic NPs/NCMPs s	0.519	0.98	0.944	-0.0097	0.723	8.1

5.4.4. Investigation of PspA4Pro structure

The primary structure of PspA4Pro was investigated using SDS-PAGE analysis. According to Figure 5-4, the molecular weight markers are represented in Lanes 2 and 7, and PspA4Pro standard in lane 1 revealed a clear band at about 55 KDa. The PspA4Pro released from anionic NPs, anionic NPs/NCMPs, cationic NPs/NCMPs and cationic NPs Lanes 3, 4, 5 and 6, respectively, also showed similar clear banding patterns to the PspA4Pro standard (Figure 5-4).
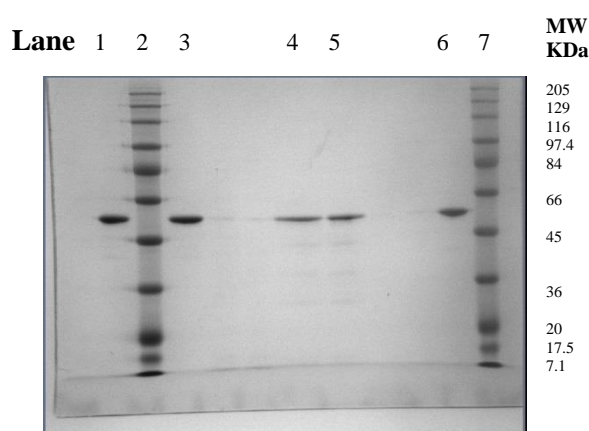
Figure 5-4: SDS-PAGE behaviour of PspA4Pro released. Lanes represent, PspA4Pro standard (1), molecular weight standard markers (2, 7), PspA4Pro released from anionic NPs (3), PspA4Pro released from anionic NPs/NCMPs (4), PspA4Pro released from cationic NPs/NCMPs (5), and PspA4Pro released from cationic NPs (6). Difference in band intensity was due to different loading.

The secondary structure analysis of PspA4Pro standard and PspA4Pro released from anionic and cationic NPs/NCMPs was performed using CD spectral data. Figure 5-5 A and B shows the structure of standard PspA4Pro and PspA4Pro released from anionic and cationic NPs/NCMPs respectively. The CD spectra show two characteristics minima at 222 and 208 nm which are known to be associated with an α-helical structure (30). In support of these data structural analysis showed that the predominant structure of standard PspA4Pro, and, PspA4Pro released from anionic and cationic NPs/NCMPs was helical displaying 50, 51 and 45 % helicity respectively (Table 5-3). Comparing the

CD results of PspA4Pro released from anionic and cationic NPs/NCMPs with that of standard PspA4Pro, the content of α-helix increased by 1 and 5 %, respectively.

A

B
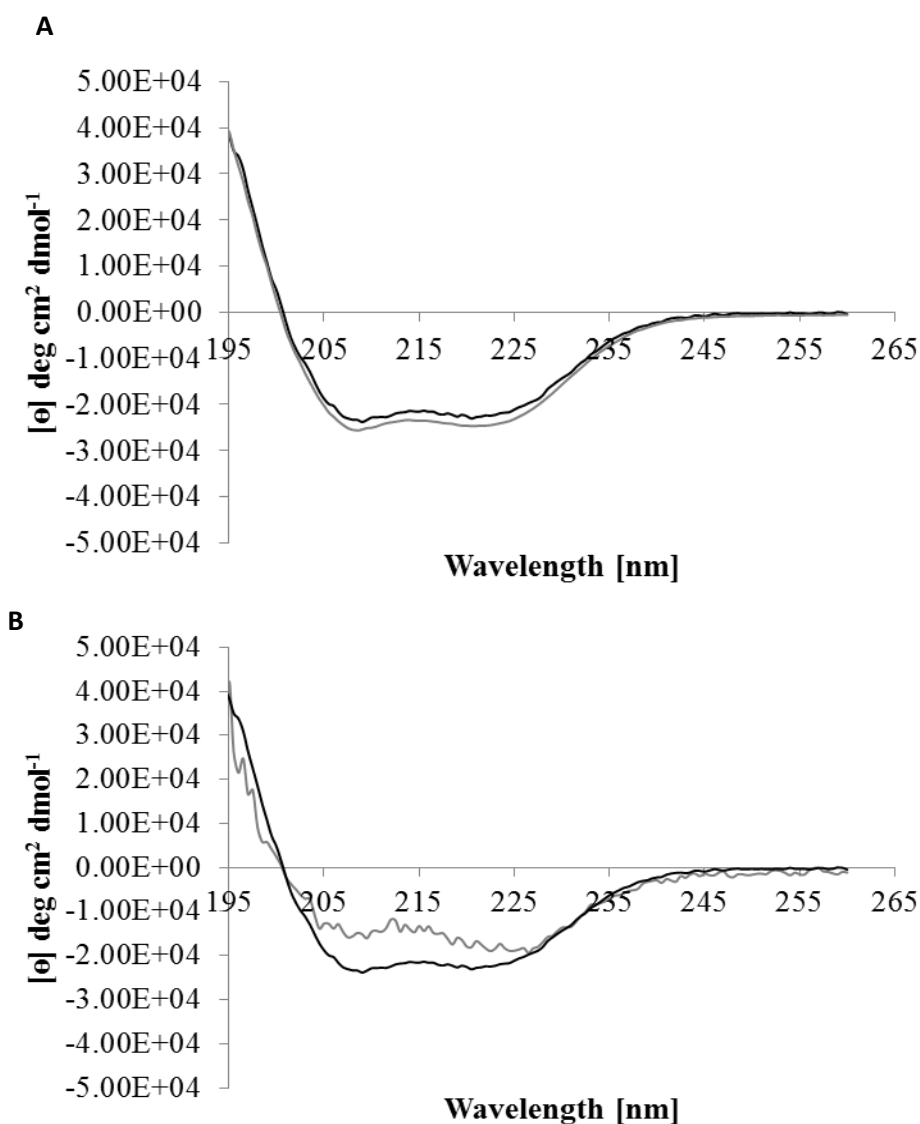
Figure 5-5: The CD spectra of PspA4Pro released from anionic NPs/NCMPs (grey) and PspA4Pro standard (black) (A) and PspA released from cationic NPs/NCMPs (grey) and PspA4Pro standard (black) (A).

Table 5-3: The percentage of secondary structure conformation for PspA4Pro standard and PspA4Pro released from anionic and cationic NPs/NCMPs.

	Helix	Strands	Turns	Unordered
PspA standard	50.0 ± 0	22.0 ± 0.014	7.5 ± 0.007	21.0 ± 0.014
PspA released from anionic NPs/NCMPs	51.0 ± 0.04	21.0 ± 0.0566	7.50 ± 0.007	21.0 ± 0
PspA released from cationic NPs/NCMPs	45.0 ± 0.0212	28.0 ± 0.0212	7.00 ± 0	20.0 ± 0

5.4.5. *In vitro* antigenicity study of PspA4Pro

The antigenicity of PspA4Pro released from anionic and cationic NPs/NCMPs were evaluated using ELISA with specific PspA monoclonal antibody and presented as relative antigenicity. The ELISA assay measures the ability of released PspA4Pro to bind and be recognized by an anti-PspA antibody. The results show that the relative antigenicity of PspA4Pro is maintained after release from the anionic NPs/NCMPs (0.95±0.14) and from cationic NPs/NCMPs (0.26±0.00).

5.4.6. Cytotoxicity study

The cytotoxicity of unloaded anionic and cationic NPs on DCs cell line was assessed after 4 h exposure using MTT assay (219). Figure 5-6 shows decreasing cell viability with increasing NPs concentration. The anionic NPs displayed a cell viability of 86.38±5.5 % at 5 mg/ml concentration after 4 h exposure. On the other hand, cationic NPs displayed a DCs viability of 69.82±5.28 % at 5 mg/ml concentration after 4 h exposure. Both NPs showed cell viability more than the A549 cell viability after 24 h reported in section 3.4.9 and 4.4.10. This could be due to short period of exposure.
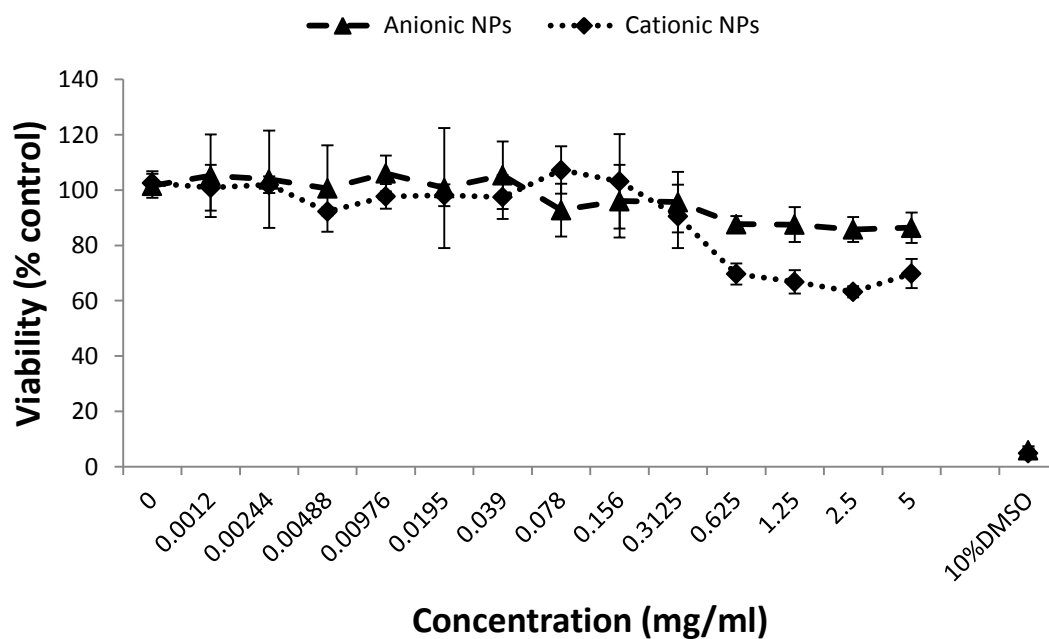
Figure 5-6: DCs viability measured by MTT assay after 4 h exposure to anionic and cationic NPs. Data represent mean ± SD, n=3.

5.4.7. NPs cellular uptake by DCs

The uptake of FITC-BSA loaded anionic and cationic NPs by DCs was confirmed by CLSM. The cell wall of the DCs was stained with WGA TR, the nucleus was stained with DAPI and the NPs loaded with FITC-BSA were observed under red, blue and green channel, respectively. Regardless of the surface charge of NPs, the green fluorescence was seen inside DCs confirming the presence of NPs. Figure 5-7 shows NPs intracellular localisation inside DCs after 1 h of co-incubation in cell culture media.
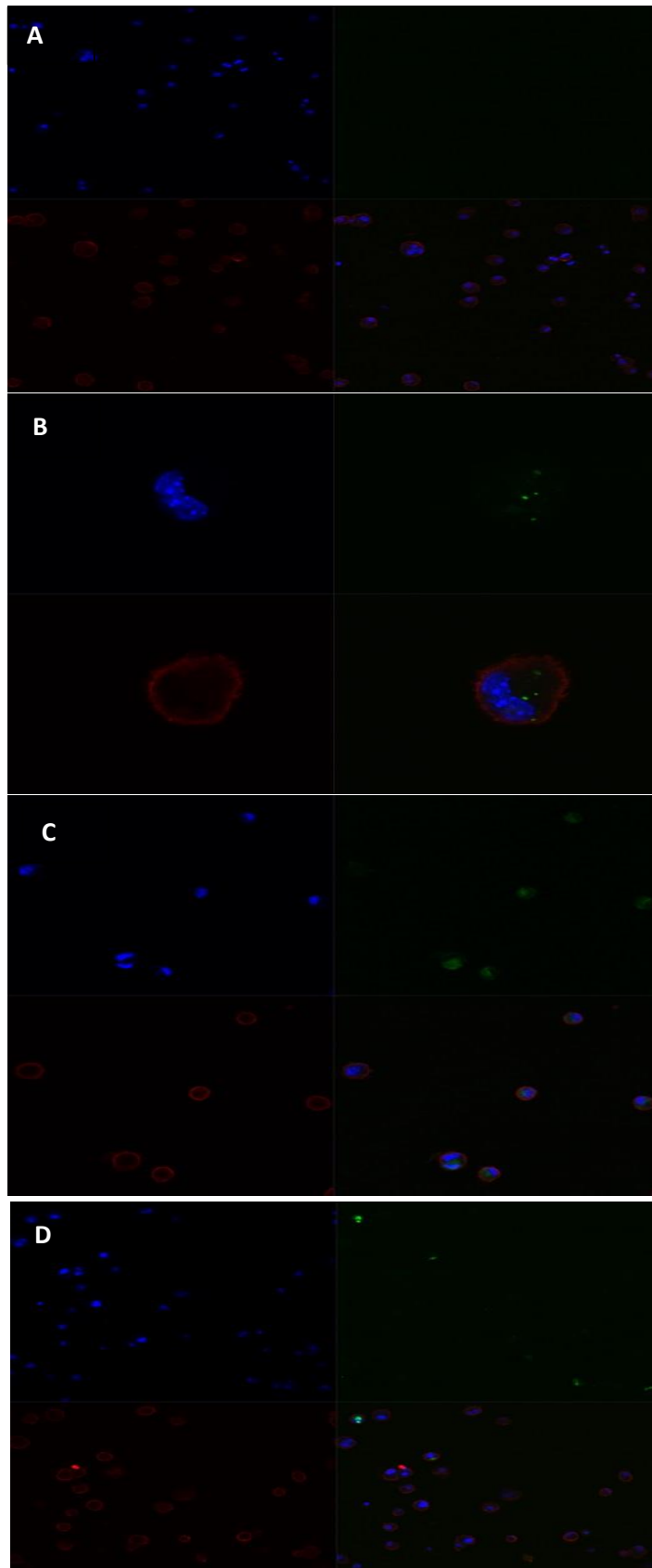
Figure 5-7: Confocal microscopic image of anionic NPs uptake by DCs. (A) DCs incubated without NPs at 20x, (B) DCs incubated with anionic NPs at 63x, and (C) DCs incubated with anionic NPs at 20x, and (D) DCs incubated with cationic NPs at 20x (red channel for WGA TR), (blue channel for DAPI), and (green channel for FITC-BSA).

5.5. Discussion

The results obtained with BSA as a model antigen in chapters 3 and 4 were promising so further work was performed on PspA4Pro as a therapeutic antigen. However, it should be taken into account that each protein has a different molecular weight, and chemical structure. In this study, the optimum parameters inferred from BSA for PspA4Pro encapsulation into anionic and cationic NPs followed by spray drying with L-leucine to produce NCMPs as pneumococcal protein vaccine against *S. pneumonia* to be administered by dry powder inhalation were used.

The particle size of anionic NPs increased when CHL was incorporated (Table 5-1). The increase in size observed can be related to the increased viscosity of EAP due to the presence of CHL, which lowered the shear stress on polymer OP during sonication and produced larger emulsion droplets and consequently larger NPs. Also, it could be attributed to the presence of CHL on the surface of the cationic NPs. However, the CHL: PGA-co-PDL ratio in the final cationic NPs was lower than the theoretical ratio, due to the fact that a certain amount of CHL was remained in the EAP and removed by washing (212) (more detail discussed in section 4.5.1).

Also, it could be observed that the particle size of BSA loaded anionic and cationic NPs (Table 4-2) were larger than the PspA4Pro loaded anionic and cationic NPs (Table 5-1). This could be attributed to the fact that the PspA4Pro has an elongated shape structure (Figure 5-1.B) and a lower Mwt (55 kDa) while the BSA has a heart shape structure (Figure 3-1) and larger Mwt (66 kDa) thus enhance increase in particle size of NPs.

The efficiency of NP surface coating can be measured by estimating the zeta potential of the aqueous suspension containing NPs. The surface charge values may be positive or negative depending upon the nature of the polymer or the material used for coating. The zeta potential of the anionic NPs was negative, as expected, because of the hydroxyl end groups on PGA-co-PDL (Table 5-1). The cationic NPs were

electropositive confirming the presence of CHL on the PGA-co-PDL NPs surface Table 5-1. This could be explained by electrostatic interactions between the negatively charged groups of PGA-co-PDL and the positively charged CHL that induce adsorption of CHL onto the NPs surface. Only a fraction of the amino groups were required to neutralize the negative charges of PGA-co-PDL, whereas the remaining free amino groups were responsible for the resulting positive zeta potential (109; 211).

The encapsulation efficiency of PspA4Pro in the anionic NPs 75.3±6.2% was significantly higher than for cationic NPs 50.2±7.1%. This could be explained by electrostatic interactions between the negative charge of PspA4Pro and the positive charge of CHL (214). The CHL attracts some of the PspA4Pro to the surface of the NPs during the preparation and hardening process, which significantly decreases the encapsulation efficiency (214). This was confirmed by the first initial burst release phase (section 0) at time 0 h which was considered as a result of loss of surface PspA4Pro.

The PspA4Pro loading in anionic NPs (65.73±5.6 µg/mg) decreased substantially (9.84±1.4 µg/mg) when CHL was added to the EAP to produce cationic NPs. This was expected from predictions based on equation 1-2 in which DL is inversely proportional to the polymer amount (PGA-co-PDL alone for NPs and PGA-co-PDL and CHL for CHL-NPs) (147).

Also, it could be observed that EE% and DL of BSA loaded anionic and cationic NPs (Table 4-4) were lower than the PspA4Pro loaded anionic and cationic NPs (Table 5-1). This could be attributed to the fact that BSA has a heart shape structure (Figure 3-1) and larger Mwt (66 kDa) while PspA4Pro has an elongated shape structure (Figure 5-1.B) and a lower Mwt (55 kDa) thus providing more space to encapsulate more protein inside the NPs.

It has been reported a dose of 1-5 µg of PspA was sufficient to stimulate an immune response in mice when injected intramuscularly or subcutaneously (30; 157; 220). However, when PspA was delivered nasally (a mucosal site) with an adjuvant (nontoxic A subunit mutant of cholera toxin S61F), a dose of only 100 ng was needed to stimulate an immune response correspondent to the response produced by oral delivery of 7.5 µg (221). Assuming that PGA-co-PDL particles developed in this study were delivered via inhalation (through mucosal site), the dose needed would be about 100 ng of PspA for mice which is equivalent to a dose of 4 µg of anionic NPs/NCMPs and 25 µg of cationic NPs/NCMPs. Also, one should consider that the dose of PspA4Pro would be changed when applied to human vaccination (although it would be based on the animal studies).

The anionic and cationic NPs/NCMPs were produced via spray drying using L-leucine as a carrier. The photomicrograph of anionic and cationic NPs/NCMPs shows irregular and corrugated surface texture (for more detail and discussion see section 3.5.2).

The higher burst release observed with the cationic NPs/NCMPs formulations at time zero (12.75±0.1%) compared to anionic NPs/NCMPs may be due to some of the PspA not being encapsulated in the particles, but instead was on the surface, due to interactions between the positive CHL and negative PspA, affecting the real encapsulation efficiencies (110).

The *in vitro* release data of anionic NPs/NCMPs formulations showed a lower cumulative release achieving 21 % release after 48 h. The cationic NPs/NCMPs formulation showed higher cumulative releases, with nearly 83 % of PspA4Pro released at the end of 48 h. These differences in release pattern of the formulations may be due to a combination of factors, such as PspA4Pro loading, and presence of CHL on the surface of NPs (88). For both formulations the noticed change in release profile at 20-24h after the initial burst release could be due to the distribution of PspA4Pro inside NPs or a change in degradation rate f NPs due to changed surface porosity (141).

CHL coating NPs dissolves in water and therefore does not slow down drug diffusion from NPs (156; 110).

The *in vitro* release kinetics were studied to determine the PspA4Pro release mechanism. PspA4Pro was released from anionic NPs/NCMPs formulations according to Higuchi diffusion model. Therefore, the sustained release of PspA4Pro from anionic NPs/NCMPs appears to be a diffusion-limited process (66). PspA4Pro was released from cationic NPs/NCMPs formulations according to dual pattern first order model and Higuchi diffusion model. First order kinetics equation describes release of PspA4Pro which is not effectively encapsulated in NPs and is ready to dissolve from NPs surface. This is a rapid process occurring immediately after placing the formulation into the release medium (215). The Higuchi model describes the second and third phase of PspA4Pro release which appears to be a diffusion-limited process.

The primary structure of PspA4Pro was investigated using SDS-PAGE analysis. The identical bands observed for PspA4Pro standard and released suggests the primary structure has been maintained and was not degraded or affected by the procedure.

The secondary structure of PspA4Pro in the formulation was analysed using CD spectroscopy (172). The PspA4Pro released from anionic NPs/NCMPs confirmed the presence of α-helix structure. However, the PspA4Pro released from cationic NPs/NCMPs confirmed the decreased (~ 5 %) of α-helix structure compared to standard PspA4Pro. This has been related to electrostatic interaction between the positive charge of CHL and the negative charge of PspA4Pro (172).

The ELISA was used to examine the ability of PspA antibody to bind to PspA4Pro released from anionic and cationic NPs/NCMPs (30). This assay determines the ability of PspA4Pro released from anionic and cationic NPs/NCMPs to be identified by a specific anti-PspA antibody. The results indicated the relative antigenicity of the PspA4Pro released from anionic NPs/NCMPs was preserved. These results demonstrate

that PspA4Pro was not susceptible to the conformational changes as those observed with other proteins. However, it was observed that PspA4Pro released from cationic NPs/NCMPs showed 25 % of relative antigenicity. This could be attributed to changes in secondary structure of PspA4Pro after release and could be due to the release of CHL from the surface of the particles and interact with PspA4Pro released in the medium.

The formulation is designed to target DCs so cytotoxicity studies were performed on a DCs cell line. The anionic and cationic NPs were well tolerated by DCs with approximately 90 % viability at 0.312 mg/ml which decreased to 86.38±5.5 % with anionic NPs and 69.82±5.28 % with cationic NPs at 5 mg/ml concentration. This provides an indication about the feasibility of using anionic and cationic NPs as safe carriers to target DCs.

The uptake of anionic and cationic NPs by JAWS II DC cell type after 1h co-incubation was confirmed by CLSM. Wischke *et al.* reported similar results with FITC-BSA loaded PLGA microparticles where the FITC-BSA loaded microparticles internalized successfully by DCs (135). In this study the fluorescence signal visualized have not quantified due to non specific staining visible in some parts of the well and to prevent false positive data.

5.6. Conclusion

This study introduced a successful method for preparing anionic and cationic NPs/NCMPs for encapsulating and delivering PspA4Pro as a dry powder. The results showed reproducible size and entrapment efficiency with a good antigen loading and morphological characteristics. The PspA4Pro antigen entrapped in NPs preserved its primary and secondary structure to a large extent. The relative antigenicity (i.e. activity) has been retained for anionic NPs/NCMPs while less antigenicity was observed for cationic NPs/NCMPs. Furthermore, cell viability studies on DCs showed that the particles were well tolerated. DCs uptake studies provide evidence of NPs uptake by

DCs within 1 h of incubation. This study suggests that PGA-co-PDL NPs/NCMPs could be further investigated for evaluating the activity and immunogenicity of the released PapA4Pro.

6. General Discussion

6.1. Overview

S. pneumoniae is one of the most significant human pathogens, causing high morbidity and mortality rates globally (3). It is implicated in both non-invasive diseases (e.g. otitis media, sinusitis, and bronchitis) which are generally non-life threating conditions, but lead to discomfort and loss of school or work days and invasive diseases (e.g. pneumonia, bacterial meningitis, and septicaemia) which are life threating conditions (4). There are two types of pneumococcal vaccine available: PPV and PCV. However, they are expensive and do not cover all serotypes (3; 4; 23; 24). Universal research is presently concentrated on establishing other pneumococcal-vaccine approaches that compromise these defects. PspA has gained a special focus because it is a surface protein located on the cell wall in all strains of pneumococci (29). *S. pneumoniae* are generally transmitted by air droplets or direct contact with contaminated respiratory secretions (7) so it is ideal to deliver the vaccine through the pulmonary route. There are limited studies published in literature regarding the development of a delivery system for PspA as a vaccine. The aim of this project was to formulate and characterise nanocomposite microparticles encapsulating PspA4Pro as a vaccine for the prevention of pneumococcal disease by dry powder pulmonary delivery.

6.2. Optimisation of size and drug loading of NPs

Precise adjustment of the various formulation and processing parameters is important to obtain NPs of a desired size and antigen loading. In this study, a particle size of ≤ 500 nm was desired to facilitate uptake of NPs by DCs (43; 98; 156). BSA was used as a model antigen and Taguchi experimental design was applied to optimize the double emulsion solvent evaporation method to achieve desired size and loading.

It was found that the NPs size was influenced by different parameters in the following order: polymer mass > OP volume > sonication amplitude > surfactant concentration > EAP sonication time IAP sonication time > IAP volume > BSA concentration. While

the influence on BSA loading had the following order: BSA concentration > IAP volume > polymer mass > surfactant concentration > OP volume > EAP sonication time > sonication amplitude > IAP sonication time.

It was found that that the polymer mass followed by the OP volume and sonication amplitude had the greatest influence on the particle size of NPs.

In general, an increase in the mass of substances used will increase the particle size. This effect of the polymer mass on the particle size attributed to the increased viscosity of the OP leading to a less efficient stirring of the medium and to increased NPs coalescence (144). Also, a low OP volume produces a concentrated and viscous polymer solution therefor it is more difficult to break up the polymer solution into smaller droplets during the second emulsification (222). This size increase was also observed with PLGA protein-loaded NPs, when using a double emulsion solvent evaporation method. When the polymer mass increased from 200 mg to 400mg the particle size increased from 207±6 nm to 1090±210 nm (143). The presence of high concentrations of the surfactant (PVA) in the IAP leads to increase in the viscosity of the primary emulsion (w/o) and lead to the formation of larger particles. Yang et al. investigate the effects of the presence of PVA into the IAP on the different characteristics of BSA loaded PCL microspheres. They noticed that at higher concentrations of PVA in the IAP the viscosity of the primary emulsion increased and lead to difficulty in breaking up the emulsion into smaller droplets (222). A similar result was reported in previous study in which the size of IgG loaded PCL microspheres increased with the presence of PVA in the IAP (223).

Furthermore, the rate of size reduction decreased considerably when sonication was carried out beyond the amplitude of 45 % or when the EAP and IAP sonication time increased. This effect could be attributed to more cavitation created by increasing the amplitude, which reduced the efficiency of energy transmission and decreased the

ultrasonic effect (145). Similar results reported by Ito *et al.* who found that the particle size of PLGA microspheres was not affected by stirring time period (224). In contrast to Yang et al. who found that the speed of stirring is the predominant factor affecting particle size of PCL: PLGA microspheres encapsulating BSA (222).

A successful drug delivery system should have a high loading capacity in order to decrease the amount of drug and excipients used for manufacturing the delivery system. (143). The influence of different parameters on the DL of NPs had the following order: BSA concentration>IAP volume > polymer mass > PVA concentration > OP volume > EAP sonication time and IAP sonication time > sonication amplitude. While the effect on the EE % had the following order: polymer mass > PVA concentration BSA concentration > IAP volume > OP volume > EAP sonication time and IAP sonication time > sonication amplitude.

BSA concentration had the greatest influence on the DL. The DL increased profoundly as the BSA concentration increased from 0.2 to 1 %. This was expected from predictions based on equation used for DL calculation in which DL is positively proportional to the amount of BSA. Similar results were reported in literatures. Bilati *et al.* prepared FITC-BSA loaded PLGA NPs at different concentrations. When FITC-BSA concentration increased the DL increased subsequently (143). Also, Youan *et al.* fabricated PCL microparticles using the w/o/w emulsion solvent evaporation method and BSA as a model drug. When the BSA: polymer ratio increased from 5:100 to 37.5:100, an increase in BSA loading (11.8 times higher) was reported (225).

Also, BSA concentration was the third factor that affects EE %. The EE % of BSA increased when BSA concentration increased from 0.2 to 0.5% but interestingly it decreased considerably as the BSA concentration increased further to 1%. In fact, an increase in BSA concentration to high levels (1 %) is not always beneficial; this trend has been explained by the amount of polymer used being insufficient to completely

encapsulate the BSA (143). Furthermore, higher concentration of BSA provide a higher BSA concentration in IAP droplets and thus increase the concentration gradient between the IAP droplets and the EAP and so increases the amount of BSA transported into the EAP (153). Yang *et al.* reported similar results. They prepared PCL: PLGA 65: 35 microspheres encapsulating BSA. At higher BSA theoretical loading (0.57 to 4.8 %), the EE % decreased significantly (79.1 to 55 %) (222).

IAP volume played an important role on DL and EE %, such that, the larger the volume of IAP used, the higher the BSA loading. This effect has been previously reported (147; 152) and is thought to be due to a decrease in the concentration gradient between IAP and EAP. In contrast, Youan *et al.* found that an increase of IAP volume (0.25 to 1.25 ml) lead to decrease in BSA EE % and loading (70 times lower) (225).

The third factor affecting DL was polymer mass. DL decreases substantially with increasing polymer mass, as it was expected from predictions based in the respective equation 2-1 in which DL is inversely proportional to the polymer amount (147). Similar observation was reported by Baras *et al.* They found that the DL of BSA decreased with an increase in PCL concentrations. At a 0.5 % (w/w) concentration of PCL a 24 % BSA loading were obtained while at 3 % (w/w) concentration of PCL the BSA loading decreased to 3 % (w/w) (226).

On the other hand, the polymer mass had the greatest influence on EE % of BSA. This could be correlated with the increased mass of the polymer resulting in a further stabilization of the primary emulsion and limiting the diffusion of BSA through and out of the OP due to higher viscosity of the OP (92). Similar observations were reported by Devineni *et al.* They found that the BSA EE % for microparticles prepared by 4 and 8% (w/v) PCL concentrations increased from 12 to 25% (227). In contrast, Baras et al. reported that the EE % of BSA decreased with an increase in PCL concentrations. At 0.5 % (w/w) concentration of PCL a 73 % BSA encapsulation efficiency were obtained

while at 3 % (w/w) concentration of PCL the BSA encapsulation efficiency decreased to 42 % (226).

The fourth factor affecting DL was PVA concentration. Among the PVA concentrations used, 1 % PVA was found to result in a considerably higher BSA loading. One possible explanation is that 1% PVA concentration provided sufficient covering of the organic/aqueous interface so as to reduce possible leaching of the BSA. Consequently, any further increase in PVA concentration (5, 10 %) resulted in more BSA molecules partitioning rapidly into the aqueous phase during the emulsification procedure due to the emulsifying effect of PVA, resulting in decreased DL (146). Although the PVA concentrations ranked the second factor affecting EE % but there effects on EE % were similar to DL. Mao *et al.* reported similar results when preparing PLGA microspheres by double emulsion solvent evaporation method using PVA as a surfactant. When PVA concentration increased (0.1 to 0.5%) the results shows no further increase in DL and EE % (148). In contrast Yang *et al.* reported that increasing PVA concentration (from 0.025 to 0.05 to 0.1 %) of the IAP results in an increase in EE % and loading of BSA encapsulated PCL microsphere (222).

In addition, the results showed that reducing the OP volume increased DL and EE%. This could be due to the higher viscosity of the organic phase leading to a further stabilization of the primary emulsion and minimize the diffusion of BSA through the OP. This was consistent with Baras *et al*. who observed that the use of a lower OP volume leads to a significant increase in the BSA EE % (from 7 to 13 %) (226).

EAP sonication time and IAP sonication time exert similar effects on DL and EE%. Increasing the sonication time of IAP and EAP resulted in higher encapsulation efficiency % and DL. These results were consistent with the results obtained by Bilati *et al.* They reported that increasing sonication time of IAP up to 30 seconds increased loading efficiency of BSA loaded PLGA microspheres (143).

The factor that has the least effect was sonication amplitude. Increasing sonication amplitude (30 to 45 or 65%) had almost no effect on the BSA encapsulation efficiency % or DL. This effect have been reported in literature and is thought to be caused by a BSA precipitation within the sonication probe due to high pressure and increased fluid cavitations during sonication (136; 149). Similar results were obtained by Bilati *et al.* They reported that increasing sonication intensity from 35 to 65 W increased loading efficiency of BSA loaded PLGA microspheres (143).

From the suggested optimized run produced NPs (HDL NPs) with DL 43.67±2.3 µg/mg, particle size of 445±46.8 nm and zeta potential of −17.44±1.2 mV was selected for further investigations.

6.3. Optimisation of size, drug loading and charge of cationic NPs

Cationic NPs are effectively taken up by DCs. The ionic interaction between the positive charge on the particles surface and the negative charge on cell surface generates a successful bond and promotes particle uptake (87). Furthermore, cationic NPs have greater ability to interact with the proteoglycans on the surface of macrophages and DCs (173). Incorporation of cationic polymers such as chitosan or chitosan derivatives have been shown to enhance uptake of antigens by DCs and subsequently induce a strong immune responses (174). CHL adsorption to PGA-co-PDL NPs was used as a successful strategy to produce cationic NPs. In this study two strategies were used to adsorb CHL to NPs. The first strategy involved adsorption of CHL onto the surface of the already formed NPs by physical adsorption. The second strategy involved addition of CHL to EAP during the process of NPs preparation by double emulsion solvent evaporation method.

In the first strategy, different concentrations of CHL were used with and without 1% PVA. When 1% PVA was used, upon addition of CHL, the zeta potential changed from negative to neutral regardless of CHL concentration. This was due to the ability of the

PVA layer to screen CHL charges leading to an almost neutral zeta potential value (228). These results were consistent with previous work carried out by Mura *et al.* They prepared PLGA NPs by emulsion solvent evaporation method and in the presence of PVA in EAP the fabricated NPs had neutral zeta potential (211).

When PVA was not included the zeta potential changed from negative to neutral at lower CHL concentrations (4 and 8 mg/ml) but at higher CHL concentrations (20 and 30 mg/ml) the zeta potential changed to positive. Chronopoulou *et al* reported similar pattern with chitosan coated PLGA NPs, in the case of lower concentration, the relative PLGA and chitosan concentrations correspond to a concentration close to the one of the isoelectric condition, justifying the finding that the zeta potential of the resulting coated PLGA NPs was very close to zero and then at higher concentration inverts its charge, indicating that the adsorbed chitosan reversed the NPs charge (110). At the highest concentration of CHL tested (34 mg/ml) the NPs surface charge was neutral, probably because of the high viscosity of the CHL solution and steric hindrance created by CHL molecules in the solution which would decrease the efficiency of adsorption (111; 229).

The particle size increased significantly when the concentration of CHL increased to 8 mg/ml. The increase in particle size has been attributed to either the increased viscosity of the CHL solution, which lowered the shear stress on NPs during stirring, and/or the increasing amounts of CHL on the surface of the NPs (212). Similar results reported by Yuan *et al* (212)*.* It was reported that the NPs size increased (182 to 543 nm) with the increase of initial chitosan concentration (0 to 0.17%). However, at CHL concentration of 20 and 34 mg/ml there was no significant change in particle size. This indicated a complete coating of CHL on the surface leading to CHL molecules repelling each other, preventing particle aggregation and hence an increase in particle size (111).

At the same concentration of CHL there was no effect of different PVA concentration on the particle size. But when no PVA was used the particle size increased significantly this is because the PVA is known to prevent particle aggregation (80).

The second strategy produced successfully CHL-NPs with positive charge in the whole range of CHL concentrations examined (2, 4, 6, 8, 10, 16, 20 mg/ml) while the first strategy failed to.

The zeta-potential of cationic NPs increased with CHL feed concentrations until a zeta-potential plateau was reached at approximately +24 mV (CHL concentration of approximately 16–20 mg/ml). This could be indicative of saturation in adsorption of CHL on the NPs (191; 111; 212). The particle size of cationic NPs was different with two groups of NPs present regardless of CHL concentrations. The particle size of cationic NPs increased significantly at low concentration of CHL ranging from 2 to 4m g/ml. This could be attributed to the increased viscosity of CHL, lowering the shear stress of the OP during sonication producing larger emulsion droplets and subsequently larger NPs (212). Higher concentrations of CHL (6, 10, 16 mg/ml) the particle size did not change significantly. This has been attributed to a complete coating of the NPs by CHL molecules so additional CHL would repel each and prevent particles aggregation.

Similar results were reported by Guo *et al.* Cationic PLGA NPs were produced by adsorption of different chitosan concentrations (0–2.4 g/L) on PLGA, via double emulsion solvent evaporation method. They found that the NPs size increased from 261.5 nm to 972.7 nm with increase in chitosan concentration from 0 to 2.4 g/L. These increase in size accompanied by increase in zeta potential from - 20.3 to +55 mV which confirm the adsorption of chitosan on PLGA NPs (111).

Also, the pattern of change in particle size when CHL was added to the EAP was similar to that when CHL was added after NPs formation. It was observed that all cationic NPs regardless of preparation method displayed a neutral or positive charge

that could be due to electrostatic interactions between the negatively charged groups (-OH) of PGA-co-PDL and the positively charged CHL inducing adsorption of CHL onto the NPs surface. Also, the change in zeta potential need a small ratio of the amino groups to neutralize the negative charges of PGA-co-PDL while the reset of free amino groups could be reason behind the change in zeta potential (211; 230).

As the concentration of CHL increased the amount of adsorbed CHL per mg of NPs increased over the entire range of CHL concentrations examined (0–20 mg/ml) and there was no plateau of adsorption was reached. In contrast, the zeta potential did not change with increased amount of CHL adsorbed on the NPs at high concentrations of CHL (greater than approximately 16–20 mg/ml). This could be attributed to the multiple layers model of CHL adsorption on NPs. In this model only a small ratio of CHL influenced the zeta-potential (the first few layers) and the layers after do not change the zeta-potential due to the apparent surface charge (amine groups) per unit area is constant (111).

The second strategy was selected to examine CHL adsorption onto NPs and to explain the mechanism of adsorption because it gave positive zeta potential over the entire range of CHL concentrations examined. The four adsorption isotherms (Langmuir, BET, Freundlich, and Halsey) models evaluated to describe the adsorption mechanism of CHL onto NPs. It was found that the adsorption of CHL on NPs complied with multilayer adsorption pattern irrespective of which model was examined. The leading factor particularly in the development of the first adsorption layer was electrostatic force between CHL (with positive charge) and PGA-co-PDL surface (with negative charge). When the CHL concentration increased it is likely that the following layers of CHL adsorbed on the first layer of CHL without interaction with the NPs surface. When more CHL layers adsorbed the CHL molecules would repel each due to similar charge other because of the same charge however CHL molecules interacted via hydrogen bonds,

hydrophobic interactions, and van der Waal's forces. Mainly, the NPs great surface energy and surface area had a significant function in CHL multilayer adsorption (111). The cationic NPs prepared at a CHL concentration of 10 mg/ml was selected for further investigations in this study because these particles had a similar size (480.23±32.2 nm) to the anionic NPs.

6.4. Preparation and characterisation of PspA loaded anionic and cationic NPs

When the optimised conditions applied for the preparation of PspA encapsulated NPs the particle size of anionic NPs was 310.4±25.3 nm and for cationic NPs was 409.7±49.5 nm. The presence of CHL increased the particle size significantly and changed zeta potential of anionic NPs (-29.17±0.09 mV) to positive (+21.33±1.2 mV).

The EE % of Psp4ProA in the anionic NPs was 75.3±6.2% and it was significantly higher than EE% of cationic NPs 50.2±7.1%. Also, the PspA4Pro loading in cationic NPs (9.84±1.4 µg/mg) decreased significantly in comparison with anionic NPs (65.73±5.6 µg/mg). Similar results reported by Anish *et al*. (157). They prepared PLA microparticles encapsulating PspA using double emulsion solvent evaporation method. The EE % of PspA obtained ranged from 43 to 78 % and PspA loading of 2.5 to 3.67 µ/mg (157).

The dose of PspA in range of 1-5 µg has been shown to be sufficient to evoke immunity in mice when delivered intramuscularly or subcutaneously (30; 157; 220). On the other hand, when PspA was delivered through nasal route (i.e. mucosal site) with an adjuvant, only a dose of 100 ng was needed to stimulate immunity compared to the immunity produced by oral delivery of 7.5 µg (221). Assuming that PGA-co-PDL NPs/NCMPs developed in this study were to be delivered by inhalation (through mucosal site), the PspA dose would be about 100 ng for mice, which is equivalent dose of 4 µg of anionic NPs/NCMPs and 25 µg of cationic NPs/NCMPs. In addition, one should consider that

the dose of PspA4Pro would be changed when apply to human vaccination (although it would be based on the animals studies).

The anionic and cationic NPs appear to be well tolerated by DCs. This provides an indication about the feasibility of using anionic and cationic NPs as safe carriers to target DCs.

The uptake of anionic and cationic NPs by JAWS II DCs cell line after incubation for 1 h was confirmed by CLSM. There was good agreement between particle size (around 200 and 445 nm) and the ability for an uptake by DCs (89; 135).

Similar results reported by Foged *et al.* (89). They examined the DCs uptake of a wide size range and surface charge characteristics of model fluorescent polystyrene particles. They found that the optimal size of particles for efficient uptake by DCs was 500 nm and below. Also, they found that the larger particles uptake enhanced by modifying the surface charge (89).

So we may conclude that anionic and cationic NPs are efficiently ingested by DCs and could be applied for the delivery of antigens to DCs.

6.5.   Optimisation of spray drying of NPs into NCMPs

The PGA-co-PDL NPs were dispersed into L-leucine solution and spray dried to produce NCMPs carriers suitable for pulmonary delivery via DPIs. The Taguchi experimental design was applied to evaluate the influence of the spray drying parameters on the yield % of NCMPs powder and the order was as follows: the feed rate > aspirator capacity > air flow rate > inlet drying temperature > the feed concentration. The highest yield (Run H, 50.96±2.26 %) was obtained when the suggested combinations were as following: the feed rate= 10 %, aspirator capacity= 100 %, air flow rate=400 L/h, inlet drying temperature= 100 ºC, the feed concentration= 12.5 mg/ml.

The most important factor was feed rate at 15 %, the atomizing air may not be able to penetrate the stream of liquid. Consequently, insufficient atomization and drying may cause deposition of a large amount of NCMPs on the walls of the drying chamber and the cyclone separator (161). Similar observation was reported by Motlekar *et. al.* (161). They found that the high feed rate (25 %) of the spray suspension lead to almost no yield of dry powder (161).

The second important factor was aspiration as a high aspirator flow rate created greater centrifugal force leading to an increase in the collection efficiency (162). Airflow can have a negative effect on powder yield % at high spray flow small droplets are produced, which are collected less efficiently by the centrifugal force (162). Shi and Hickey optimised spray drying condition to prepare PLGA microparticles suitable for inhalation. They found that the airflow and aspirator capacity had significant effect on the yield of dry powder. Where the airflow had negative effect, showing that powder yield decreased with the increase of the airflow while the aspirator capacity had positive effect, showing that powder yield increased with the increase of the aspirator capacity (162).

The inlet temperature of drying air had considerable effects on the yield of dry powder. It was noticed that as inlet temperature increased from 50 to 100 ℃ this resulted in an increased powder yield. It has been reported that high inlet temperature can reduce the drying time and inhibit particle aggregation (163). Furthermore, a higher inlet temperature promotes a decrease of residual moisture by enhancing water evaporation resulting in less particles stick in the drying chamber (164).

Also, it was observed that the change in the concentration of total solid in the spray dried suspension showed no improvement in the yield of dry powder. This observation was in contrast to the results reported by Jensen *et al.* were they found that as the

concentration of solid in the suspension increased the yield of dry powder increased (92).

Optimum conditions for the production of the highest yield% of dry powder resulted in 50.96±2.26 % of NCMPs (92).

Photomicrographs of NCMPs showed irregular and porous microparticles. This occurred due to excessive build-up of vapour pressure during water evaporation in the spray drying process and occurs with hydrophobic amino acids, such as L-leucine, for improved aerosolisation performance (100; 165; 169). These observations were in contrast to results reported by Tawfeek *et al* (66). They produced PGA-coPDL/L-leucine microparticles with smooth surface.

Anionic NPs/NCMPs produced a higher FPD, and FPF % 45.00±4.70 μg and 78.57±0.1 %, respectively, than cationic NPs/NCMPs 32.51±6.67 μg and 46.79±11.21 %, respectively. This could be attributed to incomplete powder de-aggregation as van der Waals forces between particles were not completely overcome upon inhalation despite the low density of the particles. In addition, powder aggregation of cationic NPs/NCMPs was confirmed with a Carr's index of ≥32, indicating the flow was very poor (66). Similar results were reported previously where PGA-co-PDL/L-leucine NCMPs aerosolisation studies showed FPF% of 76.95±5.61% (68).

As the anionic and cationic NPs/NCMPs deposition in term of MMAD will reach bronchial-alveolar region in the lung, cytotoxicity studies were carried out on A 549 cell line. The anionic and cationic NPs/NCMPs appear to be well tolerated by the cell line at 2.5 mg/ml concentration indicating a good toxicity profile. This provides an indication about the feasibility of using anionic and cationic NPs/NCMPs as safe carriers for pulmonary drug delivery (68).

6.6. Investigation of *In vitro* release of protein

In vitro release studies of NPs/NCMPs formulations showed biphasic release profile with a first initial burst release followed by a second continuous sustained release phase over 48h. In the cationic NPs/NCMPs formulations the observed high-burst release at time zero (22.41±6.7%) could be explained by the majority of the BSA being adsorbed onto the surface (110). Also, the cationic NPs/NCMPs formulations showed a higher cumulative BSA release at the end of 48 h compared to anionic NPs/NCMPs. These differences in release patterns may be due to a combination of factors, such as BSA loading, and presence of BSA on the surface of the NPs (152). Similar results reported by Wang *et al.* (230). They found that chitosan modified PLGA NPs showed higher burst release of the drug than the PLGA NPs.

For both formulations the notable change in release profile at 20-24h after the initial burst release could be due to the distribution of BSA inside NPs or a change in degradation rate due to changed surface porosity (152). Furthermore, it is worth noting that CHL adsorbed on NPs dissolves in water and therefore does not hinder drug diffusion from the NPs (156; 110). These results were consistent with results reported by Gupta *et al*. where they found that poly-ω-caprolactone and chitosan coated poly-ω-caprolactone NPs had similar *in vitro* percentage cumulative release of hemagglutinin protein irrespective of presence of chitosan coat on NPs surface (54).

A study of the *in vitro* release kinetics was carried out to determine the mechanism of BSA release. BSA was released from anionic NPs/NCMPs formulations according to the Higuchi diffusion model. However, BSA was released from cationic NPs/NCMPs formulations according to a dual pattern first order model and Higuchi diffusion model. A first order kinetics equation described the release of BSA which was not effectively encapsulated in cationic NPs and is readily to dissolve from cationic NPs surface. This was a rapid process occurring immediately after introducing the formulation into the

release medium (215). The Higuchi model describes the second part of the BSA release which appears to be a diffusion-limited process.

The *in vitro* release data of anionic and cationic NPs/NCMPs formulations showed similar results with PspA4Pro encapsulated.

6.7. Investigation of structure and relative antigenicity of released protein

In this study the released BSA and PspA4Pro from anionic and cationic NPs/NCMPs maintained their structure and preserved its activity. The BSA and PspA4Pro released maintained their primary structure and was not degraded or affected by the procedure. The secondary structure of BSA and PspA4Pro released from anionic NPs/NCMPs confirmed the presence of α-helix. However, the BSA and PspA4Pro released from cationic NPs/NCMPs confirmed the presence of decreased α-helix (8.5 and 5 %, respectively) compared to standard BSA and PspA4Pro. This could be due to electrostatic interaction between positive charge of CHL and negative charge of BSA and PspA4Pro (172). This relative low decrease in α-helix content has also been reported in literature (140; 231; 232).

The relative antigenicity of the PspA4Pro released from anionic NPs/NCMPs was preserved. These results demonstrate that PspA4Pro was not susceptible to formulation parameters induced conformational changes as those observed with other proteins. However, it was observed that PspA4Pro released from cationic NPs/NCMPs showed 25% of relative antigenicity. This could be attributed to changes in secondary structure of PspA4Pro after release.

7.Future Work

7.1. Future work

These results would be helpful in improving optimised processes for producing polymeric particles to enhance the immunogenicity and stability of protein antigens. The selected formulations encapsulating PspA4Pro have been provided to Instituto Butantan, Brazil to examine the activity, immunogenicity, and pneumococcal challenge *in vivo* (233).

Moreover, the immunogenicity of the formulation can be examined by measuring the up regulation of MHC II, CD 40, CD 80, CD83, and CD86 surface markers expressed on DCs surfaces by flow cytometry.

The biological activity of PspA4Pro released from anionic and cationic NPs/NCMPs can be evaluated by *Escherichia coli* killing assay (30). This assay depends on the role of apolactoferrin as bactericidal. The function of PspA in pneumococcal infection is to interact with apolactoferrin and avoid its bactericidal action. Shortly, the *E. coli* culture will be grown to early log growth phase then it will be inoculated at predetermined number in a microtiter plate. Apolactoferrin will be dissolved in medium at a selected concentration, followed by the addition of control PspA or PspA released from NP/NCMPs. Then *E. coli* will be added. After overnight incubation colony forming units will be detected by counting colonies grown on plates. The log colony forming units killed will be figured out by subtracting the experimental readings from control bacteria cultures grown under the same conditions.

The bio distribution of PspA after inhalation can be examined by radioisotope counting assay (35). Briefly, PspA will be labeled with indium chloride via N-terminal and ε-Lys amino groups, using diethylenetriaminepentaacetic acid then it will be delivered alone or as a complex with the formulation. The radioisotope counts in the body tissue (mouth, olfactory area, nasopharynx, bronchi, and lungs) at 0.5, 1, 4, 8, 20, and 40 h after inhalation will be evaluated with a γ-counter.

Further studies will evaluate the long term stability of the dry powder formulation at various temperature and humidity conditions. Stability of the formulation at ambient conditions is beneficial in order to prevent cold-chain requirements, avoid moisture adsorption which can lead to powder aggregation and poor flow and aerosolisation behaviour; moreover it will affect the stability and integrity of PspA4Pro. The stability of the dry powder will be examined using DSC and X-ray powder diffraction to determine changes in the crystallinity of the particles. PspA4Pro stability, integrity and activity will be evaluated by SDS-PAGE, CD and lactoferrin assay, respectively (30).

Moreover, the biochemical response of NPs/NCMPs dry powder administered via inhalation into rat lung (*in vivo*) can be assessed. The potential inflammatory reactions will be evaluated by testing the following factors: lung fluid protein activity, lactate dehydrogenase activity, and existance of inflammatory polymorphonuclear cells (234).

Briefly, the bronchoalveolar lavage fluid samples will be added to Coomassie- plus protein assay reagent and will be measured by spectrophotometer at 595 nm. The amount of total protein will be calculated by using a standard curve prepared with BSA (234).

To examine lactate dehydrogenase activity in bronchoalveolar lavage fluid, samples will be centrifuged; then, the supernatant will be added to NADH in Tris/NaCl solution, followed by the addition of pyruvate solution. Lactate dehydrogenase activity was evaluated by kinetic measurements (234).

To evaluate the existance of inflammatory polymorphonuclear cells the bronchoalveolar lavage fluid samples will be centrifuged and the pellet will be dissolved in saline then it will be stained with Diff-Quik and examined by light microscopy to identify macrophage and polymorphonuclear cells (234).

References

References

1. **Klugman, J. and Grabenstein, K.** A century of pneumococcal vaccination research in humans. *Clinical Microbiology and Infection.* 2012, Vol. 18, pp. 15–24.

2. **Watson, D., Musher, D., Jacobson, J., Verhoef, J.** A Brief History of the Pneumococcus in Biomedical Research: A Panoply of Scientific Discovery. *Clinical Infectious Diseases.* 1993, Vol. 17, pp. 913-924.

3. **Barocchi, M., Censini, S. and Rappuoli, R.** Vaccines in the era of genomics: The pneumococcal challenge. *Vaccine.* 2007, Vol. 25, pp. 2963–2973.

4. **Driver, C.** Pneumonia part 2: signs, symptoms and vaccinations. *British Journal of Nursing.* 2012, Vol. 21, pp. 245-249.

5. **Lamb, K., Flasche, S., Diggle, M., Inverarity, D., Greenhalgh, D., Jefferies, J., Smith, A., Edward, G., Denhame, B., McMenaming, J., McDonaldg, E., Mitchellh, T., Chri, S.** Trends in serotypes and sequence types among cases of invasive pneumococcal disease in Scotland, 1999–2010. *Vaccine.* 2014, Vol. 32, pp. 4356–4363.

6. **Bhatty, M., Pruett, S., Swiatlo, E., Nanduri, B.** Alcohol abuse and Streptococcus pneumoniae infections: consideration of virulence factors and impaired immune responses. *Alcohol.* 2011, Vol. 45, pp. 523-539.

7. **Briles, D., Tart, R., Swiatlo, E., Dillard, J., Smith, P., Benton, K., Ralph, B., Brooks-Walter, A., Crain, M., Hollingshead, S., McDaniel, L.** Pneumococcal Diversity: Considerations for New Vaccine Strategies with Emphasis on Pneumococcal Surface Protein A (PspA). *Clinical Microbiology Reviews.* 1998, Vol. 11, pp. 645-657.

8. **Mook-Kanamori, B., Geldhoff, M., van der Poll, T., van de Beek, D.** Pathogenesis and Pathophysiology of Pneumococcal Meningitis. *Clinical Microbiology Reviews.* 2011, Vol. 24, pp. 557–591.

9. **Murphy, L., Travers, P., Walport, M.** *Janeway's Immunobiology.* 7th . New York : Garland Science, 2008.

10. **Nair, G., Niederman, M.** Community-acquired pneumonia: an unfinished battle. *Medical Clinics of North America.* 2011, Vol. 95, pp. 1143–1161.

11. **Gray, C., Mercer, M., Shayne, L., Kriel, C.** Streptococcal Pneumoniae Meningitis. *Immunopaedia.* [Online] 2010. [Cited: november 30, 2014.] http://www.immunopaedia.org.za/index.php?id=750.

12. **Weisfelt, M., de Gans, J., ven der Poll, T., van de Beek, D.** Pneumococcal meningitis in adults: new approaches to management and prevention. *Lancet Neurology.* 2006, Vol. 5, pp. 332–342.

13. **Patterson, C., Loebinger, M.** Community acquired pneumonia: assessment and treatment. *Clinical Medicine.* 2012, Vol. 12, pp. 283-286.

14. **Welte, T., Torres, A., Nathwani, D.** Clinical and economic burden of community-acquired pneumonia among adults in Europe. *Thorax.* 2012, Vol. 67, pp. 71-79.

15. **WHO/UNICEF.** WHO/Global Action Plan for Prevention and Control of Pneumonia (GAPP). *WHO World health organization.* [Online] 2009. [Cited: Jun 26, 2012.] http://www.who.int/maternal_child_adolescent/documents/fch_cah_nch_09_04/en/.

16. **Loebinger, M., Wilson, R.** Bacterial pneumonia. *Medicine.* 2008, Vol. 36, pp. 285–290.

17. **Drijkoningen, J., Rohde, G.** Pneumococcal infection in adults: burden of disease. *Clinical Microbiology and Infection.* 2014, Vol. 20, pp. 45-51.

18. **Almirall, J., BolõÂbar, I., Vidal, J., Sauca, G., Coll, P., Niklasson, B., Bartolome, M., Balanzo, X.** Epidemiology of community-acquired pneumonia in adults: a population-based study. *European Respiratory Journal.* 2000, Vol. 15, pp. 757-763.

19. **Marrie, T., Huang, J.** Epidemiology of community-acquired pneumonia in Edmonton, Alberta: an emergency department-based study. *Canadian Respiratory Journal.* 2005, Vol. 12, pp. 139-142.

20. **Broulette, J., Yu, H., Pyenson, B., Iwasaki, K., Sato, R.** The incidence rate and economic burden of community-acquired pneumonia in a working-age population. *American Health and Drug Benefits.* 2013, Vol. 8, pp. 494-503.

21. **Ferreira, D., Jambo, K. and Gordon, S.** Experimental human pneumococcal carriage models for vaccine research. *Trends in Microbiology.* 2011, Vol. 19, pp. 464-470.

22. **Mundargi, R., Babu, V., Rangaswamy, V., Patel, P., Aminabhavi, T.** Nano/micro technologies for delivering macromolecular therapeutics using poly(D,L-lactide-co-glycolide) and its derivatives. *Journal of Controlled Release.* 2008, Vol. 125, pp. 193–209.

23. **Clutterbuck, E., Lazarus, R., Yu, L., Bowman, J., Bateman, E., Diggle, L., Angus, B., Peto, T., Beverley, P., Mant, D., Pollard, A.** Pneumococcal Conjugate and Plain Polysaccharide Vaccines Have Divergent Effects on Antigen-Specific B Cells. *The Journal of Infectious Diseases.* 2012, Vol. 205, pp. 1408–16.

24. **Pletz, M., Maus, U., Krug, N., Welte, T., Lode, H.** Pneumococcal vaccines: mechanism of action, impacton epidemiology and adaption of the species. *International Journal of Antimicrobial Agents.* 2008, Vol. 32, pp. 199–206.

25. **Peabody, R., Hippisley-Cox, J., Harcourt, S., Pringle, M., Painter, M., Smith, G.** Uptake of pneumococcal polysaccharide vaccine in at-risk populations in England and Wales 1999–2005. *Epidemiological Infection.* 2008, Vol. 136, pp. 360–369.

26. **Paradiso, P.** Essential criteria for evaluation of pneumococcal conjugate vaccine candidates. *Vaccine.* 2009, Vols. Vaccine 27S (2009) C15–C18, pp. C15–C18.

27. **Jiang, Y., Gauthier, A., Keeping, S., Carroll, S.** A public health and budget impact analysis of vaccinating the elderly and at-risk adults with the 23-valent pneumococcal polysaccharide vaccine or 13-valent pneumococcal conjugate vaccine in the UK. *Expert Review of Pharmacoeconomics & Outcomes Research. Early online.* 2014, pp. 1-11.

28. **Ogunniyi, A., Grabowicz, M., Briles, D., Cook, A., Paton, J.** Development of a Vaccine against Invasive Pneumococcal Disease Based on Combinations of Virulence Proteins of Streptococcus pneumoniae. *Infection and Immunity.* 2007, Vol. 75, pp. 350–357.

29. **Linder, A., Hollingshead, S., Janulczyk, R., Christensson, B., Akesson, P.** Human antibody response towards the pneumococcal surface proteins PspA and PspC during invasive pneumococcal infection. *Vaccine.* 2007, Vol. 25, pp. 341–345.

30. **Haughney, S., Petersen, L., Schoofs, A., Ramer-Tait, A., King, J., Briles, D., Wannemuehler, M., Narasimhan, B.** Retention of structure, antigenicity, and biological function of pneumococcal surface protein A (PspA) released from polyanhydride nanoparticles. *Acta Biomaterialia.* 2013.

31. **Swiatlo, E., Ware, D.** Novel vaccine strategies with protein antigens of Streptococcus pneumoniae. *FEMS Immunology and Medical Microbiology.* 2003, Vol. 38, pp. 1-7.

32. **Kang, H., Srinivasan, J., Curtiss, R.** Immune responses to recombinant pneumococcal PspA antigen delivered by live attenuated Salmonella enterica serovar Typhimurium vaccine. *Infection and Immunity .* 2002, Vol. 70, pp. 1739–1749.

33. **Oliveira, M., Miyaji, E., Ferreira, D., Moreno, A., Ferreira, P., Lima, F., Santos, F., Sakauchi, M., Takata, C., Higashi, H., Raw, I., Kubrusly, F., Ho, P.** Combination of pneumococcal surface protein A (PspA) with whole cell pertussis vaccine increases protection against pneumococcal challenge in mice. *PLoS ONE.* 2010, Vol. ;5:e10863.

34. **Safari, D., Marradi, M., Chiodo, F., Th Dekker, H., Shan, Y., Adamo, R., Oscarson, S., Rijkers, G., Lahmann, M., Kamerling, J., Penadés, S., Snippe, H.** Gold nanoparticles as carriers for a synthetic Streptococcus pneumoniae type 14 conjugate vaccine. *Nanomedicine (Lond).* 2012, Vol. 7, pp. 651–662.

35. **Kong, G., Sato, A., Yuki, Y., Nochi, T., Takahashi, H., Sawada, S., Mejima, M., Kurokawa, S., Okada, K., Sato, S., Briles, D., Kunisawa, J., Inoue, Y., Yamamoto, M., Akiyoshi, K., Kiyonoa, H.** Nanogel-Based PspA Intranasal Vaccine Prevents Invasive Disease and Nasal Colonization by Streptococcus pneumoniae. *Infection and Immunity.* 2013, Vol. 81, pp. 1625–1634.

36. **Kunda, N., Somavarapu, S., Gordon, S., Hutcheon, G., Saleem, I.** Nanocarriers targeting dendritic cells for pulmonary vaccine delivery. *Pharmaceutical Research.* 2013, Vol. 30, pp. 325-341.

37. **Kleinstreuer, C., Zhang, Z., Li, Z.** Modeling airflow and particle transport/deposition in pulmonary airways. *Respiratory Physiology & Neurobiology.* 2008, Vol. 163, pp. 128–138.

38. **Saluja, V., Amorij, J-P., Kapteyn, J., Boer, A., Frijlink, H., Hinrichs, W.** A comparison between spray drying and spray freeze drying to produce an influenza subunit vaccine powder for inhalation. *Journal of Controlled Release.* 2010, Vol. 144, pp. 127-133.

39. **Kersten, G., Hirschberg, H.** Needle-free vaccine delivery. *Expert opinion drug delivery.* 2007, Vol. 4, pp. 459-474.

40. **Vyas, S., Gupta, P.** Implication of nanoparticles/microparticles in mucosal vaccine delivery. *Expert Review Vaccines.* 2007, Vol. 7, pp. 401-418.

41. **Jaganathan, K., Vyas, S.** Strong systemic and mucosal immune responses to surface-modified PLGA microspheres containing recombinant hepatitis B antigen administered intranasally. *Vaccine.* 2006, Vol. 24, pp. 4201 -4211.

42. **Hokey, D., Misra, A.** Aerosol vaccines for tuberculosis: A fine line between protection and pathology. *Tuberculosis.* 2011, Vol. 91, pp. 82-85.

43. **Pulliam, B., Sung, J., Edwards, D.** Design of nanoparticle-based dry powder pulmonary vaccines. *Expert Opinion on Drug Delivery.* 2007, Vol. 4, pp. 651-663.

44. **Spiers, I., Eyles, J., Baillie, L., Williamson, E., Oya Alpar, H.** Biodegradable microparticles with different release profiles: effect on the immune response after a single administration via intranasal and intramuscular routes. *Journal of Pharmacy and Pharmacologyl.* 2000, Vol. 52, pp. 1195–1201.

45. **Gutierro, I., Hernandez, R., Igartua, M., Gascon, A., Pedraz, J.** Size dependent immune response after subcutaneous, oral and intranasal administration of BSA loaded nanospheres. *Vaccine.* 2002, Vol. 21, pp. 67–77.

46. **McNeela, E., O'Connor, D., Jabbal-Gil,l I., Illum, L., Davis, S., Pizza, M., et al.** A mucosally delivered vaccine against diphtheria: formulation chitosan enhances local and systemic and Th2 responses following nasal delivery. *Vaccine .* 2000, Vol. 19, pp. 1188–1198.

47. **Van der Lubben, I., Kersten, G., Fretz, M., Beuvery, C., Verhoef, J., Junginger, H.** Chitosan microparticles for mucosal vaccination against diphtheria: oral and nasal efficacy studies in mice. *Vaccine.* 2003, Vol. 21, pp. 1400–1408.

48. **Venkatesan, N., and Vyas, S.** Polysaccharide coated liposomes for oral immunization—development and characterization. *International Journal of Pharmaceutics.* 2000, Vol. 203, pp. 169–177.

49. **Perrie, Y., Frederik, P., Gregoriadis, G.** Loposome-mediated DNA vaccination: the effect of vesicle composition. *Vaccine.* 2001, Vol. 19, pp. 3301–3310.

50. **Wu H-Y, Russel MW.** Induction of mucosal and systemic immune responses by intranasal immunization using recombinant cholera toxin B subunit as an adjuvant. *Vaccine.* 1998, Vol. 16, pp. 286–292.

51. **Isaka, M., Komiya, T., Takahashi, M., Yasuda, Y., Taniguchi, T., Zhao, Y., et al.** Recombinant cholera toxin B subunit (rCTB) as a mucosal adjuvant enhances induction of diphtheria and tetanus antitoxin antibodies in mice by intranasal administration with diphtheria-pertusistetanus (DPT) combination vaccine. *Vaccine.* 2004, Vol. 22, pp. 3061–3068. .

52. **Amidi, M., Pellikaan, H., Hirschberg, H., de Boer, A., Crommelin, D., Hennink, W., Kersten, G., Jiskoot, W.** Diphtheria toxoid-containing microparticulate preparation, characterization and evaluation in guinea pigs. *Vaccine.* 2007, Vol. 25, pp. 6818–6829.

53. **Rafiq, K., Bergtold, A., Clynes, R.** Immune complex-mediated antigen presentation induces tumor immunity. *The Journal of Clinical Investigation.* 2002, Vol. 110, pp. 71-79.

54. **Gupta, N., Tomar, P., Sharma, V., Dixit, V.** Development and characterization of chitosan coated poly-(-caprolactone) nanoparticulate system for effective immunization against influenza. *Vaccine.* 2011, Vol. 29, pp. 9026– 9037.

55. **Foged, C., Sundblad, A., Hovgaard, L.** Targeting Vaccines to Dendritic Cells. *Pharmaceutical Research.* 2002, Vol. 19, pp. 229–238.

56. **Delves, P., Maitin, S., Burton, D., Roitt, I.** *Roitt's Essential Immunology.* 12. s.l. : Wiley-Blackwell: Hoboken, 2011.

57. **Banchereau, J., Steinman, R.** Dendritic cells and the control of immunity. *Nature.* 1998, Vol. 392, pp. 245-252.

58. **Lambrecht, B., Hammad, H.** Biology of Lung Dendritic Cells at the Origin of Asthma. *Immunity.* 2009, Vol. 18, pp. 412–424.

59. **von Garnier, C., Nicod, L.** Immunology taught by lung dendritic macrophages. *Swiss Medical Weekly.* 2009, Vol. 139, pp. 186–192.

60. **Demedts, I., Brusselle, G., Vermaelen, K., Pauwels, R.** Identification and characterization of human pulmonary dendritic cells. *Am J Respir Cell Mol Biol.* 2005, Vol. 32, pp. 177–184.

61. **Singh, M., Chakrapani, A., O'Hagan, D.** Nanoparticles and microparticles as vaccine delivery systems. *Expert Review Vaccines.* 2007, Vol. 6, pp. 797-808.

62. **Thompson, C., Hansford, D, Higgins, S, Hutcheon, G., Rostron, C., Munday, D.** Enzymatic synthesis and evaluation of new novel x-pentadecalactone polymers for the production of biodegradable microspheres. *Journal of Microencapsulation.* 2006, Vol. 23, pp. 213–226.

63. **Kallinteri, P., Higgins, S., Hutcheon, G., St Pourcain, C., Garnett, M.** Novel functionalized biodegradable polymers for nanoparticle drug delivery system. *Biomacromolecules.* 2005, Vol. 6, pp. 1885–1894.

64. **Gaskell, E., Hobbs, G., Rostron, C., Hutcheon, G.** Encapsulation and release of a-chymotrypsin from poly(glyceroladipate-co-x-pentadecalactone) microparticles. *Journal of Microencapsulation.* 2008, Vol. 25, pp. 187–195.

65. **Thompson, C., Hansford, D., Higgins, S., Rostron, C., Hutcheon, G., Munday, D.** Evaluation of ibuprofen-loaded microspheres prepared from novel copolyesters. *International Journal of Pharmaceutics.* 2007, Vol. 329, pp. 53–61.

66. **Tawfeek, H., Khidr, S., Samy, E., Ahmed, S., Murphy, M., Mohammed, A., Shabir, A., Hutcheon, G., Saleem, I.** Poly(Glycerol Adipate-co-ω-Pentadecalactone) Spray-Dried Microparticles as Sustained Release Carriers for Pulmonary Delivery. *Pharmaceutical Research.* 2011, Vol. 28, pp. 2086-2097.

67. **Tawfeek, H., Evans, A., Iftikar, A., Mohammed, A., Shabir, A., Somavarapud, S., Hutcheon, G., Saleem, I.** Dry powder inhalation of macromolecules using novel PEG-copolyester microparticle carriers. *Journal of Pharmaceutics.* 2013, Vol. 441, pp. 611-619.

68. **Kunda, N., Alfagih, I., Dennison, S., Tawfeek, H., Somavarapu, S., Hutcheon, G., Saleem, I.** Bovine Serum Albumin Adsorbed PGA-co-PDL Nanocarriersfor Vaccine Delivery via Dry Powder Inhalation. *Pharmaceutical Research.* 2014, Vol. Oct.

69. **Nicolas, J., Mura, S., Brambilla, D., Mackiewicz, N., Couvreur, P.** Design, functionalization strategies and biomedical applications of targeted biodegradable/biocompatible polymer-based nanocarriers for drug delivery. *Chemical Society Reviews.* 2013, Vol. 42, pp. 1147-1235.

70. **Vila, A., Sánchez, A., Janes, K., Behrens, I., Kissel, T., Vila Jato, J., Alonso, M.** Low molecular weight chitosan nanoparticles as new carriers for nasal vaccine delivery in mice. *European Journal of Pharmaceutics and Biopharmaceutics .* 2004 , Vol. 57, pp. 123-131.

71. **Sayın, B., Somavarapu, S., Li, X., Thanou, M., Sesardic, D., Alpar, H., Senel, S.** Mono-N-carboxymethyl chitosan (MCC) and N-trimethyl chitosan (TMC) nanoparticles for non-invasive vaccine delivery. *International Journal of Pharmaceutics.* 2008, Vol. 363, pp. 139–148.

72. **Pawar, D., Goyal, A., Mangal, S., Mishra, N., Vaidya, B., Tiwari, S., Jain, A., Vyas, S.** Evaluation of Mucoadhesive PLGA Microparticles for Nasal Immunization. *American Association of Pharmaceutical Scientists Journal.* 2010, Vol. 12, pp. 130-137.

73. **Thomas, C., Rawat, A., Hope-Weeks, L., Ahsan, A.** Aerosolized PLA and PLGA Nanoparticles Enhance Humoral, Mucosal and Cytokine Responses to Hepatitis B Vaccine. *Molecular Pharmaceutics.* 2011, Vol. 8, pp. 405-415.

74. **Muttil, P., Prego, C., Garcia-Contreras, L., Pulliam, B., Fallon, J., Wang, C., Hickey, A., Edwards, D.** Immunization of Guinea Pigs with Novel Hepatitis B Antigen as Nanoparticle Aggregate Powders Administered by the Pulmonary Route. *The AAPS Journal.* 2010, Vol. 12, pp. 330-337.

75. **Bivas-Benita, M., van Meijgaarden, K., Franken, K.** Pulmonary delivery of chitosan-DNA nanoparticles enhances the immunogenicity of a DNA vaccine encoding HLA-A0201-restricted T cells epitopes of M. tuberculosis. *Vaccine.* 2004, Vol. 22, pp. 1609-1615.

76. **Eyles, J., Williamson, E., Spiers, I., Alpar, H.** Protection studies following bronchopulmonary and intramuscular immunisation with yersinia pestis F1 and V subunit vaccines coencapsulated in biodegradable microspheres: a comparison of efficacy. *Vaccine.* 2000, Vol. 18, pp. 3266-3271.

77. **Yadav, S., Kumari, A., Yadav, R.** Development of peptide and protein nanotherapeutics by nanoencapsulation and nanobioconjugation. *Peptides.* 2011, Vol. 32, pp. 173–187.

78. **Ye, M., Kim, S., Park, K.** Issues in long-term protein delivery using biodegradable microparticles. *Journal of Controlled Release.* 2010, Vol. 146, pp. 241–260.

79. **Giunchedi, P., Conti, B., Genta, I., Conte, U., Puglisi, G.** Emulsion Spray-Drying for the Preparation of Albumin-Loaded PLGA Microspheres. *Drug Development and Industrial Pharmacy.* 2001, Vol. 27, pp. 745-750.

80. **Jain, R.** The manufacturing techniques of various drug loaded biodegradable poly(lactide-co-glycolide) (PLGA) devices. *Biomaterials.* 2000, Vol. 21, pp. 2475-2490.

81. **Singh, J., Pandit, S., Bramwell, V., Alpar, H.** Diphtheria toxoid loaded poly-(ε-caprolactone) nanoparticles as mucosal vaccine delivery systems. *Methods.* 2006, Vol. 38, pp. 96–105.

82. **Konan, Y., Gurny, R., Allémann, E.** Preparation and characterization of sterile and freeze-dried sub-200 nm nanoparticles. *International Journal of Pharmaceutics.* 2002, Vol. 233, pp. 239–252.

83. **Yoshida, M., Babensee, J.** Molecular aspects of microparticle phagocytosis by dendritic cells. *Journal of Biomaterials Science.* 2006, Vol. 17, pp. 893–907.

84. **Thiele, L., Rothen-Rutishauser, B., Jilek, S., Wunderli- Allenspach, H., Merkle, H., Walter, E.** Evaluation of particle uptake in human blood monocyte-derived cells in vitro. Does phagocytosis activity of dendritic cells measure up with macrophages? *Journal of Controlled Release.* 2001, Vol. 76, pp. 59–71.

85. **Thomasin, C., Corradin, G., Men, Y., Merkle, H., Gander, B.** Tetanus toxoid and synthetic malaria antigen containing poly(lactide)/ poly(lactide-co-glycolide) microspheres: importance of polymer degradation and antigen release for immune response. *Journal of Controlled Release.* 1996, Vol. 41, pp. 131–145.

86. **Walter, E., Dreher, D., Kok, M., Thiele, L., Kiama, S., Gehr, P., Merkle, H.** Hydrophilic poly(DL-lactide-co-glycolide) microspheres for the delivery of DNA to human-derived macrophages and dendritic cells. *Journal of Controlled Release.* 2001, Vol. 76, pp. 149–168.

87. **Hamdy, S., Haddadi, A., Hung, R., Lavasanifar, A.** Targeting dendritic cells with nano-particulate PLGA cancer vaccine formulations. *Advanced Drug Delivery Reviews.* 2011, Vol. 63, pp. 943–955.

88. **Thomas, C., Gupta, V., Ahsan, F.** Influence of surface charge of PLGA particles of recombinant hepatitis B surface antigen in enhancing systemic and mucosal immune responses. *International Journal of Pharmaceutics.* 2009, Vol. 379, pp. 41–50.

89. **Foged, C., Brodin, B., Frokjaer, S., Sundblad, A.** Particle size and surface charge affect particle uptake by human dendritic cells in an in vitro model. *International Journal of Pharmaceutics.* 2005, Vol. 298, pp. 315–322.

90. **Manolova, V., Flace, A., Bauer, M., Schwarz, K., Saudan, P., Bachmann, M.** Nanoparticles target distinct dendritic cell populations according to their size. *European Journal of Immunology.* 2008, Vol. 38, pp. 1404-14013.

91. **Sung, J., Pulliam, B., Edwards, D.** Nanoparticles for drug delivery to the lungs. *Trends in Biotechnology.* 2007, Vol. 25, pp. 563-570.

92. **Jensen, D., Cun, D., Maltesen, M., Frokjaer, S., Nielsen, H., Foged, C.** Spray drying of siRNA-containing PLGA nanoparticles intended for inhalation. *Journal of Controlled Release.* 2010, Vol. 142, pp. 138–145.

93. **Ungaro, F., d' Angelo, I., Miro, A., La Rotonda, M., Quaglia, F.** Engineered PLGA nano- and micro-carriers for pulmonary delivery: challenges and promises. *Journal of Pharmacy and pharmacology.* 2012, Vol. 64, pp. 1217–1235.

94. **Al-fagih, I., Alanazi, F.,Hutcheon, G., Saleem, I.** Recent Advances Using Supercritical Fluid Techniques for Pulmonary Administration of Macromolecules via Dry Powder Formulations. *Drug Delivery Letters.* 2011, Vol. 1, pp. 128-134.

95. **Pilcer, G., Amighi, K.** Formulation strategy and use of excipients in pulmonary drug delivery. *International Journal of Pharmaceutics.* 2010, Vol. 392, pp. 1–19.

96. **Amorij, J, Saluja, V., Petersen, A., Hinrichs, W., Huckriede, A., Frijlink, H.** Pulmonary delivery of an inulin-stabilized influenza subunit vaccine prepared by spray-freeze drying induces systemic, mucosal humoral as well as cell-mediated immune responses in BALB/c mice. *Vaccine.* 2007, Vol. 25, pp. 8707–8717.

97. **Basavaraj, K., Nanjwade, Sagar A. Adichwal, Kishori R. Gaikwad, et al.** Pulmonary Drug Delivery: Novel Pharmaceutical Technologies Breathe New Life into the Lungs. *PDA Journal of Pharmaceutical Science and Technology.* 2011, Vol. 65, pp. 513-534.

98. **Lu, D., Hickey, A.** Pulmonary vaccine delivery. *Expert Review Vaccine.* 2007, Vol. 6, pp. 213-226.

99. **Sou, T., Meeusen, E., deVeer, M., Morton, D., Kaminskas, L., McIntosh, M.** New developments in drypowder pulmonary vaccine delivery. *Trends in Biotechnology.* 2011, Vol. 29, pp. 191-198.

100. **Vehring, R.** Pharmaceutical Particle Engineering via Spray Drying. *Pharmaceutical Research.* 2008, Vol. 25, pp. 999-1022.

101. **Mansour, H., Rhee, Y. & Wu, X.** Nanomedicine in pulmonary delivery. *International Journal of Nanomedicine.* 2009, Vol. 4, pp. 299–319.

102. **Sezer, Ali Demir.** Recent Advances in Novel Drug Carrier Systems. s.l. : InTech, 2012, 3.

103. **Ohtake, S., Martin, R., Yee, L., Chen, D., Kristensen, D., Lechuga-Ballesteros, D., Truong-Le, V.** Heat-stable measles vaccine produced by spray drying. *Vaccine.* 2010, Vol. 28, pp. 1275–1284.

104. **Burger, J., Cape, S., Braun, C., McAdams, D., Best, J., Bhagwat, P., Pathak, P., Rebits, L., Sievers, R.** Stabilizing formulations for inhalable powders of live-attenuated measles virus vaccine. *Journal of Aerosol Medicine and Pulmonary Drug Delivery.* 2008, Vol. 21, pp. 25–34.

105. **Sullivan, V., Mikszta, J., Laurent, P., Huang, J., Ford, B.** Noninvasive delivery technologies: respiratory delivery of vaccines. *Expert Opinion on Drug Delivery.* 2006 , Vol. 3, pp. 87-95.

106. **Garcia-Contreras, L., Wong, Y., Mutti, P., Padilla, D., Sadoff, J., Derousse, J., Germishuizen, W., Goonesekera, S., Elbert, K., Bloom, B., Miller, R., Fourie, P., Hickey, A., Edwards, D.** Immunization by a bacterial aerosol. *Proceedings of the National Academy of Sciences of the United States of America .* 2008, Vol. 105, pp. 4656–4660.

107. **Lu, D., Garcia-Contreras, L., Muttil, P., Padilla, D., Xu, D., Liu, J., Braunstein, M., McMurray, D., Hickey, A.** Pulmonary immunization using antigen 85-B polymeric microparticles to boost tuberculosis immunity. *AAPS J.* 2010, Vol. 12, pp. 338–347.

108. **Agarkhedkar, S., Kulkarni, P., Winston, S., Sievers, R., Dhere, R., Gunale, B., Powell, K., Rota, P., Papania, M., MVDP author group.** Safety and immunogenicity of dry powder measles vaccineadministered by inhalation: A randomized controlled Phase I clinical trial. *Vaccine.* 2014, Vol. 32, pp. 6791-6797.

109. **Wang, M., Zhang, Y., Feng, J., Gu, T., Dong, Q., Yang, X., Sun, Y., Wu, Y., Chen, Y., Kong, W.** Preparation, characterization, and in vitro and in vivo investigation of chitosan-coated poly (d,l-lactide-co-glycolide) nanoparticles for intestinal delivery of exendin-4. *International Journal of Nanomedicine.* 2013, Vol. 8, pp. 1141–1154.

110. **Chronopoulou, L., Massimi, M., Giardi, M., Cametti, C., Devirgiliis, L., Dentini, M., Palocci, C.** Chitosan-coated PLGA nanoparticles: A sustained drug release strategy for cell cultures. *Colloids and Surfaces B: Biointerfaces.* 2013, Vol. 103, pp. 310– 317.

111. **Guo, C., Gemeinhart, R.** Understanding the adsorption mechanism of chitosan onto poly(lactide-co-glycolide) particles. *European Journal of Pharmaceutics and Biopharmaceutics.* 2008, Vol. 70, pp. 597–604.

112. *United States Pharmacopeia 31—National Formulary 26.* s.l. : United States Pharmacopeial Convention Inc, 2008, 601.

113. **Wong, W., Crapper, J., Chan, H., Traini, D., Young, P.** Pharmacopeial methodologies for determining aerodynamic mass distributions of ultra-high dose inhaler medicines. *Journal of Pharmaceutical and Biomedical Analysis.* 2010, Vol. 51, pp. 853–857.

114. **Swarbrick, J.** *Encyclopedia of Pharmaceutical Technology.* third. New York : Informa healthcare, 2007.

115. **Greenfield, N.** Using circular dichroism spectra to estimate protein secondary structure. *Nature Protocols.* 2007, Vol. 1, pp. 2876–2890.

116. **Henzler Wildman, K., Lee, D-K. and Ramamoorthy, A.** Mechanism of Lipid Bilayer Disruption by the Human Antimicrobial Peptide, LL-37. *Biochemistry.* 2003, Vol. 42, pp. 6545–6558.

117. **Whitmore, L., Woollett, B., Miles, A., Janes, R., Wallance, B.** The protein circular dichrosim data bank, a Web-based site for access to circular dichrosim spectroscopic data. *Structure.* 2010, Vol. 18, pp. 1267-1269.

118. **Whitmore, L., Wallace, B.** Protein secondary structure analyses from circular dichroism spectroscopy: methods and reference databases. *Biopolymers.* 2008, Vol. 89, pp. 392–400.

119. **Whitmore, L. and Wallace, B.** DICHROWEB, an online server for protein secondary structure analyses from circular dichroism spectroscopic data. *Nucleic Acids Res.* 2004, Vol. 32, pp. W668–73.

120. **Horta, A., Sargo, C., da Silva, A., de Carvalho, Gonzaga M., Dos Santos, M., Gonçalves, V., Zangirolami, T., de Campos Giordano, R.** Intensification of high cell-density cultivations of rE. coli for production of S. pneumoniae antigenic surface protein, PspA3, using model-based adaptive control. *Bioprocess and Biosystems Engineering .* 2012, Vol. 35, pp. 1269-1280.

121. **Carvalho, R., Cabrera-Crespo, J., Tanizaki, M., Gonçalves, V.** Development of production and purification processes of recombinant fragment of pneumococcal surface protein A in Escherichia coli using different carbon sources and chromatography sequences. *Applied Microbiology and Biotechnology .* 2012, Vol. 94, pp. 683-694.

122. **Horta, A., Silva, A., Sargo, C., Velez, A., Gonzaga, M., Giordano, R., Gonçalves, V., Zangirolami, T.** A supervision and control tool based on artificial intelligence for high cell density cultivations. *Brazilian Journal of Chemical Engineering.* 2014, Vol. 31, pp. 457 - 468.

123. **Brito, L., Singh, M.** Aceptable levels of endotoxin in accine formulations duringpreclinical research. *Journal of Pharmaceutical Science.* 2011, Vol. 100, pp. 34-37.

124. **des Rieux, A., Fievez, V., Garinot, M., Schneider, Y. J., Preat, V.** Nanoparticles as potential oral delivery systems of proteins and vaccines: a mechanistic approach. *Journal of Controlled Release.* 2006, Vol. 116, pp. 1–27.

125. **Feng, A., Boraey, M., Gwina, M., Finlay, P., Kuehl, P., Vehring, R.** Mechanistic models facilitate efficient development of leucine containing microparticles for pulmonary drug delivery. *International Journal of Pharmaceutics.* 2011, Vol. 409, pp. 156-163.

126. **Yang, S., Zhu, J.** Preparation and Characterization of Camptothecin Solid Lipid Nanoparticles. *Drug Development and Industrial Pharmacy.* 2002, Vol. 28, pp. 265–274 .

127. **Tekade, R., Chougule, M.** Formulation Development and Evaluation of Hybrid Nanocarrier for Cancer Therapy: Taguchi Orthogonal Array Based Design. *BioMed Research International.* 2013, Vol. 2013, p. ID 712678.

128. **Taguchi, G.** Taguchi Method: Design of Experiments. *Quality Engineering Series.* 1993, Vol. 4.

129. **Lee, S., Heng, D., Ng, W., Chan, H., Tana, R.** Nano spray drying: A novel method for preparing protein nanoparticles for protein therapy. *International Journal of Pharmaceutics.* 2011, Vol. 403, pp. 192–200.

130. **Chawla, V., Saraf, S.** Rheological studies on solid lipid nanoparticle based carbopol gels of aceclofenac. *Colloids and Surfaces B: Biointerfaces.* 2012, Vol. 92, pp. 293– 298.

131. **Asghar, A., Abdul Raman, A., WD, WA.** A Comparison of Central Composite Design and Taguchi Method for Optimizing Fenton Process. *The Scientific World Journal.* 2014, Vol. 2014, p. ID 869120.

132. **´opez-Cacho, J., Gonz´alez-R, P., Talero, B., Rabasco, B., Gonz´alez-Rodr´ıguez, M.** Robust Optimization of Alginate-Carbopol 940 Bead Formulations. *The ScientificWorld Journal.* 2012, Vol. 2012, p. ID 605610.

133. **Saroja, C., Lakshmi, P.** Formulation and optimization of fenofibrate lipospheres using Taguchi's experimental design. *Acta Pharmaceutica.* 2013, Vol. 63, pp. 71–83.

134. **Baras, B., Benoit, M.-A. and Gillard, J.** Parameters influencing the antigen release from spray-dried poly(DL-lactide) microparticles. *Int J Pharm.* 2000, Vol. 200, pp. 133–145.

135. **Wischke, C., Lorenzen, D., Zimmermann, J., Borchert, H.** Preparation of protein loaded poly(D,L-lactide-co-glycolide) microparticles for the antigen delivery to dendritic cells using a static micromixer. *European Journal of Pharmaceutics and Biopharmaceutics.* 2006, Vol. 62, pp. 247–253.

136. **Wischke, C., Borchert, H.** Influence of the primary emulsification procedure on the characteristics of small protein-loaded PLGA microparticles for antigen delivery. *Journal of Microencapsulation.* 2006, Vol. 23, pp. 435–448.

137. **Huang, B., Kim, H.** Probing Three-Dimensional Structure of Bovine Serum Albumin by Chemical Cross-Linking and Mass Spectrometry. *Journal of the American Society for Mass Spectrometry .* 2004, Vol. 15, pp. 1237–1247.

138. **Hamidi, M., Zarei, N.** A reversed-phase high-performance liquid chromatography method for bovine serum albumin assay in pharmaceutical dosage forms and protein/antigen delivery systems. *Drug Testing and Analysis.* 2009, Vol. 1, pp. 214-8.

139. Preparation for inhalation: Aerodynamic assessment of fine particles. Eur. pharmacopoeia 7.0. Strasbourg: Council of Europe, European Directorate for the Quality of Medicines & HealthCare. 2010, pp. 274-275.

140. **Zhang, J., Ma, X., Guo, Y., Yang, L., Shen, Q., Wang, H., Ma, Z.** Size-controllable preparation of bovine serum albumin-conjugated PbS nanoparticles. *Material Chemistry and Physics.* 2010, Vol. 119, pp. 112–117.

141. **He, J., Feng, M., Zhou, X., Ma, S., Jiang, Y., Wang, Y., Zhang, H.** Stabilization and encapsulation of recombinant human erythropoietin into PLGA microspheres using human serum albumin as a stabilizer. *International Journalof Pharmaceutics.* 2011, Vol. 416, pp. 69-76.

142. **Morsi, H., Yong, K., Jewell, A.** Evaluation of the Taguchi methods for the simultaneous assessment of the effects of multiple variables in the tumour microenvironment. *International Seminars in Surgical Oncology.* 2004, Vol. 1:7.

143. **Bilati, U., Allemann, E., Doelker, E.** Poly(D,L-lactide-co-glycolide) protein-loaded nanoparticles prepared by the double emulsion method—processing and formulation issues for enhanced entrapment efficiency. *Journal of Microencapsulation.* 2005, Vol. 22, pp. 205–214.

144. **Li, X., Deng, X., Yuan, M., Xiong, C., Huang, Z., Zhang, Y., Jia, W.** Investigation on process parameters involved in preparation of poly-D,LL-lactide-poly(ethylene glycol) microspheres containing Leptospira Interrogans antigens. *International Journal of Pharmaceutics.* 1999, Vol. 178, pp. 245–255.

145. **Tang, E., Huang, M., Lim, L.** Ultrasonication of chitosan and chitosan nanoparticles. *International Journal of Pharmaceutics.* 2003, Vol. 265, pp. 103–114.

146. **Sanad, R., Abdel Malak, N., El-Bayoomy, T., Badawi, A.** Preparation and characterization of oxybenzone-loaded solid lipid nanoparticles (SLNs) with enhanced safety and sunscreening efficacy: SPF and UVA-PF. *Drug Discoveries and Therapeutics.* 2010, Vol. 4, pp. 472-483.

147. **Brunner, C., Baran, E., Pinho, E., Reis, R., Neves, N.** Performance of biodegradable microcapsules of poly(butylene succinate), poly(butylene succinate-co-adipate) and poly(butylene terephthalate-co-adipate) as drug encapsulation systems. *Colloids Surf B Biointerfaces.* 2011, Vol. 84, pp. 498–507.

148. **Mao, S., Shi, Y., Li, L., Xu, J., Schaper, A., Kissel, T.** Effects of process and formulation parameters on characteristics and internal morphology of poly(D,L-lactide-co-glycolide) microspheres formed by the solvent evaporation method. *European Journal of Pharmaceutics and Biopharmaceutics.* 2008, Vol. 68, pp. 214–223.

149. **Zhang, J., Chen, D., Wang, S., Zhu, K.** Optimizing double emulsion process to decrease the burst release of protein from biodegradable polymer microspheres. *Journal of Microencapsulation.* 2005, Vol. 22, pp. 413–422.

150. **Ruana, G., Feng, S.** Preparation and characterization of poly(lactic acid)–poly(ethylene glycol)–poly(lactic acid) (PLA–PEG–PLA) microspheres for controlled release of paclitaxel. *Biomaterials.* 2003, Vol. 24, pp. 5037–5044.

151. **Feczkó, T., Tóth, J., Dósa, Gy., Gyenis, J.** Optimization of protein encapsulation in PLGA nanoparticles. *Chemical Engineering and Processing.* 2011, Vol. 50, pp. 757– 765.

152. **Cun, D., et al., et al.** High loading efficiency and sustained release of siRNA encapsulated in PLGA nanoparticles: Quality by design optimization and characterization. *Eur J Pharm Biopharm.* 2011, Vol. 77, pp. 26–35.

153. **Yang, Y., Chung, T.** Polymeric microspheres containing protein fabricated by double-emulsion solvent extraction/evaporation method. *Biomaterials.* 2001, Vol. 22, pp. 231–241.

154. **Bittner, B., Kissel, T.** Ultrasonic atomizatio n for spray drying : a versatile technique for the preparation of protein loaded biodegradable microspheres. *Journal of Microencapsulation.* 1999, Vol. 16, pp. 325-341.

155. **Walter, E., Moelling, K., Pavlovic, J., Merkle, H.** Microencapsulation of DNA using poly(DL-lactide-co-glycolide): stability issues and release characteristics. *Journal of Controlled Release.* 1999, Vol. 61, pp. 361-374.

156. **Slütter, B., Bal, S., Keijzer, C., Mallants, R., Hagenaars, N., Que, I., Kaijzel, E., Ede, W., Augustijns, P., Löwik, C., Bouwstra, J., Broere, F., Jiskoot, W.** Nasal vaccination with N-trimethyl chitosan and PLGA based nanoparticles: Nanoparticle characteristics determine quality and strength of the antibody response in mice against the encapsulated antigen. *Vaccine.* 2010, Vol. 28, pp. 6282-6291.

157. **Anish, C., Upadhyay, A., Sehgal, D., Panda, A.** Influences of process and formulation parameters on powder properties and immunogenicity of spray dried polymer particles entrapping recombinant pneumococcal surface protein A. *International Journal of Pharmaceutics.* 2014, Vol. 466, pp. 198-210.

158. **Gutierro, I., Hernandez, R., Igartua, M., Gascon, A., Pedraz, J.** Size dependent immune response after subcutaneous, oral and intranasal administration of BSA loaded nanospheres. *Vaccine.* 2002, Vol. 21, pp. 67-77.

159. **Shakweh, M., Ponchel, G., Fattal, E.** Particle uptake by Peyer'spatches: a pathway for drug and vaccine delivery. *Expert Opinion on Drug Delivery.* 2004, Vol. 1, pp. 141-163.

160. **Briles, D., Hollingshead, S., Nabors, G., Paton, J., Brooks-Walter, A.** The potential for using protein vaccines to protect against otitis media caused by Streptococcus pneumoniae. *Vaccine.* 2001, Vol. 19, pp. 87-95.

161. **Motlekar, N., Youan, B.** Optimization of experimental parameters for the production of LMWH-loaded polymeric microspheres. *Drug Design, Development and Therapy.* 2, 2008, pp. 39–47.

162. **Shi, S., Hickey, A.** PLGA Microparticles in Respirable Sizes Enhance an In Vitro T Cell Response to Recombinant Mycobacterium Tuberculosis Antigen TB10.4-Ag85B. *Pharmaceutical Research.* 2010, Vol. 27, pp. 350-360.

163. **Mohajel, N., Roholamini Najafabadi, A., Azadmanesh, K., Vatanara, A., Moazeni, E., Rahimi, A., Gilani, K.** Optimization of a spray drying process to prepare dry powder microparticles containing plasmid nanocomplex. *International Journal of Pharmaceutics.* 2012, Vol. 423, pp. 577-585.

164. **Billon, A., Bataille, B., Cassanas, G., Jacob, M.** Development of spray-dried acetaminophen microparticles using experimental designs. *International Journal of Pharmaceutics.* 2000, Vol. 203, pp. 159–168.

165. **Adler, M., Unger, M., Lee, G.** Surface composition of spray-dried particles of bovine serum albumin/trehalose/surfactant. *Pharmaceutical Research.* 2000, Vol. 17, pp. 863-70.

166. **Li, H., Seville, P., Williamson, I., Brichall, J.** The use of amino acids to enhance the aerosolisation of spray-dried powders for pulmonary gene therapy. *Journal of Gene Medicine.* 2005, Vol. 7, pp. 343-353.

167. **Li, H., Neill, H., Innocent, R., Seville, P., Williamson, I., Brichall, J.** Enhanced dispersibility and deposition of spray-dried powders for pulmonary gene therapy. *Journal of Drug Targeting.* 2003, Vol. 11, pp. 425-432.

168. **Seville, P., Learoyd, T., Li, H., Williamson, I., Birchall, J.** Amino acid modified spray-dried powders with enhanced aerosolisation properties for pulmonary drug delivery. *Powder Technology.* 2007, Vol. 178, pp. 40-50.

169. **Sou, T., Kaminskas, L., Nguyen, T., Carlberg, R., Mc Intosh, M., Morton, D.** The effect of amino acid excipients on morphology and solid-state properties of multi-component spray-dried formulations for pulmonary delivery of biomacromolecules. *European Journal of Pharmaceutics and Biopharmaceutics.* 2013, Vol. 83, pp. 234-243.

170. **Rabbani, N., Seville, P.** The influence of formulation components on the aerosolisation properties of spray-dried powders. *Journal of Controlled Release.* 2005, Vol. 110, pp. 130-140.

171. **Cal, K., Sollohub, K.** Spray drying technique. I: hardware and process parameters. *Journal of pharmaceutical science.* 2010, Vol. 99, pp. 575-586.

172. **Yang, L., Guo, Y., Ma, X., Hu, Z., Zhu, S., Zhang, X., Jiang, K.** Cooperativity between pepsin and crystallization of calcium carbonate in distilled water. *Journal of Inorganic Biochemistry.* 2003, Vol. 93, pp. 197–203.

173. **Chen, H., Zheng, Y., Tian, G., Tian, Y., Zeng, X., Liu, G.** Oral delivery of DMAB-modified docetaxel-loaded PLGA-TPGS nanoparticles for cancer chemotherapy. *Nanoscale Research Letters.* 2011, Vol. 6, p. 4.

174. **Andrade, F., Goycoolea, F., Chiappetta, D., dasNeves, J., Sosnik, A., Sarmento, B.** Chitosan-Grafted Copolymers and Chitosan-Ligand Conjugates as Matrices for Pulmonary Drug Delivery. *International Journal of Carbohydrate Chemistry.* 2011, Vol. 2011, pp. Article ID 865704, 14 pages.

175. **Thomann-Harwood, L., Kaeuper, P., Rossi, N., Milona, P., Herrmann, B., McCullough, K.** Nanogel vaccines targeting dendritic cells: Contributions of the surface decoration and vaccine cargo on cell targeting and activation. *Journal of Controlled Release.* 2013, Vol. 166, pp. 95–105.

176. **Bhardwaj, V., Ankola, D., Gupta, S., Schneider, M., Lehr, C., Kumar, M.** PLGA nanoparticles stabilized with cationic surfactant: safety studies and application in oral delivery of paclitaxel to treat chemical-induced breast cancer in rat. *Pharmaceutical Research.* 2009, Vol. 26, pp. 2495-2503.

177. **Hariharan, S., Bhardwaj, V., Bala, I., Sitterberg, J., Bakowsky, U., Ravi Kumar, M.** Design of Estradiol Loaded PLGA Nanoparticulate Formulations: A Potential Oral Delivery System for Hormone Therapy. *Pharmaceutical Research.* 2006, Vol. 23, pp. 184-195.

178. **Jensen, D., Jensen, L., Koocheki, S., Bengtson, L., Cun, D., Nielsen, H., Foged, C.** Design of an inhalable dry powder formulation of DOTAP-modified PLGA nanoparticles loaded with siRNA. *Journal of Controlled Release.* 2012, Vol. 157, pp. 141-148.

179. **Bento, D., Staats, H., Gonçalves, T., Borges, O.** Development of a novel adjuvanted nasal vaccine: C48/80 associated with chitosan nanoparticles as a path to enhance mucosal immunity. *European Journal of Pharmaceutics and Biopharmaceutics.* 2015, Vol. 26, p. doi: 10.1016/j.

180. **Biswas, S., Chattopadhyay, M., Sen, K., Saha, M.** Development and characterization of alginate coated low molecular weight chitosan nanoparticles as new carriers for oral vaccine delivery in mice. *Carbohydrate Polymer.* 2015, Vol. 121, pp. 403-410.

181. **Xu, J., Dai, W., Chen, B., Fan, X.** Mucosal immunization with PsaA protein, using chitosan as a delivery system, increases protection against acute otitis media and invasive infection by Streptococcus pneumoniae. *Scandinavian Journal of Immunology.* 2015, Vol. 81, pp. 177-185.

182. **Ma, F., Zhang, Q, Zheng, L.** Interleukin/chitosan (JY) adjuvant enhances the mucosal immunity of human papillomavirus 16 L1 virus-like particles in mice. *Biotechnology Letters.* 2015, Vol. 37, pp. 773-777.

183. **Cui, Z., Han, D., Sun, X., Zhang, M., Feng, X., Sun, C., Gu, J., Tong, C., Lei, L., Han, W.** Mannose-modified chitosan microspheres enhance OprF-OprI-mediated protection of mice against Pseudomonas aeruginosa infection via induction of mucosal immunity. *Applied Microbiology and Biotechnology .* 2015, Vol. 99, pp. 667-680.

184. **Barhate, G., Gautam, M., Gairola, S., Jadhav, S., Pokharkar, V.** Enhanced mucosal immune responses against tetanus toxoid using novel delivery system comprised of chitosan-functionalized gold nanoparticles and botanical adjuvant: characterization, immunogenicity, and stability assessment. *Journal of Pharmaceutical Sciences.* 2014, Vol. 103, pp. 3448-3456.

185. **Dehghan, S., Tafaghodi, M., Bolourieh, T., Mazaheri, V., Torabi, A., Abnous, K., Tavassoti Kheiri, M.** Rabbit nasal immunization against influenza by dry-powder form of chitosan nanospheres encapsulated with influenza whole virus and adjuvants. *International Journal of Pharmaceutics.* 2014, Vol. 475, pp. 1-8.

186. **Bucarey, S., Pujol, M., Poblete, J., Nuñez, I., Tapia, C., Neira-Carrillo, A., Martinez, J., Bassa, O.** Chitosan microparticles loaded with yeast-derived PCV2 virus-like particles elicit antigen-specific cellular immune response in mice after oral administration. *Virology Journal.* 2014, Vol. 11, pp. doi: 10.1186/1743-422X-11-149.

187. **Zhang, S., Zhang, F., Li, A., Liu, L., Wu, W., Li, C., Zhang, Q., Liang, M., Li, D.** Study on adjuvant effect of oral recombinant subunit vaccine formulated with chitosan against human enterovirus 71. *Bing Du Xue Bao.* 2014, Vol. 30, pp. 221-225.

188. **Harde, H., Agrawal, A., Jain, S.** Tetanus toxoids loaded glucomannosylated chitosan based nanohoming vaccine adjuvant with improved oral stability and immunostimulatory response. *Pharmaceutical Research .* 2015 , Vol. 32, pp. 122-134.

189. **Sawaengsak, C., Mori, Y., Yamanishi, K., Srimanote, P., Chaicumpa, W., Mitrevej, A., Sinchaipanid, N.** Intranasal chitosan-DNA vaccines that protect across influenza virus subtypes. *International Journal of Pharmaceutics.* 2014, Vol. 473, pp. 113-125.

190. **Ye, T., Yue, Y., Fan, X., Dong, C., Xu, W., Xiong, S.** M cell-targeting strategy facilitates mucosal immune response and enhances protection against CVB3-induced viral myocarditis elicited by chitosan-DNA vaccine. *Vaccine.* 2014, Vol. 32, pp. 4457-4465.

191. **Pawar, D., Jaganathan, K.** Mucoadhesive glycol chitosan nanoparticles for intranasal delivery of hepatitis B vaccine: enhancement of mucosal and systemic immune response. *Drug Delivery.* 2014, Vol. 14, pp. 1-11.

192. **Liu, Q., Zhang, C., Zheng, X., Shao, X., Zhang, X., Zhang, Q., Jiang, X.** Preparation and evaluation of antigen/N-trimethylaminoethylmethacrylate chitosan conjugates for nasal immunization. *Vaccine.* 2014, Vol. 32, pp. 2582-2590.

193. **Klein, K., Mann, J., Rogers, P., Shattock, R.** Polymeric penetration enhancers promote humoral immune responses to mucosal vaccines. *Journal of Controlled Release.* 2014, Vol. 183, pp. 43-50.

194. **Nanda, R., Hajam, I., Edao, B., Ramya, K., Rajangam, M., Chandra Sekar, S., Ganesh, K., Bhanuprakash, V., Kishore, S.** Immunological evaluation of mannosylated chitosan

nanoparticles based foot and mouth disease virus DNA vaccine, pVAC FMDV VP1-OmpA in guinea pigs. *Biologicals.* 2014 , Vol. 42, pp. 153-159.

195. **Chai, D., Yue, Y., Xu, W., Dong, C., Xiong, S.** Mucosal co-immunization with AIM2 enhances protective SIgA response and increases prophylactic efficacy of chitosan-DNA vaccine against coxsackievirus B3-induced myocarditis. *Human Vaccines & Immunotherapeutics.* 2014, Vol. 10, pp. 1284-1294.

196. **Harde, H., Agrawal, A., Jain, S.** Development of stabilized glucomannosylated chitosan nanoparticles using tandem crosslinking method for oral vaccine delivery. *Nanomedicine.* 2014, Vol. 16, pp. 2511-2529.

197. **Ozbılgın, N., Saka, O., Bozkır, A.** Preparation and in vitro/in vivo evaluation of mucosal adjuvant in situ forming gels with diphtheria toxoid. *Drug Delivery.* 2014, Vol. 2, pp. 140-147.

198. **Sawaengsak, C., Mori, Y., Yamanishi, K., Mitrevej, A., Sinchaipanid, N.** Chitosan nanoparticle encapsulated hemagglutinin-split influenza virus mucosal vaccine. *AAPS PharmSciTech.* 2014, Vol. 2, pp. 317-325.

199. **Jiang, T., Singh, B., Li, H., Kim, Y., Kang, S., Nah, J., Choi, Y., Cho, C.** Targeted oral delivery of BmpB vaccine using porous PLGA microparticles coated with M cell homing peptide-coupled chitosan. *Biomaterials.* 2014, Vol. 35, pp. 2365-2373 .

200. **Wang, M., Yue, Y., Dong, C., Li, X., Xu, W., Xiong, S.** Mucosal immunization with high-mobility group box 1 in chitosan enhances DNA vaccine-induced protection against coxsackievirus B3-induced myocarditis. *Clinical and vaccine immunology.* 2013 , Vol. 11, pp. 1743-1751.

201. **Chen, L., Zhu, J., Li, Y., Lu, J., Gao, L., Xu, H., Fan, M., Yang, X.** Enhanced nasal mucosal delivery and immunogenicity of anti-caries DNA vaccine through incorporation of anionic liposomes in chitosan/DNA complexes. *Plos one.* 2013, Vol. 8, p. e71953.

202. **Hausner, M., Schamberger, A., Naumann, W., Jacobs, E., Dumke, R.** Development of protective anti-Mycoplasma pneumoniae antibodies after immunization of guinea pigs with the combination of a P1-P30 chimeric recombinant protein and chitosan. *Microbial Pathogenesis.* 2013, Vols. 64:23-32., pp. 23-32.

203. **Primard, C., Poecheim, J., Heuking, S., Sublet, E., Esmaeili, F., Borchard, G.** Multifunctional PLGA-based nanoparticles encapsulating simultaneously hydrophilic antigen and hydrophobic immunomodulator for mucosal immunization. *Molecular pharmaceutics.* 2013, Vol. 10, pp. 2996-3004.

204. **Pawar, D., Mangal, S., Goswami, R., Jaganathan, K.** Development and characterization of surface modified PLGA nanoparticles for nasal vaccine delivery: effect of mucoadhesive coating on antigen uptake and immune adjuvant activity. *European Journal of Pharmaceutics and Biopharmaceutics.* 2013, Vol. 85, pp. 550-559.

205. **Mishra, N., Khatri, K., Gupta, M., Vyas, S.** Development and characterization of LTA-appended chitosan nanoparticles for mucosal immunization against hepatitis B. *Artificial Cells, Nanomedicine, and Biotechnology.* 2014, Vol. 42, pp. 245-255.

206. **Suksamran, T., Ngawhirunpat, T., Rojanarata, T., Sajomsang, W., Pitaksuteepong, T., Opanasopit, P.** Methylated N-(4-N,N-dimethylaminocinnamyl) chitosan-coated electrospray OVA-loaded microparticles for oral vaccination. *International Journal of Pharmaceutics.* 2013, Vol. 448, pp. 19-27.

207. **Kobayashi, T., Fukushima, K., Sannan, T., Saito, N., Takiguchi, Y., Sato, Y., Hasegawa, H., Ishikawa, K.** Evaluation of the effectiveness and safety of chitosan derivatives as adjuvants for intranasal vaccines. *Viral Immunology.* 2013, Vol. 2, pp. 133-142.

208. **Tafaghodi, M., Saluja, V., Kersten, G., Kraan, H., Slütter, B., Amorij, J., Jiskoot, W.** Hepatitis B surface antigen nanoparticles coated with chitosan and trimethyl chitosan: Impact of formulation on physicochemical and immunological characteristics. *Vaccine.* 2012, Vol. 30, pp. 5341-5348.

209. **Wu, Y., Wu, S., Hou, L., Wei, W., Zhou, M., Su, Z., Wu, J., Chen, W., Ma, G.** Novel thermal-sensitive hydrogel enhances both humoral and cell-mediated immune responses by intranasal vaccine delivery. *European Journal of Pharmaceutics and Biopharmaceutics.* 2012, Vol. 81, pp. 486-497.

210. **Zhang, Y., Niu, Y., Luo, Y., Ge, M., Yang, T., Yu, L., Wang, Q.** Fabrication, characterization and antimicrobial activities of thymolloaded loaded zein nanoparticles stabilized by sodium caseinate–chitosan hydrochloride double layers. *Food Chemistry.* 2014, Vol. 142, pp. 269–275.

211. **Mura, S., Hillaireau, H., Nicolas, J., Nicolas, B., Gueutin, C., Zanna, S., Tsapis, N., Fattal, E.** Influence of surface charge on the potential toxicity of PLGA nanoparticles towards Calu-3 cells. *International Journal of Nanomedicine.* 2011, Vol. 6, pp. 2591–2605.

212. **Yuan, X., Shah, B., Kotadia, N., Li, J., Gu, H., Wu, Z.** The Development and Mechanism Studies of Cationic Chitosan-Modified Biodegradable PLGA Nanoparticles for Efficient siRNA Drug Delivery. *Pharmaceutical Research.* 2010, Vol. 27, pp. 1285–1295.

213. **Muherei, M., Junin, R.** Equilibrium Adsorption Isotherms of Anionic, Nonionic Surfactants and Their Mixtures to Shale and Sandstone. *Modern Applied Science.* 2009, Vol. 3, pp. 158-167.

214. **Li, X., Kong, X., Shi, S., Zheng, X., Guo, G., Wei, Y., Qian, Z.** Preparation of alginate coated chitosan microparticles for vaccine delivery. *BMC Biotechnology.* 2008, Vol. 8, pp. 89-99.

215. **Balcerzak, J., Mucha, M.** Analysis of model drug release kinetics from complex matrices of polylactide-chitosan. *Progress on Chemistry and Application of Chitin and Its Derivatives.* 2010, Vol. 25, pp. 117-126.

216. **Bhardwaj, V., Ankola, D., Gupta, S., Schneider, M., Lehr, C., Kumar, M.** PLGA nanoparticles stabilized with cationic surfactant: safety studies and application in oral delivery of paclitaxel to treat chemical-induced breast cancer in rat. *Pharmaceutical Research.* 2009, Vol. 26, pp. 2495–2503.

217. **Kwon, Y., Standley, S., Goh, S., Frechet, J.** Enhanced antigen presentation and immunostimulation of dendritic cells using acid-degradable cationic nanoparticles. *Journal of Controlled Release.* 2005, Vol. 105, pp. 199-212.

218. **Jedrzejas, M.** Pneumococcal Virulence Factors: Structure and Function. *Microbiology and molecular biology reviews.* 2001, Vol. 65, pp. 187–207.

219. **Mosmann, T.** Rapid colorimetric assay for cellular growth and survival: Application to proliferation and cytotoxicity assays. *J Immunol Methods.* 1983, Vol. 65, pp. 55-63.

220. **Lima, F., Miyaji, E., Quintilio, W., Raw, I., Ho, P., Oliveira, M.** Pneumococcal surface protein A dose not affect the immune responses to a combined diphheria tetanus and pertusis vaccine in mice. *Vaccine.* 2013, Vol. 31, pp. 2465-2470.

221. **Yamamoto, M., Briles, D., Yamamoto, S., Ohmura, M., Kiyono, H., Mc Ghee, J.** A nontoxic adjuvent for mucosal immunity to pneumococcal surface protein A. *Journal of Immunology.* 1998, Vol. 161, pp. 4115-4121.

222. **Yang, Y., Chung, T., Ng, N.** Morphology, drug distribution, and in vitro release profiles of biodegradable polymeric microspheres containing protein fabricated by double-emulsion solvent extraction/evaporation method. *Biomaterials.* 2001, Vol. 22, pp. 231-241.

223. **Erdemli, Ö., Keskin, D., Tezcaner, A.** Influence of excipients on characteristics and release profiles of poly(ε-caprolactone) microspheres containing immunoglobulin G. *Materials Science and Engineering C.* 2015, Vol. 48, pp. 391–399.

224. **Ito, F., Fujimori, H., Makino, K.** Factors affecting the loading efficiency of water-soluble drugs in PLGA microspheres. *Colloids and Surfaces B: Biointerfaces.* 2008, Vol. 61, pp. 25–29.

225. **Youan, B., Benoit, M., Baras, B., Gillard, J.** Prote in -load e d poly(e-caprolac ton e) m ic ropartic le s. I. Optim iz ation of th e pre paration by (w ate r-in -oil)-in w ate r em u l sion solv e n t e v aporation. *Journal of Microencapsulation.* 1999, Vol. 16, pp. 587-599.

226. **Baras, B., Benoit, M.-A., Gillard, J.** influence of various technological parameters on the preparation of spray-dried poly(e-caprolactone) microparticles containing a model antigen. *Journal of Microencapsulation.* 2000, Vol. 17, pp. 485-498.

227. **Devineni, D., Ezekwudo, D., Palaniapp, R.** Formulation of maltodextrin entrapped in polycaprolactone microparticles for protein and vaccine delivery: Effect of size determining formulation process variables of microparticles on the hydrodynamic diameter of BSA. *Journal of Microencapsulation.* 2007, Vol. 24, pp. 358–370.

228. **Pisani, E., Fattal, E., Paris, J., Ringard, C., Rosilio, V., Tsapis, N.** Surfactant dependent morphology of polymeric capsules of perfluorooctyl bromide: influence of polymer adsorption at the dichloromethane-water interface. *Journal of Colloid and Interface Science.* 2008, Vol. 326, pp. 66–71.

229. **Dotto, G., Pinto, L., Hachicha, M., Knani, S.** New physicochemical interpretations for the adsorption of food dyes on chitosan films using statistical physics treatment. *Food Chemistry .* 2015, Vol. 171, pp. 1–7.

230. **Wang, Y., Li, P. and Kong, L.** Chitosan-Modified PLGA Nanoparticles with Versatile Surface for Improved Drug Delivery. *AAPS Pharm Sci Tech.* 2013, Vol. 14, pp. 585-592.

231. **Jiang, M., Wu, Y., He, Y., Nie, J.** Synthesis and characterisation of an amphiphilic hyperbranched poly(amine-ester)-co-D,L-lactide (HPAE-co-PLA) copolymers and their nanoparticles for protein drug delivery. *Journal of Applied Polymer Science.* 2010, Vol. 117, pp. 1156-1167.

232. **Determan, A., Trewyn, B., Lin, V., Nilsen-Hamilton, M., Narasimhan, B.** Encapsulation, stabilisation, and release of BSA-FITC from polyanhydride microspheres. *Journal of Controlled Release.* 2004, Vol. 100, pp. 97-109.

233. **Vadesilho, C., Ferreira, D., Moreno, A., Chavez-Olortegui, C., de Avila, R., Oliveira, M., Ho, P., Miyaji, E.** Characterization of the antibody response elicited by immunization with pneumococcal surface protein A (PspA) as recombinant protein or DNA vaccine and analysis of protection against an intranasal lethal challenge with Streptococcus pneumoniae. *Microbial Pathogenesis.* 2012, Vol. 53, pp. 243-249.

234. **Huang, Y., Vieira, A., Huang, K., Yeh, M., Chiang, C.** Pulmonary inflammation caused by chitosan microparticles. *Journal of Biomedical Materials Research Part A.* 2005, Vol. 75, pp. 283-287.

Appendices

Appendix- 1

SDS-PAGE analysis of protein integrity

Sodium dodecyl sulfate poly (acrylamide) gels (10 cm W × 8 cm L × 0.5 mm thick) were freshly cast for all experiments. The resolving layer solution prepared using 6 mL protogel solution (to produce a final acrylamide concentration of 7.5%), 5 mL resolving buffer, and 8.78 mL water. Polymerization was initiated by adding 100 μl of freshly prepared 10% ammonium persulfate (APS) and 10 μl N, N, N`, N`,-tetramethyl ethylenediamine (TEMED). Then the solution was poured between the gel casting plates and allowed to set for 15 minutes. The stacking layer gel was prepared using 1.3 mL protogel solution (to produce 4% acrylamide final concentration), 2.5 mL stacking buffer, and 6 mL water. Polymerization was initiated by adding 50 μl of freshly prepared 10% APS and 10 μl TEMED. Then the solution was poured between the gel casting plates to the top of plates and the comb inserted between the plates. The gel was allowed to polymerise for 15 minutes then the comb gently removed. The gel was then placed into the electrophoresis tank, filled with fresh (10X) Tris-glycine-SDS Buffer. Protein samples and standard were treated with protein loading buffer in a ratio (1:1) for 3 min at 95°C. The protein molecular weight marker, standard, and samples were loaded into the wells (25 μl per well). The gel was transferred to colloidal Coomassie Brilliant Blue stain (to stain the protein band) and placed on a shaker for 24 h. Then the gel was rinsed with water and placed on the shaker for a further 24 h (to destain the gel).

List of Publications

List of Publications

Publications

1.   Kunda NK, <u>Alfagih IM</u>, Saleem IY, Hutcheon GA. " Polymer based delivery systems for the pulmonary delivery of macromolecules" in Pulmonary Drug Delivery: Advances and Challenges by Professor Ali Nokhodchi and Gary Martin (Book Chapter). John Wiley & Sons (Accepted, launch Mar 2015).

2.   Kunda NK, <u>Alfagih IM</u>, Dennison SR, Tawfeek HM, Somavarapu S, Hutcheon GA, Saleem IY. 2014. Bovine Serum Albumin Adsorbed PGA-co-PDL Nanocarriers for Vaccine Delivery via Dry Powder Inhalation. Pharmaceutical Research, <u>doi: 10.1007/s11095-</u>014-1538-5.

3.   Merchant Z, Taylor K, Stapleton P, Razak S, Kunda N, <u>Alfagih I</u>, Sheikh K, Saleem I, Somavarapu S. 2014. Engineering hydrophobically modified chitosan for enhancing the dispersion of respirable microparticles of levofloxacin. European Journal of Pharmaceutics and Biopharmaceutics, <u>doi:10.1016/j.ejpb.2014.09.005</u>.

4.   <u>Alfagih IM</u>, Alanazi FK, Hutcheon GA, Saleem IY. 2011. Recent Advances Using Supercritical Fluid Techniques for Pulmonary Administration of Macromolecules via Dry Powder Formulations. *Drug Delivery Letters*, vol. 1(2), 128-134.

Conference proceeding (4-page abstract)

1.   <u>Alfagih IM</u>, Alanzi FK, Kunda NK, Hutcheon GA, Saleem IY. Protein loaded PGA-co-PDL Nanocomposite Microparticles for Inhalation. Drug Delivery to the Lungs – DDL 23- December 2012, Edinburgh, Scotland, UK (Published in Juournal of Aerosol Medicine and Pulmonary Drug Delivery. October 2013: A13).

2.   Kunda NK, <u>Alfagih IM</u>, Somavarapu S, Hutcheon GA, Saleem IY. Pulmonary Vaccine Delivery of Protein Adsorbed PGA-co-PDL Nanocomposite Microparticles. Drug Delivery to the Lungs – DDL 23- : December 2012, Edinburgh, Scotland, UK

(Published in Juournal of Aerosol Medicine and Pulmonary Drug Delivery. October 2013: A9).

Selected Abstract

1. <u>Alfagih IM</u>, Kunda NK, Alanzi FK, Hutcheon GA, Saleem IY. Cationic PGA-co-PDL nanocomposite microparticles for antigen delivery via inhalation. Drug Delivery to the Lungs – DDL 25: 10th –12th December 2014, Edinburgh, Scotland, UK.

2. <u>Alfagih IM</u>, Kunda NK, Alanzi FK, Hutcheon GA, Saleem IY. Pulmonary antigen delivery using surface modified PGA-co-PDL nanocomposite microparticles. 8th Vaccine & ISV Congress, 26-28 Oct 2014, Philadelphia, PA, USA.

3. <u>Alfagih IM</u>, Alanzi FK, Kunda NK, Hutcheon GA, Saleem IY. Protein loaded PGA-co-PDL Nanocomposite Microparticles for Inhalation. Drug Delivery to the Lungs – DDL 23: 5th –7th December 2012, Edinburgh, Scotland, UK.

4. N K Kunda, <u>I M Alfagih</u>, S Somavarapu, G A Hutcheon, I Y Saleem. Pulmonary Vaccine Delivery of Protein Adsorbed PGA-co-PDL Nanocomposite Microparticles. Drug Delivery to the Lungs – DDL 23: 5th –7th December 2012, Edinburgh, Scotland, UK.

5. <u>Alfagih IM</u>, Alanzi FK, Satyanarayana S, Chavan T, Hutcheon GA, Saleem IY. PGA-co-PDL Nanocomposite Microparticles as Carriers of Protein for Pulmonary Delivery. 8th World Meeting on Pharmaceutics, Biopharmaceutics and Pharmaceutical Technology, 19-21 March 2012, Istanbul, Turkey.

Funding

Recent Advances Using Supercritical Fluid Techniques for Pulmonary Administration of Macromolecules via Dry Powder Formulations

Iman M. Al-fagih[a,b], Fars K. Alanazi[b], Gillian A. Hutcheon[a] and Imran Y. Saleem[a,*]

[a]*School of Pharmacy & Biomolecular Sciences, Liverpool John Moores University, Liverpool, UK;* [b]*Department of Pharmaceutics, College of Pharmacy, King Saud University, Riyadh, Saudi Arabia*

Abstract: Growing demands on a suitable formulation method that ensures the stability of the active compound coupled with the limitations of current methods (milling, lyophilization, spray drying, and freeze spray drying) has brought wide attention to supercritical fluid (SCF) technology. Advantages of using the SCF technology comprise its high abilities, adaptability in providing alternative processing methods, high compressibility and diffusivity of the supercritical fluid, capability as an alternative for conventional organic solvents, and the option to attain different processing parameters which would be otherwise difficult to conduct with traditional methods. This review proposes to present an up-to-date outlook on dry powder pulmonary formulations of macromolecules using SCF technology.

Keywords: Dry powder, inhalation, macromolecules, microparticles, peptide, protein, super critical fluid.

1. INTRODUCTION

Over the past two decades a rapid growth of innovative technologies for producing novel therapeutic agents has arisen. This growth has mostly been initiated by the discovery of new therapeutic agents, such as macromolecules, together with an increased understanding and knowledge of pathophysiology [1]. Consequently, novel macromolecules (also known as biotechnology-derived pharmaceuticals, biotherapeutics, or biological drugs and include recombinant therapeutic proteins, monoclonal antibody based products and nucleic acid-based medicinal products) can now be produced with preferential selectivity for definite targets [1, 2]. To date many macromolecule based drugs are in clinical trials or at approval phase (Table **1**) [3]. Over the past decade pharmaceutical research and development has been focused on developing macromolecules for treatment of many diseases, and are preferred due to their greater selectivity; lower disruption of normal biological processes; effective substitutional therapy in mutated or deleted normal protein and less clinical development time in addition to a shorter FDA approval period [4,5].

However, most of these macromolecules must be administered repeatedly using an invasive manner to reach a therapeutic concentration, even though these procedures would be painful to the patients [6-8]. As an alternative to repeated injection, pulmonary inhalation could enhance macromolecule administration because it is a non-invasive technique for local and systemic drug delivery. The lungs own many favorable features, including large surface area for absorption, highly vasculatures, thin epithelium in the alveolar tissue and short path of gas–blood exchange movement [8].

However, formulating macromolecules into suitable pulmonary delivery systems remains a challenge.

A variety of micro/nanoparticulate systems such as polymer based micro/nanoparticles, liposomes and solid lipid micro/nanoparticles have been used for the encapsulation of macromolecules serving specific therapeutic purposes such as controlled release or targeted drug delivery. Major concerns on the formulation method of macromolecules must be addressed when dealing with these molecules [7]. The stability and biological activity of macromolecules are extensively dependent on their entire structures, and can be easily altered by physical means (e.g. denaturation, adsorption, or noncovalent aggregation) or chemical means (e.g. oxidation, deamidation, or peptide cleavage). The impact of modifications can be very complicated (losses in therapeutic activity, changes in absorption, biodistribution, elimination, toxicity and immunogenecity). In addition, these intact structures are important characteristics which have impact on the physicochemical properties of the final therapeutic products, especially in the case of pulmonary drug delivery that require careful manipulation of the particle size, shape, density, and surface properties (Table **2**). Many different routes are employed to achieve solid-state formulations, including milling, freeze drying (lyophilization), spray drying (SD), and spray–freeze drying (SFD) (Table **3**).

Growing demands on a suitable formulation method that ensures the stability of the active compound coupled with the limitations of current methods (milling, lyophilization, spray drying, and freeze spray drying) brought wide attention to supercritical fluid (SCF) technology [2]. SCF are gases and liquids above their critical pressure (P_c) and critical temperature (T_c), and under these conditions, the molecules exhibit the flow, polarity, and solvency properties common of liquids but have the diffusion and reactivity characteristics of gases. SCF technique can be performed using carbon dioxide (CO_2), water, propane, acetone, nitrous oxide (N_2O),

*Address correspondence to this author at the School of Pharmacy and Biomolecular Sciences, Liverpool John Moores University, James Parson Building, Byrom Street, Liverpool, L3 3AF UK; Tel: +44(0)151 231 2265; Fax: +44(0)151 231 2170; E-mail: I.Saleem@ljmu.ac.uk

Table 1.   Examples of Therapeutic Macromolecules being Investigated for Systemic Delivery via the Pulmonary Route

Type	Active Agent	Disease	Ref.
Hormone	Erythropoeitin	Anaemia	[15]
	Insulin	Diabetes	[15]
	Parathyroid hormone	Osteoporosis	[14, 15]
	Cetrorelix	LH-RH antagonist	[15]
	Follicle stimulating hormone	Fertility treatment	[15]
	LH-RH analogues	Endometriosis, prostate cancer	[15]
Growth factor	Sargramostim	Sarcoma	[15]
	Growth hormone releasing factor	Pituitary dwarfism	[14]
Blood derivative	Immunoglobulin	Trigger/modulate immune response	[15]
Interferon-beta	Interferon	Multiple sclerosis	[14, 15]
Natural extract	Calcitonin-salmon	Osteoporosis	[14, 15]
	Heparin	Inhibit thrombosis	[14, 15]
	Cyclosporine	immunosuppression	[15]
Recombinant protein	Human recombinant F.IX	Hemophilia B	[15]
Vaccine	HBsAg	Hepatitis B	[16]
	P30B2, (NANP)6P2P30	Malaria	[16]
	SPf66	Malaria	[16]
	Hemagglutinin	Influenza	[16]
	Mtb8.4 peptide	Tuberculosis	[16]
	HLA-A*0201 plasmid	Tuberculosis	[16]
	Diphtheria toxoid	Diphtheria	[16]
	Tetanus toxoid	Tetanus	[16]
	Formalin- inactived rotovirus	Rotavirus	[16]

Table 2.   Product Parameters and Pharmaceutical Considerations in Drug Product Design

Parameter	Importance/Effect	Ref.
Particle size and distribution	Precise targeting Content uniformity Rates of dissolution, Rates of release, Dose delivery	[18-20]
Particle shape (morphology)	Flow property Dispersibility	[21]
Particle density	Flow property Dispersibility	[22]
Particle surface charge	Optimal surface properties of particles must be obtained to prevent particles agglomeration Flow property Dispersibility Precise targeting	[16, 21, 23]
Crystal form	Crystal form influences all steps of the development from discovery to marketing	[10]

Table 3.   Common Methods for Formulations of Macromolecules

Method	Description	Disadvantages	Excipients	Ref.
Jet Milling	Bulk particles are introduced into the milling chamber. Air or nitrogen, fed through nozzles at high pressure, accelerates the solid particles to sonic velocities. The particles collide and fracture. While flying around the mill, larger particles are subjected to higher centrifugal forces and are forced to the outer perimeter of the chamber. Small particles exit the mill through the central discharge stream	Broad particle size Physical/chemical degradation	e.g. trehalose	[21]
Freeze drying (Lyophilization)	The formulation is frozen and the bulk water is removed by sublimation. The resulting cake is composed of the protein, any nonvolatile excipients, and a small amount of residual water tightly associated with the protein	Time consuming Broad particle size distribution	e.g. trehalose, inulin, dextran	[6, 11]
Spray drying	Uses atomization to form microdispersed droplets. The water in these droplets quickly evaporates when passed through a stream of hot gas, resulting in the formation of a fine powder of microparticles containing protein and excipients	Degradation Low process efficacy Time consuming	e.g. leucine, lactose, trehalose, dipamitoyl-phosphatidylcholine (DPPC), albumin	[8, 11, 22, 24, 25]
Spray-freeze drying	The microdispersed liquid particles are generated through the jet nozzle in the absence of heat, then collected and frozen in liquid nitrogen before sublimation occurs. The frozen particles are then lyophilized	Degradation Low process efficacy Time consuming	e.g. inulin, trehalose, manitol	[6, 8, 21, 24]
Supercritical Fluid	SCF are gases and liquids above their critical pressure and critical temperature. SCF technique can be performed using carbon dioxide (CO_2), water, propane, acetone, nitrous oxide (N_2O), trifluoromethane, chlorodifluoromethane, diethyl ether, water, or CO_2 with ethanol	Solubility of molecules in solvent Degradation Particle size control Residue of organic solvent Scale up of this process is restricted by particle aggregation and nozzle blockage due to rapid expansion cooling.	e.g. sucrose, trehalose, manitol	[2, 8, 11, 13]

trifluoromethane, chlorodifluoromethane, diethyl ether, water, or CO_2 with ethanol [13]. In addition SCF possess several fundamental advantages as solvents and/or anti-solvents for processing heat-labile solutes at low temperature. For example, supercritical CO_2 is a good solvent for water-insoluble as well as water-soluble compounds under suitable low critical conditions (T_c = 31.2 °C, P_c = 7.4 MPa) [8]. In addition, compressed CO_2 is accessible in ample proportions with a higher degree of purity [9]. Moreover, CO_2 is non-toxic, nonflammable, and inexpensive [8]. Therefore, supercritical CO_2 has potential as an alternative for conventional organic solvents used in solvent-based processes for forming solid dosage forms. Furthermore, the general consideration of SCF as a "green" substitute has become very significant as the harmful effects of residual organic solvents, from both a processing and environmental point of view, have been known, and in addition, the regulatory specifications for the utilization and residual amounts of organic solvents in the final pharmaceutical product become more stringent [10].

There are two major principles based on SCF. The first process utilizes supercritical fluids as a solvent. The Rapid Expansion of a Supercritical Solution (RESS) process is the method that represents this first principle. Initially the solute

must dissolve in a SCF followed by sudden decompression, after which the solution is rapidly expanded at low pressure by passing through an orifice. The restrictions facing application of RESS for macromolecules formulations include: it is restricted to molecules that are soluble in SCF CO_2, relatively high temperature required for the rapid expansion (typical temperature of 40 ºC) which can destroy proteins, lacking control of particle size, and scale up of this process is restricted by particle aggregation and nozzle blockage due to rapid expansion cooling [8].

The second process involves the solute being insoluble in SCF and hence utilizes SCF as an antisolvent. Many macromolecules which are suitable as therapeutic agents are slightly soluble in SCF and have high solubility in water. These processes use SCF as an antisolvent where a solute is dissolved in an organic solvent then precipitated by SCF. Precipitation develops when the SCF is absorbed by the organic solvent followed by expansion of the liquid phase and decreases in the solvent power leading to particle formation. The Gas Anti-Solvent (GAS), Aerosol Solvent Extraction System (ASES), Supercritical Fluid Antisolvent (SAS), Precipitation with Compressed Antisolvent (PCA), Solution Enhanced Dispersion by Supercritical Fluids (SEDS), and

supercritical fluid extraction of emulsion (SFEE) are the processes that exemplify this second group Fig. (**1**). The main disadvantage of the second process that applies SCF as antisolvent is the difficulty to remove the residual organic solvent completely [8].

Thorough discussions of differences in the above techniques have been recently published elsewhere [8-13]. This review proposes to present an up-to-date outlook on the progression of dry powder formulations for inhalation of macromolecules using SCF techniques, covering its challenges, possibilities and recent developments.

2. SUPERCRITICAL FLUID APPLICATIONS IN PREPARATION OF MACROMOLECULES FOR DRY POWDER INHALATION

Unlike conventional methods of particle formation such as milling, lyophilization, spray-drying, and freeze-spray drying, where large particles are reduced to the intended size, SCF technology includes developing the particles in a controlled approach to achieve the intended size. Therefore the negative effect of the energy transmitted to the system such as denaturation of protein to produce the desired size can be avoided. Ideally, the particles once formed must not be subjected to further treatment and this property makes SCF technology suitable to produce macromolecules in their native pure state and/or encapsulating these agents [13].

Advantages of using the SCF technology comprise its high abilities, adaptability in providing alternative processing methods, the high compressibility and diffusivity of SCF, capability as an alternative for conventional organic solvents,

and the ability to reach different processing parameters (such as pressure and the rate of solvent evaporation) which would otherwise be difficult to conduct with conventional methods [10].

2.1. Encapsulation of Insulin

SCF have unique properties as mentioned above that makes them applicable for various processing methods such as particle formation and extractions. Recently, a significant interest in SCF technology has been revealed in an attempt to find other preferable approaches of insulin processing.

Todo *et al.* [26] examined the absorption of insulin dry powders processed with mannitol (carrier) and citric acid (an absorption enhancer) by the SCF process known as solution enhanced dispersion by supercritical fluids (SEDS) with that prepared by spray drying (SD) technique. In this investigation insulin powder was precipitated by dispersing the insulin aqueous solutions through V-type nozzles into supercritical CO_2/ethanol/water ternary system. Water feed rate, liquid CO_2 feed rate, ethanol feed rate, pressure, and temperature were 0.035 mL/min, 5.7 g/min, 0.665 mL/min, 15 MPa, and 35 ºC, respectively. These operating conditions enabled the water to be miscible with the non-polar CO_2. A manual injector was used to introduce aqueous 0.25 % insulin solution with 0.2% citric acid and 5.0 % mannitol into the water stream. For dry powders (0.25 % insulin solutions containing 5 % mannitol and 0.20 % citric acid) prepared by SD technique the following standard operating parameters were used: an inlet temperature of 90 ºC, a drying air flow rate of 0.75 m^3/min, a solution feed rate of 5 mL/min, and an atomizing air pressure of 100 kPa. The authors found that insulin

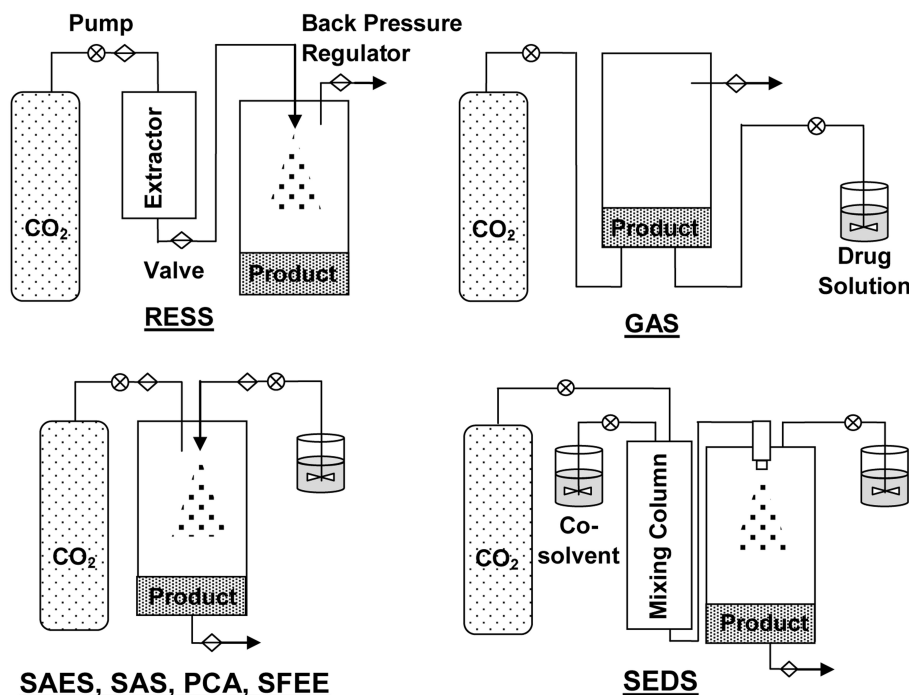**Fig. (1).** Schematic diagrams of various particle-formation processes using supercritical fluid technology. RESS: Rapid Expansion of a Supercritical Solution, GAS: Gas Anti-Solvent, ASES: Aerosol Solvent Extraction System, SAS: Supercritical Fluid Antisolvent, PCA: Precipitation with Compressed Antisolvent, SEDS: Solution Enhanced Dispersion by Supercritical Fluids, and SFEE: supercritical fluid extraction of emulsion.

powder prepared by the SCF method showed enhanced aerosolisation efficiency at 28 L/min using an Andersen Cascade Impactor in comparison with insulin powder prepared by the SD method. For example, SCF insulin powders had the greatest quantity of powder retrieved from stages 2–7 and a mass median aerodynamic diameter of 3.2 µm with respirable fraction of 47.6 %. The hypoglycemic effect of insulin powder processed by SCF after intratracheal application was higher than that produced by SD. In addition, they found that SCF technique provided the largest yield of insulin powder (>80 %) although it was on a laboratory scale production. These results demonstrated that the SCF process would be beneficial to prepare inhalable insulin powder.

Amidi *et al.* [27] demonstrated that PCA-type SCF technology is an appropriate method to manufacture inhalable insulin-loaded microparticles with specific particle properties and retained structure of insulin. The authors used N-trimethyl chitosan (TMC), as a mucoadhesive absorption enhancer, and dextran as carriers for insulin, and prepared two formulations of 10 % (w/w) of insulin/TMC or insulin/dextran. The particles were formed by spraying an acidic water/dimethyl sulfoxide (DMSO) solution of insulin and polymer within supercritical CO_2. The flow rates of polymer-insulin solution and CO_2 were 4.5 mL/min and 333 g/min, respectively. The pressure and temperature were maintained at 110 bar and 40 °C. The mass median aerodynamic diameter was 4 µm and the percentages of the emitted dose were 62 and 67 % for insulin/TMC and insulin/dextran respectively. The water content of the particles was 4 % (w/w), and neither crumpled nor agglomerated after formation and storage. The intact structure of insulin in the freshly formulated dried insulin powders were monitored by circular dichroism spectroscopy, which indicated the secondary and tertiary structures of insulin was retained in all preparations. Furthermore, at the end of one-year storage at 4 °C, the particle properties were preserved and the insulin structure almost retained in the TMC powders.

Kim *et al.* [28] compared micronized insulin using mannitol as a stabilizer alone or with the addition of trehalose as a second stabilizer using a process known as aerosol solvent extraction system (ASES) SCF technology. They injected co-currently the solution of insulin/mannitol (15/85 wt.%) with or without 10 and 15 wt.% trehalose with the CO_2 into the precipitation vessel using the solvent, N,N-dimethylformamide (DMF) at 35 °C, 180 bar, 8 mg/mL solution concentration, and 5 ml/min solution flow rate. Results indicated that when trehalose was used as a second stabilizer, the particles were almost uniform, more spherical, less adhesive, and less aggregated in air flow, in comparison to insulin mannitol particles alone. The mass median aerodynamic diameter of the insulin/mannitol particles was ~5 µm and of the insulin/mannitol/trehalose particles was ~2.32 µm, which are appropriate for inhalable dosage from. *In vitro* aerosolisation deposition test conducted with a micro-orifice uniform deposit impactor (MOUDI-II™Impactor) at 30 L/min revealed 69 % by weight of the insulin/mannitol and 41 % by weight of the insulin/manitol/trehalose particles was deposited on stages 3, 4, 5 and 6. This study showed the ASES process was able to retain the secondary structures of insulin in both insulin/mannitol and insulin/manitol/trehalose particles.

2.2. Gene Powders

Polymer based non-viral gene delivery systems have been shown to offer protection from nuclease degradation, increased plasmid DNA (pDNA) uptake and sustained duration of pDNA action [29]. These gene delivery systems can be prepared from biologically compatible and degradable polymers e.g. poly (d,l-lactic-co-glycolic) acid (PLGA). The effectiveness of gene therapeutic systems depends on the ability of such system to deliver nucleic acid into the target cells. Gene dry powders are anticipated to have further advantage of prolonged shelf life of the preparation [29].

Okamoto *et al.* [29] compared stability of a chitosan–pDNA complex powder processed by a SEDS-type SCF technique and gene solution alone for inhalation. They precipitated the gene powder by dispersing an aqueous chitosan–pDNA complex solution with mannitol into the stream of a SCF CO_2/ethanol admixture. In the mixing column, the CO_2 was admixed with ethanol at a flow rate of 5.7 g/min and 0.665 mL/min respectively. Using these operating conditions resulted in complete miscibility of ethanol, water, and CO_2. The admixture was dispersed into the particle formation vessel at 35 °C and 15 MPa using one end of the V-shaped nozzle, while the other end of the V-shaped nozzle was used to disperse water at a flow rate of 0.035 mL/min. The aqueous chitosan–pDNA complex solution (0.4 mL) was manually injected into the water stream and the dry powder was collected from the depressurized vessel. This procedure resulted in powder yields of ~80 % and aerodynamic particle sizes of ~3 µm, which was appropriate for pulmonary delivery. Scanning electron microscopy examination revealed the powders to have rectangular shape. Gene integrity and transfection potency were determined by electrophoresis and *in vivo* pulmonary transfection test in mice. The SCF technique minimized the supercoiled DNA during the formulation processing; although, the reduction in the remaining supercoiled and open circular DNA in the powders during storage was more prolonged than in solutions. As a result, the powders generated using SEDS had increased transfection potency in comparison to the gene solutions for the same quantity of DNA.

Mayo *et al.* [30] developed a SCF extraction of emulsions (SFEE) technique based on CO_2 for formulating nanoparticles having high plasmid (pFlt23K, an anti-angiogenic pDNA capable of inhibiting vascular endothelial growth factor (VEGF) secretion) loading and loading efficiency. First they prepared a lipophilic phase by dissolving PLGA into ethyl acetate and the inner aqueous phase composed of pFlt23K Tris-EDTA buffer. The aqueous phase was sonicated for 1 min (15W) with the lipophilic phase to obtain a 1° emulsion (w/o). The outer aqueous phase consisted of 0.5 % (w/v) polyvinyl alcohol (PVA) saturated with ethyl acetate. The 1° emulsion was further sonicated with the outer aqueous phase for 3 min to obtain the 2° emulsion (w/o/w). The emulsion extraction and particle production was performed using coaxial SFEE apparatus consisting of a cylindrical pressure vessel, placed in a temperature controlled water bath at 45 °C. Supercritical CO_2 was injected via a syringe pump to the base of this vessel. The emulsion was introduced counter currently by means of a 100 µm capillary

tube within a 1/16" stainless steel high pressure tubing at the top of the vessel, permiting CO_2 to flow continually from the vessel. During the process the pressure and flow rate of the emulsion were kept at 8 MPa and 0.4 ml/ min, respectively. Results revealed spherical particles with smooth surface and 280 nm in diameter. In addition, a high loading of pFlt23K (19.7 %, w/w) and high encapsulation efficiency (>98 %) was achieved, while a low residual solvents (<50 ppm), attributed to rapid particle formation due to successful solvent removal afforded by the SFEE technique. *In vitro* transfection of pFlt23K-PLGA nanoparticles were able to significantly reduce secreted VEGF from human lung alveolar epithelial cells (A549) with normoxic and hypoxic status, with no cytotoxicty detected.

2.3. Vaccination

Recently immunization by inhalation has been investigated as a substituent for parenteral vaccination. Vaccines delivered via the lung route can initiate both systemic and local immune responses due to the presence of extensive dendritic cells and macrophages lining the respiratory epithelium.

Amidi *et al.* [31] examined the potential of N-Trimethyl chitosan (TMC) and dextran microparticles for pulmonary delivery of diphtheria toxoid (DT). DT-loaded microparticles were formulated by spraying an aqueous solution of DT/dextran (w/w) or DT/TMC into supercritical CO_2 and ethanol using SEDS type SCF technology. When the operating temperature (38 ºC) and pressure (100 bar) was achieved, CO_2 and ethanol were completely miscible forming a single supercritical phase. The ethanol/CO_2 mixture was immediately introduced via a concentric coaxial two-fluid nozzle and sprayed into the vessel for 5 min. This was subsequently followed by pumping the aqueous polymer-DT solution into the T-mixer at a flow rate of 0.5 ml/min using two syringe pumps. This was mixed with SCF-CO_2 (367 g/min) and ethanol (25 ml/min) and fed into the precipitation vessel through the concentric coaxial two-fluid nozzle. Smooth spherical particles were produced with median volume diameter of ~3 μm and the fine particle mass fractions less than 5 μm, as revealed by cascade impactor analysis at 30 L/min, were 35 % for the dextran and 56 % for the TMC formulations.

This study demonstrated that the generated powders had a significant mass fraction of particles less than 5 μm, suitable for inhalation. In addition, this investigation revealed that TMC microparticles were a potent pulmonary delivery system for DT antigen. Pulmonary immunization with DT-TMC microparticles containing 2 or 10 Lf of DT produced a strong immune response as manifested by the production of IgM, IgG, IgG subclasses (IgG1 and IgG2) antibodies similar to or significantly greater than those gained after subcutaneous application of alum-adsorbed DT (2 Lf). In addition, the IgG2/IgG1 ratio after pulmonary immunization with DT-TMC microparticles was significantly greater in comparison with subcutaneous administered alum-adsorbed DT. While pulmonary administrations of DT-dextran particles produced a very poor immune response.

3. CONCLUSION

There has been great progress in supercritical CO_2 techniques to increase performance of macromolecules without losing the biological activity of these sensitive molecules. However, there are still possibilities for optimizing processing parameters, such as temperature, pressure, flow rates, and concentration of ingredients. In addition, processing of therapeutic macromolecules with supercritical CO_2 permit a wide range of macromolecules to be processed, and in the future it is expected that SCF techniques will provide a more favorable alternative to producing formulations encapsulating macromolecules.

ACKNOWLEDGEMENTS

REFERENCES

[1]   Tibbitts, J.; Cavagnaro, J.; Haller, C.; Ben Marafino, B.; Andrews, P.; Sullivan, J. Practical approaches to dose selection for first-in-human clinical trials with novel biopharmaceuticals. *Reg. Toxicol. Pharmacol.*, **2010**, *58*(2), 243–251.

[2]   Walsh, G. Biopharmaceuticals: recent approvals and likely directions. *Trends Biotechnol.*, **2005**, *23*(11), 553–558.

[3]   Leader, B.; Baca, Q.J.; Golan, DE. Protein therapeutics: a summary and pharmacological classification. *Nat. Rev. Drug Discov.*, **2008**, *7*(1), 21–39.

[4]   Reichert, JM. Trends in development and approval times for new therapeutics in the United States. *Nat. Rev. Drug Discov.*, **2003**, *2*(9), 695–702.

[5]   Fox, JL. Turning plants into protein factories. *Nat. Biotechnol.*, **2006**, *24*(10), 1191–1193.

[6]   Swarbrick, J. Encyclopedia of Pharmaceutical Technology, 3^{ed} ed.; Informa healthcare: New York, **2007**.

[7]   Kayser, O., Muller, R.H. Pharmaceutical Biotechnology Drug Discovery and Clinical Application, 1st ed.; Wiley-VCH Verlag GmbH & Co. KGaA, Weinheim: New York, **2004**.

[8]   Shoyele, S. A.; Cawthorne, S. Particle engineering techniques for inhaled biopharmaceuticals. *Adv. Drug Deliv. Rev.*, **2006**, *58*(9-10), 1009–1029.

[9]   Vemavarapu, C.; Mollan, M. J.; Lodaya, M.; Needhamb, T.E. Design and process aspects of laboratory scale SCF particle formation systems. *Int. J. Pharm.*, **2005**, *292*(1-2), 1–16.

[10]   Pasquali, I.; Bettini, R.; Giordano., F. Supercritical fluid technologies: An innovative approach for manipulating the solid-state of pharmaceuticals. *Adv. Drug Deliv. Rev.*, **2008**, *60*(3), 399–410.

[11]   Okamoto, H.; Danjo, K. Application of supercritical fluid to preparation of powders of high-molecular weight drugs for inhalation. *Adv. Drug Deliv. Rev.*, **2008**, *60*(3), 433–446.

[12]   Mishima, K. Biodegradable particle formation for drug and gene delivery using supercritical fluid and dense gas. *Adv. Drug Deliv. Rev.*, **2008**, *60*(3), 411–432.

[13]   Byrappa, K.; Ohara, S.; Adschiri., T. Nanoparticles synthesis using supercritical fluid technology – towards biomedical applications. *Adv. Drug Deliv. Rev.*, **2008**, *60*(3), 299–327.

[14]   Laube, B. L. The expanding role of aerosols in systemic drug delivery, gene therapy, and vaccination. *Respir. Care*, **2005**, *50*(9), 1161-1176.

[15]   Cryan, S.A.; Sivadas, N.; Garcia-Contreras, L. In vivo animal models for drug delivery across the lung mucosal barrier. *Adv. Drug Deliv. Rev.*, **2007**, *59*(11), 1133-1151.

[16]   Pulliam , B.; Sung, J. C.; Edwards, D. A. Design of nanoparticle-based dry powder pulmonary vaccines. *Expert Opin. Drug Deliv.*, **2007**, *4*(6), 651-663.

[17]   U.S. Food and drug administration. Drugs: Development & Approval Process (Drugs), How Drugs are Developed and Approved. http://www.fda.gov/Drugs/DevelopmentApprovalProcess/HowDru

gsareDevelopedandApproved/DrugandBiologicApproval Reports/ucm242674.htm (Accessed May 22, 2011).

[18] Jain, K. K. Drug Delivery Systems, 1ˢᵗed.; Humana Press: Totowa, 2008.

[19] Niazi, S. K. Handbook of Preformulation Chemical, Biological, and Botanical Drugs, 1ˢᵗed.; Informa healthcare: New York, **2007**.

[20] Hillery, A. M.; Lloyd, A. W.; Swarbrick. J. Drug Delivery and Targeting for Pharmacists and Pharmaceutical Scientists, 1ˢᵗed.; Taylor & Francis: New York, **2001**.

[21] Pilcer, G.; Amighi. K. Formulation strategy and use of excipients in pulmonary drug delivery. *Int. J. Pharm*., **2010**, *392*(1-2), 1–19.

[22] Vehring, R. Pharmaceutical particle engineering via spray drying. *Pharm. Res*., **2008**, 25(5), 999-1022.

[23] Singh, M.; Chakrapani, A.; O'Hagan, D. Nanoparticles and microparticles as vaccine-delivery systems. *Expert Rev.Vaccines*, **2007**, *6*(5), 797-808.

[24] Amorij, J-P.; Huckriede, A.; Wilschut, J.; Frijlink, H. W.; Hinrichs, W. L. J. Development of stable influenza vaccine powder formulations: challenges and possibilities. *Pharm. Res*., **2008**, *25*(6), 1256-1273.

[25] Sollohub, K.; Cal, K. Spray drying technique: II. Current applications in pharmaceutical technology. *J. Pharm. Sci.*, **2010**, *99*(2), 587-597.

[26] Todo, H.; Iida, K.; Okamoto, H.; Danjo, K. Improvement of insulin absorption from intratracheally administrated dry powder prepared by supercritical carbon dioxide process. *J. Pharm. Sci.*, **2003**, *92*(12), 2475-2468.

[27] Amidi, M.; Pellikaan, H. C.; de Boer, A. H.; Crommelin, D. J. A.; Hennink, W. E.; Jiskoo, W. Preparation and physicochemical characterization of supercritically dried insulin-loaded microparticles for pulmonary delivery. *Eur. J. Pharm. Biopharm.*, **2008**, *68*(2), 191–200.

[28] Kim, Y.H.; Sioutas, C.; Shing, K.S. Influence of stabilizers on the physicochemical characteristics of inhaled insulin powders produced by supercritical antisolvent process. *Pharm. Res.,* **2009**, *26*(1), 61-71.

[29] Okamoto, H.; Sakakura, Y.; Shiraki, K.; Oka, K.; Nishida, S.; Todo, H.; Iida, K.; Danjo, K. Stability of chitosan–pDNA complex powder prepared by supercritical carbon dioxide process. *Int. J. Pharm.*, **2005**, *290*(1-2), 73-81.

[30] Mayo, A. S.; Ambati, B. K.; Kompella, U. B. Gene delivery nanoparticles fabricated by supercritical fluid extraction of emulsions. *Int. J. Pharm.*, **2010**, *387*(1-2), 278-285.

[31] Amidi, M.; Pellikaan, H. C.; Hirschberg, H.; de Boer, A. H.; Crommelin , D. J. A.; Hennink, W. E.; Kersten, G.; Jiskoot, W. Diphtheria toxoid-containing microparticulate powder formulations for pulmonary vaccination: Preparation, characterization and evaluation in guinea pigs. *Vaccine*, **2007**, *25*(37-38), 6818–6829

PGA-co-PDL NANOCOMPOSITE MICROPARTICLES AS CARRIERS OF PROTEIN FOR PULMONARY DELIVERY

I.M. Alfagih[1,2], F.K. Alanazi[2], S. Satyanarayana[3], T. Chavan[3], G.A. Hutcheon[1], I.Y. Saleem[1]

(1) School of Pharmacy & Biomolecular Sciences, Liverpool John Moores University, Liverpool, UK.
(2) Department of Pharmaceutics, King Saud University, Riyadh, Saudi Arabia.
(3) The School of Pharmacy, University of London, London, UK.

Introduction

As an alternative to repeated injection, dry powder pulmonary inhalation offers a non-invasive technique for local and systemic delivery of protein-based formulation (1). The lungs possess many favourable features (2). In our laboratory we have been investigating and developing alternative biodegradable polyester polymers [poly (glycerol adipate-co-ω-pentadecalactone, PGA-co-PDL)]. Using this polymer we have successfully encapsulated a model protein (α-chymotrypsin enzyme). In addition, release studies revealed most of the protein released over several hours (3). Furthermore, we have successfully demonstrated that PGA-co-PDL microparticles could be used as an alternative carrier for pulmonary delivery with enhanced aerosol performance and reduced toxicity to normal lung cells compared to PLGA microparticles (4).

In this study we aim to produce PGA-co-PDL nanocomposite microparticles (NMs) loaded with bovine serum albumin (BSA), a model protein, which may be administered to the lung via dry powder inhalation. The impact of these characteristics on important aspects of pulmonary delivery such as aerosolization, and release will be determined.

Methods

Nanoparticles Preparation

BSA (Avenchem, UK) loaded PGA-co-PDL nanoparticles (NPs) were prepared by probe sonication (sonics, VCX 500) of water-in-oil-in-water (w/o/w) double emulsion/solvent evaporation method (Table 1). The double emulsion was stirred for 2 h at room temperature and the NPs were collected by centrifugation at 30,000 g (Beckman J2-2IM/E) for 45 min at 4 °C. Control empty NPs were prepared.

Spray drying NPs

The NMs were prepared by spray drying NPs suspension in aqueous L-leucine solutions (1.5%w/w) using a mini-spray dryer (Büchi, B-290) with two-fluid nozzle (0.7 mm diameter), feed rate of 15 ml/min, air flow of 414 L/h, aspirator at 40m³/h, inlet and outlet temperature of 100 and 47 °C, respectively.

Nanocomposite Microparticles characterisation
Particle size & zeta potential

The particle size & zeta potential were measured using a Zetaplus. Briefly, 100µl of the suspension was diluted to 5 ml using double distilled water and the measurements recorded at 25ºC (n=3).

Spray dried yeild & drug loading

The yield of spray dried NMs was quantified as a percentage mass of expected total powder yield (n=3). The amount of BSA loaded in the NPs was determined by measuring the amount of BSA remaining in the supernatant with a QuantiPro BCA protein assay (Sigma) after centrifugation (n=3).

Particle morphology

Spray dried NMs were mounted on gold coated aluminium stubs (EmiTech K 550X Gold Sputter Coater, 25mA for 3 min), and visualised by scanning electron microscopy.

In-vitro relese study

20mg of BSA encapsulated spray dried NMs were placed in an eppendorf and dispersed in 1.2ml of PBS (pH 7.4). The samples were incubated at 37°C in the orbital shaker set at 250 rpm. At predetermined time intervals up to 24h, the samples were centrifuged (30,000 g for 20 min) and 1ml of the supernatant removed and replaced with fresh buffer. The supernatant was analysed by QuantiPro BCA protein assay as mentioned above (n=3).

Table 1 Different formulation parameters for preparation of NPs by (w/o/w) double emulsion solvent evaporation

Formula No.	Polymer conc. (mg/ml)	BSA Conc. (%)	IAP volume (µl)	PVA Conc. IAP (%)	PVA Conc. EAP (%)	EAP volume (ml)
NM1	25	0.5	500	1	13	25
NM2	25	0.5	500	5	13	25
NM3	25	0.5	250	5	13	25

*IAP: internal aqueous phase **EAP: external aqueous phase

Aerosolisation studies

Dry powder samples (10mg) were manually loaded into hydroxypropyl methylcellulose capsules (size 3), and aerosolised via a cyclohaler into a Next Generation Impactor (NGI), coated with 5% tween 80: acetone solution, at a flow rate of 60L/min for 4s to determine aerodynamic particle size. The samples were collected by washing with DCM/0.15 M NaCl mixture (2:1) to dissolve the polymer and the encapsulated BSA, which was determined by QuantiPro BCA protein assay as mentioned above (n=3). The FPF (%) was determined as the fraction of emitted dose deposited in the NGI with aerodynamic diameters less than 4.6 µm, and the MMAD was calculated from log-probability analysis.

Results & Discussion

Nanocomposite Microparticles characterisation

The particle size achieved ranged from 196.6±1.9 – 290.6±7.5 and the yield of NMs achieved after spray drying ranged from 24.4±4.7 – 35.9±5.1 (Table 2). All particles had a negative zeta potential, possibly due to PVA remaining on the particles after centrifugation and washing. The drug loading ranged from 14.6±2.5 to 20.54±3.1 µg/mg particle. There was a significant increase in drug loading between NM1 and NM2, due to an increase in PVA concentration in the IAP. However, decreasing IAP volume led to no significant difference in BSA loading between NM2 and NM3.

SEM analysis indicated that NMs (NM2) had a corrugated surface with pores visible on the surface (Fig. 1). This occurred due to excessive build-up of vapor pressure during solvent evaporation in the spray drying process and occurs with hydrophobic amino acids, such as L-leucine, for improved aerosolization performance (5). The size of the NM was approximately 2-3 µm according to SEM analysis.

Table 2 The drug loading, particle size, zeta potential, spray dried yield & drug loading of different NMs formulations.

Formula No.	Particle size (nm)	Zeta potential (mV)	Yield (%)	BSA loading (µg/mg)
NM1	275.5±12.7	-24.5±1.3	25.4±5.3	14.6±2.5
NM2	196.6±1.9	-19.3±3.3	24.4±4.7	20.5±3.1
NM3	290.6±7.5	-12.4±2.1	35.9±5.1	19.5±0.6

The data in Fig.2 represents the % cumulative release of BSA as a percentage of the drug loading. All formulation showed biphasic release profile with a first initial burst release followed by a second continuous sustained release phase over 24h. All formulations had a similar initial burst release of BSA ranging from 9.6±1.0 – 11.5±2.3%.
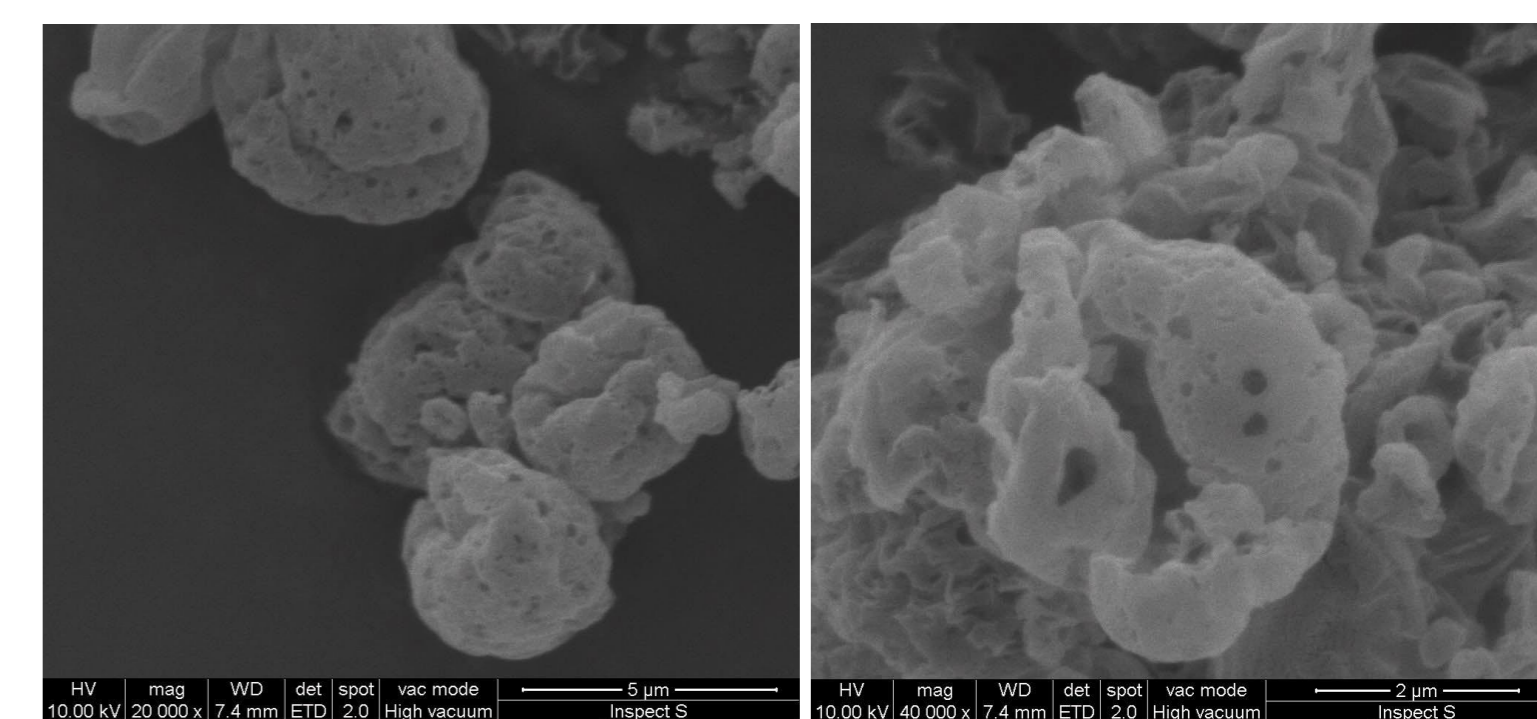

Figure 1 SEM images of NMs (NM2). Scale bar represents 5 µm (A) & 2 µm (B) respectively.

Significant difference was noted in release profile (2 – 24 h) between NM1 and NM3, with NM1 achieving 19.8±1.5% release after 24 h compared to NM3 (14.1±2.0%).
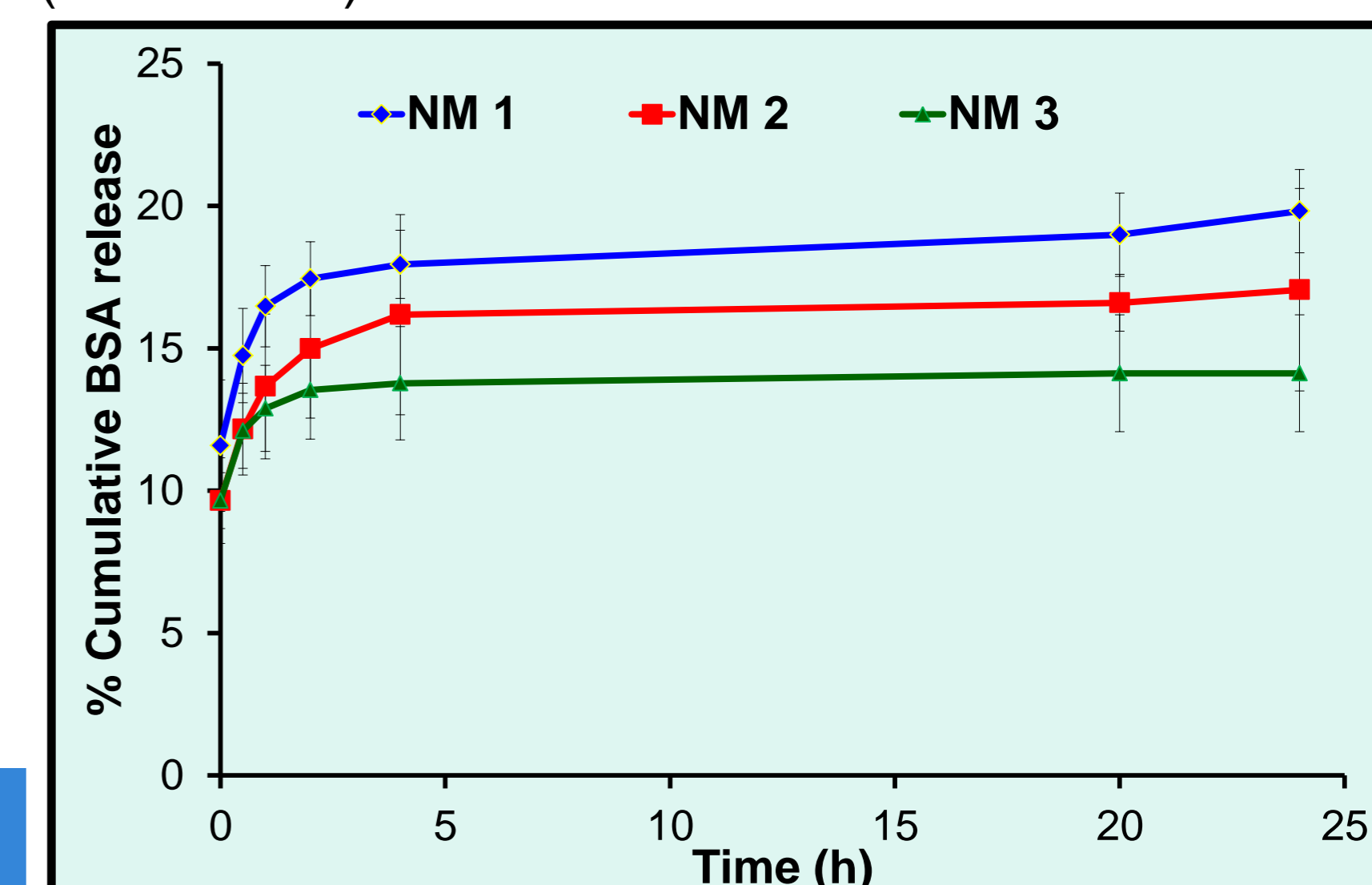

Figure 2 % cumulative in-vitro release profiles for different BSA-PGA-co-PDL NMs as a percentage of drug loading in phosphate buffer saline, pH 7.4.

NM2 was chosen for aerosolisation studies due to a high drug loading and reasonable drug release profile compared to NM1 and NM3. The results in Tab.3 indicate good aerosolisation properties and the MMAD corresponds to particle size data achieved with SEM.
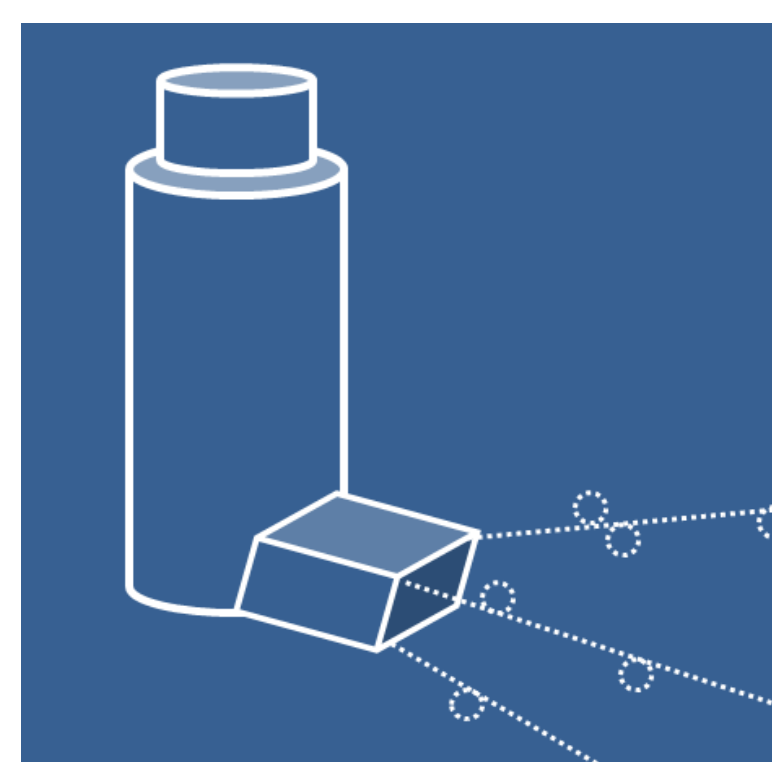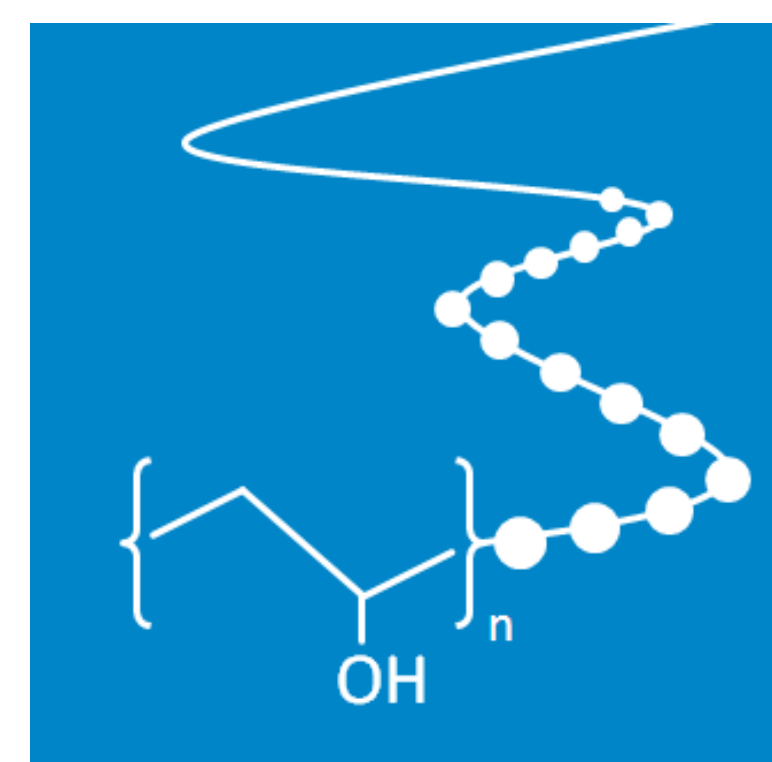
Table 3 Aerosolisation performance of NM2

Formula No.	FPF (%)	MMAD (µm)
NM2	70.1 ±13.2	1.6 ± 0.4

Conclusion

we have shown the potential for encapsulating proteins within PGA-co-PDL NMs as carriers for pulmonary delivery using double emulsion/spray drying as a preparation method. Future studies will involve improving the drug loading, stability studies and release by optimising the preparation method.

References

[1] Sou, T., et al. Trends Biotechnol. 29,191-198 (2011).
[2] Bivas-Benita, M., et al. Eur. J. Pharm. and Biopharm. 58, 1–6 (2004).
[3] Gaskell, E., et al. J. Microencapsul. 25, 187-195 (2008).
[4] Tawfeek, H., et al. Pharm. Res. 28, 2086-97 (2010).
[5] Alder, M., et al. Pharm. Res. 17, 863-870 (2000).

Protein Loaded PGA-co-PDL Nanocomposite Microparticles for Inhalation

I M Alfagih[1, 2], F K Alanazi[2], N K Kunda[1], G A Hutcheon[1], I Y Saleem[1]

1. School of Pharmacy and Biomolecular Sciences, Liverpool John Moores University, UK.
2. Department of Pharmaceutics, King Saud University, Riyadh, Saudi Arabia.

Introduction

Over the past decade pharmaceutical research has been focused on developing macromolecules for treatment of many diseases [1]. Most of these macromolecules are administered using an invasive manner to reach a therapeutic concentration, even though these procedures would be painful to the patients. As an alternative, pulmonary inhalation could enhance macromolecules administration because it is a non-invasive technique for local and systemic drug delivery. The lungs own many favourable features, including large surface area for absorption, high vasculatures, thin epithelium in the alveolar tissue and short path of gas–blood exchange movement [2]. However, formulating these macromolecules into suitable pulmonary delivery systems remains a challenge. .

The most common method for the encapsulation of proteins in polymer-based nanoparticles (NPs) is the water/oil/water (w/o/w) double-emulsion solvent evaporation method [3]. NPs can also be formulated into dry powders for inhalation by spray-drying.

Here at Liverpool John Moores University we have been investigating poly glycerol adipate-co-ω-pentadecalactone (PGA-co-PDL) as alternative to PLGA as a carrier for pulmonary delivery of macromolecules [4]. The results revealed that these polyesters could exhibit an alternative pulmonary delivery as they provide a protective matrix and faster release in a short period of time in comparison with other similar polymers, such as PLGA.

Objective

The aim of this study was to formulate PGA-co-PDL NPs encapsulating bovine serum albumin (BSA), a model protein, incorporated into a microparticle L-leucine matrix via spray drying to produce nanocomposite microparticle (NCMPs) carriers suitable for pulmonary delivery via dry powder inhalation.

Methods

Nanocomposite microparticles preparation

The protein solution 1% 0.5 ml was emulsified in dichloromethane,DCM containing 50 mg PGA-co-PDL, by a probe sonicator at 45% amplitude over an ice. Then emulsified into a 1% PVA solution 25ml at 45% ampliyude and stirred for 2h at room temperature to evaporate DCM. NPs collected by centrifugation at 25,750xg and 4°C.

NCMPs were prepared by spray drying NPs suspended in L-leucine solution (1:1.5w/w) using a mini-spray dryer (Büchi, B-290) at pump: 10%, air flow: 50 mm, aspirator: 50 % and inlet temperature:100 °C.

Nanocomposite microparticles characterization

- NCMPs zeta potential and size were carried out using a Zetaplus, Brookhaven Instruments, U.K.
- BSA loaded in NPs was determined by measuring BSA remaining in the supernatant and wash after centrifugation using a QuantiPro BCA protein assay kit (Sigma-aldrich).
- NCMPs were visualised by scanning electron microscopy (SEM) (FEI – Inspect S Low VAV Scanning).
- The yield of NCMPs was quantified as a percentage mass of expected total powder yield.

In-vitro release study

Ten mg of NCMPs were dispersed in 1.2ml of phosphate buffer saline, PBS (pH7.4) at 37°C and rotated on a mixer (HulaMixer, Life Technologies).

Aerosolisation study (Next Generation Impactor, NGI)

Ten mg of NCMPs were loaded into HMC capsules and aerosolised via a cyclohaler into a NGI, coated with tween 80: acetone solution,flow rate of 60L/min for 4s. Samples were collected by washing with DCM/0.15M NaCl mixture. FPF%: the fraction of emitted dose deposited in NGI with aerodynamic diameters < 4.6µm and the MMAD was calculated from log-probability analysis.

Results and Discussion
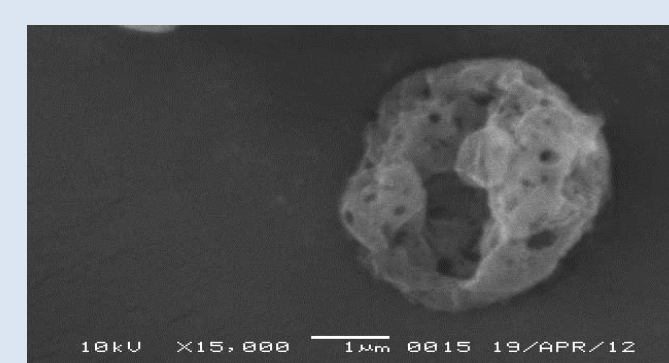
Nanocomposite microparticles characterization

The selected w/o/w double emulsion solvent evaporation process produced particles in the nanometer size range with a narrow particle size distribution (Table 1). The %EE of BSA loaded NPs was 39.49±2.63 % with BSA loading of 35.9±2.39 µg/mg and a zeta potential of -17.17±0.61 mV. NPs were further spray-dried to produce NCMPs with a reasonable yield for BSA loaded (38.22±1.17 %) and empty NCMPs (61.32±5.67 %).

Table 1 The particle size, polydispersity index (PDI), zeta potential, encapsulation efficiency (%EE), drug loading (DL), and yield (%) of NCMPs (n=3).

Formulation	Particle size (nm)	PDI	Zeta potential (mV)	EE (%)	DL (µg/mg)	Yield (%)
BSA-PGA-co-PDL	203.03±5.4	0.145	-17.17±0.61	39.49±2.63	35.9±2.39	38.22±1.17
Empty PGA-co-PDL	284.1±9.9	0.280	-15.86±0.85	-	-	61.32±5.67

SEM analysis (Figure 1) indicated that NCMPs were irregular and corrugated with a porous surface. The geometrical particle size of the produced nanocomposite microparticles as observed by SEM was approximately 2-4 µm.
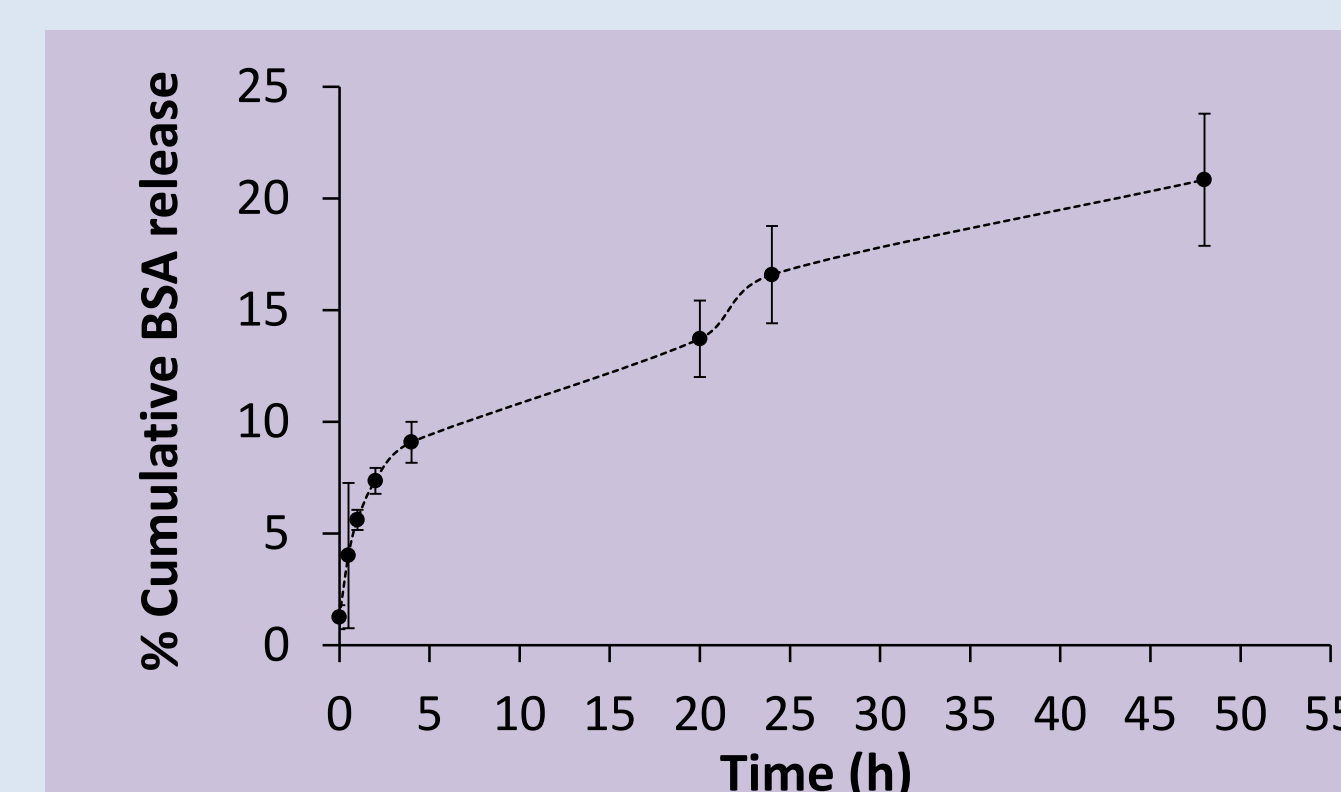
Figure 1 SEM images of spray dried BSA-PGA-co-PDL NCMPs. (The scale bar represents 1µm).

In-vitro release study

BSA showed biphasic release profile (Figure 2) with an initial burst release followed by a second continuous sustained release phase over 48h. The initial burst release of BSA from NCMPs was 1.26±1.5% which after 4 h increased rapidly to 9.08±3.4%, which then slowed to 20.84±4.2% after 48 h.

Figure 2 In-vitro release profiles of BSA –PGA-co-PDL NCMPs in PBS, pH 7.4 (n=3).

Aerosolisation study (Next Generation Impactor, NGI)

Aerodynamic particle characteristics revealed that the studied formulation yielded NCMPs capable of delivering efficient BSA with %FPF of 70.97±4.7% and a MMAD of 1.5±0.35 µm, indicating deposition in the bronchial-alveolar region. As NCMPs penetrate to the bronchial-alveolar region it is anticipated the L-leucine component will dissolve, releasing PGA-co-PDL NPs which will eventually degrade into its individual components (glycerol, divinyl adipate, and caprolactone) releasing BSA for uptake.

Table 2 The % fine particle fraction & MMAD(µm) of BSA-PGA-co-PDL nanocomposite NCMPs (n=3).

Formulation	%FPF	MMAD (µm)
BSA-PGA-co-PDL	70.97±4.7	1.5±0.35

Conclusions

The water-oil-water double emulsion solvent evaporation technique was able to manufacture PGA-co-PDL NPs with suitable BSA EE % (39.49%) and sustained release over 48h. Incorporating L-leucine during spray drying to produce NCMPs yielded FPF (70%) and MMAD (1.5 µm) allowing for high efficient delivery of protein to the lungs.

References

1) J. Fox. Turning plants into protein factories. *Nat. Biotechnol.*, **24**: 1191–1193 (2006).
2) S. Shoyele and S. Cawthorne. Particle engineering techniques for inhaled biopharmaceuticals. *Adv. Drug Del. Rev.* **58**: 1009–1029 (2006).
3) Pilcer, G. and Amighi. Formulation strategy and use of excipients in pulmonary drug delivery. *Int J Pharm.* **392**: 1–19 (2010).
4) H. Tawfeek, S. Khidr, E. Samy, S. Ahmed, M. Murphy, A. Mohamme, A. Shabir, G. Hutcheon and I. Saleem. Poly(Glycerol Adipate-co-ω-Pentadecalactone) spray-dried microparticles as sustained release carriers for pulmonary delivery. *Pharm Res.,* **28**: 2086-2097 (2011).

Cationic PGA-co-PDL nanocomposite microparticles for antigen delivery via inhalation

I M Alfagih[1, 2], N K Kunda[1], F K Alanazi[2], G A Hutcheon[1], I Y Saleem[1]

1. School of Pharmacy and Biomolecular Sciences, Liverpool John Moores University, UK.
2. Department of Pharmaceutics, King Saud University, Riyadh, Saudi Arabia.

Introduction

Pulmonary vaccine delivery has gained major attention to produce both mucosal and systemic immunity (1). The encapsulation of antigens in nanoparticles (NPs) has been investigated extensively as an approach to enhance immunogenicity (2).

A number of polymers have been studied for pulmonary vaccine delivery. In recent years, poly glycerol adipate-co-ω-pentadecalactone (PGA-co-PDL) was studied as a drug carrier (3), (4).

Chitosan hydrochloride (CHCl) has been described as a water-soluble and a positively charged polyelectrolyte, which may overcome the low water solubility of chitosan at neutral pH. However, like other cationic polymers, the strong positive charge of CHCl contributes to the toxicity of the polymer. The amount of CHCl can be decreased by making CHCl-coated PGA-co-PDL NPs, because only a lower amount of CHCl was expected to coat on the surface of a particle compared to CHCl NPs (5).

Objective

The aim of this study was to prepare CHCl coated PGA-co-PDL NPs encapsulating bovine serum albumin (BSA), a model antigen to produce cationic NPs which further spray dried to form nanocomposite microparticles (NCMPs) suitable for antigen delivery via inhalation.

Methods

Nanocomposite microparticles preparation

The protein solution 1%, 0.5ml was emulsified in 2ml of dichloromethane,DCM containing 50mg of PGA-co-PDL, by sonication using a probe sonicator at 45% amplitude (VC X 500 Vibra-CellTM, Sonics & Materials, Inc., USA) for 5s over an ice bath. Then it was emulsified into a a mixture of 1% CHCl and 1% PVA solution 25ml using a probe sonicator at 45% amplitude for 15s. Then it was stirred magnetically for 2h to evaporate DCM. The NPs were collected by centrifugation (SIGMA 3-30 K, SIGMA Laborzentrifugen GmbH, Germany) at 40,000xg for 1h at 4°C, and washed with distilled water.

NCMPs were prepared by spray drying NPs suspended in aqueous L-leucine solutions (1:1.5 w/w) using a mini-spray dryer (Büchi, B-290) with a standard two-fluid nozzle, feed rate of 10ml/min, air flow of 535L/h, aspirator at 50% and inlet temperature of 100°C.

Nanocomposite microparticles characterization
- NCMPs zeta potential and size were carried out using a Malvern NanoZS (Malvern Instruments Ltd., Worcestershire, UK).
- The amount of BSA loaded in the NPs was determined by measuring the amount of BSA remaining in the supernatant and wash after centrifugation using a QuantiPro bicinchoninic acid (BCA) protein assay kit (Sigma-aldrich).
- Spray dried NCMPs were visualised by scanning electron microscopy (SEM) (FEI – Inspect S Low VAV Scanning Electron Microscope).

In-vitro release study
Ten mg of NCMPs were dispersed in 1.2ml of phosphate buffer saline (pH7.4) at 37°C and rotated on a sample mixer (HulaMixer, Life Technologies).

Aerosolisation study (Next Generation Impactor, NGI)
Fifteen mg of NCMPs were loaded into HMC capsules, and aerosolised via a cyclohaler into a NGI, coated with 1% tween 80: acetone solution, at a flow rate of 60L/min for 4s. The samples were collected by washing with DCM/0.15M NaCl mixture (2:1). The FPF (%) was determined as the fraction of emitted dose deposited in the NGI with aerodynamic diameters less than 4.6μm, and the MMAD was calculated from log-probability analysis.

Results and Discussion
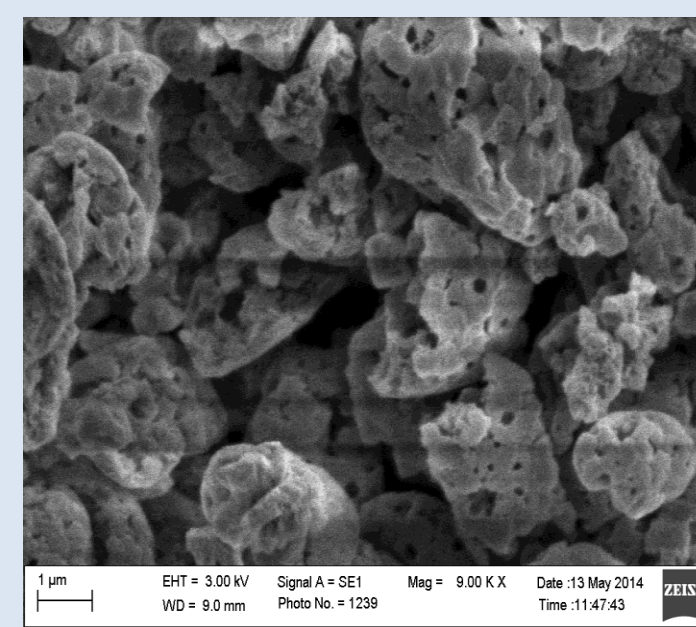
Nanocomposite microparticles characterization

The w/o/w double emulsion solvent evaporation process produced particles in the nanometer size range with a narrow particle size distribution (Table 1). The BSA loading for CHCl coated and uncoated PGA-co-PDL nanoparticles were 7.2±1.3 and 33.1±3 μg/mg respectively. The change in BSA loading observed attributed to increased amount of solid. The surface charge of CHCl coated PGA-co-PDL nanoparticles changed to +14.2±0.7mV.

Table 1 The particle size, polydispersity index (PDI), zeta potential, and drug loading (DL) for nanocomposite microparticles (n=3).

Formulation	Particle size (nm)	Zeta Potential (mV)	DL (μg/mg)	Polydispersity (PDI)
PGA-co-PDL	445±46.8	-17.4±1.2	33.1±3	0.145
CHCl-PGA-co-PDL	480.2±32.2	+14.2±0.7	7.2±1.3	0.280

SEM analysis (Figure 1) indicated that NCMPs were irregular and corrugated with a porous surface. The geometrical particle size of the produced nanocomposite microparticles as observed by SEM was approximately 2-4 μm.
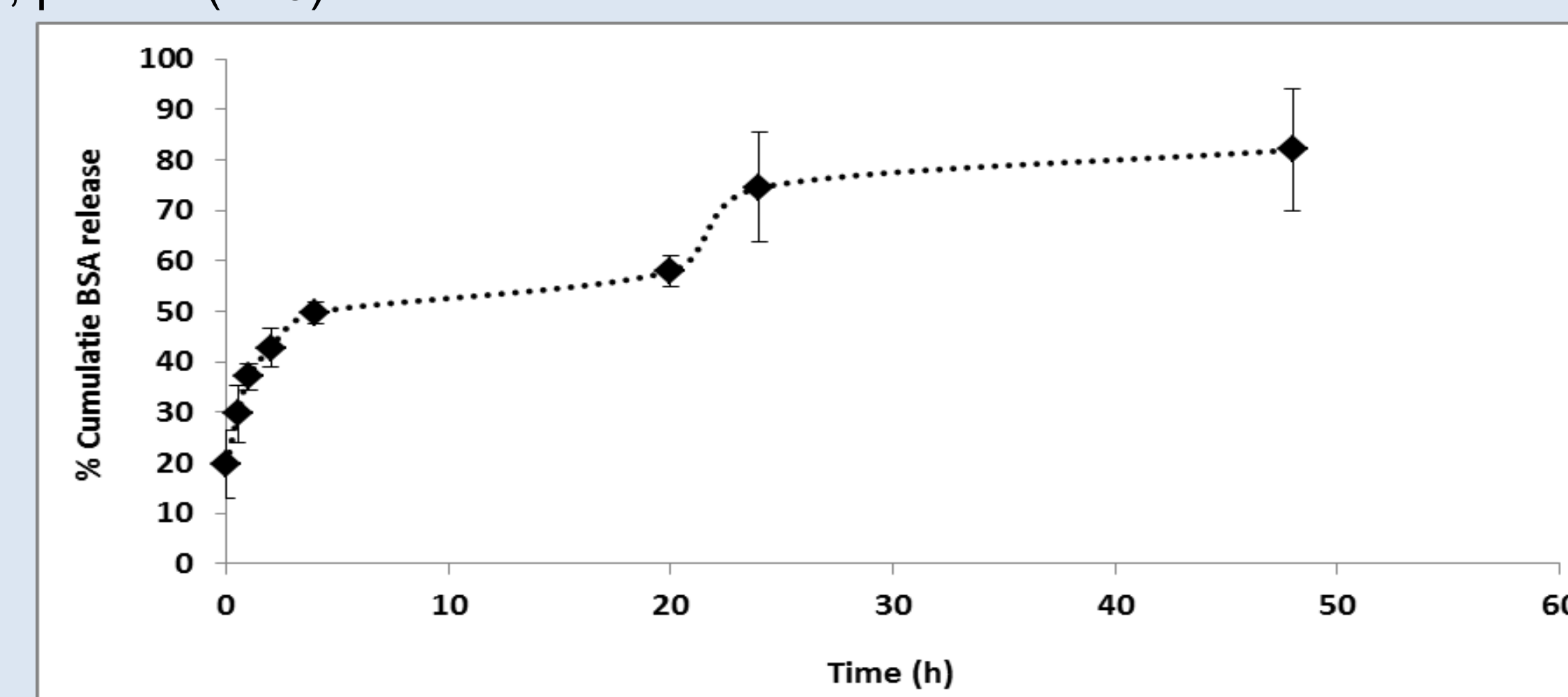
Figure 1 SEM images of spray dried CHCl-PGA-co-PDL nanocomposite microparticles. (The scale bar represents 1μm).

In-vitro release study

BSA showed biphasic release profile (Figure 2) with a first initial burst release followed by a second continuous sustained release phase over 48h. The initial burst release of BSA from NCMPs was 19.6±6% which after 4 h increased rapidly to 49.7±2%, which then slowed to 57.96±3.03% after 20 h then increased to 74.52±10% after 24 h followed by slow release to 81.9±12% after 48 h. This could be attributed to the distribution of BSA inside NPs matrix or a change in matrix degradation rate due to changed surface porosity.

Figure 2 In-vitro release profiles for CHCl-PGA-co-PDL nanocomposite microparticles in phosphate buffer saline, pH 7.4 (n=3).

Aerosolisation study (Next Generation Impactor, NGI)
Aerodynamic particle characteristics revealed that formulation yielded NCMPs capable of delivering BSA with %FPF of 47.3±12% and a MMAD of 1.7±0.29 μm, indicating deposition in the bronchial-alveolar region. As NCMPs penetrate to the bronchial-alveolar region it is anticipated that the L-leucine component will dissolve, releasing CHCl-PGA-co-PDL NPs for cells uptake.

Conclusions

The water-oil-water double emulsion solvent evaporation technique was able to manufacture CHCl-PGA-co-PDL NPs with suitable BSA loading (7μg/mg) and sustained release over 48h. The use of L-leucine during spray drying produced NCMPs with FPF (47%) and MMAD of 1.7±0.29 μm allowing for high efficient delivery of protein to the lungs.

References
1. Kunda, N., Somavarapu, S., Gordon, S., Hutcheon, G., Saleem, I. Nanocarriers targeting dendritic cells for pulmonary vaccine delivery. *Pharm Res.* 2013, Vol. 30, pp. 325-341.
2. Koppolu, B., Zaharoff, D. The effect of antigen encapsulation in chitosan particles on uptake, activation and presentation by antigen presenting cells. *Biomaterials.* 2013, Vol. 34, pp. 2359-2369.
3. Thompson, C., Hansford, D., Higgins, S., Hutcheon, G., Rostron, C., Munday, D. Enzymatic synthesis and evaluation of new novel pentadecalactone polymers for the production of biodegradable microspheres. *Journal of Microencapsulation.* 2006, Vol. 23, pp. 213-226.
4. Kallinteri, P., Higgins, S., Hutcheon, G., St Pourçain C., Garnett, M. Novel functionalized biodegradable polymers for nanoparticle drug delivery systems. *Biomacromolecules.* 2005, Vol. 6, pp. 1885-94.
5. Zhang, Y., Niu, Y., Luo, Y., Ge, M., Yang, T., Yu, L., Wang, Q.,. Fabrication, characterisation and antimicrobial actiities of thymol loaded zein nanoparticles stabilized by sodium caseinate-chitosan hydrochloride double layers. *Food chemistry.* 2014, Vol. 142, pp. 269-275.

PGA-co-PDL NANOCOMPOSITE MICROPARTICLES AS CARRIERS OF PROTEIN FOR PULMONARY DELIVERY

I.M. Alfagih[1,2], F.K. Alanazi[2], S. Satyanarayana[3], T. Chavan[3], G.A. Hutcheon[1], I.Y. Saleem[1]

(1) School of Pharmacy & Biomolecular Sciences, Liverpool John Moores University, Liverpool, UK.
(2) Department of Pharmaceutics, King Saud University, Riyadh, Saudi Arabia.
(3) The School of Pharmacy, University of London, London, UK.

Introduction

As an alternative to repeated injection, dry powder pulmonary inhalation offers a non-invasive technique for local and systemic delivery of protein-based formulation (1). The lungs possess many favourable features (2). In our laboratory we have been investigating and developing alternative biodegradable polyester polymers [poly (glycerol adipate-co-ω-pentadecalactone, PGA-co-PDL)]. Using this polymer we have successfully encapsulated a model protein (α-chymotrypsin enzyme). In addition, release studies revealed most of the protein released over several hours (3). Furthermore, we have successfully demonstrated that PGA-co-PDL microparticles could be used as an alternative carrier for pulmonary delivery with enhanced aerosol performance and reduced toxicity to normal lung cells compared to PLGA microparticles (4).

In this study we aim to produce PGA-co-PDL nanocomposite microparticles (NMs) loaded with bovine serum albumin (BSA), a model protein, which may be administered to the lung via dry powder inhalation. The impact of these characteristics on important aspects of pulmonary delivery such as aerosolization, and release will be determined.

Methods

Nanoparticles Preparation
BSA (Avenchem, UK) loaded PGA-co-PDL nanoparticles (NPs) were prepared by probe sonication (sonics, VCX 500) of water-in-oil-in-water (w/o/w) double emulsion/solvent evaporation method (Table 1). The double emulsion was stirred for 2 h at room temperature and the NPs were collected by centrifugation at 30,000 g (Beckman J2-2IM/E) for 45 min at 4 °C. Control empty NPs were prepared.

Spray drying NPs
The NMs were prepared by spray drying NPs suspension in aqueous L-leucine solutions (1.5%w/w) using a mini-spray dryer (Büchi, B-290) with two-fluid nozzle (0.7 mm diameter), feed rate of 15 ml/min, air flow of 414 L/h, aspirator at 40m³/h, inlet and outlet temperature of 100 and 47 °C, respectively.

Nanocomposite Microparticles characterisation
Particle size & zeta potential
The particle size & zeta potential were measured using a Zetaplus. Briefly, 100µl of the suspension was diluted to 5 ml using double distilled water and the measurements recorded at 25ºC (n=3).

Spray dried yeild & drug loading
The yield of spray dried NMs was quantified as a percentage mass of expected total powder yield (n=3). The amount of BSA loaded in the NPs was determined by measuring the amount of BSA remaining in the supernatant with a QuantiPro BCA protein assay (Sigma) after centrifugation (n=3).

Particle morphology
Spray dried NMs were mounted on gold coated aluminium stubs (EmiTech K 550X Gold Sputter Coater, 25mA for 3 min), and visualised by scanning electron microscopy.

In-vitro relese study
20mg of BSA encapsulated spray dried NMs were placed in an eppendorf and dispersed in 1.2ml of PBS (pH 7.4). The samples were incubated at 37°C in the orbital shaker set at 250 rpm. At predetermined time intervals up to 24h, the samples were centrifuged (30,000 g for 20 min) and 1ml of the supernatant removed and replaced with fresh buffer. The supernatant was analysed by QuantiPro BCA protein assay as mentioned above (n=3).

Table 1 Different formulation parameters for preparation of NPs by (w/o/w) double emulsion solvent evaporation

Formula No.	Polymer conc. (mg/ml)	BSA Conc. (%)	IAP volume (µl)	PVA Conc. IAP (%)	PVA Conc. EAP (%)	EAP volume (ml)
NM1	25	0.5	500	1	13	25
NM2	25	0.5	500	5	13	25
NM3	25	0.5	250	5	13	25

*IAP: internal aqueous phase **EAP: external aqueous phase

Aerosolisation studies
Dry powder samples (10mg) were manually loaded into hydroxypropyl methylcellulose capsules (size 3), and aerosolised via a cyclohaler into a Next Generation Impactor (NGI), coated with 5% tween 80: acetone solution, at a flow rate of 60L/min for 4s to determine aerodynamic particle size. The samples were collected by washing with DCM/0.15 M NaCl mixture (2:1) to dissolve the polymer and the encapsulated BSA, which was determined by QuantiPro BCA protein assay as mentioned above (n=3). The FPF (%) was determined as the fraction of emitted dose deposited in the NGI with aerodynamic diameters less than 4.6 µm, and the MMAD was calculated from log-probability analysis.

Results & Discussion

Nanocomposite Microparticles characterisation
The particle size achieved ranged from 196.6±1.9 – 290.6±7.5 and the yield of NMs achieved after spray drying ranged from 24.4±4.7 – 35.9±5.1 (Table 2). All particles had a negative zeta potential, possibly due to PVA remaining on the particles after centrifugation and washing. The drug loading ranged from 14.6±2.5 to 20.54±3.1 µg/mg particle. There was a significant increase in drug loading between NM1 and NM2, due to an increase in PVA concentration in the IAP. However, decreasing IAP volume led to no significant difference in BSA loading between NM2 and NM3.

SEM analysis indicated that NMs (NM2) had a corrugated surface with pores visible on the surface (Fig. 1). This occurred due to excessive build-up of vapor pressure during solvent evaporation in the spray drying process and occurs with hydrophobic amino acids, such as L-leucine, for improved aerosolization performance (5). The size of the NM was approximately 2-3 µm according to SEM analysis.

Table 2 The drug loading, particle size, zeta potential, spray dried yield & drug loading of different NMs formulations.

Formula No.	Particle size (nm)	Zeta potential (mV)	Yield (%)	BSA loading (µg/mg)
NM1	275.5±12.7	-24.5±1.3	25.4±5.3	14.6±2.5
NM2	196.6±1.9	-19.3±3.3	24.4±4.7	20.5±3.1
NM3	290.6±7.5	-12.4±2.1	35.9±5.1	19.5±0.6

The data in Fig.2 represents the % cumulative release of BSA as a percentage of the drug loading. All formulation showed biphasic release profile with a first initial burst release followed by a second continuous sustained release phase over 24h. All formulations had a similar initial burst release of BSA ranging from 9.6±1.0 – 11.5±2.3%.
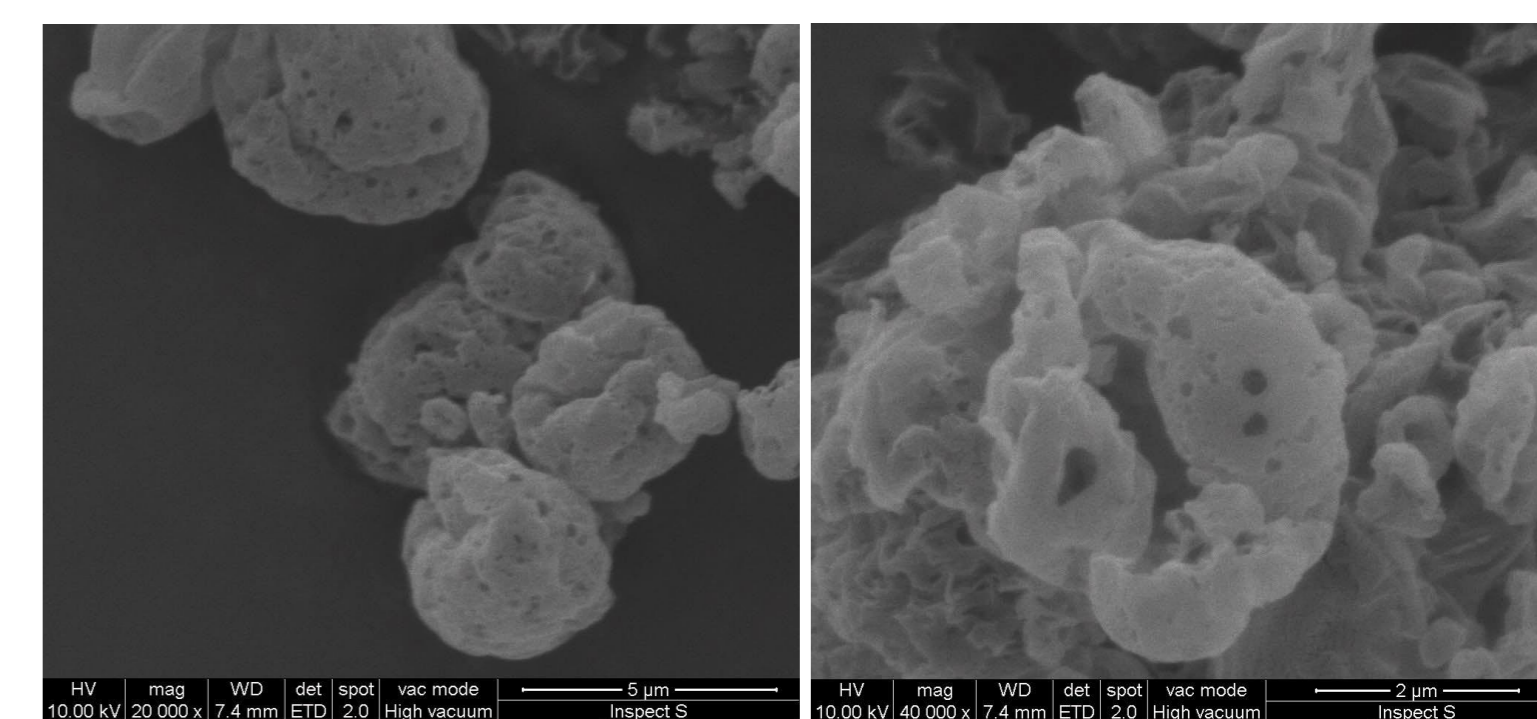

Figure 1 SEM images of NMs (NM2). Scale bar represents 5 µm (A) & 2 µm (B) respectively.

Significant difference was noted in release profile (2 – 24 h) between NM1 and NM3, with NM1 achieving 19.8±1.5% release after 24 h compared to NM3 (14.1±2.0%).
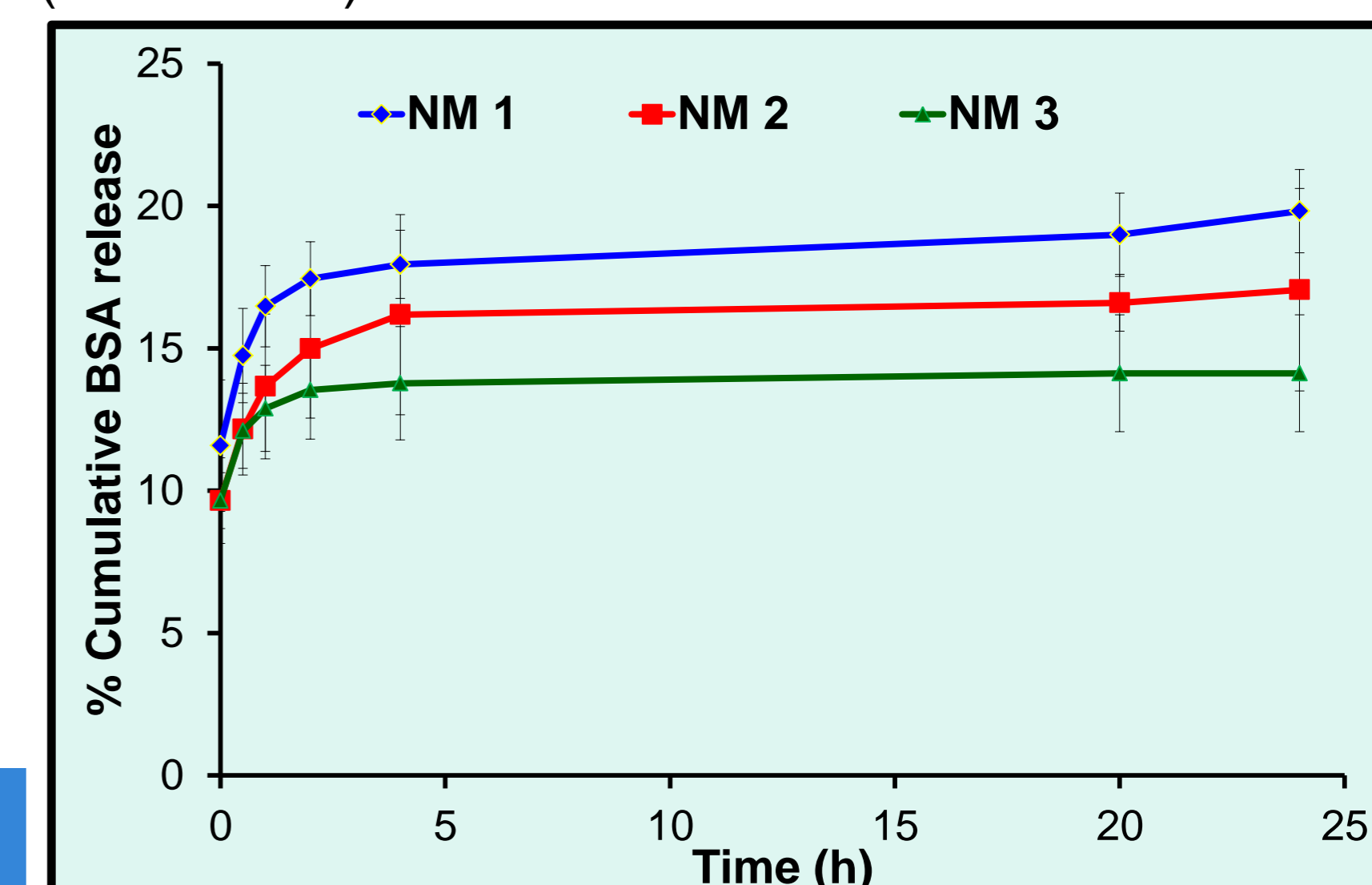

Figure 2 % cumulative in-vitro release profiles for different BSA-PGA-co-PDL NMs as a percentage of drug loading in phosphate buffer saline, pH 7.4.

NM2 was chosen for aerosolisation studies due to a high drug loading and reasonable drug release profile compared to NM1 and NM3. The results in Tab.3 indicate good aerosolisation properties and the MMAD corresponds to particle size data achieved with SEM.
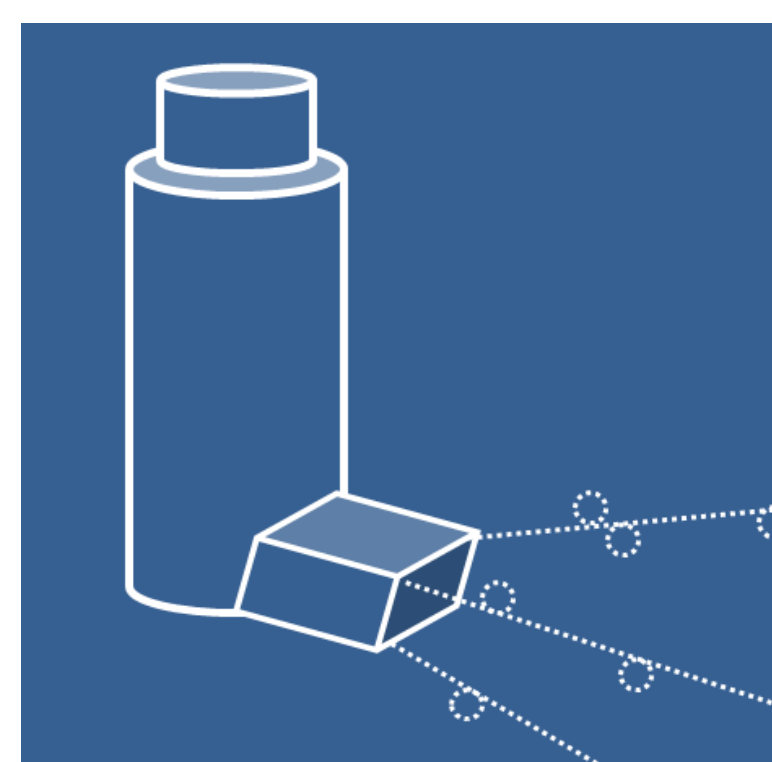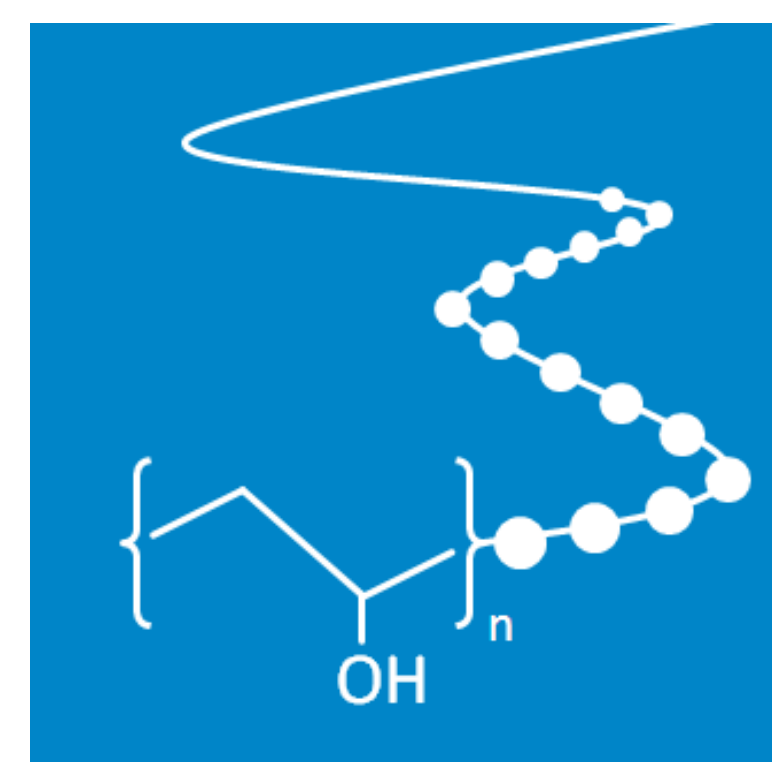
Table 3 Aerosolisation performance of NM2

Formula No.	FPF (%)	MMAD (µm)
NM2	70.1 ±13.2	1.6 ± 0.4

Conclusion

we have shown the potential for encapsulating proteins within PGA-co-PDL NMs as carriers for pulmonary delivery using double emulsion/spray drying as a preparation method. Future studies will involve improving the drug loading, stability studies and release by optimising the preparation method.

References

[1] Sou, T., et al. Trends Biotechnol. 29,191-198 (2011).
[2] Bivas-Benita, M., et al. Eur. J. Pharm. and Biopharm. 58, 1–6 (2004).
[3] Gaskell, E., et al. J. Microencapsul. 25, 187-195 (2008).
[4] Tawfeek, H., et al. Pharm. Res. 28, 2086-97 (2010).
[5] Alder, M., et al. Pharm. Res. 17, 863-870 (2000).

Protein Loaded PGA-co-PDL Nanocomposite Microparticles for Inhalation

I M Alfagih[1, 2], F K Alanazi[2], N K Kunda[1], G A Hutcheon[1], I Y Saleem[1]
1. School of Pharmacy and Biomolecular Sciences, Liverpool John Moores University, UK.
2. Department of Pharmaceutics, King Saud University, Riyadh, Saudi Arabia.

Introduction

Over the past decade pharmaceutical research has been focused on developing macromolecules for treatment of many diseases [1]. Most of these macromolecules are administered using an invasive manner to reach a therapeutic concentration, even though these procedures would be painful to the patients. As an alternative, pulmonary inhalation could enhance macromolecules administration because it is a non-invasive technique for local and systemic drug delivery. The lungs own many favourable features, including large surface area for absorption, high vasculatures, thin epithelium in the alveolar tissue and short path of gas–blood exchange movement [2]. However, formulating these macromolecules into suitable pulmonary delivery systems remains a challenge. .

The most common method for the encapsulation of proteins in polymer-based nanoparticles (NPs) is the water/oil/water (w/o/w) double-emulsion solvent evaporation method [3]. NPs can also be formulated into dry powders for inhalation by spray-drying.

Here at Liverpool John Moores University we have been investigating poly glycerol adipate-co-ω-pentadecalactone (PGA-co-PDL) as alternative to PLGA as a carrier for pulmonary delivery of macromolecules [4]. The results revealed that these polyesters could exhibit an alternative pulmonary delivery as they provide a protective matrix and faster release in a short period of time in comparison with other similar polymers, such as PLGA.

Objective

The aim of this study was to formulate PGA-co-PDL NPs encapsulating bovine serum albumin (BSA), a model protein, incorporated into a microparticle L-leucine matrix via spray drying to produce nanocomposite microparticle (NCMPs) carriers suitable for pulmonary delivery via dry powder inhalation.

Methods

Nanocomposite microparticles preparation

The protein solution 1% 0.5 ml was emulsified in dichloromethane,DCM containing 50 mg PGA-co-PDL, by a probe sonicator at 45% amplitude over an ice. Then emulsified into a 1% PVA solution 25ml at 45% ampliyude and stirred for 2h at room temperature to evaporate DCM. NPs collected by centrifugation at 25,750xg and 4°C.

NCMPs were prepared by spray drying NPs suspended in L-leucine solution (1:1.5w/w) using a mini-spray dryer (Büchi, B-290) at pump: 10%, air flow: 50 mm, aspirator: 50 % and inlet temperature:100 °C.

Nanocomposite microparticles characterization

- NCMPs zeta potential and size were carried out using a Zetaplus, Brookhaven Instruments, U.K.
- BSA loaded in NPs was determined by measuring BSA remaining in the supernatant and wash after centrifugation using a QuantiPro BCA protein assay kit (Sigma-aldrich).
- NCMPs were visualised by scanning electron microscopy (SEM) (FEI – Inspect S Low VAV Scanning).
- The yield of NCMPs was quantified as a percentage mass of expected total powder yield.

In-vitro release study

Ten mg of NCMPs were dispersed in 1.2ml of phosphate buffer saline, PBS (pH7.4) at 37°C and rotated on a mixer (HulaMixer, Life Technologies).

Aerosolisation study (Next Generation Impactor, NGI)

Ten mg of NCMPs were loaded into HMC capsules and aerosolised via a cyclohaler into a NGI, coated with tween 80: acetone solution,flow rate of 60L/min for 4s. Samples were collected by washing with DCM/0.15M NaCl mixture. FPF%: the fraction of emitted dose deposited in NGI with aerodynamic diameters < 4.6µm and the MMAD was calculated from log-probability analysis.

Results and Discussion
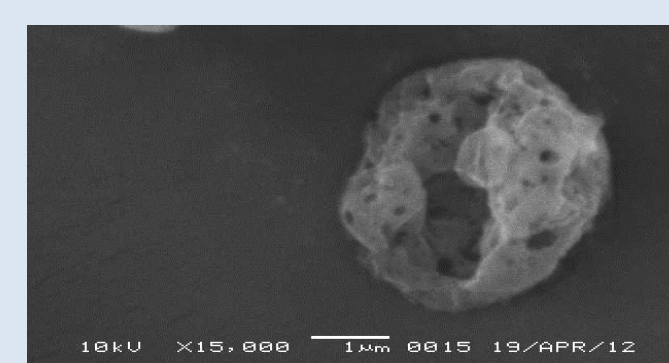
Nanocomposite microparticles characterization

The selected w/o/w double emulsion solvent evaporation process produced particles in the nanometer size range with a narrow particle size distribution (Table 1). The %EE of BSA loaded NPs was 39.49±2.63 % with BSA loading of 35.9±2.39 µg/mg and a zeta potential of -17.17±0.61 mV. NPs were further spray-dried to produce NCMPs with a reasonable yield for BSA loaded (38.22±1.17 %) and empty NCMPs (61.32±5.67 %).

Table 1 The particle size, polydispersity index (PDI), zeta potential, encapsulation efficiency (%EE), drug loading (DL), and yield (%) of NCMPs (n=3).

Formulation	Particle size (nm)	PDI	Zeta potential (mV)	EE (%)	DL (µg/mg)	Yield (%)
BSA-PGA-co-PDL	203.03±5.4	0.145	-17.17±0.61	39.49±2.63	35.9±2.39	38.22±1.17
Empty PGA-co-PDL	284.1±9.9	0.280	-15.86±0.85	-	-	61.32±5.67

SEM analysis (Figure 1) indicated that NCMPs were irregular and corrugated with a porous surface. The geometrical particle size of the produced nanocomposite microparticles as observed by SEM was approximately 2-4 µm.
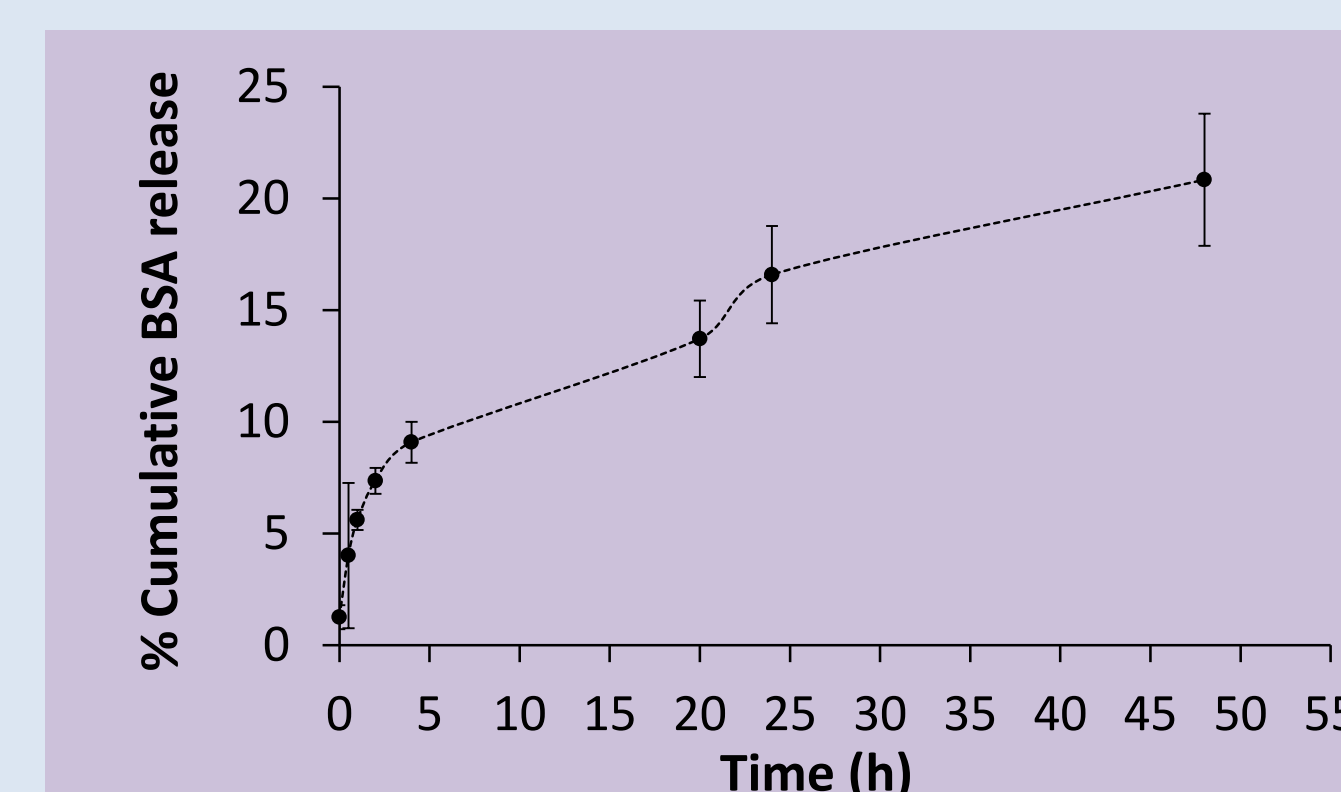
Figure 1 SEM images of spray dried BSA-PGA-co-PDL NCMPs. (The scale bar represents 1µm).

In-vitro release study

BSA showed biphasic release profile (Figure 2) with an initial burst release followed by a second continuous sustained release phase over 48h. The initial burst release of BSA from NCMPs was 1.26±1.5% which after 4 h increased rapidly to 9.08±3.4%, which then slowed to 20.84±4.2% after 48 h.

Figure 2 In-vitro release profiles of BSA –PGA-co-PDL NCMPs in PBS, pH 7.4 (n=3).

Aerosolisation study (Next Generation Impactor, NGI)

Aerodynamic particle characteristics revealed that the studied formulation yielded NCMPs capable of delivering efficient BSA with %FPF of 70.97±4.7% and a MMAD of 1.5±0.35 µm, indicating deposition in the bronchial-alveolar region. As NCMPs penetrate to the bronchial-alveolar region it is anticipated the L-leucine component will dissolve, releasing PGA-co-PDL NPs which will eventually degrade into its individual components (glycerol, divinyl adipate, and caprolactone) releasing BSA for uptake.

Table 2 The % fine particle fraction & MMAD(µm) of BSA-PGA-co-PDL nanocomposite NCMPs (n=3).

Formulation	%FPF	MMAD (µm)
BSA-PGA-co-PDL	70.97±4.7	1.5±0.35

Conclusions

The water-oil-water double emulsion solvent evaporation technique was able to manufacture PGA-co-PDL NPs with suitable BSA EE % (39.49%) and sustained release over 48h. Incorporating L-leucine during spray drying to produce NCMPs yielded FPF (70%) and MMAD (1.5 µm) allowing for high efficient delivery of protein to the lungs.

References

1) J. Fox. Turning plants into protein factories. Nat. Biotechnol., **24**: 1191–1193 (2006).
2) S. Shoyele and S. Cawthorne. Particle engineering techniques for inhaled biopharmaceuticals. Adv. Drug Del. Rev. **58**: 1009–1029 (2006).
3) Pilcer, G. and Amighi. Formulation strategy and use of excipients in pulmonary drug delivery. Int J Pharm. **392**: 1–19 (2010).
4) H. Tawfeek, S. Khidr, E. Samy, S. Ahmed, M. Murphy, A. Mohamme, A. Shabir, G. Hutcheon and I. Saleem. Poly(Glycerol Adipate-co-ω-Pentadecalactone) spray-dried microparticles as sustained release carriers for pulmonary delivery. Pharm Res., **28**: 2086-2097 (2011).

Cationic PGA-co-PDL nanocomposite microparticles for antigen delivery via inhalation

I M Alfagih[1, 2], N K Kunda[1], F K Alanazi[2], G A Hutcheon[1], I Y Saleem[1]
1. School of Pharmacy and Biomolecular Sciences, Liverpool John Moores University, UK.
2. Department of Pharmaceutics, King Saud University, Riyadh, Saudi Arabia.

Introduction

Pulmonary vaccine delivery has gained major attention to produce both mucosal and systemic immunity (1). The encapsulation of antigens in nanoparticles (NPs) has been investigated extensively as an approach to enhance immunogenicity (2).

A number of polymers have been studied for pulmonary vaccine delivery. In recent years, poly glycerol adipate-co-ω-pentadecalactone (PGA-co-PDL) was studied as a drug carrier (3), (4).

Chitosan hydrochloride (CHCl) has been described as a water-soluble and a positively charged polyelectrolyte, which may overcome the low water solubility of chitosan at neutral pH. However, like other cationic polymers, the strong positive charge of CHCl contributes to the toxicity of the polymer. The amount of CHCl can be decreased by making CHCl-coated PGA-co-PDL NPs, because only a lower amount of CHCl was expected to coat on the surface of a particle compared to CHCl NPs (5).

Objective

The aim of this study was to prepare CHCl coated PGA-co-PDL NPs encapsulating bovine serum albumin (BSA), a model antigen to produce cationic NPs which further spray dried to form nanocomposite microparticles (NCMPs) suitable for antigen delivery via inhalation.

Methods

Nanocomposite microparticles preparation
The protein solution 1%, 0.5ml was emulsified in 2ml of dichloromethane,DCM containing 50mg of PGA-co-PDL, by sonication using a probe sonicator at 45% amplitude (VC X 500 Vibra-CellTM, Sonics & Materials, Inc., USA) for 5s over an ice bath. Then it was emulsified into a a mixture of 1% CHCl and 1% PVA solution 25ml using a probe sonicator at 45% amplitude for 15s. Then it was stirred magnetically for 2h to evaporate DCM. The NPs were collected by centrifugation (SIGMA 3-30 K, SIGMA Laborzentrifugen GmbH, Germany) at 40,000xg for 1h at 4°C, and washed with distilled water.
NCMPs were prepared by spray drying NPs suspended in aqueous L-leucine solutions (1:1.5 w/w) using a mini-spray dryer (Büchi, B-290) with a standard two-fluid nozzle, feed rate of 10ml/min, air flow of 535L/h, aspirator at 50% and inlet temperature of 100ºC.

Nanocomposite microparticles characterization
- NCMPs zeta potential and size were carried out using a Malvern NanoZS (Malvern Instruments Ltd., Worcestershire, UK).
- The amount of BSA loaded in the NPs was determined by measuring the amount of BSA remaining in the supernatant and wash after centrifugation using a QuantiPro bicinchoninic acid (BCA) protein assay kit (Sigma-aldrich).
- Spray dried NCMPs were visualised by scanning electron microscopy (SEM) (FEI – Inspect S Low VAV Scanning Electron Microscope).

In-vitro release study
Ten mg of NCMPs were dispersed in 1.2ml of phosphate buffer saline (pH7.4) at 37°C and rotated on a sample mixer (HulaMixer, Life Technologies).

Aerosolisation study (Next Generation Impactor, NGI)
Fifteen mg of NCMPs were loaded into HMC capsules, and aerosolised via a cyclohaler into a NGI, coated with 1% tween 80: acetone solution, at a flow rate of 60L/min for 4s. The samples were collected by washing with DCM/0.15M NaCl mixture (2:1). The FPF (%) was determined as the fraction of emitted dose deposited in the NGI with aerodynamic diameters less than 4.6μm, and the MMAD was calculated from log-probability analysis.

Results and Discussion

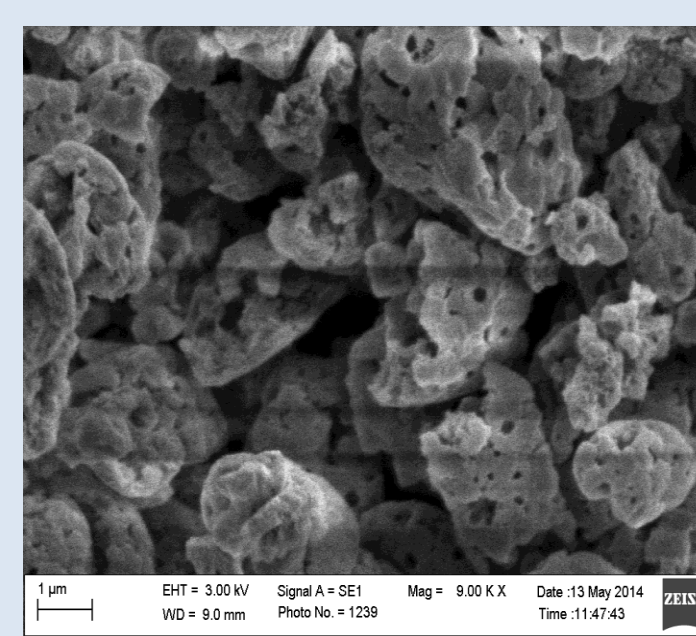### Nanocomposite microparticles characterization

The w/o/w double emulsion solvent evaporation process produced particles in the nanometer size range with a narrow particle size distribution (Table 1). The BSA loading for CHCl coated and uncoated PGA-co-PDL nanoparticles were 7.2±1.3 and 33.1±3 μg/mg respectively. The change in BSA loading observed attributed to increased amount of solid. The surface charge of CHCl coated PGA-co-PDL nanoparticles changed to +14.2±0.7mV.

Table 1 The particle size, polydispersity index (PDI), zeta potential, and drug loading (DL) for nanocomposite microparticles (n=3).

Formulation	Particle size (nm)	Zeta Potential (mV)	DL (μg/mg)	Polydispersity (PDI)
PGA-co-PDL	445±46.8	-17.4±1.2	33.1±3	0.145
CHCl-PGA-co-PDL	480.2±32.2	+14.2±0.7	7.2±1.3	0.280

SEM analysis (Figure 1) indicated that NCMPs were irregular and corrugated with a porous surface. The geometrical particle size of the produced nanocomposite microparticles as observed by SEM was approximately 2-4 μm.
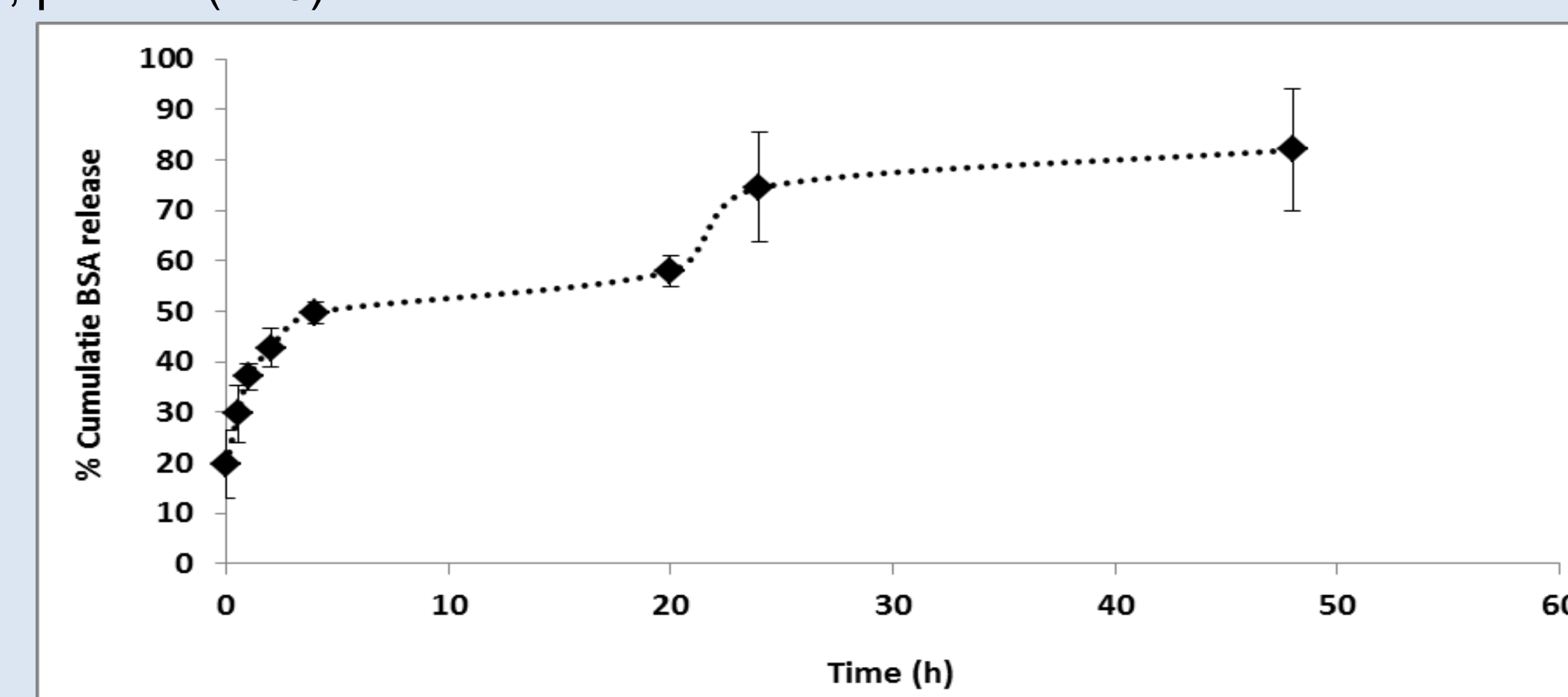
Figure 1 SEM images of spray dried CHCl-PGA-co-PDL nanocomposite microparticles. (The scale bar represents 1μm).

In-vitro release study

BSA showed biphasic release profile (Figure 2) with a first initial burst release followed by a second continuous sustained release phase over 48h. The initial burst release of BSA from NCMPs was 19.6±6% which after 4 h increased rapidly to 49.7±2%, which then slowed to 57.96±3.03% after 20 h then increased to 74.52±10% after 24 h followed by slow release to 81.9±12% after 48 h. This could be attributed to the distribution of BSA inside NPs matrix or a change in matrix degradation rate due to changed surface porosity.

Figure 2 In-vitro release profiles for CHCl-PGA-co-PDL nanocomposite microparticles in phosphate buffer saline, pH 7.4 (n=3).

Aerosolisation study (Next Generation Impactor, NGI)

Aerodynamic particle characteristics revealed that formulation yielded NCMPs capable of delivering BSA with %FPF of 47.3±12% and a MMAD of 1.7±0.29 μm, indicating deposition in the bronchial-alveolar region. As NCMPs penetrate to the bronchial-alveolar region it is anticipated that the L-leucine component will dissolve, releasing CHCl-PGA-co-PDL NPs for cells uptake.

Conclusions

The water-oil-water double emulsion solvent evaporation technique was able to manufacture CHCl-PGA-co-PDL NPs with suitable BSA loading (7μg/mg) and sustained release over 48h. The use of L-leucine during spray drying produced NCMPs with FPF (47%) and MMAD of 1.7±0.29 μm allowing for high efficient delivery of protein to the lungs.

References
1. Kunda, N., Somavarapu, S., Gordon, S., Hutcheon, G., Saleem, I. Nanocarriers targeting dendritic cells for pulmonary vaccine delivery. *Pharm Res.* 2013, Vol. 30, pp. 325-341.
2. Koppolu, B., Zaharoff, D. The effect of antigen encapsulation in chitosan particles on uptake, activation and presentation by antigen presenting cells. *Biomaterials.* 2013, Vol. 34, pp. 2359-2369.
3. Thompson, C., Hansford, D., Higgins, S., Hutcheon, G., Rostron, C., Munday, D. Enzymatic synthesis and evaluation of new novel pentadecalactone polymers for the production of biodegradable microspheres. *Journal of Microencapsulation.* 2006, Vol. 23, pp. 213-226.
4. Kallinteri, P., Higgins, S., Hutcheon, G., St Pourçain C., Garnett, M. Novel functionalized biodegradable polymers for nanoparticle drug delivery systems. *Biomacromolecules.* 2005, Vol. 6, pp. 1885-94.
5. Zhang, Y., Niu, Y., Luo, Y., Ge, M., Yang, T., Yu, L., Wang, Q.,. Fabrication, characterisation and antimicrobial actiities of thymol loaded zein nanoparticles stabilized by sodium caseinate-chitosan hydrochloride double layers. *Food chemistry.* 2014, Vol. 142, pp. 269-275.